

## Photophysics of multichromophoric molecular assemblies

**Citation for published version (APA):**

Beckers, E. H. A. (2006). *Photophysics of multichromophoric molecular assemblies*. [Phd Thesis 1 (Research TU/e / Graduation TU/e), Chemical Engineering and Chemistry]. Technische Universiteit Eindhoven.  
<https://doi.org/10.6100/IR599249>

**DOI:**

[10.6100/IR599249](https://doi.org/10.6100/IR599249)

**Document status and date:**

Published: 01/01/2006

**Document Version:**

Publisher's PDF, also known as Version of Record (includes final page, issue and volume numbers)

**Please check the document version of this publication:**

- A submitted manuscript is the version of the article upon submission and before peer-review. There can be important differences between the submitted version and the official published version of record. People interested in the research are advised to contact the author for the final version of the publication, or visit the DOI to the publisher's website.
- The final author version and the galley proof are versions of the publication after peer review.
- The final published version features the final layout of the paper including the volume, issue and page numbers.

[Link to publication](#)

**General rights**

Copyright and moral rights for the publications made accessible in the public portal are retained by the authors and/or other copyright owners and it is a condition of accessing publications that users recognise and abide by the legal requirements associated with these rights.

- Users may download and print one copy of any publication from the public portal for the purpose of private study or research.
- You may not further distribute the material or use it for any profit-making activity or commercial gain
- You may freely distribute the URL identifying the publication in the public portal.

If the publication is distributed under the terms of Article 25fa of the Dutch Copyright Act, indicated by the "Taverne" license above, please follow below link for the End User Agreement:

[www.tue.nl/taverne](http://www.tue.nl/taverne)

**Take down policy**

If you believe that this document breaches copyright please contact us at:

[openaccess@tue.nl](mailto:openaccess@tue.nl)

providing details and we will investigate your claim.

**Photophysics of  
Multichromophoric  
Molecular Assemblies**



# **Photophysics of Multichromophoric Molecular Assemblies**

**Proefschrift**

ter verkrijging van de graad van doctor aan de Technische Universiteit  
Eindhoven, op gezag van de Rector Magnificus, prof.dr.ir. C.J. van Duijn,  
voor een commissie aangewezen door het College voor Promoties in het  
openbaar te verdedigen op dinsdag 24 januari 2006 om 16.00 uur

door

Edwin Hendrikus Anne Beckers

geboren te Maastricht

Dit proefschrift is goedgekeurd door de promotor:

prof.dr.ir. R.A.J. Janssen

Copromotor:

dr. S.C.J. Meskers

This research has been financially supported by the Council for Chemical Sciences of the Netherlands Organization for Scientific Research (NWO-CW).

Omslagontwerp: Bianca Beckers en Edwin Beckers

Druk: Universiteitsdrukkerij, Technische Universiteit Eindhoven

CIP-DATA LIBRARY TECHNISCHE UNIVERSITEIT EINDHOVEN

Beckers, Edwin H.A.

Photophysics of multichromophoric molecular assemblies / by Edwin H.A.

Beckers. – Eindhoven : Technische Universiteit Eindhoven, 2005.

Proefschrift. – ISBN 90-386-2957-5

NUR 913

Trefwoorden: donor-acceptor systemen / geconjugeerde materialen /  
fotogeïnduceerde elektronenoverdracht / energie overdracht / waterstof-  
bruggen / aggregatie / zelf-assemblage

Subject headings: donor-acceptor systems / conjugated materials /  
photoinduced electron transfer / energy transfer / hydrogen bonding /  
aggregation / self-assembly

*“Er komt nergens zoveel aan het licht als in een donkere kamer”*

W. F. Hermans

*“De grootste kunstenaar kan niets verzinnen dat niet vooraf al in het steen bestaat, maar als zijn hand niet met zijn geest meegaat zal hij het nooit van het ruwe marmer winnen”*

Michelangelo

# Table of Contents

## Chapter 1

### *Photoinduced Electron Transfer in Multichromophoric Assemblies*

1.1	Introduction	2
1.2	Artificial Donor-Acceptor Systems	3
	<i>Covalent Donor-Acceptor systems</i>	3
	<i>Supramolecular Donor-Acceptor systems</i>	5
	<i>Aggregated and Self-Assembled D-A Systems and <math>\pi</math>-<math>\pi</math> Stacking</i>	6
1.3	Photophysics Processes in $\pi$ -Conjugated Organic Molecules	7
	<i>Energy Transfer</i>	7
	<i>Electron Transfer</i>	8
1.4	Photoinduced Absorption Spectroscopy	10
1.5	Aim and Scope of this Thesis	12
1.6	References	13

## Chapter 2

### *Charge Transfer Kinetics in Fullerene-Oligomer-Fullerene Triads Containing Alkylpyrrole Units*

2.1	Introduction	20
2.2	Results and Discussion	21
	<i>Energy Levels</i>	21
	<i>Photoluminescence Quenching</i>	21
	<i>Gibbs-free Energy for Charge Separation</i>	23
	<i>Time-Resolved Photoluminescence</i>	24
	<i>Near Steady-State Photoinduced Absorption</i>	26
	<i>Transient Photoinduced Absorption</i>	27
	<i>Modelling of the Transient PIA Trace</i>	28
2.3	Conclusions	30
2.4	Experimental Section	30
2.5	References and Notes	31

## Chapter 3

### *Charge Separation and Recombination in Photoexcited Oligo(p-Phenylene Vinylene) – Perylene Bisimide Arrays close to the Marcus Inverted Region*

3.1	Introduction	36
3.2	Results and Discussion	36
3.3	Conclusions	41
3.4	Experimental Section	42
3.5	References and Notes	43

## Chapter 4

### *Photoinduced Multistep Electron Transfer in an Oligoaniline–Oligo(p-phenylene vinylene) – Perylene Bisimide Molecular Array*

4.1	Introduction	46
4.2	Results	46
	<i>Absorption Spectroscopy</i>	46
	<i>Electrochemistry</i>	48
	<i>Energetic Considerations</i>	49
	<i>Transient Absorption Spectroscopy</i>	50
	<i>Array 1 in Toluene</i>	51
	<i>Array 1 in Polar Solvents</i>	52
	<i>Array 2 in Polar Solvents</i>	53
4.3	Discussion	55
4.4	Conclusions	56
4.5	Experimental Section	57
4.6	References	57

## Chapter 5

### *The Influence of Intermolecular Orientation on the Charge Transfer Kinetics in Self-assembled Oligo(p-phenylene vinylene) – Perylenebisimide Arrays*

5.1	Introduction	62
5.2	Results and Discussion	64
	<i>Intermolecular Organization in the Aggregates from Absorption Spectroscopy</i>	64
	<i>Molecular Mechanics Calculations</i>	68
	<i>Photoinduced Charge Separation and Recombination</i>	70
5.3	Conclusions	75
5.4	Experimental Section	75
5.5	References	76

## Chapter 6

### *Supramolecular OPV-Fullerene Architectures by Using the Ureido-pyrimidinone Quadruple Hydrogen-bonding Unit*

6.1	Introduction	80
6.2	Monofunctional OPV-Fullerene Ureido-Pyrimidinone Systems	81
	<i>Optical Properties of OPV4-UP1 and OPV4-UP2</i>	82
	<i>Keto-Enol Equilibrium</i>	83
	<i>Fluorescence Quenching</i>	84
	<i>Förster Energy Transfer</i>	87
	<i>Electron Transfer</i>	88
6.3	Bifunctional OPV-Fullerene Ureido-Pyrimidinone Systems	89
6.4	Conclusions	92



6.5	Experimental Section	93
6.6	References and Notes	93

## Chapter 7

### *Hydrogen-bonded Oligo(p-phenylene vinylene) – Perylene Bisimide Arrays*

7.1	Introduction	98
7.2	Ureido-Pyrimidinone Coupled OPV-PERY Arrays	98
	<i>Optical properties</i>	98
	<i>Transient Photoinduced Absorption (PIA)</i>	99
	<i>Electron Transfer</i>	100
7.3	Diaminotriazine Coupled OPV-PERY Arrays	101
	<i>Chlorine-Substituted OPV-PERY Systems</i>	102
	<i>Phenoxy-Substituted OPV-PERY Systems</i>	104
7.4	Analysis of Aggregate Packing	108
7.5	Conclusions	113
7.6	Experimental Section	114
7.7	References and Notes	119

## Chapter 8

### *Charge Transfer in Supramolecular Co-Aggregates of Oligo(p-phenylene vinylene) and Perylene Bisimide in Water*

8.1	Introduction	124
8.2	Results and Discussion	124
	<i>UV/Vis Absorption Spectroscopy</i>	124
	<i>Transient Photoinduced Absorption Spectroscopy</i>	126
	<i>Photoluminescence Quenching</i>	127
8.3	Conclusions	128
8.4	Experimental Section	128
8.5	References and Notes	128

	<i>Summary</i>	131
--	----------------	-----

	<i>Samenvatting</i>	133
--	---------------------	-----

	<i>Curriculum Vitae</i>	137
--	-------------------------	-----

	<i>List of Publications</i>	139
--	-----------------------------	-----

	<i>Dankwoord</i>	141
--	------------------	-----

# Chapter 1

## Photoinduced Electron Transfer in Multichromophoric Assemblies

### *Abstract*

*In this chapter an introduction on photoinduced energy and electron transfer reactions in donor-acceptor systems is presented in relation to the scope of the thesis. Knowledge of these transfer processes is vital in elucidating the working principles of natural photosynthesis and of artificial systems that aim to convert solar energy into electricity or fuels. For covalently linked donor-acceptor molecules numerous studies have advanced the insights into the energetics and kinetics of photoinduced charge transfer processes. The photophysical properties of isolated donor-acceptor arrays can often be rationalized by Marcus theory. In contrast, our understanding of the same reactions in solid state organic semiconductors is not nearly as advanced. One of the reasons is that intermolecular interactions between donor-acceptor molecules that occur in the solid state have to be taken into account in addition to intrinsic and intramolecular interactions of the chromophores. More knowledge of the intermolecular effects within ensembles of molecules is essential to begin to understand and eventually control the complex interplay of processes that direct photoinduced electron transfer in solid state organic semiconductors and future devices based on these materials.*

## 1.1 Introduction

The conversion of solar light into valuable energy by natural or artificial photosynthesis is an appealing and intriguing process, making it an interesting topic for researchers in biology, physics and chemistry.<sup>1-4</sup> A well-studied and illustrative system is the photosynthetic reaction system in purple bacteria. The solar light is captured in the two pigment-protein light-harvesting complexes and preserved by circulating the energy within the cyclic arrays of bacteriochlorophyll molecules.<sup>5-7</sup> Following the initial charge separation reaction in the heart of the reaction center, the photogenerated positive and negative charges are moved apart to suppress the recombination reaction. The energy of the resulting long-lived charges is subsequently used to drive biochemical processes within the bacteria.<sup>3,4</sup>

The important mechanistic information extracted from studies on natural processes<sup>8-11</sup> also led to ideas for the design of artificial reaction systems to mimic and possibly improve the solar energy conversion process based on photoinduced electron transfer between electron donor and acceptor systems.<sup>12-15</sup> Mimicking natural systems with synthetic analogues has provided valuable insight on how charge separation and recombination reactions proceed in donor-acceptor  $\pi$ -conjugated molecules following photoexcitation. These studies have shown that both electronic properties (excitation energy and redox potentials) and structural elements (distance, orientation, and nature of the bridge) are critical parameters that control the kinetics of charge transfer reactions in molecular systems. The photophysical and photochemical properties of isolated donor-acceptor molecules and those molecularly dissolved in solution can often be described by theories based on Marcus equation.

In contrast, attempts to extrapolate these insights to the behavior of composite organic semiconductors in the solid state have repeatedly failed. The origin of this discrepancy can be found in the importance of intermolecular interactions in the solid state. Similar to the proteins surrounding the chromophores in the natural systems, the environment of the photoactive compounds is of immense importance for the final properties of organic solid state semiconductors. This makes control over the intermolecular orientation and morphology an essential prerequisite to influence and improve charge separation, charge transport, and collection of charges at the electrodes in photovoltaic devices based on organic molecules. Determining and controlling the interactions between different chromophores in the solid state is far from trivial and, hence, detailed studies on model compounds in solution remain important to deepen our insights in the effects of orientation and distance on electron transfer reactions. This thesis addresses the kinetics of the photophysical processes in covalently linked, hydrogen-bonded, and self-assembled nanoaggregated donor-acceptor systems in an attempt to elucidate some of the principles that govern photoinduced electron transfer reactions in solid state organic compounds (Figure 1). By increasing the complexity from a single molecule in solution to self-assembled molecular ensembles it will be possible to determine some of the structural factors that control the kinetics of electron transfer in the solid state.

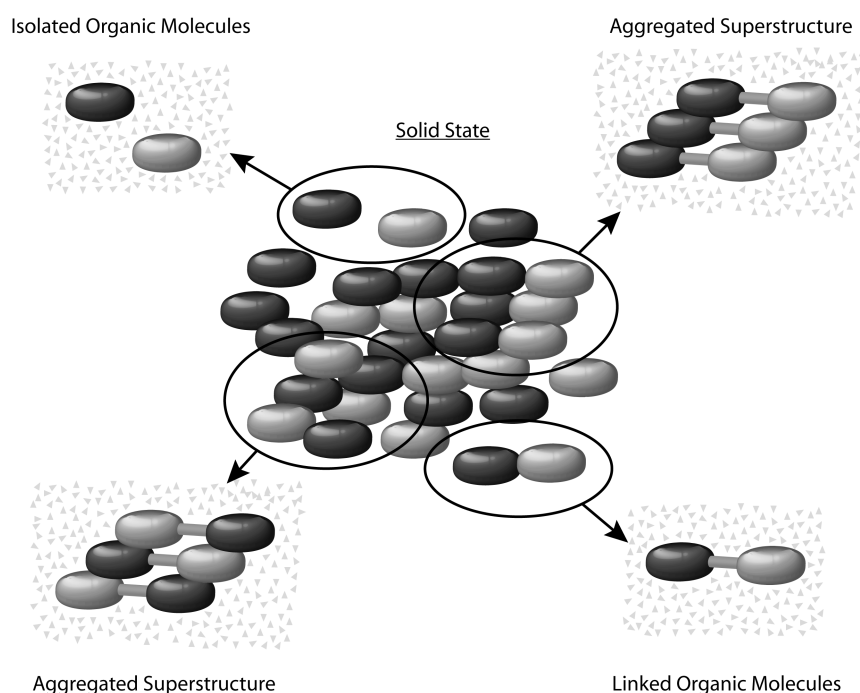


**Figure 1:** Schematic representation of the morphology of a donor-acceptor system in the solid-state. The various compositions of chromophores in solution can mimic the nanoscopic domains within the solid state.

## 1.2 Artificial Donor-Acceptor Systems

Numerous attempts have been made to mimic the chromophoric system used by nature in artificial systems. Often the donor and acceptor unit are covalently linked to ensure that donor and acceptor are in close proximity and –in many cases– have a more or less rigid mutual orientation. In nature, however, the photoactive molecules are rarely covalently bound but rather carefully positioned by supramolecular interactions. Therefore photoinduced energy and electron transfer reactions in supramolecularly organized donor-acceptor dyads increasingly receive attention in recent years. Finally, the first examples are emerging where many chromophores with donor and acceptor electronic properties self-assemble into larger architectures by noncovalent bonding. Ultimately supramolecular interactions and self-assembly might lead to multichromophoric systems having carefully designed ensembles of molecules that are able to transfer light into solar energy or solar fuels, much like nature does. In this paragraph some illustrative examples of chromophore systems will be discussed to give an introduction on the current state-of-the-art of this fascinating research area.

**Covalent Donor-Acceptor Systems.** Extensive efforts on synthetic modification of  $\pi$ -conjugated materials have created a wide variety of possibilities to link donor and acceptor materials in almost every desired way. By introducing a covalent linker between the chromophores it is possible to study interactions between different photoactive and electroactive chromophores in close proximity.

Influenced by the light-harvesting system nature uses, many studies focus on porphyrin units in artificial donor-acceptor arrays.<sup>13,15,16</sup> Recently, this is often in combination with fullerenes after the

potential of this unit as an electron acceptor was established.<sup>17-19</sup> In this way it is possible to examine the existing theories on electron transfer reaction in great detail. Examples on the dependence of the strength of the redox couple have been reported for various covalently linked donor-fullerene arrays often in combination with studies on the differences between intra and intermolecular processes.<sup>20-25</sup> The type of linkage is still of major influence, in particular control over the rigidity of the linker deepened the knowledge as the orientation of the donor and acceptor could be fixed.<sup>26,27</sup>

Synthetically more demanding is the extension of the lifetime of the created charges by the incorporation of additional chromophores in the system, much like in the natural photosynthetic reaction center.<sup>12,13,15,28,29</sup> This has led to the creation of appealing, complex structures and demonstrates the large degree of control that has been achieved in fine tuning energy levels towards tailoring the outcome of the photophysical processes. Of the many examples that can be found in literature, only two are briefly mentioned here as an illustration of the state-of-the art in this field.

The hexadec porphyrin- $C_{60}$  compound described by Kuciauskas *et al.* shows how an artificial system can benefit from knowledge obtained from the natural photosynthetic reaction center (Figure 2).<sup>30</sup> The four zinc porphyrins in  $(P_{ZP})_3-P_{ZC}-P-C_{60}$  are used as a light-harvesting antenna. Subsequently, an energy transfer reaction occurs from the excited state of the zinc porphyrin to the free base porphyrin. Finally, a charge transfer reaction results in the formation of the  $(P_{ZP})_3-P_{ZC}-P^+-C_{60}^-$  radical ion pair.

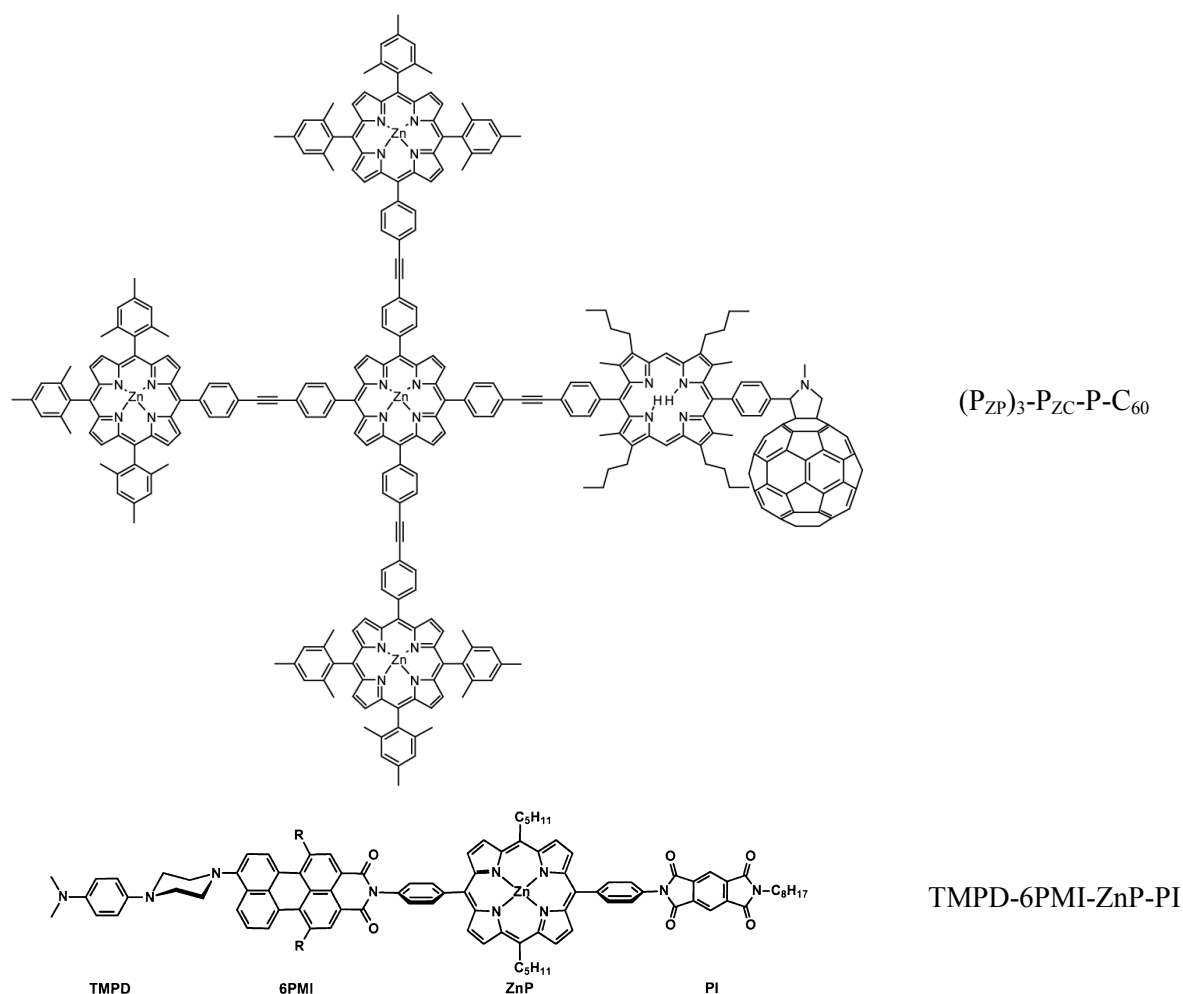


**Figure 2:** Examples of multichromophoric covalent donor-acceptor arrays.<sup>30,31</sup>

Andersson *et al.* reported an impressive example of control over reaction pathways resulting in an exceptional enhancement of the lifetime of the photoinduced charges.<sup>31</sup> By covalently linking two donor-acceptor systems they synthesized the TMPD-6PMI-ZnP-PI tetramer (Figure 2). The  $\text{TMPD}^+-6\text{PMI}^- \cdot \text{ZnP}^{++} \cdot \text{PI}^-$  state is created after double photoexcitation, which recombines to the  $\text{TMPD}^+-6\text{PMI}^- \cdot \text{ZnP} \cdot \text{PI}^-$  state. This distant ion pair has a lifetime of around 650 ns, over four orders of magnitude longer than the separate  $\text{TMPD}^+ \cdot 6\text{PMI}^-$  and  $\text{ZnP}^{++} \cdot \text{PI}^-$  ion pairs.

**Supramolecular Donor-Acceptor Systems.** Besides the fixation of donor and acceptor units by covalent bonding, it is also possible to use supramolecular linkers. The types of bonding most frequently used are metal interactions<sup>32,33</sup> and hydrogen bonding.<sup>34</sup> Again, the inspiration for supramolecular donor-acceptor systems mainly results from natural systems where the presence of intermolecular interactions is of vital importance.<sup>3,35-39</sup>

Like for covalently coupled arrays, the porphyrin/fullerene couple is the most intensely studied supramolecular donor-acceptor system (Figure 3). In contrast to the covalent analogs, resolving the structure of the supramolecular architecture is typically the main goal<sup>40-44</sup> and the actual photophysical processes are only rarely studied in detail.<sup>45-47</sup> Interestingly, some of these supramolecular systems have already been used to create working devices.<sup>48-50</sup>

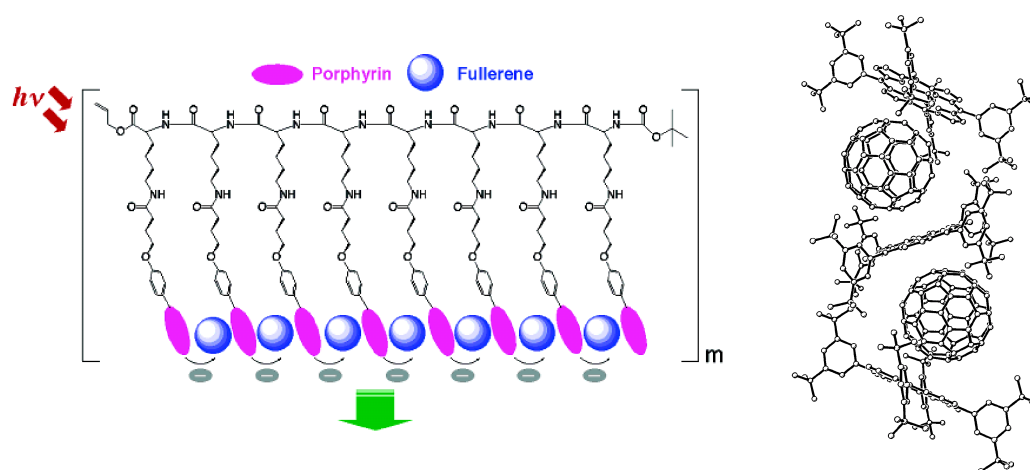


**Figure 3:** Examples of supramolecular porphyrin/fullerene structures.<sup>40,47</sup>

Segura *et al.* have reported an example of an electron transfer in hydrogen-bonded donor-acceptor dyads.<sup>51</sup> They elegantly showed the use of a guanidinium-carboxylate hydrogen bonding couple to link a TTF donor to a  $\text{C}_{60}$  acceptor in various ways (Figure 4). In these dyads, a through-space electron transfer reaction was observed resulting in the  $\text{C}_{60}^- \cdot \text{TTF}^{++}$  radical ion pair.

Another example of the use of supramolecular interactions in well-defined donor-acceptor systems is shown by Ramos *et al.*<sup>52</sup> An oligo(*p*-phenylene vinylene) (OPV) donor is linked by a *m*-phenylene ethynylene foldamer to a perylene bisimide (PERY) acceptor. The extended configuration of this spacer in polar solvents introduces a large chromophore distance that prevents the photoinduced charge transfer reaction. On the other hand, a folded configuration in apolar solvent places both chromophores at a close distance, resulting in the efficient formation of radical ion pairs.

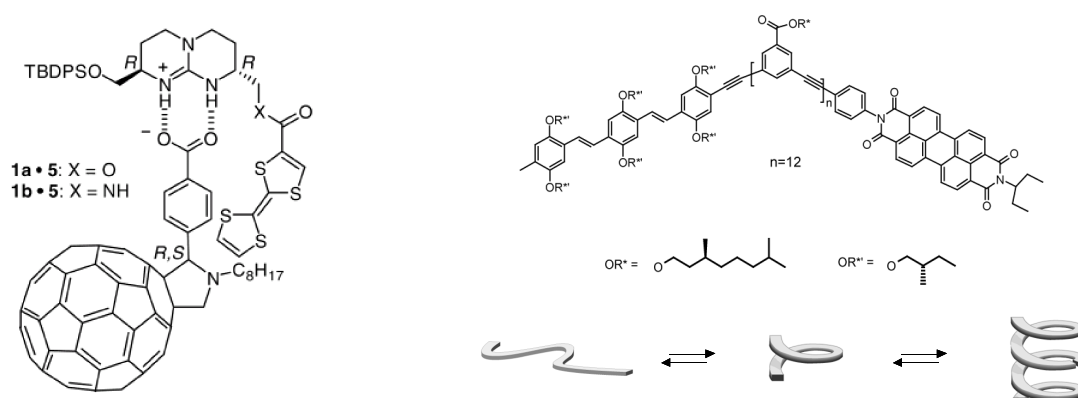


**Figure 4:** Illustrative examples of a hydrogen bonded TTF-C<sub>60</sub> dyad<sup>51</sup> (left) and a covalently linked oligo(*p*-phenylene vinylene)-perylene foldamer<sup>52</sup> (right).

**Aggregated and Self-Assembled Donor-Acceptor Systems and  $\pi$ - $\pi$  Stacking.**<sup>53</sup> The combination of a large flat  $\pi$ -system together with an acceptor-strength superior to that of the fullerene unit has made the perylene chromophore an ideal compound for the study of photophysics in aggregated systems. Its versatility is shown by examples of the use in supramolecular structures ranging from metal-linked structures containing porphyrins<sup>54</sup> to stacked three-fold symmetric discs<sup>55</sup> and organogels of cholesteric perylenes<sup>56</sup>. An additional advantage of the perylene unit is that after only a slight modification of the core it can act not only as an acceptor, but also as a donor unit.<sup>57,58</sup>

One of the first studies on the special properties of aggregated donor-acceptor systems was published by Wasielewski.<sup>59</sup> Tetrakis(perylene bisimide) substituted zinc tetraphenylporphyrin self-assembles in solution and solid state into ordered 150 nm nanoparticles by van der Waals stacking (Figure 5). Photoinduced charge transfer in the nanoparticles occurred with near unit efficiency at a rate of  $k_{CS} = 3.1 \times 10^{11} \text{ s}^{-1}$  in toluene and the charges recombine with  $k_{CR} = 1.4 \times 10^8 \text{ s}^{-1}$ . The charge transfer is faster than for model compounds consisting of one zinc porphyrin containing only one or two perylene bisimides. In addition, the recombination is somewhat slower than in the model compounds. Charge recombination within the nanoaggregates not only provided the ground state, but also the perylene bisimide triplet state. The latter is a consequence of radical ion pairs that intersystem cross from the primary singlet radical ion pair. The average radical ion pair distance was estimated to be 21 Å, while the chromophore center-to-center distance in the compound is only 14.4 Å. This implies that the electron on the perylene bisimide is five layers removed from the layer with the hole on the porphyrin. A similar effect was observed for oligo(*p*-phenylene vinylene)-fullerene dyads. It was shown that the forward electron transfer in these dyads can be up to an order of magnitude faster in the solid state than the same reaction in the most polar solvents.<sup>60</sup> In these molecules, acceleration of charge separation would only be expected in more polar solvents. Taking into account that organic solids have a much lower relative dielectric constant (typically  $\epsilon_r = 3$  to 4) compared to the most polar solvents used ( $\epsilon_r = 25$ ), the increased transfer speed cannot be explained by polarity.

Another design proposed in a recent report on photophysical processes in a supramolecular oligo(*p*-phenylene)vinylene, porphyrin, and C<sub>60</sub> shows that indeed the pathways of electron transfer can be adjusted by synthetic design of energy levels and supramolecular interactions.<sup>61</sup> However, it also

reveals the current limitations of the available detection techniques that prevent clarification of real fundamental issues in complex systems.

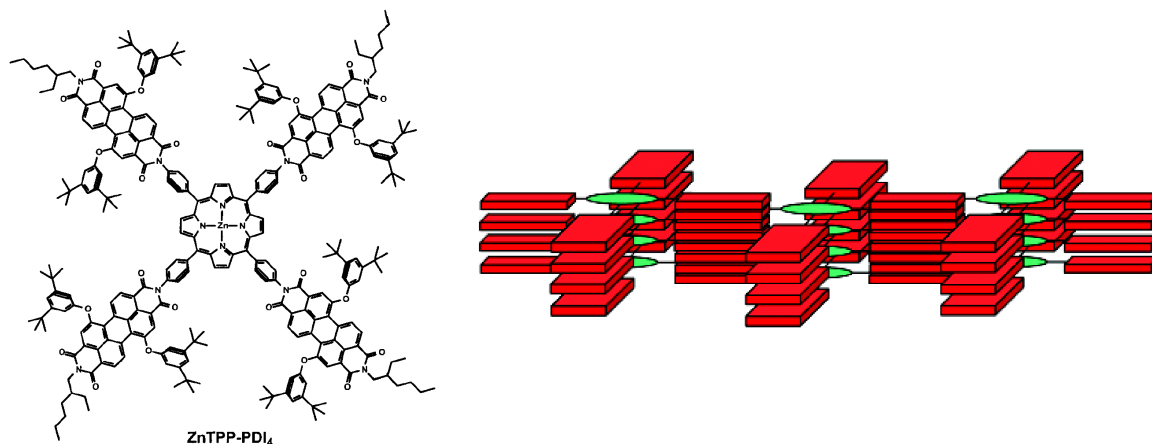


**Figure 5:** Structure and cartoon of the self-assembled nanoparticles.<sup>59</sup>

### 1.3 Photophysical Processes in $\pi$ -Conjugated Materials

Two different chromophores in close proximity with complementary electronic properties often exhibit photophysical processes that are not found in either of the pure materials. Two of the most startling - and potentially useful- photophysical reactions are energy transfer and electron (or charge) transfer. These transfer reactions form the heart of natural photosynthesis and are fundamental to the operation of artificial organic systems for solar fuels and photovoltaics. In this section the basic principles of photoinduced energy and electron transfer reaction will be briefly discussed.

**Energy Transfer.** When two different materials or molecules with different excited state energy levels exist in a single system, an energy transfer reaction may occur after photoexcitation. Provided that the excited state of one molecule (the donor) is higher in energy than that of the other (the acceptor), the excitation energy of the photoexcited donor can be transferred to the acceptor. In this process the donor material returns to the ground state, and the acceptor material is formed in the excited state.

Energy transfer may occur via different mechanisms, and three models have been proposed for various types of energy transfer reactions. The most trivial one is the radiative energy transfer mechanism in which the donor emits a photon that is subsequently absorbed by the acceptor material and brings it to the excited state. A second mechanism, proposed by Dexter,<sup>62</sup> involves a non-radiative energy transfer mechanism based on a double electron exchange mechanism via overlapping orbitals. For Dexter energy transfer, the donor and acceptor have to be in close contact and an exponential ( $\exp(-R)$ ) distance dependence is observed. This mechanism is of particular interest for triplet energy transfer reactions and may also play a role in intramolecular energy transfer reactions when the two chromophores are in close proximity. In the latter case, it may be difficult to distinguish from direct delocalization (strong coupling). The most studied mechanism for energy transfer, however, is the dipole-dipole based Förster<sup>63</sup> model. In Förster energy transfer, two transition dipole moments are coupled via classical dipole-dipole coupling, leading to a  $R^{-6}$  distance dependence. As a result, Förster



energy transfer is particularly important at intermediate distances for donor and acceptor chromophores with electrical dipole allowed transitions. Many singlet energy transfer reactions fulfill these criteria.

The most commonly used technique to quantify energy transfer reactions is recording the quenching of the intensity or lifetime of photoluminescence of the photoexcited donor in combination with an increase of emission of the acceptor. Since energy transfer is a competing pathway for the radiative decay of the singlet state of the donor, the lifetime of the excited state of the donor material provides a direct measure for the energy transfer rate.

**Electron Transfer.** In addition to *energy* transfer, *electron* transfer may also occur upon illumination of a pair of chromophores. For electron transfer, either the donor or the acceptor may be photoexcited. Electron transfer can occur when the change in free energy for charge separation ( $\Delta G_0$ ) is negative. In a first approximation, this is achieved when the excited-state energy exceeds the energy difference between the oxidation potential of the donor ( $E_{ox}(D)$ ) and the reduction potential of the acceptor ( $E_{red}(A)$ ). For donor-acceptor systems in solutions, the likelihood of an electron transfer reaction can be predicted by analyzing the various contributions to the free energy ( $\Delta G_0$ ) according to equation 1, which also contains terms for the spatial separation of the ions and their solvation.<sup>64</sup>

$$-\Delta G_0 = -e[E_{ox}(D) - E_{red}(A)] + E_{00} + \frac{e^2}{4\pi\epsilon_0\epsilon_s R_{cc}} + \frac{e^2}{8\pi\epsilon_0} \left( \frac{1}{r^+} + \frac{1}{r^-} \right) \left( \frac{1}{\epsilon_{ref}} - \frac{1}{\epsilon_s} \right) \quad (1)$$

The parameters involved in equation 1 are the electron charge ( $-e$ ), the vacuum permittivity ( $\epsilon_0$ ), the relative permittivities of the solvent ( $\epsilon_s$ ) and the reference solvent ( $\epsilon_{ref}$ ) used to determine the redox potentials, the center-to-center distance of positive and negative charges in the chromophores ( $R_{cc}$ ), and the radii of the positive and negative ions ( $r^+$  and  $r^-$ ).

The driving force ( $-\Delta G_0$ ) can be directly linked to the kinetics of the reaction by the theory proposed by Marcus (equation 2).<sup>65</sup> Marcus theory predicts that three kinetic regimes exist depending on the relative size of  $-\Delta G_0$  and the reorganization energy  $\lambda$  (Figure 6). The reorganization energy is the energy required to bring the geometry of the photoexcited (DA)\* complex to the geometry of the charge-separated ( $D^+A^-$ ) state. The  $\lambda$  parameter is the sum of internal ( $\lambda_i$ ) and solvent ( $\lambda_s$ ) contributions. In the “normal region” ( $-\Delta G_0 < \lambda$ ), the rate for electron transfer increases with increasing driving force due to a decreasing barrier for the reaction ( $\Delta G_0^\ddagger$ , equation 3). Typical values for the internal reorganization energy of  $\pi$ -conjugated molecules are  $\lambda_i = 0.2 - 0.5$  eV, while the additional solvent reorganization energy ( $\lambda_s$ ) can exceed values of 0.7 eV. This implies that the total reorganization energy ( $\lambda = \lambda_s + \lambda_i$ ) is mostly larger than the driving force for the electron transfer reaction and that electron transfer often occurs in the normal region.

When the driving force is similar to the reorganization energy ( $-\Delta G_0 \approx \lambda$ ) the more rare case of the “optimal region” occurs in which the barrier for charge transfer becomes zero. Because there is no barrier, the rate for charge separation maximizes and only depends on the electronic coupling ( $V$ ). Upon increasing the driving force even further, the “inverted region” ( $-\Delta G_0 > \lambda$ ) is reached. Here the rate will decrease again with increasing driving force because the barrier increases.

$$k_0 = \left( \frac{\pi}{\hbar^2 \lambda k_B T} \right)^{1/2} V^2 \exp \left( - \frac{\Delta G_0^\ddagger}{k_B T} \right) \quad (2)$$

$$\Delta G_0^\ddagger = \frac{(\Delta G_0 + \lambda)^2}{4\lambda} \quad (3)$$

The first observation of all three regimes was by Gloss and Miller, nearly 25 years after the prediction was made by Marcus.<sup>66,67</sup> Whereas it is becoming more common to observe inverted region behavior for the charge recombination reaction,<sup>68-72</sup> it is still very rarely observed for a photoinduced intramolecular charge separation reaction.<sup>73,74</sup>

The theory for electron transfer reactions is of immense importance for numerous fields of science, which has been acknowledged by awarding the Nobel Prize to Rudolph Marcus in 1992.<sup>75,76</sup> However, debates on the exact limits of the applicability of the predictions are still lively.<sup>77-79</sup> In particular, consensus on the exact role of the solvent<sup>80-85</sup> and the importance of tunneling effects<sup>80,86,87</sup> in the reaction has not yet been reached. In addition, claimed observations on extremely long-lived charges have been hard to justify by the existing theories, resulting in arguments on both the validity of theory and experiments.<sup>88-91</sup>

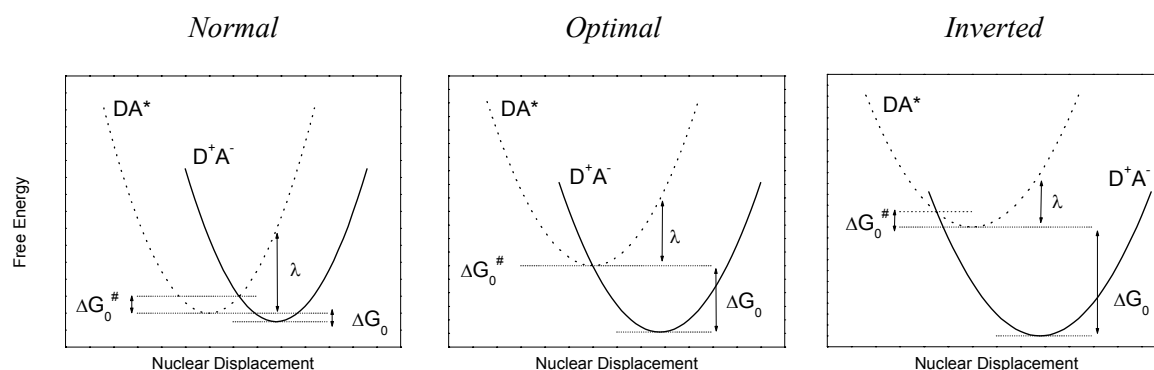


**Figure 6:** Energy diagrams for the three possible regions for electron transfer as described by Marcus theory.

The most important adaptation to Marcus equations has been done by Joshua Jortner (equation 4).<sup>92-94</sup> Jortner recognized the importance of higher vibrational levels in direct and superexchange interactions. This enabled a more accurate description of the inverted region and explained the temperature independence of the electron transfer reaction at low temperatures. Jortner's model incorporates the effective mode vibrational energy ( $\hbar\omega$ ) and the Huang-Rhys factor  $S (= \lambda_i/\hbar\omega)$  into Marcus theory. For most  $\pi$ -conjugated systems a value of  $1500 \text{ cm}^{-1}$  (0.186 eV) is used for  $\hbar\omega$ , referring to the frequency of the stretch vibration of the carbon-carbon double bond in aromatic systems.

$$k_0 = \left( \frac{\pi}{\hbar^2 \lambda_s k_B T} \right)^{1/2} V^2 \sum_{n=0}^{\infty} e^{-S} \frac{S^n}{n!} \exp \left( - \frac{(\Delta G_0 + \lambda_s + n\hbar\omega)^2}{4\lambda_s k_B T} \right) \quad (4)$$

Although the theory of charge separation and recombination is rather well developed for most experimental conditions, this does not imply that it can be directly applied to construct a synthetically designed system having all the desired properties. For application of donor-acceptor systems in photovoltaics or in solar fuels, it is generally beneficial to have a fast charge separation to attain the highest conversion of excitations into charges. The recombination should be as slow as possible to retain the charges as long as possible. As indicated above, most systems have charge separation in the normal region and the recombination in the inverted region. Therefore a high driving force is desired for both reactions. Unfortunately, the sum of both driving forces equals the excitation energy, i.e. if one driving force increases; the other decreases (Figure 7). This makes a delicate balance between both processes inevitable for optimal performances.

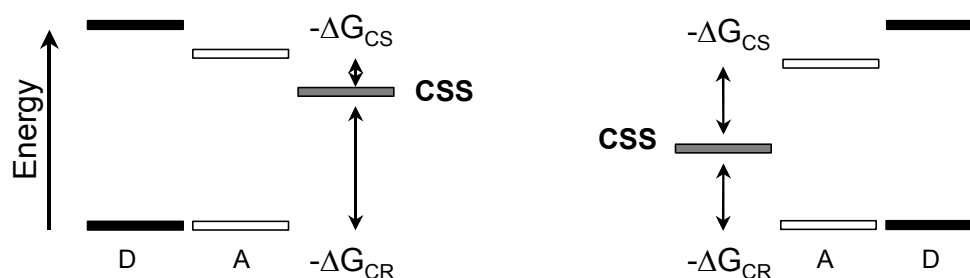


**Figure 7:** Schematic representation of the excited state energy levels of a donor-acceptor system with different driving forces for charge separation and recombination.

#### 1.4 Photoinduced Absorption (PIA) Spectroscopy.

In this section the experimental technique for determining the temporal evolution of primary photoexcitations as used in this thesis is briefly outlined. The method used to accurately measure photoinduced energy and electron transfer processes on various timescales is pump-probe photoinduced absorption spectroscopy. In this technique an excited state is created by illumination of the sample with laser light (*pump*-beam). The evolving processes after photoexcitation are subsequently monitored by detection of the species formed with a second laser beam or white-light source (*probe*-beam). In contrast to photoluminescence quenching, this technique allows the direct measurement of excited-state species and since it probes the bulk of the sample it is less sensitive to small impurities that limit the use of fluorescence quenching in determining rate constants.

For most studies reported in this thesis, a pump-probe setup (Figure 8) is used based on a laser system with 800 nm laser pulses with duration of 150 fs at a repetition frequency of 1 kHz. The wavelengths of pump and probe beams can be adjusted in this setup via two optical parametric amplifiers (OPA). These provide a wide range of wavelengths ranging from the visible to the infrared (450 nm – 1700 nm).

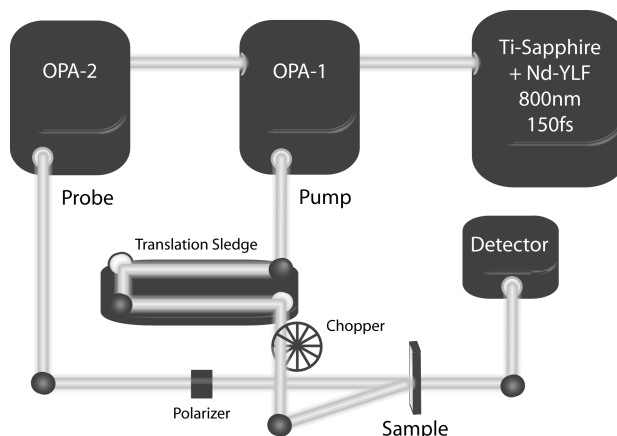


**Figure 8:** Experimental pump-probe setup for photoinduced absorption (PIA) spectroscopy in the picosecond time regime.

In the actual experiment, the pump-beam is mechanically chopped at a frequency of 500 Hz, thereby blocking every second pulse of this beam and creating an on/off sequence for the excitation of the sample (Figure 9). This facilitates the detection of absorption difference between the “on-state” (with species in their excited state) and the “off-state” (with molecules in their ground state) because the probe beam still has a 1 kHz frequency.

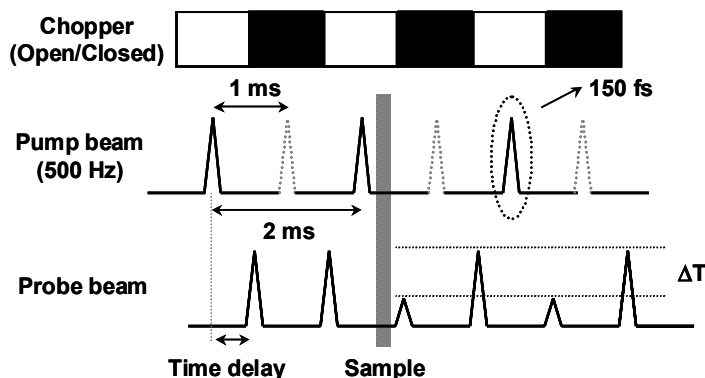


**Figure 9:** Pulse sequence for the used pump-probe photoinduced absorption setup. Time delay is not drawn to scale and may vary from 10 fs to 1500 ps.

The difference in transmission between these two probe pulses ( $\Delta T$ ) is monitored by a lock-in amplifier and referenced to the intensity of the probe-beam ( $T$ ), resulting in the desired photoinduced absorption signal ( $\Delta T/T$ ). By using a translation stage, the time delay between the pump and probe pulse arriving at the sample can be adjusted, giving time resolution in the femtosecond to nanosecond time range. The translation stage used in this setup can extend the pathway of the beam by 0.5 meter, thereby providing the detection of the first 1500 ps after photoexcitation. This makes it suitable for the investigation of the dynamics of singlet states and charges created at close distance between a donor

and acceptor. Diffusion processes and the formation of triplet excited states are negligible at the timescale of 1 nanosecond and will therefore not interfere with measurements of the dynamics at the used short timescales.

## 1.5 Aim and Scope of this Thesis

Existing theories on photophysical processes for isolated  $\pi$ -conjugated molecules are often adequate in describing intramolecular energy and electron transfer reactions, but applying these insights to the same reactions in solid state organic semiconductors remains cumbersome. The actual difficulty of adapting theories for electron transfer to organic molecules in the solid-state properties lies in the poor understanding of the effects of intermolecular interactions. While orientation effects are well studied in covalent donor-acceptor arrays and the determination of geometry of aggregates is currently a tremendously active field, the influence of organizational effects on the photophysics within a superstructure is rarely the topic of interest. Nevertheless, the importance of the interplay between different molecules is indeed acknowledged in the rare cases that it has been studied. Examples of such studies range from energy transfer reactions<sup>95</sup> and exciton migration studies<sup>96-99</sup> in supramolecular aggregates to the observation of intermolecular interactions for charged oligomers<sup>100,101</sup> and the enhancement of the electron transfer reaction upon aggregation.<sup>52,102</sup> Interestingly, there is also an example where it was demonstrated that different effects that emerge upon aggregation cancel out, leaving the photophysical properties in solution unaltered in the solid state.<sup>103</sup>

In this thesis an attempt is made to investigate the effects of aggregation in a more systematical way. A variety of compounds is studied in the aggregated state and compared to the same species in the molecularly dissolved state, providing more information of the actual influence of the aggregation. For future research, these aggregated structures can serve as ideal model compounds to mimic and elucidate phenomena of conjugated materials in the solid state that were previously unattainable. In previous studies the lack of available reference materials like non-aggregated species prevents the opportunity to explicitly scrutinize the influence of the intermolecular effects.

In chapters 2 to 4 the focus is on covalently linked arrays. The applicability of the theories of Marcus and Weller is investigated by varying the strength of the redox couple, the type of linker and the solvent polarity. The studied compounds consist of oligothiophene<sup>104,105</sup>-fullerene<sup>106-113</sup> and oligo(*p*-phenylene vinylene)<sup>20,114-116</sup>-perylene<sup>117-133</sup> donor-acceptor systems. These molecules complement the previous studies on oligothiophene-fullerene<sup>134-143</sup> and oligo(*p*-phenylene vinylene)-perylene,<sup>116,144,145</sup> and provide basis for further experiments on supramolecularly bound and aggregated systems. One example of achieving a long charge-separated state lifetime via a cascaded energy-electron transfer reaction in a pentadic array containing three different chromophores will be presented in chapter 4.

Supramolecularly linked and aggregated systems are studied in chapters 5 to 8. Both the effects of having a reversible linkage between the donor and the acceptor unit as well as the interactions within superstructures are investigated in detail. For this purpose the oligo(*p*-phenylene vinylene)-perylene bisimide couple was chosen because of the excellent possibilities to study these chromophores in their aggregated state<sup>54-59,146-162</sup> and their characteristic features in optical spectroscopy. First, the type of packing and its influence on the charge transfer dynamics is studied for covalent OPV-PERY arrays. In addition, the influence of linkage via hydrogen bonding is studied in both molecularly dissolved

hydrogen bonded OPV-PERY arrays as well as their aggregated analogs. Finally, the aggregation of OPV and PERY compounds is investigated in an aqueous environment.

## 1.6 References

- 1 Huber, R. *Angew. Chem., Int. Ed.* **1989**, 28, 848.
- 2 Moser, C. C.; Keske, J. M.; Warncke, K.; Farid, R. S.; Dutton, P. L. *Nature* **1992**, 355, 796.
- 3 *The Photosynthetic Reaction Center*, Deisenhofer, J.; Norris, J. R. Eds. Academic Press, **1993**.
- 4 *Molecular Mechanisms of Photosynthesis*, Blankenship, R. E. Blackwell Science, Oxford, U.K., **2002**.
- 5 McDermott, G.; Prince, S. M.; Freer, A. A.; Hawthornthwaitelawless, A.M.; Papiz, M. Z.; Cogdell, R. J.; Isaacs, N. W. *Nature* **1995**, 374, 517.
- 6 Yang, M.; Agarwal, R.; Fleming, G. R. *J. Photochem. Photobiol.* **2001**, 142, 107.
- 7 Roszak, A. W.; Howard, T. D.; Southall, J.; Gardiner A. T.; Law, C. J.; Isaacs, N.W.; Cogdell, R. J. *Science* **2003**, 302, 1969.
- 8 Jortner, J. *J. Chem. Phys.* **1976**, 64, 4860.
- 9 Jortner, J. *J. Am. Chem. Soc.* **1980**, 102, 6676.
- 10 Franzen, S.; Goldstein, R. F.; Boxer, S. G. *J. Phys. Chem.* **1993**, 97, 3040.
- 11 Page, C. C.; Moser, C. C.; Chen, X.; Dutton, P. L. *Nature* **1999**, 402, 47.
- 12 Wasielewski, M. R. *Chem. Rev.* **1992**, 92, 435.
- 13 Gust, D.; Moore, T. A.; Moore, A. L. *Acc. Chem. Res.* **1993**, 26, 198.
- 14 Gray, H. B.; Winkler, J. R. *Ann. Rev. Biochem.* **1996**, 65, 537.
- 15 Gust, D.; Moore, T. A.; Moore, A. L. *Acc. Chem. Res.* **2001**, 34, 40.
- 16 Holten, D.; Bocian, D. F.; Lindsey, J. S. *Acc. Chem. Res.* **2002**, 35, 57.
- 17 Williams, R. M.; Zwier, J. M.; Verhoeven, J. W. *J. Am. Chem. Soc.* **1995**, 117, 4093.
- 18 Guldi, D. M. *Chem. Soc. Rev.* **2002**, 31, 22.
- 19 Fukuzumi, S. *Org. Biomol. Chem.* **2003**, 1, 609.
- 20 Peeters, E.; Van Hal, P. A.; Knol, J.; Brabec, C. J.; Sariciftci, N. S.; Hummelen, J. C.; Janssen, R. A. J. *J. Phys. Chem. B* **2000**, 104, 10174.
- 21 Fujitsuka, M.; Ito, O.; Yamashiro, T.; Aso, Y.; Otsubo, T. *J. Phys. Chem. A* **2000**, 104, 4876.
- 22 Matsumoto, K.; Fujitsuka, M.; Sato, T.; Onodera, S.; Ito, O. *J. Phys. Chem. B* **2000**, 104, 11632.
- 23 Van Hal, P. A.; Knol, J.; Langeveld-Voss, B. M. W.; Meskers, S. C. J.; Hummelen, J. C.; Janssen, R. A. J. *J. Phys. Chem. A* **2000**, 104, 5974.
- 24 Van Hal, P. A.; Beckers, E. H. A.; Peeters, E.; Apperloo, J. J.; Janssen, R. A. J. *Chem. Phys. Lett.* **2000**, 328, 403.
- 25 Van Hal, P. A.; Janssen, R. A. J.; Lanzani, G.; Cerullo, G.; Zavelani-Rossi, M.; De Silvestri, S. *Phys. Rev. B* **2001**, 64, 075206/1.
- 26 Wasielewski, M. R.; Niemczyk, M. P. *J. Am. Chem. Soc.* **1984**, 106, 5043.
- 27 Paddon-Row, M. N. *Acc. Chem. Res.* **1994**, 27, 18.
- 28 Guldi, D. M. *Chem. Soc. Rev.* **2002**, 31, 22.
- 29 Imahori, H.; Mori, Y.; Matano, J. *Photochem. Photobiol. C* **2003**, 4, 51.
- 30 Kuciauskas, D.; Liddell, P. A.; Lin, S.; Johnson, T. E.; Weghorn, S. J.; Lindsey, J. S.; Moore, A. L.; Moore, T. A.; Gust, D. *J. Am. Chem. Soc.* **1999**, 121, 8604.
- 31 Andersson, M.; Sinks, L. E.; Hayes, R. T.; Zhao, Y.; Wasielewski, M. R. *Angew. Chem., Int. Ed.* **2003**, 42, 3139.
- 32 Armaroli, N. *Photochem. Photobiol. Sci.* **2003**, 2, 73.

- 33 Balaban, T. S. *Acc. Chem. Res.* **2005**, *38*, 612.
- 34 Sánchez, L.; Martín, N.; Guldi, D. *Angew. Chem., Int Ed.* **2005**, *44*, 5374.
- 35 Breton, J.; Boullais, C.; Burie, J. R.; Nabedryk, E.; Mioskowski, C. *Biochemistry* **1994**, *33*, 14378.
- 36 Diner, B. A.; Force, D. A.; Randall, D. W.; Britt, R. D. *Biochemistry* **1998**, *37*, 17931.
- 37 Lubitz, W.; Lenzian, F.; Bittl, R. *Acc. Chem. Res.* **2002**, *35*, 313.
- 38 Ferreira, K. N.; Iverson, T. M.; Maghlaoui, K.; Barber, J.; Iwata, S. *Science* **2004**, *303*, 1831.
- 39 Okamoto, K.; Fukuzumi, S. *J. Phys. Chem. B* **2005**, *109*, 7713.
- 40 Boyd, P. D. W.; Hodgson, M. C.; Rickard, C. E. F.; Oliver, A. G.; Chaker, L.; Brothers, P. J.; Bolskar, R. D.; Tham, F. S.; Reed, C. A. *J. Am. Chem. Soc.* **1999**, *121*, 10487.
- 41 Wang, Y.-B.; Lin, Z. *J. Am. Chem. Soc.* **2003**, *125*, 6072.
- 42 Shirakawa, M.; Fujita, N.; Shinkai, S. *J. Am. Chem. Soc.* **2003**, *125*, 9902.
- 43 Shoji, Y.; Tashiro, K.; Aida, T. *J. Am. Chem. Soc.* **2004**, *126*, 6570.
- 44 Guldi, D. M.; Gouloumis, A.; Vazquez, P.; Torres, T.; Georgakilas, V.; Prato, M. *J. Am. Chem. Soc.* **2005**, *127*, 5811.
- 45 Yamaguchi, T.; Ishii, N.; Tashiro, K.; Aida, T. *J. Am. Chem. Soc.* **2003**, *125*, 13934.
- 46 D'Souza, F.; Smith, P. M.; Zandler, M. E.; McCarty, A. L.; Itou, M.; Araki, Y.; Ito, O. *J. Am. Chem. Soc.* **2004**, *126*, 7898.
- 47 Hasobe, T.; Kamat, P. V.; Troiani, V.; Solladie, N.; Ahn, T. K.; Kim, S. K.; Kim, D.; Kongkanand, A.; Kuwabata, S.; Fukuzumi, S. *J. Phys. Chem. B* **2005**, *109*, 19.
- 48 Hasobe, T.; Kashiwagi, Y.; Absalom, M. A.; Sly, J.; Hosomizu, K.; Crossley, M. J.; Imahori, H.; Kamat, P. V.; Fukuzumi, S. *Adv. Mater.* **2004**, *16*, 975.
- 49 Hasobe, T.; Kamat, P. V.; Absalom, M. A.; Kashiwagi, Y.; Sly, J.; Crossley, M. J.; Hosomizu, K.; Imahori, H.; Fukuzumi, S. *J. Phys. Chem. B* **2004**, *108*, 12865.
- 50 Hasobe, T.; Imahori, H.; Kamat, P. V.; Ahn, T. K.; Kim, S. K.; Kim, D.; Fujimoto, A.; Hirakawa, T.; Fukuzumi, S. *J. Am. Chem. Soc.* **2005**, *127*, 1216.
- 51 Segura, M.; Sánchez, L.; De Mendoza, J.; Martín, N.; Guldi, D. M. *J. Am. Chem. Soc.* **2003**, *125*, 15093.
- 52 Ramos, A. M.; Meskers, S. C. J.; Beckers, E. H. A.; Prince, R. B.; Brunsveld, L.; Janssen, R. A. J. *J. Am. Chem. Soc.* **2004**, *126*, 9630.
- 53 Hoeben, F. J. M.; Jonkheijm, P.; Meijer, E. W.; Schenning, A. P. H. J. *Chem. Rev.* **2005**, *105*, 1491.
- 54 Prodi, A.; Chiorboli, C.; Scandola, F.; Iengo, E.; Alessio, E.; Dobrawa, R.; Würthner, F. *J. Am. Chem. Soc.* **2005**, *127*, 1454.
- 55 Rybtchinski, B.; Sinks, L. E.; Wasielewski, M. R. *J. Phys. Chem. A* **2004**, *108*, 7497.
- 56 Sugiyasu, K.; Fujita, N.; Shinkai, S. *Angew. Chem., Int. Ed.* **2004**, *43*, 1229.
- 57 Rybtchinski, B.; Sinks, L. E.; Wasielewski, M. R. *J. Am. Chem. Soc.* **2004**, *126*, 12268.
- 58 Fuller, M. J.; Sinks, L. E.; Rybtchinski, B.; Giaimo, J. M.; Li, X. Y.; Wasielewski, M. R. *J. Phys. Chem. A* **2005**, *109*, 970.
- 59 Van der Boom, T.; Hayes, R. T.; Zhao, Y.; Bushard, P. J.; Weiss, E. A.; Wasielewski, M. R. *J. Am. Chem. Soc.* **2002**, *124*, 9582.
- 60 Van Hal, P. A.; Meskers, S. C. J.; Janssen, R. A. J. *Appl. Phys. A* **2004**, *79A*, 41.
- 61 Wolffs, M.; Hoeben, F. J. M.; Beckers, E. H. A.; Schenning, A. P. H. J.; Meijer, E. W. *J. Am. Chem. Soc.* **2005**, *127*, 13484.
- 62 Dexter, D. L. *J. Chem. Phys.* **1953**, *21*, 836.
- 63 Förster, T. *Discuss. Faraday Soc.* **1959**, *27*, 7.

- 64 Weller, A. Z. *Phys. Chem. Neue Folge* **1982**, 133, 93.
- 65 Marcus, R. A. *J. Chem. Phys.* **1965**, 43, 679.
- 66 Miller, J. R.; Calcaterra, L. T.; Closs, G. L. *J. Am. Chem. Soc.* **1984**, 106, 3047.
- 67 Closs, G. L.; Miller, J. R. *Science* **1988**, 240, 440.
- 68 Kroon, J.; Oevering, H.; Verhoeven, J. W.; Warman, J. M.; Oliver, A. M.; Paddon-Row, M. N. *J. Phys. Chem.* **1993**, 97, 5065.
- 69 Guldi, D. M.; Luo, C. P.; Da Ros, T.; Bozi, S.; Prato, M. *Chem. Commun.* **2002**, 2320.
- 70 Yoshida, N.; Ishizuka, T.; Yofu, K.; Murakami, M.; Miyasaka, H.; Okada, T.; Nagata, Y.; Itaya, A.; Cho, H. S.; Kim, D.; Osuka, A. *Chem. Eur. J.* **2003**, 9, 2854.
- 71 Guldi, D. M.; Luo, C. P.; Kotov, N. A.; Da Ros, T.; Bosi, S.; Prato, M. *J. Phys. Chem. B* **2003**, 107, 7293.
- 72 Guldi, D. M.; Hirsch, A.; Scheloske, M.; Dietel, E.; Troisi, A.; Zerbetto, F.; Prato, M. *Chem. Eur. J.* **2003**, 9, 4968.
- 73 Mataga, N.; Chosrowjan, H.; Taniguchi, S.; Shibata, Y.; Yoshida, N.; Osuka, A.; Kikuzawa, T.; Okada, T. *J. Phys. Chem. A* **2002**, 106, 12191.
- 74 Mataga, N.; Taniguchi, S.; Chosrowjan, H.; Osuka, A.; Kurotobi, K. *Chem. Phys. Lett.* **2005**, 403, 163.
- 75 Marcus, R. A. *Angew. Chem.* **1993**, 105, 1161.
- 76 Marcus, R. A. *Rev. Mod. Phys.* **1993**, 65, 599.
- 77 Tachiya, M. *J. Phys. Chem.* **1993**, 97, 5911.
- 78 Barbara, P. F.; Meyer, T. J.; Ratner, M. A. *J. Phys. Chem.* **1996**, 100, 13148.
- 79 Tributsch, H.; Pohlmann, L. *Science* **1998**, 279, 1891.
- 80 Zimmt, M. B.; Waldeck, D. H. *J. Phys. Chem. A* **2003**, 107, 3580.
- 81 Benten, H.; Ohkita, H.; Ito, S.; Yamamoto, M.; Tohda, Y.; Tani, K. *J. Chem. Phys.* **2005**, 123, 084901.
- 82 Read, I.; Napper, A.; Zimmt, M. B.; Waldeck, D. H. *J. Phys. Chem. A* **2000**, 104, 9385.
- 83 Vath, P.; Zimmt, M. B.; Matyushov, D. V.; Voth, G. A. *J. Phys. Chem. B* **1999**, 103, 9130.
- 84 Small, D. W.; Matyushov, D. V.; Voth, G. A. *J. Am. Chem. Soc.* **2003**, 125, 7470.
- 85 Weaver, M. J. *Chem. Rev.* **1992**, 92, 463.
- 86 Mikkelsen, K. V.; Ratner, M. A. *Chem. Rev.* **1987**, 87, 113.
- 87 Sumi, H.; Kakitani, T. *J. Phys. Chem. B* **2001**, 105, 9603.
- 88 Ohkubo, K.; Kotani, H.; Shao, J. G.; Ou, Z. P.; Kadish, K. M.; Li, G. L.; Pandey, R. K.; Fujitsuka, M.; Ito, O.; Imahori, H.; Fukuzumi, S. *Angew. Chem., Int. Ed.* **2004**, 43, 853.
- 89 Harriman, A. *Angew. Chem., Int. Ed.* **2004**, 43, 4985.
- 90 Fukuzumi, S.; Kotani, H.; Ohkubo, K.; Ogo, S.; Tkachenko, N. V.; Lemmetyinen, H. *J. Am. Chem. Soc.* **2004**, 126, 1600.
- 91 Benniston, A. C.; Harriman, A.; Li, P. Y.; Rostron, J. P.; Verhoeven, J. W. *Chem. Commun.* **2005**, 2701.
- 92 Kestner, N. R.; Logan, J.; Jortner, J. *J. Phys. Chem.* **1974**, 78, 2148.
- 93 Ulstrup, J.; Jortner, J. *J. Chem. Phys.* **1975**, 63, 4358.
- 94 Jortner, J.; Bixon, M. *Adv. Chem. Phys. volume 106*, **1999**.
- 95 Hoeben, F. J. M.; Herz, L. M.; Daniel, C.; Jonkheijm, P.; Schenning, A.; Silva, C.; Meskers, S. C. J.; Beljonne, D.; Phillips, R. T.; Friend, R. H.; Meijer, E. W. *Angew. Chem., Int. Ed.* **2004**, 43, 1976.
- 96 Daniel, C.; Herz, L. M.; Silva, C.; Hoeben, F. J. M.; Jonkheijm, P.; Schenning, A.; Meijer, E. W. *Phys. Rev. B* **2003**, 68, 235212.
- 97 Herz, L. M.; Daniel, C.; Silva, C.; Hoeben, F. J. M.; Schenning, A.; Meijer, E. W.; Friend, R. H.; Phillips, R. T. *Phys. Rev. B* **2003**, 68, 045203.



- 98 Hennebicq, E.; Pourtois, G.; Scholes, G. D.; Herz, L. M.; Russell, D. M.; Silva, C.; Setayesh, S.; Grimsdale, A. C.; Müllen, K.; Bredas, J. L.; Beljonne, D. *J. Am. Chem. Soc.* **2005**, *127*, 4744.
- 99 Beljonne, D.; Hennebicq, E.; Daniel, C.; Herz, L. M.; Silva, C.; Scholes, G. D.; Hoeben, F. J. M.; Jonkheijm, P.; Schenning, A.; Meskers, S. C. J.; Phillips, R. T.; Friend, R. H.; Meijer, E. W. *J. Phys. Chem. B* **2005**, *109*, 10594.
- 100 Apperloo, J. J.; Janssen, R. A. J.; Malenfant, P. R. L.; Fréchet, J. M. J. *J. Am. Chem. Soc.* **2001**, *123*, 6916.
- 101 Sakai, T.; Satou, T.; Kaikawa, T.; Takimiya, K.; Otsubo, T.; Aso, Y. *J. Am. Chem. Soc.* **2005**, *127*, 8082.
- 102 Schenning, A. P. H. J.; Van Herrikhuyzen, J.; Jonkheijm, P.; Chen, Z.; Würthner, F.; Meijer, E. W. *J. Am. Chem. Soc.* **2002**, *124*, 10252.
- 103 Rybtchinski, B.; Sinks, L. E.; Wasielewski, M. R. *J. Phys. Chem. A* **2004**, *108*, 7497.
- 104 Roncali, J. *Chem. Rev.* **1992**, *92*, 711.
- 105 Tour, J. M. *Chem. Rev.* **1996**, *96*, 537.
- 106 Williams, R. M.; Zwiernicki, J. M.; Verhoeven, J. W. *J. Am. Chem. Soc.* **1995**, *117*, 4093.
- 107 Imahori, H.; Sakata, Y. *Adv. Mater.* **1997**, *9*, 537.
- 108 Martín, N.; Sanchez, L.; Illescas, B.; Perez, I. *Chem. Rev.* **1998**, *98*, 2527.
- 109 Imahori, H.; Sakata, Y. *Eur. J. Org. Chem.* **1999**, 2445.
- 110 Guldi, D. M.; Prato, M. *Acc. Chem. Res.* **2000**, *33*, 695.
- 111 Imahori, H.; Tamaki, K.; Guldi, D. M.; Luo, C.; Fujitsuka, M.; Ito, O.; Sakata, Y.; Fukuzumi, S. *J. Am. Chem. Soc.* **2001**, *123*, 2607.
- 112 Guldi, D. M.; Martín, N. *J. Mater. Chem.* **2002**, *12*, 1978.
- 113 Segura, J. L.; Martín, N.; Guldi, D. M. *Chem. Soc. Rev.* **2005**, *34*, 31.
- 114 Armaroli, N.; Eckert, J.-F.; Nierengarten, J.-F. *Chem. Commun.* **2000**, 2105.
- 115 Meier, H.; Gerold, J.; Kolshorn, H.; Baumann, W.; Bletz, M. *Angew. Chem., Int. Ed.* **2002**, *41*, 292.
- 116 Neuteboom, E. E.; Meskers, S. C. J.; Van Hal, P. A.; Van Duren, J. K. J.; Meijer, E. W.; Janssen, R. A. J.; Dupin, H.; Pourtois, G.; Cornil, J.; Lazzaroni, R.; Bredas, J.-L.; Beljonne, D. *J. Am. Chem. Soc.* **2003**, *125*, 8625.
- 117 Kircher, T.; Lohmannsroben, H. G. *Phys. Chem. Chem. Phys.* **1999**, *1*, 3987.
- 118 Schlichting, P.; Duchschere, B.; Seisenberger, G.; Basché, T.; Bräuchle, C.; Müllen, K. *Chem. Eur. J.* **1999**, *5*, 2388.
- 119 Yang, S. I.; Prathapan, S.; Miller, M. A.; Seth, J.; Bocian, D. F.; Lindsey, J. S.; Holten, D. *J. Phys. Chem. B* **2001**, *105*, 8249.
- 120 Prathapan, S.; Yang, S. I.; Seth, J.; Miller, M. A.; Bocian, D. F.; Holten, D.; Lindsey, J. S. *J. Phys. Chem. B* **2001**, *105*, 8237.
- 121 Yang, S. I.; Lammi, R. K.; Prathapan, S.; Miller, M. A.; Seth, J.; Diers, J. R.; Bocian, D. F.; Lindsey, J. S.; Holten, D. *J. Mater. Chem.* **2001**, *11*, 2420.
- 122 Miller, S. E.; Zhao, Y.; Schaller, R.; Mulloni, V.; Just, E. M.; Johnson, R. C.; Wasielewski, M. R. *Chem. Phys.* **2002**, *275*, 167.
- 123 Lukas, A. S.; Zhao, Y.; Miller, S. E.; Wasielewski, M. R. *J. Phys. Chem. B* **2002**, *106*, 1299.
- 124 Muthukumar, K.; Loewe, R. S.; Kirmaier, C.; Hindin, E.; Schwartz, J. K.; Sazanovich, I. V.; Diers, J. R.; Bocian, D. F.; Holten, D.; Lindsey, J. S. *J. Phys. Chem. B* **2003**, *107*, 3431.
- 125 Schweitzer, G.; Gronheid, R.; Jordens, S.; Lor, M.; De Belder, G.; Weil, T.; Reuther, E.; Müllen, K.; De Schryver, F. C. *J. Phys. Chem. A* **2003**, *107*, 3199.

- 126 Jordens, S.; De Belder, G.; Lor, M.; Schweitzer, G.; Van der Auweraer, M.; Weil, T.; Reuther, E.; Müllen, K.; De Schryver, F. C. *Photochem. Photobiol. Sci.* **2003**, *2*, 177.
- 127 Guo, X.; Zhang, D.; Zhang, H.; Fan, Q.; Xu, W.; Ai, X.; Fan, L.; Zhu, D. *Tetrahedron* **2003**, *59*, 4843-4850
- 128 Ino, D.; Watanabe, K.; Takagi, N.; Matsumoto, Y. *Chem. Phys. Lett.* **2004**, *383*, 261.
- 129 Neuteboom, E. E.; Van Hal, P. A.; Janssen, R. A. J. *Chem. Eur. J.* **2004**, *10*, 3907.
- 130 Ahrens, M. J.; Sinks, L. E.; Rybtchinski, B.; Liu, W.; Jones, B. A.; Giaimo, J. M.; Gusev, A. V.; Goshe, A. J.; Tiede, D. M.; Wasielewski, M. R. *J. Am. Chem. Soc.* **2004**, *126*, 8284.
- 131 Kaletas, B. K.; Dobrawa, R.; Sautter, A.; Würthner, F.; Zimine, M.; De Cola, L.; Williams, R. M. *J. Phys. Chem. A* **2004**, *108*, 1900.
- 132 Cremer, J.; Mena-Osteritz, E. M.; Pschierer, N. G.; Müllen, K.; Bäuerle, P. *Org. Biomol. Chem.* **2005**, *3*, 985.
- 133 Fukuzumi, S.; Ohkubo, K.; Ortiz, J.; Gutierrez, A. M.; Fernandez-Lazaro, F.; Sastre-Santos, A. *Chem. Commun.* **2005**, 3814.
- 134 Yamashiro, T.; Aso, Y.; Otsubo, T.; Tang, H.; Harima, Y.; Yamashita, K. *Chem. Lett.* **1999**, 443.
- 135 Van Hal, P. A.; Knol, J.; Langeveld-Voss, B. M. W.; Meskers, S. C. J.; Hummelen, J. C.; Janssen, R. A. J. *J. Phys. Chem. A* **2000**, *104*, 5974.
- 136 Fujitsuka, M.; Ito, O.; Yamashiro, T.; Aso, Y.; Otsubo, T. *J. Phys. Chem. A* **2000**, *104*, 4876.
- 137 Zhang, F.; Svensson, M.; Andersson, M. R.; Maggini, M.; Bucella, S.; Menna, E.; Inganas, O. *Adv. Mater.* **2001**, *13*, 1871.
- 138 Fujitsuka, M.; Matsumoto, K.; Ito, O.; Yamashiro, T.; Aso, Y.; Otsubo, T. *Res. Chem. Intermed.* **2001**, *27*, 73.
- 139 Van Hal, P. A.; Janssen, R. A. J.; Lanzani, G.; Cerullo, G.; Zavelani-Rossi, M.; De Silvestri, S., *Chem. Phys. Lett.* **2001**, *345*, 33.
- 140 Van Hal, P. A.; Knol, J.; Langeveld-Voss, B. M. W.; Meskers, S. C. J.; Hummelen, J. C.; Janssen, R. A. J. *Synth. Met.* **2001**, *116*, 123.
- 141 Van Hal, P. A.; Beckers, E. H. A.; Meskers, S. C. J.; Janssen, R. A. J.; Joussetme, B.; Blanchard, P.; Roncali, J. *Chem. Eur. J.* **2002**, *8*, 5415.
- 142 Ikemoto, J.; Takimiya, K.; Aso, Y.; Otsubo, T.; Fujitsuka, M.; Ito, O. *Org. Lett.* **2002**, *4*, 309.
- 143 Hirayama, D.; Takimiya, K.; Aso, Y.; Otsubo, T.; Hasobe, T.; Yamada, H.; Imahori, H.; Fukuzumi, S.; Sakata, Y. *J. Am. Chem. Soc.* **2002**, *124*, 532.
- 144 Peeters, E.; Van Hal, P. A.; Meskers, S. C. J.; Janssen, R. A. J.; Meijer, E. W. *Chem. Eur. J.* **2002**, *8*, 4470.
- 145 Syamakumari, A.; Schenning, A. P. H. J.; Meijer, E. W. *Chem. Eur. J.* **2002**, *8*, 3353.
- 146 Würthner, F.; Thalacker, C.; Sautter, A. *Adv. Mater.* **1999**, *11*, 754.
- 147 Würthner, F.; Thalacker, C.; Sautter, A.; Schärfl, W.; Ibach, W.; Hollricher, O. *Chem. Eur. J.* **2000**, *6*, 3871.
- 148 Jonkheijm, P.; Fransen, M.; Schenning, A. P. H. J.; Meijer, E. W. *J. Chem. Soc., Perkin Trans. 2* **2001**, 1280.
- 149 Schenning, A. P. H. J.; Jonkheijm, P.; Peeters, E.; Meijer, E. W. *J. Am. Chem. Soc.* **2001**, *123*, 409.
- 150 Würthner, F.; Thalacker, C.; Diele, S.; Tschierske, C. *Chem. Eur. J.* **2001**, *7*, 224.
- 151 Herz, L. M.; Silva, C.; Friend, R. H.; Phillips, R. T.; Setayesh, S.; Becker, S.; Marsitsky, D.; Müllen, K. *Phys. Rev. B* **2001**, *64*, 195203/1.

- 152 Schmidt-Mende, L.; Fechtenkötter, A.; Müllen, K.; Moons, E.; Friend, R. H.; MacKenzie, J. D. *Science* **2001**, *293*, 1119.
- 153 Van der Boom, T.; Hayes, R. T.; Zhao, Y.; Bushard, P. J.; Weiss, E. A.; Wasielewski, M. R. *J. Am. Chem. Soc.* **2002**, *124*, 9582.
- 154 Würthner, F.; Sautter, A. *Org. Biomol. Chem.* **2003**, *1*, 240.
- 155 Wang, W.; Han, J. J.; Wang, L.-Q.; Li, L.-S.; Shaw, W. J.; Li, A. D. Q. *Nano Lett.* **2003**, *3*, 455.
- 156 Li, A. D. Q.; Wang, W.; Wang, L.-Q. *Chem. Eur. J.* **2003**, *9*, 4594.
- 157 Ajayaghosh, A.; George, S. J.; Praveen, V. K. *Angew. Chem., Int. Ed.* **2003**, *42*, 332.
- 158 Arnaud, A.; Belleney, J.; Boue, F.; Bouteiller, L.; Carrot, G.; Wintgens, V. *Angew. Chem., Int. Ed.* **2004**, *43*, 1718.
- 159 Würthner, F. *Chem. Commun.* **2004**, 1564.
- 160 Neuteboom, E. E.; Meskers, S. C. J.; Meijer, E. W.; Janssen, R. A. J. *Macromol. Chem. Phys.* **2004**, *205*, 217.
- 161 Ahrens, M. J.; Sinks, L. E.; Rybtchinski, B.; Liu, W.; Jones, B. A.; Giaimo, J. M.; Gusev, A. V.; Goshe, A. J.; Tiede, D. M.; Wasielewski, M. R. *J. Am. Chem. Soc.* **2004**, *126*, 8284.
- 162 Li, X.; Sinks, L. E.; Rybtchinski, B.; Wasielewski, M. R. *J. Am. Chem. Soc.* **2004**, *126*, 10810.

# Charge Transfer Kinetics in Fullerene-Oligomer-Fullerene Triads Containing Alkylpyrrole Units\*

### *Abstract*

*A photoinduced electron transfer reaction has been observed in three fullerene-donor-fullerene triads containing an electron rich pyrrole ring in the donor moiety. The kinetics of charge separation in solution has been investigated by photoluminescence and transient absorption spectroscopy. The polarity of solvent and the distance between donor and acceptor affect the forward electron transfer reaction, in qualitative agreement with a semi-empirical model for the Gibbs-free energy for charge separation. Depending on the conditions, charge separation occurs at a rate of  $10^9$ - $10^{10}$   $s^{-1}$ . The charge recombination rate is estimated to be faster than  $2 \times 10^{10}$   $s^{-1}$ . The relatively large contribution of the singlet-excited state  $S_n \leftarrow S_1$  absorption of the fullerene moiety to the photoinduced absorption hampered a more accurate determination of the recombination rate.*

---

\* This work has been published: Beckers, E. H. A.; Van Hal, P. A.; Dhanabalan, A.; Meskers, S. C. J.; Knol, J.; Hummelen, J. C.; Janssen, R. A. J. *Journal of Physical Chemistry A* **2003**, *107*, 6218-6224.

## 2.1 Introduction

To disclose the complex processes involved in the photoinduced electron transfer reaction between a  $\pi$ -conjugated donor and a fullerene acceptor, extensive studies have addressed the photophysical properties of covalently linked oligomer- $C_{60}$  dyads and triads containing, among others, oligothiophenes<sup>1-11</sup>, oligo(*p*-phenylene vinylene)s,<sup>12-17</sup> and porphyrins<sup>18,19</sup> as the electron donor. In this study the charge transfer kinetics of fullerene-donor-fullerene triads containing a pyrrole unit in the donor are investigated. The electron-rich pyrrole unit is used to lower the oxidation potential ( $E_{ox}$ ) and thereby increase the change in free energy for electron transfer, enabling this reaction to occur in apolar media.

The three novel (ADA) triads<sup>20</sup> used in this study are shown in (Figure 1). ADA-1 consists of a thiophene-pyrrole-thiophene (T-Py-T) donor moiety coupled to two N-methylfulleropyrrolidine (MP- $C_{60}$ ) electron acceptors.<sup>21</sup> ADA-2 has a similar structure as ADA-1, but the two thiophene rings have been replaced by phenyl groups. As a result, the Ph-Py-Ph donor moiety of ADA-2 has approximately the same geometry as ADA-1, but a significantly higher oxidation potential. This allows investigation of the effect of the oxidation potential on photophysical processes without adjusting the distance between the donor and acceptor chromophores. In ADA-3, the T-Py-T donor of ADA-1 is augmented with two phenyl groups on each side, to increase the distance between the donor and acceptor, but without significantly affecting the oxidation potential.

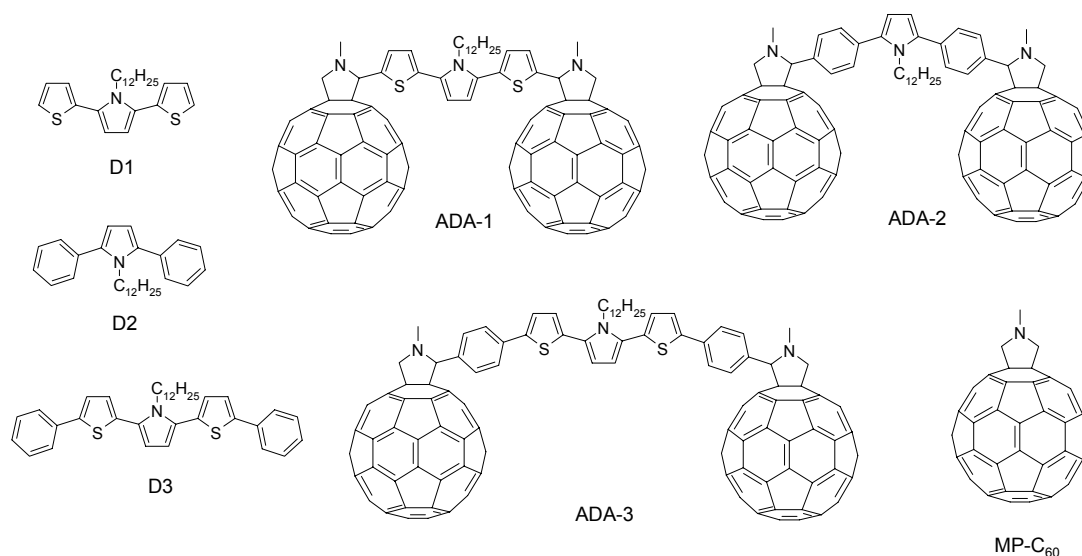


**Figure 1:** Donor molecules D1, D2, and D3; triads ADA-1, ADA-2, and ADA-3; MP- $C_{60}$ .

The kinetics for photoinduced charge separation and recombination in the triads have been studied with fluorescence quenching and lifetime spectroscopy in combination with near steady-state and transient photoinduced absorption (PIA) experiments, and have been compared to the electron transfer reactions observed in mixtures of the donor model compound D1,<sup>22</sup> D2,<sup>20</sup> or D3<sup>23</sup> with MP- $C_{60}$ <sup>24</sup> (Figure 1).

## 2.2 Results and Discussion

**Energy Levels.** The UV/Vis spectra (Figure 2) of the three triads exhibit characteristic absorption peaks at 433 and 705 nm of the fulleropyrrolidine moiety. Compared to MP-C<sub>60</sub>, ADA-1 and ADA-3 exhibit additional absorptions in the UV region, as a result of the contribution of the conjugated donor segments. The spectra were found to be independent on the polarity of the solvent. The UV/Vis spectra only show absorptions of the isolated chromophores. However, some electronic coupling between the donor and acceptor chromophores in the ground state cannot be excluded because the spectra of donor (D1, D2, and D3) and MP-C<sub>60</sub> are partially overlapping. The spectra demonstrate that the lowest singlet-excited state in the ADA triads is localized on the fulleropyrrolidine unit at 1.76 eV (~705 nm).

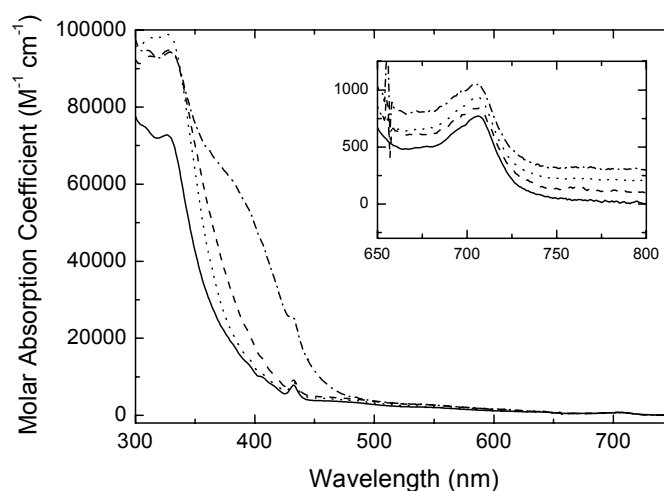


**Figure 2:** UV/Vis absorption spectra of MP-C<sub>60</sub> (solid line) and the triads ADA-1 (dashed line), ADA-2 (dotted line), and ADA-3 (dash-dotted line) in ODCB. The inset shows the spectra in the 650-800 nm region. In the inset the spectra are offset vertically for clarity.

The donor molecules undergo a reversible electrochemical oxidation at potentials 0.83, 1.02, and 0.73 V (versus SCE in CH<sub>2</sub>Cl<sub>2</sub>) for D1, D2, and D3 respectively. Compared to similarly substituted thiophene molecules (1.07 V for 3T (terthiophene), 1.42 V for Ph-T-Ph, and 0.96 for Ph-3T-Ph),<sup>6,25</sup> the introduction of the pyrrole unit reduces the oxidation potential considerably.

**Photoluminescence Quenching.** The intensity of the fullerene photoluminescence (PL) of the triads at 712 nm can be used to assess whether an intramolecular charge transfer reaction occurs from the donor to the fullerene acceptor. Figure 3 compares the PL of the fulleropyrrolidine group in the triads to that of MP-C<sub>60</sub> in three solvents of increasing polarity. The observed PL quenching for ADA-1 indicates that charge transfer already occurs in a relatively apolar solvent such as toluene ( $\epsilon = 2.38$ ). The ADA-2 molecule exhibits no PL quenching in toluene, because the high oxidation potential inhibits a photoinduced electron transfer. The PL quenching of ADA-3 in toluene is less than for ADA-1, despite its slightly lower oxidation potential. We attribute this difference to the increased distance between the pyrrole and the fullerene groups in ADA-3 as compared to ADA-1, which increases the energy of the

charge-separated state. With increasing polarity of the solvent (ODCB:  $\epsilon = 9.93$ ; benzonitrile  $\epsilon = 25.2$ ), the fullerene emission of the triads is increasingly quenched (Figure 3, Table 1).

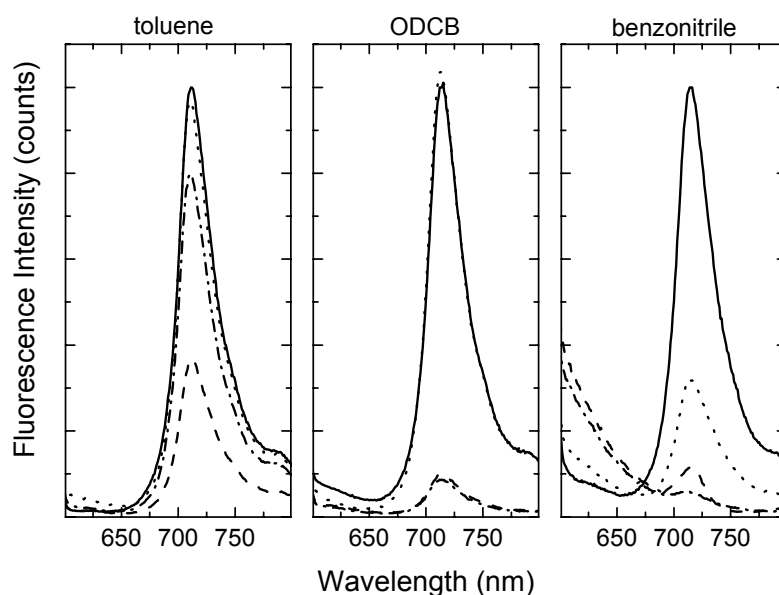


**Figure 3:** Fluorescence spectra of MP-C<sub>60</sub> (solid line) and the triads ADA-1 (dashed line), ADA-2 (dotted line), and ADA-3 (dash-dotted line) in toluene (left), ODCB (middle), and benzonitrile (right). Excitation was at 500 nm, all spectra are corrected for optical density.

**Table 1:** Fullerene fluorescence quenching factors ( $\phi(C_{60})/\phi$ ) fullerene PL lifetime ( $\tau_{\text{obs}}$ ) and rate constants for charge separation ( $k_{\text{CS}}$ ) calculated with equations 1 and 3.

Compound	Solvent	$\phi(C_{60})/\phi$	$k_{\text{CS}} (\text{s}^{-1})^{\text{a}}$	$\tau_{\text{obs}} (\text{ns})$	$k_{\text{CS}} (\text{s}^{-1})^{\text{b}}$
ADA-1	TOL	2.7	$1.2 \times 10^9$	0.77	$0.6 \times 10^9$
	ODCB	10.1	$7.0 \times 10^9$	0.12	$7.6 \times 10^9$
	BZN	8.8	$5.3 \times 10^9$	n.d.	
ADA-2	TOL	1.0	$\ll 10^8$	1.43	$< 10^7$
	ODCB	1.0	$\ll 10^8$	1.19	$0.08 \times 10^9$
	BZN	3.2	$1.5 \times 10^9$	n.d.	
ADA-3	TOL	1.3	$1.7 \times 10^8$	1.53	<i>c</i>
	ODCB	11.5	$8.0 \times 10^9$	0.12	$7.6 \times 10^9$
	BZN	17.8	$1.2 \times 10^{10}$	n.d.	
MP-C <sub>60</sub>	TOL			1.45	
	ODCB			1.31	
	BZN			1.46	

a) Calculated from  $\phi(C_{60})/\phi$  and equation 1.

b) Calculated from  $\tau_{\text{obs}}$  and equation 3.

c) Electron transfer is slow, using equation 3 would yield a negative value.

The rate constant for charge separation ( $k_{\text{CS}}$ ) can be determined from the PL lifetime of MP-C<sub>60</sub> and the fulleropyrrolidine PL quantum yield of the triad molecules ( $\phi$ ) compared to that of MP-C<sub>60</sub> ( $\phi(C_{60})$ ), via:

$$k_{\text{CS}} = \left[ \frac{\phi(\text{C}_{60})}{\phi} - 1 \right] / \tau(\text{MP} - \text{C}_{60}) \quad (1)$$

The resulting values indicate that  $k_{\text{CS}}$  is in the range of  $10^9$ -  $10^{10}$   $\text{s}^{-1}$ , depending on the nature of the triad and the solvent (Table 1).

**Gibbs-free Energy for Charge Separation.** The experimental results can be rationalized using a semi-quantitative model<sup>26</sup> (equation 2) that provides an estimate for the change in Gibbs-free energy for charge separation. In this equation,  $E_{\text{ox}}$  and  $E_{\text{red}}$  represent the oxidation and reduction potential of respectively the donor and the acceptor, measured in a solvent with relative permittivity  $\epsilon_{\text{ref}}$ .  $E_{00}$  is the energy of the excited state from which the electron transfer occurs, whereas  $e$  and  $\epsilon_0$  are the electron charge and the vacuum permittivity.  $R_{\text{cc}}$  is the center-to-center distance between the positive and the negative charges in the charge-separated state and  $r^+$  and  $r^-$  indicate the radii of the cation and anion.

$$-\Delta G_{\text{CS}} = -e[E_{\text{ox}}(\text{D}) - E_{\text{red}}(\text{A})] + E_{00} + \frac{e^2}{4\pi\epsilon_0\epsilon_s R_{\text{cc}}} + \frac{e^2}{8\pi\epsilon_0} \left( \frac{1}{r^+} + \frac{1}{r^-} \right) \left( \frac{1}{\epsilon_{\text{ref}}} - \frac{1}{\epsilon_s} \right) \quad (2)$$

The radius of the negative ion of  $\text{C}_{60}$  was set to  $r^- = 5.6 \text{ \AA}$ .<sup>6</sup> The radii of the radical cations of D1 and D3 are assumed to be equal to the  $r^+$  value for unsubstituted terthiophene ( $4.03 \text{ \AA}$ ),<sup>6</sup> because the contribution of the phenyl group to the charge distribution is assumed to be negligible.<sup>22</sup>

**Table 2:** Change in Gibbs-free energy for charge separation ( $\Delta G_{\text{CS}}$ ) in toluene (TOL), *o*-dichlorobenzene (ODCB), and benzonitrile (BZN), calculated using equation 2 for intramolecular electron transfer in ADA triads relative to the  $\text{MP-C}_{60}(\text{S}_1)$  state ( $E_{00} = 1.76 \text{ eV}$ ) and for intermolecular ( $R_{\text{cc}} = \infty$ ) electron transfer in D/MP- $\text{C}_{60}$  mixtures relative to the  $\text{MP-C}_{60}(\text{T}_1)$  state ( $E_{00} = 1.50 \text{ eV}$ ). The center-to-center distance ( $R_{\text{cc}}$ ) has been listed, other parameters are described in the text.

Sample	Solvent	$R_{\text{cc}}$ (Å)	$\Delta G_{\text{CS}}$ (eV)
ADA-1	TOL	10.5	0.11
	ODCB	10.5	-0.43
	BZN	10.5	-0.54
ADA-2	TOL	11.0	0.57
	ODCB	11.0	-0.25
	BZN	11.0	-0.40
ADA-3	TOL	14.0	0.15
	ODCB	14.0	-0.50
	BZN	14.0	-0.62
D1 + MP- $\text{C}_{60}$	TOL	$\infty$	0.95
	ODCB	$\infty$	-0.03
	BZN	$\infty$	-0.22
D3 + MP- $\text{C}_{60}$	TOL	$\infty$	0.85
	ODCB	$\infty$	-0.13
	BZN	$\infty$	-0.32



The radius for D2 is calculated to be 2.8 Å, assuming that the charge is mainly localized on the pyrrole ring. Using  $R_{cc} = 10.5$  Å, the charge-separated state for ADA-1 in toluene appears to be slightly higher in energy than the MP-C<sub>60</sub>(S<sub>1</sub>) state (Table 2). This result disagrees with the experimental observations, but charge transfer becomes exergonic when  $R_{cc}$  is (slightly) reduced to 9 Å. In agreement with the experimental results, the energy of the charge-separated states for ADA-2 and ADA-3 in toluene are higher than that of ADA-1 and the MP-C<sub>60</sub>(S<sub>1</sub>) state.

In more polar solvents, photoinduced electron transfer becomes increasingly exergonic for all triads, in agreement with the observed PL quenching (Figure 3). One other disagreement between the predictions from equation 2 and the experiment must be noted. The PL intensity of ADA-2 in ODCB is equal to that of MP-C<sub>60</sub> indicating an absence of charge separation, while the charge-separated state is predicted to be -0.25 eV below the MP-C<sub>60</sub>(S<sub>1</sub>) state.<sup>27</sup>

**Time-Resolved Photoluminescence.** Time-resolved PL measurements have been used to obtain the rate of a charge separation, independent from the PL intensity quenching, by detecting a change in the decay rate of the fulleropyrrolidine singlet state in the triads compared to MP-C<sub>60</sub> (Figure 4). In toluene solutions, a decrease of the fullerene PL lifetime is indeed observed for ADA-1, while the PL time profile of ADA-2 and ADA-3 are identical to that of MP-C<sub>60</sub>.

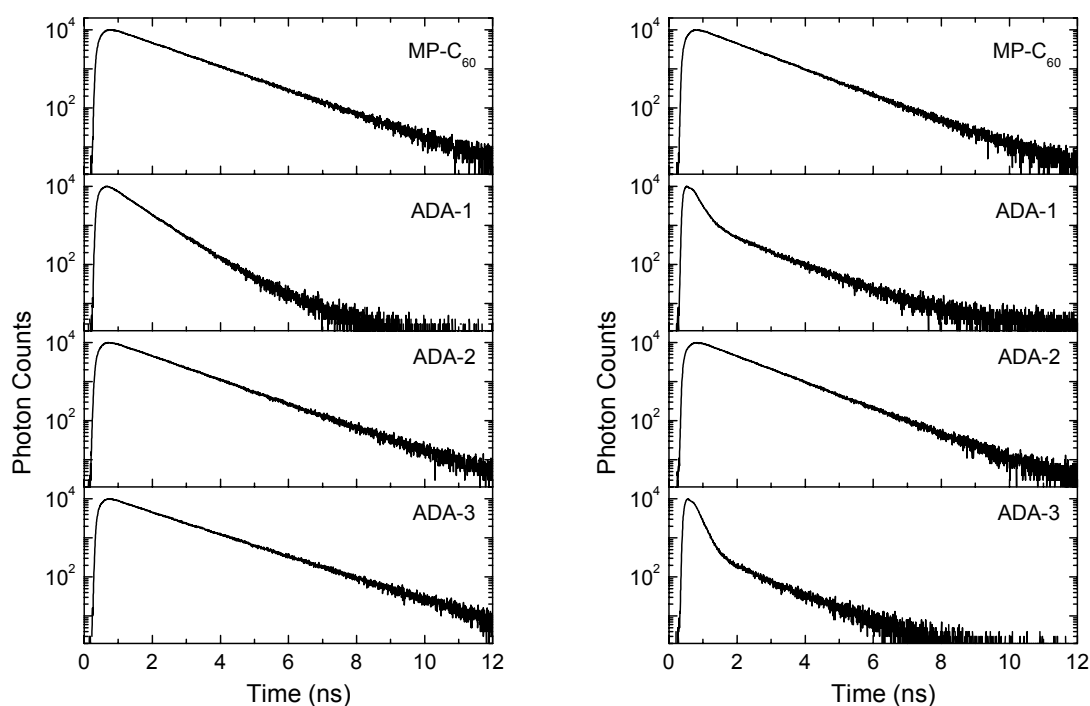


**Figure 4:** Fluorescence lifetime of MP-C<sub>60</sub> and ADA triads measured at 711 nm in toluene (left) and at 714 nm in ODCB (right). Excitation was at 400 nm.

In ODCB, the decay of both ADA-1 and ADA-3 is faster than that of MP-C<sub>60</sub>. PL lifetimes have been determined with a bi-exponential curve fitting procedure in which one time constant was kept constant

at the singlet lifetime of MP-C<sub>60</sub> in the same solvent.<sup>28</sup> The rate constants for charge separation, calculated from the fluorescence lifetimes using equation 3 are similar to those obtained from the steady-state luminescence experiments (Table 1).

$$k_{CS} = \frac{1}{\tau_{obs}} - \frac{1}{\tau(MP - C_{60})} \quad (3)$$

In addition to the rate constants, also the energy barrier ( $\Delta G_{CS}^{\ddagger}$ ) for photoinduced electron transfer has been determined for ADA-1 and ADA-3 in ODCB by temperature dependent fluorescence lifetime experiments. By using the semi-classical Marcus equation,<sup>29,30</sup> the temperature dependence of the electron transfer rate can be described with equation 4.

$$\ln(k_{CS}T^{1/2}) = \ln\left(\frac{2\pi^{3/2}|V|^2}{h(\lambda k_B)^{1/2}}\right) - \frac{\Delta G_{CS}^{\ddagger}}{k_B T} \quad (4)$$

The energy barriers in ODCB, calculated from the slope ( $-\Delta G_{CS}^{\ddagger}/k_B$ ) of a modified Arrhenius plot<sup>31-33</sup> (Figure 5), amount to 0.088 and 0.084 eV for ADA-1 and ADA-3, respectively.<sup>34</sup> The experimental energy barriers can be compared to the barriers that can be obtained using equation 5.

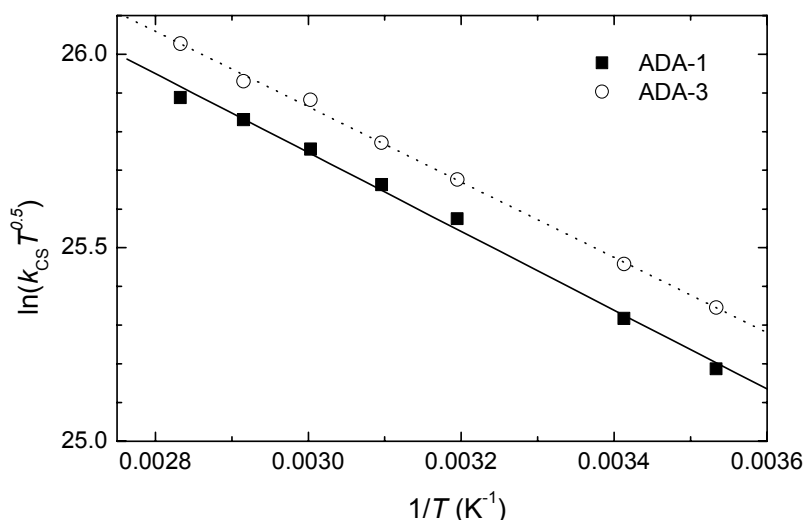


**Figure 5:** Modified Arrhenius plot of  $\ln(k_{CS}T^{0.5})$  versus  $1/T$  ( $K^{-1}$ ) for ADA-1 and ADA-3 in ODCB. The lines represent the linear fit of the experimental data to obtain the energy barrier  $\Delta G^{\ddagger}$  for the charge transfer reaction.

In equation 5,  $\lambda$  represents the reorganization energy, which is the sum of the internal ( $\lambda_i$ ) and solvent ( $\lambda_s$ ) reorganization.<sup>29</sup> The internal reorganization is set to 0.3 eV,<sup>21</sup> whereas the solvent contribution can be calculated using the Born-Hush<sup>35,36</sup> approach (equation 6).

$$\Delta G_{CS}^{\#} = \frac{(\Delta G_{CS} + \lambda)^2}{4\lambda} \quad (5)$$

$$\lambda_s = \frac{e^2}{4\pi\epsilon_0} \left( \frac{1}{2} \left( \frac{1}{r^+} + \frac{1}{r^-} \right) - \frac{1}{R_{cc}} \right) \left( \frac{1}{n^2} - \frac{1}{\epsilon_s} \right) \quad (6)$$

For ODCB as solvent, this approximation results in  $\lambda_s = 0.53$  eV and  $\Delta G_{CS}^{\#} = 0.048$  eV for ADA-1, and  $\lambda_s = 0.64$  eV and  $\Delta G_{CS}^{\#} = 0.052$  eV for ADA-3. These energy barriers are similar to the experimentally determined values. The reorganization energies of 0.83 and 0.94 eV imply that  $-\Delta G_{CS}$  is less than  $\lambda$ , such that the forward electron transfer reaction occurs in the Marcus normal region.<sup>29</sup> Using  $\lambda$  and the intercept of the modified Arrhenius plot, the electronic coupling matrix elements are determined to be  $26 \text{ cm}^{-1}$  for both ADA-1 and ADA-3 in ODCB. This result is identical to the value previously reported for oligomer-fullerene compounds.<sup>21, 37</sup>

**Near Steady-State Photoinduced Absorption.** To determine the absorption spectra of the radical cations of D1 and D3, near steady-state PIA experiments were performed on  $2 \times 10^{-4}$  M solution of these donor molecules together with an equimolar amount of MP-C<sub>60</sub> (Figure 6).<sup>38</sup> In these experiments selective excitation of the fullerene chromophore at 528 nm results in the formation of the MP-C<sub>60</sub> triplet state, which may react intermolecularly with D1 or D3 to give a radical ion pair. The PIA spectra of D1/MP-C<sub>60</sub> and D3/MP-C<sub>60</sub> in toluene both show the typical MP-C<sub>60</sub> triplet-triplet absorption with a maximum at 1.78 eV.<sup>39</sup>

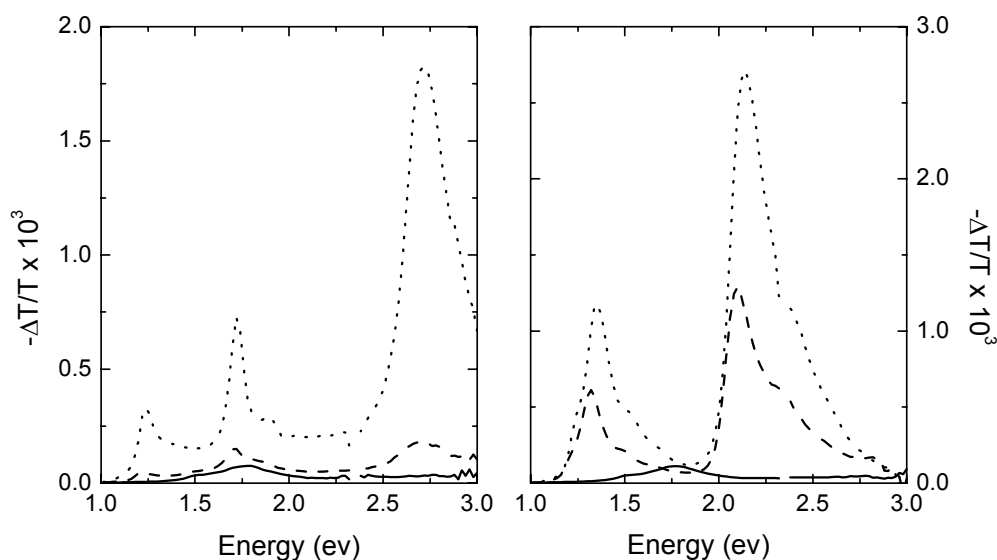


**Figure 6:** Photoinduced absorption spectra of  $2 \times 10^{-4}$  M mixtures of D1 and MP-C<sub>60</sub> (left) and D3 and MP-C<sub>60</sub> (right) in toluene (solid line), ODCB (dashed line), and benzonitrile (dotted line). Excitation was at 528 nm (2.35 eV).

Apparently, *intermolecular* charge separation does not occur in toluene, consistent with the Gibbs-free energies for charge transfer calculated with equation 2 (Table 2). In ODCB and benzonitrile, the increased polarity lowers the Gibbs-free energy of the charge-separated state below the energy of the MP-C<sub>60</sub>(T<sub>1</sub>) state from which the *intermolecular* electron transfer occurs. The PIA spectrum of D1/MP-C<sub>60</sub> shows three absorptions bands with at 1.24, 1.72, and 2.72 eV, respectively. The band at 1.24 eV is highly characteristic of the MP-C<sub>60</sub><sup>-</sup> radical anion;<sup>40</sup> the other two are assigned to absorptions of the D1<sup>+</sup> radical cation. The PIA spectrum of the D3/MP-C<sub>60</sub> mixture shows peaks at 1.33 and 2.13 eV, which are assigned to D3<sup>+</sup> absorptions. The low energy absorption shows a shoulder at 1.24 eV, again indicating the presence of MP-C<sub>60</sub><sup>-</sup>.

**Transient Photoinduced Absorption.** In addition to the (time-resolved) PL experiments, which provide rate constants for the forward charge separation reaction, transient PIA can be used to study the dynamics of charge formation and recombination when the absorption of the radical cations or anions are monitored in time. The transient differential absorption at 1030 nm (1.2 eV) of ADA-3 in ODCB was recorded to investigate the dynamics of the formation and decay of C<sub>60</sub><sup>-</sup> radical anions. The signal reaches its maximum within 1 ps (Figure 7), *i.e.* comparable to the width of the used laser pulse, and then decays exponentially with a time constant of 127 ps (Figure 7). The sub-picosecond rise indicates that at 1030 nm the differential transmission is probably not only due to C<sub>60</sub><sup>-</sup> radical anions, because these are formed at a much lower rate (Table 1).

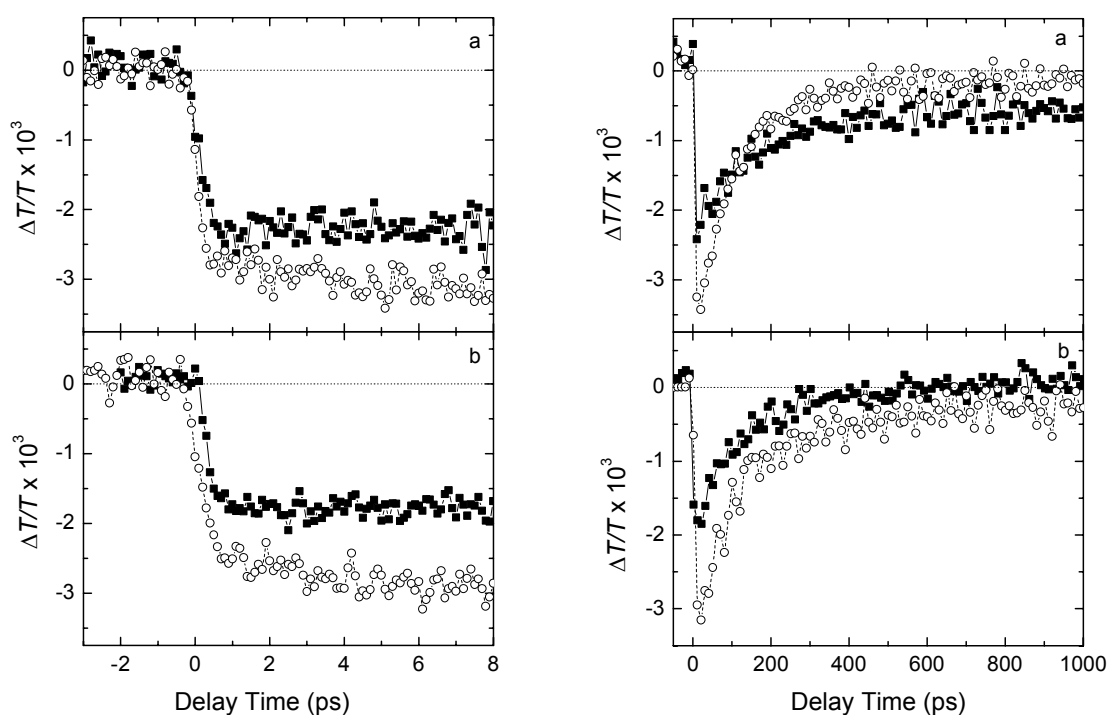


**Figure 7:** Differential transmission dynamics at (a) 1030 nm and (b) 900 nm of ADA-1 (solid squares) and ADA-3 (open circles) in ODCB from  $-3$  to  $8$  ps (left) and from  $-50$  to  $1000$  ps (right). Recorded with excitation at  $455$  nm.

Remarkably, the time constant of the decay of the differential transmission at 1030 nm is identical to the lifetime of the  $C_{60}(S_1)$  state in ADA-3 as determined by PL lifetime measurements (Table 1). Because both fluorescence and electron transfer occur from the  $C_{60}(S_1)$  state, the PL lifetime of ADA-3 corresponds to the generation of  $C_{60}^{\cdot-}$  radical anions and not to their decay. We therefore propose that the 1030 nm differential transmission signal does not primarily relate to the  $C_{60}^{\cdot-}$  radical anion, but rather originates predominantly from the  $C_{60} S_n \leftarrow S_1$  absorption.

To investigate this in more detail, the differential transmission at 900 nm has also been recorded. The molar absorption coefficient of the MP- $C_{60} S_n \leftarrow S_1$  transition ( $9000 \text{ L}\cdot\text{mol}^{-1}\cdot\text{cm}^{-1}$ ) is almost twice as high as the absorption coefficient of the MP- $C_{60}$  radical anion ( $5000 \text{ L}\cdot\text{mol}^{-1}\cdot\text{cm}^{-1}$ ) at this wavelength.<sup>39</sup> The results at 900 nm are similar to those at 1030 nm, exhibiting a rise in less than 1 ps and a decay with a time constant of 107 ps (Figure 7).

The near steady-state absorption spectra of D1 or D3 with MP- $C_{60}$  in ODCB (Figure 6) show that the absorption at 1030 nm is 4 times larger for the D3/MP- $C_{60}$  mixture as compared to the D1/MP- $C_{60}$  mixture. However, the transient differential transmission profiles at 900 and 1030 nm of ADA-1 in ODCB show only minor differences compared to the profiles of ADA-3 in ODCB. After a rise of the signal within 1 ps, the signals show an exponential decay with time constants of 156 and 135 ps at 900 and 1030 nm, respectively (Figure 7). Although these values are slightly higher than the observed fluorescence lifetime of 118 ps, they support the view that the transient PIA signal is predominantly a result of the excited state  $S_n \leftarrow S_1$  absorption of MP- $C_{60}$ .

**Modeling of the Transient PIA Trace.** Using the absorption coefficients of the charge-separated state and the excited state  $S_n \leftarrow S_1$  absorption of MP- $C_{60}$  at 900 nm in ODCB, the time profile of the transient differential absorption after excitation can be calculated as a function of the rate constants for intrinsic decay ( $k_0$ ), charge separation ( $k_{CS}$ ), and charge recombination ( $k_{CR}$ ) (Figure 8).<sup>41</sup>

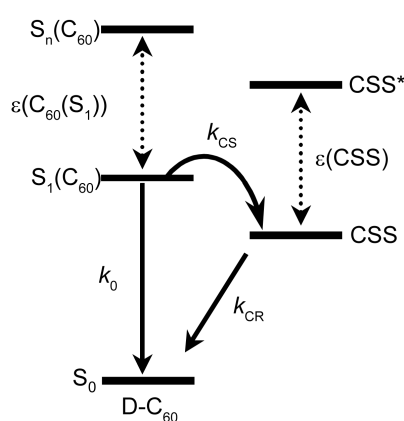


**Figure 8:** Energy diagram for the charge transfer reaction ( $k_{CS}$ ) from the MP- $C_{60}(S_1)$  state to the charge-separated state (CSS) together with intrinsic ( $k_0$ ) and charge recombination ( $k_{CR}$ ) decay pathways.

In this model, charge separation is assumed to occur exclusively from the MP- $C_{60}(S_1)$  state and the rate for charge recombination is varied, while  $k_0$  and  $k_{CS}$  are kept constant at the experimental values.<sup>41</sup>

From the steady-state PIA experiments it can be concluded that there is no significant absorption of the radical cation for the ADA-1 triad at 900 nm, therefore the absorption coefficient of the charged species is equal to that of  $\text{MP-C}_{60}^-$  ( $5000 \text{ L}\cdot\text{mol}^{-1}\cdot\text{cm}^{-1}$ ).<sup>39</sup>

The molar absorption coefficient of the radical cation of ADA-3 has been determined from the absorption spectrum of  $\text{D3}^+$ , which was obtained by oxidizing D3 with thianthrenium perchlorate.<sup>42</sup> At 900 nm, the molar absorption coefficient for  $\text{D3}^+$  is  $14000 \text{ L}\cdot\text{mol}^{-1}\cdot\text{cm}^{-1}$ . The ratio of the absorption coefficients at 900 nm (1.38 eV) of the  $\text{MP-C}_{60}(\text{S}_1)$  state and the charge-separated state (CSS) were therefore set at 9000 : 5000 for ADA-1 and at 9000 : 19000 for ADA-3.<sup>43</sup>

The calculated time profiles for values of  $k_{\text{CR}}$  ranging from  $10^{12}$  to  $2 \times 10^{10} \text{ s}^{-1}$  (Figure 9) clearly reveal that as long as charge recombination is faster than  $2 \times 10^{10} \text{ s}^{-1}$  (50 ps), the transient signal is dominated by the  $\text{S}_n \leftarrow \text{S}_1$  absorption of the  $\text{MP-C}_{60}(\text{S}_1)$  state, even if the absorption coefficient of the charge-separated state is higher than the singlet-excited state absorption.

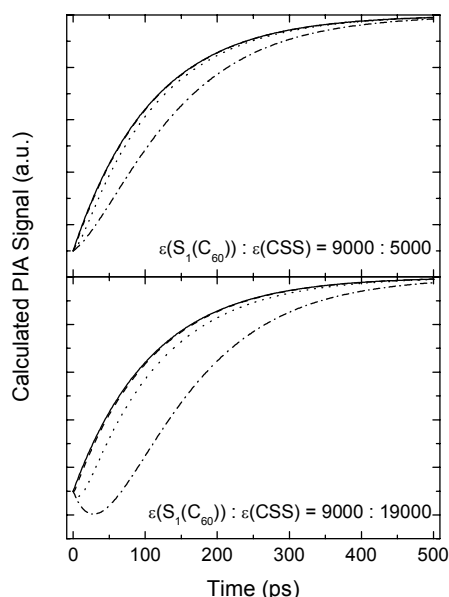


**Figure 9:** Calculated differential transmission at 900 nm for charge recombination rate constants of  $1 \text{ ps}^{-1}$  (dashed line),  $0.1 \text{ ps}^{-1}$  (dotted line), and  $0.02 \text{ ps}^{-1}$  (dash-dotted line), compared to the decay of the  $\text{MP-C}_{60}(\text{S}_1)$  state (solid line). The spectra are calculated with the model illustrated in Figure 8 with  $\epsilon(\text{C}_{60}(\text{S}_1)) : \epsilon(\text{CSS}) = 9000 : 5000$  (top) and  $\epsilon(\text{C}_{60}(\text{S}_1)) : \epsilon(\text{CSS}) = 9000 : 19000$  (bottom). The used values for  $k_{\text{CS}}$  and  $k_0$  correspond to time constants of 120 and 1310 ps, respectively.

Under these conditions the transient signal is indistinguishable from the  $\text{S}_n \leftarrow \text{S}_1$  absorption of  $\text{MP-C}_{60}$ , which hampers an accurate analysis of the recombination dynamics.<sup>44</sup> This is a general problem in donor-fullerene systems: the overlap of the  $\text{S}_n \leftarrow \text{S}_1$  and radical anion absorptions of the fullerene in the 800-1100 nm region complicates the investigation of formation and recombination kinetics.

Because the experimentally obtained time profiles are similar to the modeled curves with fast recombination, we estimate that charge recombination in ADA-1 and ADA-3 occurs within 50 ps ( $k_{\text{CR}} > 2 \times 10^{10} \text{ s}^{-1}$ ). This is in agreement with rate constants obtained for comparable thiophene- $\text{MP-C}_{60}$  dyads and triads.<sup>7,16</sup>

## 2.3 Conclusions

Intramolecular photoinduced electron transfer has been observed in three fullerene-donor-fullerene (ADA) triads that contain an electron rich pyrrole ring in the donor moiety. The charge transfer kinetics have been studied in solution with PL and transient PIA spectroscopy. In agreement with a semi-quantitative model for the Gibbs-free energy for charge separation, the photoinduced charge transfer depends on the polarity of the solvent and the distance between donor and fullerene acceptor. While charge separation occurs for ADA-1 in toluene, a higher polarity solvent is required to generate a photoinduced charge-separated state in ADA-2 and ADA-3. PL quenching and time-resolved PL studies reveal that the rate for charge separation in the ADA triads is in the range of  $k_{CS} = 10^9 - 10^{10} \text{ s}^{-1}$ . Near steady-state PIA in mixtures of the donor model compounds D1 or D3 with MP-C<sub>60</sub> reveal that an *intermolecular* charge transfer occurs from the MP-C<sub>60</sub>(T<sub>1</sub>) state, evidenced by the observation of the absorption spectra of the corresponding radical ions in the near infrared. Transient PIA in the picosecond time domain for the triads, recorded at the near-infrared absorption wavelengths of the radical ions, produced a signal that was dominated by the excited state  $S_n \leftarrow S_1$  absorption of the MP-C<sub>60</sub> moiety. A kinetic model, involving the relative absorption coefficients of the excited states, explains this behavior when the charge recombination is faster than the charge separation. A semi-quantitative analysis suggests that the recombination rate,  $k_{CR}$ , is larger than  $2 \times 10^{10} \text{ s}^{-1}$  (lifetime < 50 ps).

## 2.4 Experimental Section

**Materials.** The syntheses of ADA-1, ADA-2, and ADA-3 have been described previously.<sup>20</sup> Each of the three triads consists of a mixture of stereoisomers as a consequence of the stereocenter at each pyrrolidine ring. Compounds D1,<sup>22</sup> D2,<sup>20</sup> D3<sup>23</sup> and MP-C<sub>60</sub><sup>24</sup> have been prepared according to literature procedures.

**Electrochemistry.** Cyclic voltammograms were measured in dichloromethane ( $\epsilon = 8.93$ ), with 0.1 M tetrabutylammonium hexafluorophosphate (TBAPF<sub>6</sub>) as a supporting electrolyte, using a Potentiostat Wenking POS73 potentiostat. The working electrode was a Pt disk (0.2 cm<sup>2</sup>), the counter electrode was a Pt plate (0.5 cm<sup>2</sup>), and a saturated calomel electrode (SCE) was used as the reference electrode, calibrated against Fc/Fc<sup>+</sup> (0.46 V).

**Absorption and Fluorescence Spectroscopy.** UV/Vis absorption and fluorescence spectra were recorded with a Perkin Elmer Lambda 40P spectrometer and an Edinburgh Instruments FS920 double-monochromator luminescence spectrometer using a Peltier-cooled red-sensitive photomultiplier, respectively. All UV/Vis and fluorescence measurements were carried out in 10 mm quartz cells. Solvents for absorption and fluorescence measurements were used as received. Oxidation experiments were carried out under inert conditions by adding a solution of thianthrenium perchlorate<sup>42</sup> in dichloromethane via a syringe through a Teflon-lined septum sealing the substrate solution.

**Time-Correlated Single Photon Counting.** Time-correlated single photon counting fluorescence studies were performed using an Edinburgh Instruments LifeSpec-PS spectrometer. The LifeSpec-PS comprises a 400 nm picosecond laser (PicoQuant PDL 800B) operated at 2.5 MHz and a Peltier-cooled Hamamatsu micro-channel plate photomultiplier (R3809U-50). Lifetimes were determined from the data using the Edinburgh Instruments software package.

**Near Steady-State PIA.** Solutions containing  $2 \times 10^{-4}$  M of each compound were prepared in a nitrogen-filled glove box in order to exclude interference of oxygen during measurements. The PIA spectra were recorded between 0.5 and 3.0 eV by exciting with a mechanically modulated cw Ar ion laser ( $\lambda = 528$  nm, 275 Hz) pump beam and monitoring the resulting change in transmission of a tungsten-halogen probe light through the sample ( $\Delta T$ ) with a phase-sensitive lock-in amplifier after dispersion by a grating monochromator and detection, using Si, InGaAs, and cooled InSb detectors. The pump power incident on the sample was typically 25 mW with a beam diameter of 2 mm. The PIA ( $-\Delta T/T \approx \Delta\alpha d$ ) was directly calculated from the change in transmission after correction for the photoluminescence, which was recorded in a separate experiment. Photoinduced absorption spectra and photoluminescence spectra were recorded with the pump beam in a direction almost parallel to the direction of the probe beam. The solutions were studied in a 1 mm near-IR grade quartz cell at room temperature. Solvents for PIA measurements were distilled under nitrogen before use.

**Transient Sub-Picosecond Photoinduced Absorption.** The femtosecond laser system used for pump-probe experiments consisted of an amplified Ti/sapphire laser (Spectra Physics Hurricane). The single pulses from a cw mode-locked Ti/sapphire laser were amplified by a Nd-YLF laser using chirped pulse amplification, providing 150 fs pulses at 800 nm with an energy of 750  $\mu$ J and a repetition rate of 1 kHz. The pump pulses at 455 nm were created via optical parametric amplification (OPA) of the 800 nm pulse by a BBO crystal into infrared pulses which were then two times frequency doubled via BBO crystals. The probe beam was generated in a separate optical parametric amplification set-up in which the 900 and 1030 nm pulses were created and a RG 850 nm cut-off filter was used to avoid contributions of residual probe light (800 nm) from the OPA. The pump beam was focused to a spot size of about 1 mm<sup>2</sup> with an excitation flux of 1 mJ·cm<sup>-2</sup> per pulse. The probe beam was reduced in intensity compared to the pump beam by using neutral density filters. The pump beam was linearly polarized at the magic angle of 54.7° with respect to the probe, to cancel out orientation effects in the measured dynamics. The cross-correlation of pump and probe pulses was determined by measuring the optical Kerr effect in pure heptane using the same sample cell as in the pump-probe experiments. The pump laser pulse induces a birefringence, because the refractive index contains an intensity dependent term and becomes anisotropic under polarized illumination.<sup>45</sup> The cross-correlation, has approx. a Gaussian shape with 0.5 ps FWHM. In principle, rates for charge separation should be obtained by deconvoluting the measured signal with the cross correlation. However, numerical analysis indicates that for rates  $< 2$  ps<sup>-1</sup>, deconvolution results in only a negligible correction to the rate obtained by directly fitting an exponential function. The temporal evolution of the differential transmission was recorded using an Si detector by a standard lock-in technique at 500 Hz.

## 2.5 References and Notes

- 1 Benincori, T.; Brenna, E.; Sannicolo, F.; Trimarco, L.; Zotti, G.; Sozzani, P. *Angew. Chem., Int. Ed.* **1996**, *35*, 648.
- 2 Effenberger, F.; Grube, G. *Synthesis* **1998**, 1372.
- 3 Knorr, S.; Grupp, A.; Mehring, M.; Grube, G.; Effenberger, F. *J. Chem. Phys.* **1999**, *110*, 3502.
- 4 Yamashiro, T.; Aso, Y.; Otsubo, T.; Tang, H.; Harima, Y.; Yamashita, K. *Chem. Lett.* **1999**, 443.
- 5 Fujitsuka, M.; Ito, O.; Yamashiro, T.; Aso, Y.; Otsubo, Y. *J. Phys. Chem. A* **2000**, *104*, 4876.
- 6 Van Hal, P. A.; Knol, J.; Langeveld-Voss, B. M. W.; Meskers, S. C. J.; Hummelen, J. C.; Janssen, R. A. *J. J. Phys. Chem. A* **2000**, *104*, 5974.
- 7 Van Hal, P. A.; Janssen, R. A. J.; Lanzani, G.; Cerullo, G.; Zavelani-Rossi, M.; De Silvestri, S. *Chem. Phys. Lett.* **2001**, *345*, 33.



- 8 Fujitsuka, M.; Masahura, A.; Kasai, H.; Oikawa, H.; Nakanishi, H.; Ito, O.; Yamashiro, T.; Aso, Y.; Otsubo, T. *J. Phys. Chem. B* **2001**, *105*, 9930.
- 9 Fujitsuka, M.; Matsumoto, K.; Ito, O.; Yamashiro, T.; Aso, Y.; Otsubo, T. *Res. Chem. Intermed.* **2001**, *27*, 73.
- 10 Hirayama, D.; Takimiya, K.; Aso, Y.; Otsubo, T. Hasobe, T.; Yamada, H. Imahori, H.; Fukuzumi, S.; Sakata, Y. *J. Am. Chem. Soc.* **2002**, *124*, 532.
- 11 Van Hal, P. A.; Beckers, E. H. A.; Meskers, S. C. J.; Janssen, R. A. J.; Joussetme, B.; Blanchard, P.; Roncali, J. *Chem. Eur. J.* **2002**, *8*, 5415.
- 12 Nierengarten, J. F.; Eckert, J. F.; Nicoud, J. F.; Ouali, L.; Krasnikov, V.; Hadziioannou, G. *Chem. Commun.* **1999**, 617.
- 13 Eckert, J. F.; Nicoud, J. F.; Nierengarten, J. F.; Liu, S. G.; Echegoyen, L.; Barigelletti, F.; Armaroli, N.; Ouali, L.; Krasnikov, V. V.; Hadziioannou, G. *J. Am. Chem. Soc.* **2000**, *122*, 7467.
- 14 Armaroli, N.; Barigelletti, F.; Ceroni, P.; Eckert, J.-F.; Nicoud, J.-F.; Nierengarten, J.-F. *Chem. Commun.* **2000**, 599.
- 15 Peeters, E.; Van Hal, P. A.; Knol, J.; Brabec, C. J.; Sariciftci, N. S.; Hummelen, J. C.; Janssen, R. A. J. *J. Phys. Chem. B* **2000**, *104*, 10174.
- 16 Van Hal, P. A.; Janssen, R. A. J.; Lanzani, G.; Cerullo, G.; Zavelani-Rossi, M.; De Silvestri, S. *Phys. Rev. B* **2001**, *64*, 075206.
- 17 Nierengarten, J.-F.; Armaroli, N.; Accorsi, G.; Rio, Y; Eckert, J.-F. *Chem. Eur. J.* **2003**, *9*, 37.
- 18 Gust, D.; Moore, T. A.; Moore, A. L. *Acc. Chem. Res.* **2001**, *34*, 40.
- 19 Guldi, D. M. *Chem. Soc. Rev.* **2002**, *31*, 22.
- 20 Dhanabalan, A.; Knol, J.; Hummelen, J. C.; Janssen, R. A. J. *Synth. Met.* **2001**, *119*, 519.
- 21 Williams, R. M.; Zwier, J. M.; Verhoeven, J. W. *J. Am. Chem. Soc.* **1995**, *117*, 4093.
- 22 Van Haare, J. A. E. H.; Groenendaal, L.; Peerlings, H. W. I.; Havinga, E. E.; Vekemans, J. A. J. M.; Janssen, R. A. J.; Meijer, E. W. *Chem. Mater.* **1995**, *7*, 1984.
- 23 In addition to the photophysics described in this chapter, the synthesis of compound 3 has also been reported in: Beckers, E. H. A.; Van Hal, P. A.; Dhanabalan, A.; Meskers, S. C. J.; Knol, J.; Hummelen, J. C.; Janssen, R. A. J. *J. Phys. Chem. A* **2003**, *107*, 6218.
- 24 Maggini, M.; Scorrano, G.; Prato, M. *J. Am. Chem. Soc.* **1993**, *115*, 9798.
- 25 Apperloo, J. J.; Groenendaal, L.; Verheyen, H.; Jayakannan, M.; Janssen, R. A. J.; Dkhissi, A.; Beljonne, D.; Lazzaroni, R.; Brédas, J. L. *Chem. Eur. J.* **2002**, *8*, 2384.
- 26 Weller, A. *Z. Phys. Chem.* **1982**, *133*, 93.
- 27 The apparent failure of equation 2 in correctly predicting the energy of the charge-separated state for ADA-2, is tentatively attributed to two inaccuracies: (i) The relatively short distance between donor and acceptor moieties results in an unrealistic estimate of Coulomb term when using equation 2, because the electrostatic attraction of positive and negative charges depends on the actual charge distribution, which is not accurately represented by point charges at the centers of donor and acceptor as assumed in equation 2. (ii) The last term of equation 2 assumes that donor and acceptor are fully solvated. For a small-sized donor positioned between two large fullerene moieties, complete solvation is unlikely.
- 28 This contribution is a result of a small fluorescent impurity and typically accounts for less than 5% of the total signal.
- 29 Marcus, R. A. *J. Chem. Phys.* **1965**, *43*, 679.
- 30 Marcus, R. A. *Angew. Chem.* **1993**, *105*, 1161.
- 31 Zeng, Y.; Zimmt, M. B. *J. Phys. Chem.* **1992**, *96*, 8395.

- 32 Komamine, S.; Fujitsuka, M.; Ito, O.; Moriwaki, K.; Miyata, T.; Ohno, T. *J. Phys. Chem. A* **2000**, *104*, 11497.
- 33 Yamazaki, M.; Araki, Y.; Fujitsuka, M.; Ito, O. *J. Phys. Chem. A* **2001**, *105*, 8615.
- 34 Calculated under the assumption that both the reorganization energy and the barrier are temperature independent. In addition, the temperature dependence of the solvent polarity is assumed to have an insignificant effect on the Gibbs-free energy for the electron transfer reaction.
- 35 Oevering, H.; Paddon-Row, M. N.; Heppener, M.; Oliver, A. M.; Cotsaris, E.; Verhoeven, J. W.; Hush, N. S. *J. Am. Chem. Soc.* **1987**, *109*, 3258.
- 36 Kroon, J.; Verhoeven, J. W.; Paddon-Row, M. N.; Oliver, A. M. *Angew. Chem., Int. Ed.* **1991**, *30*, 1358.
- 37 Williams, R. M.; Koeberg, M.; Lawson, J. M.; An, Y. Z.; Rubin, Y.; Paddon-Row, M. N.; Verhoeven, J. W. *J. Org. Chem.* **1996**, *61*, 5055.
- 38 With this technique it is not possible to detect charges formed in the triads because near steady-state PIA operates in the microsecond to millisecond time domain, and this is orders of magnitude slower than the intramolecular charge recombination.
- 39 Guldi, D. M.; Prato, M. *Acc. Chem. Res.* **2000**, *33*, 695.
- 40 Guldi, D. M.; Hungerbühler, H.; Janata, E.; Asmus, K. D. *J. Phys. Chem.* **1993**, *97*, 11258.
- 41 The intensity of the differential transmission at 900 nm equals the sum of the signals of the C<sub>60</sub> singlet-excited state and the charge-separated state (CSS) via:  $\Delta T \propto -\{\varepsilon(C_{60}(S_1))[C_{60}(S_1)] + \varepsilon(CSS)[CSS]\}$ . The concentrations of C<sub>60</sub>(S<sub>1</sub>) and CSS depend on the kinetic constants shown in Figure 8, the initial concentration of C<sub>60</sub>(S<sub>1</sub>) ( $[C_{60}(S_1)]_0$ ) and amount to:  $[C_{60}(S_1)] = [C_{60}(S_1)]_0 \exp[-(k_{CS} + k_0)t]$  and  $[CSS] = [C_{60}(S_1)]_0 \left\{ \frac{k_{CS}}{k_{CR} - k_{CS} - k_0} (\exp[-(k_{CS} + k_0)t] - \exp[-k_{CR}t]) \right\}$ , respectively.
- 42 Murata, Y.; Shine, H. J. *J. Org. Chem.* **1969**, *34*, 3368.
- 43 For ADA-3, both the radical cation and radical anion absorb at 900 nm. Both contributions to the signal are accounted for in the absorption coefficient and the concentration of charged species ([CSS]) is not doubled.
- 44 Fujitsuka *et al.*<sup>5</sup> previously reported that in picosecond PIA measurements of a quaterthiophene-fulleropyrrolidine dyad (4T-C<sub>60</sub>) in an apolar solvent the fulleropyrrolidine S<sub>n</sub> ← S<sub>1</sub> excited-state absorption can be observed at wavelengths around 800-1000 nm. However, it was not mentioned that this absorption also contributes to the PIA signal during the formation of the 4T<sup>+</sup>-C<sub>60</sub><sup>-</sup> charge-separated state in more polar solvents.
- 45 *Physical Optics*, Akhmanov, S.A.; Nikitin, S. Y. Clarendon, Oxford, **1997**.



# Charge Separation and Recombination in Photoexcited Oligo(*p*-Phenylene Vinylene) – Perylene Bisimide Arrays close to the Marcus Inverted Region\*

### *Abstract*

*The kinetics of photoinduced intramolecular charge separation and subsequent charge recombination of three oligo(*p*-phenylene vinylene)-perylene bisimide-oligo(*p*-phenylene vinylene) arrays have been studied using femtosecond pump-probe spectroscopy in solvents of different polarity. The reduction potentials of three donor-acceptor-donor molecules differ strongly as a consequence of the four substituents ( $R = \textit{tert}$ -butyl-phenoxy,  $H$ , or  $Cl$ ) on the bay-position of the central perylene bisimide unit. The experiments indicate that charge separation in these molecules occurs from the first excited singlet state of the perylene bisimide moiety to the charge-separated state (CSS) and to the lowest electronically excited-state level of the charge-separated state (CSS\*). For  $R = H$  and  $R = Cl$ , the rates for charge separation and charge recombination decrease with increasing change in Gibbs-free energy, and hence the molecules represent an exceptional example of molecules in which both charge separation and recombination occur close to, or in the Marcus inverted region.*

---

\* This work has been published: Beckers, E. H. A.; Meskers, S. C. J.; Schenning, A. P. H. J.; Chen, Z.; Würthner, F.; Janssen, R. A. J. *Journal of Physical Chemistry A* **2004**, *108*, 6933-6937.

### 3.1 Introduction

The kinetics of photoinduced charge separation reactions in  $\pi$ -conjugated donor-acceptor systems is important to natural and artificial light energy conversion.<sup>1,2</sup> Marcus theory for electron transfer predicts that this reaction can occur in different regions, depending on the relative magnitude of the change in Gibbs-free energy ( $-\Delta G_0$ ) and the reorganization energy ( $\lambda$ ).<sup>3-5</sup> In the ‘normal region’ ( $-\Delta G_0 < \lambda$ ), the rate constant increases with increasing driving force ( $-\Delta G_0$ ), while in the ‘inverted region’ ( $-\Delta G_0 > \lambda$ ) the rate constant should decrease with increasing  $-\Delta G_0$ . This prediction of Marcus theory has attracted considerable interest and was experimentally first verified by Closs and Miller 20 years ago.<sup>6,7</sup> Presently, numerous examples of inverted region behavior have been reported for charge recombination, but it remains quite elusive in photoinduced charge separation.<sup>8-13</sup> One exception is the recent work of Mataga *et al.* who elegantly demonstrated inverted region behavior in charge separation in porphyrin-imide dyads, utilizing the higher energy  $S_2$  state to increase  $-\Delta G_0$ .<sup>14</sup>

Here, the photoinduced electron transfer and recombination kinetics are described for three oligo(*p*-phenylene vinylene) – perylene bisimide – oligo(*p*-phenylene vinylene) (OPV-PERY-OPV) arrays (1-3, Figure 1) and it is demonstrated that for 2 and 3, both forward and backward electron transfer occur in the ‘inverted region’. These donor-acceptor-donor arrays differ only by the substituents on the bay positions of the central PERY moiety. The substituents, *tert*-butylphenoxy, hydrogen, and chlorine were chosen to create an increasing reduction potential of the perylene bisimide and thereby an increase of  $-\Delta G_0$ .

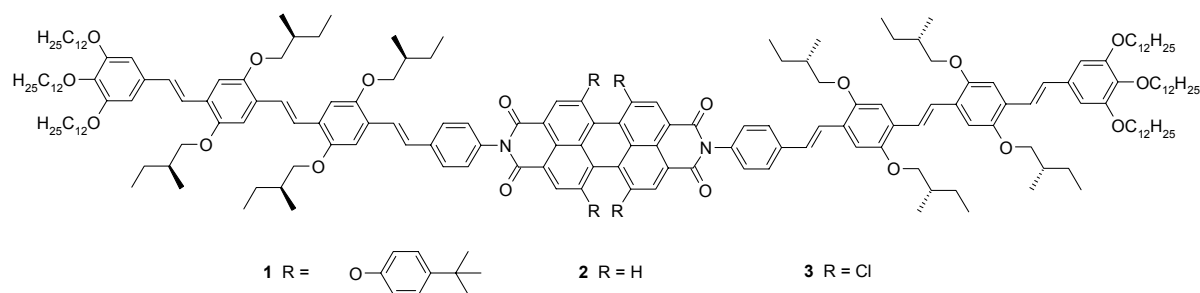


**Figure 1:** Structures of the three donor-acceptor-donor arrays 1-3.

### 3.2 Results and Discussion

The UV/Vis absorption spectra of 1-3 are shown in Figure 2. The spectra exhibit the characteristic  $\pi$ - $\pi^*$  absorption of the OPV unit at  $\sim 435$  nm for each triad. The absorptions at higher wavelength are the vibronically resolved transitions of the perylene bisimide chromophores. Going from 1 to 3, there is a continuous shift of this band to higher energy and, accordingly, the energy of the lowest singlet-excited state increases ( $E_{00} = 2.13, 2.32,$  and  $2.38$  eV, for respectively 1-3, recorded in  $\text{CH}_2\text{Cl}_2$ ).

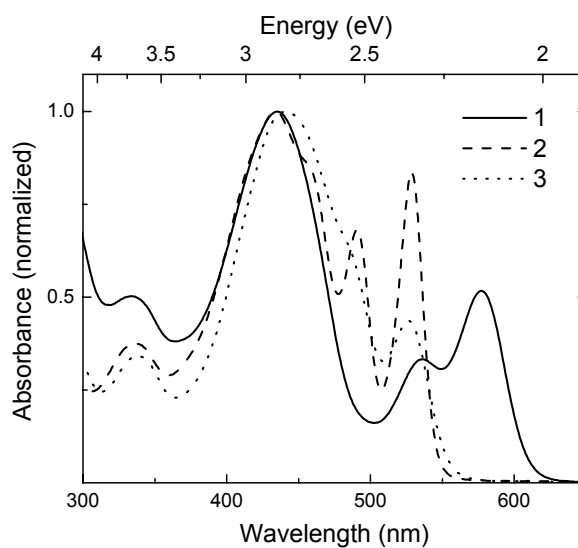


**Figure 2:** Normalized UV/Vis absorption spectra of compounds 1-3.

Each of the three triads 1-3 exhibits a reversible oxidation wave in the cyclic voltammogram (Figure 3). The first oxidation potentials of 1-3 are very similar ( $E_{\text{ox}} = +0.34$ ,  $+0.31$ , and  $+0.33$  V vs.  $\text{Fc}/\text{Fc}^+$  in  $\text{CH}_2\text{Cl}_2$ , respectively). The reduction potentials vary much more ( $E_{\text{red}} = -1.17$ ,  $-1.02$ , and  $-0.80$  V) and reflect the difference in the electron donation and accepting character of the substituents on the perylene bisimide moiety.

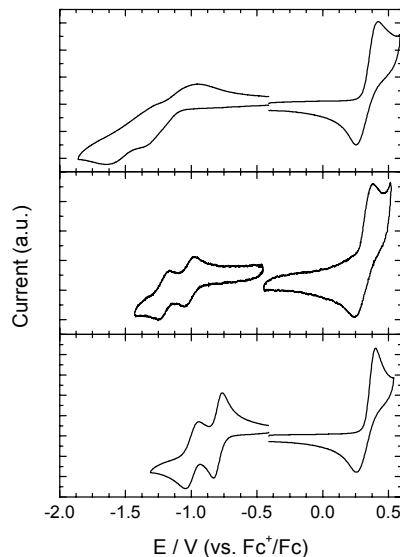


**Figure 3:** Cyclic voltammograms of compounds 1 (top), 2 (middle) and 3 (bottom) in  $\text{CH}_2\text{Cl}_2$ , scan rate  $0.1 \text{ V}\cdot\text{s}^{-1}$ , supporting electrolyte  $0.1 \text{ mol}\cdot\text{L}^{-1} \text{NBu}_4\text{PF}_6$ .

The rates for charge separation ( $k_{\text{CS}}$ ) and recombination ( $k_{\text{CR}}$ ) were determined for 1-3 in six solvents with varying polarity ( $\epsilon_s = 2.38 - 25.3$ ), by monitoring the transient absorption of the  $\text{OPV}^{+\cdot}$  radical cation at  $1450 \text{ nm}$ ,<sup>15</sup> after excitation of the OPV ( $450 \text{ nm}$ ) or PERY ( $520 \text{ nm}$ ) chromophore with femtosecond pump-probe photoinduced absorption spectroscopy.

Figure 4 shows an example of the transient traces that have been obtained. For each triad,  $k_{CS}$  and  $k_{CR}$  were extracted from the data by fitting a biexponential function. These data are collected in Table 1. For all three triads, charge separation is extremely fast ( $k_{CS} = 2.2 \times 10^{11}$  to  $1.6 \times 10^{12} \text{ s}^{-1}$ , Table 1). The charge recombination varies more strongly with the solvent and is in general slower ( $k_{CR} = < 8 \times 10^8$  to  $2.6 \times 10^{11} \text{ s}^{-1}$ ).

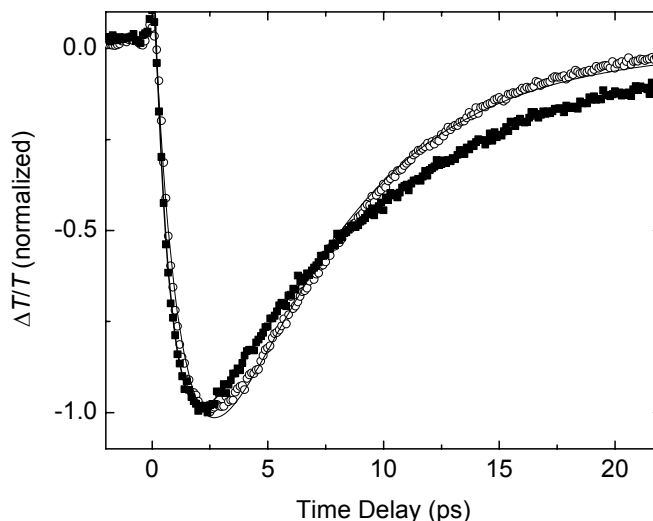


**Figure 4:** Normalized differential transmission dynamics of 3 in  $\text{CHCl}_3$  ( $\epsilon_s = 4.81$ , closed squares) and benzonitrile ( $\epsilon_s = 25.3$ , open circles) recorded at 1450 nm with excitation at 450 nm, together with a biexponential fit to the data (solid lines).

We found that values obtained for  $k_{CS}$  (or  $k_{CR}$ ) pertaining to the same solute-solvent combination were independent of the excitation wavelength (450 or 520 nm) used. This indicates that an ultrafast singlet-energy transfer from the singlet-excited state of OPV (2.52 eV) to the PERY moiety precedes the electron transfer, which therefore originates from PERY singlet excited state  $S_1$ . The strong quenching of the OPV fluorescence supports this conclusion. Therefore, the change in free energy for charge separation ( $-\Delta G_0$ ) was determined relative to the energy level of the PERY( $S_1$ ) state ( $E_{00}$ ) and the redox potentials of the donor ( $E_{ox}(D)$ ) and the acceptor ( $E_{red}(A)$ ) state using a continuum model:<sup>16</sup>

$$-\Delta G_0 = -e[E_{ox}(D) - E_{red}(A)] + E_{00} + \frac{e^2}{4\pi\epsilon_0\epsilon_s R_{cc}} + \frac{e^2}{8\pi\epsilon_0} \left( \frac{1}{r^+} + \frac{1}{r^-} \right) \left( \frac{1}{\epsilon_{ref}} - \frac{1}{\epsilon_s} \right) \quad (1)$$

The radius of the OPV radical cation and the perylene bisimide anion are set to  $r^+ = 5.05 \text{ \AA}$  and  $r^- = 4.71 \text{ \AA}$  respectively,<sup>17</sup> whereas the center-to-center chromophore distance ( $R_{cc}$ ) was set at 14  $\text{\AA}$  for all three compounds.

**Table 1:** Experimental rate constants ( $k$ ) and estimates for the change in Gibbs-free energy ( $\Delta G$ ) and activation energy ( $\Delta G^\ddagger$ ) for charge separation (CS) and recombination (CR) in different solvents. Calculated rate constants were obtained using equation 2.

Solvent	$-\Delta G_{CS}$ (eV)	$\Delta G_{CS}^{\ddagger a}$ (eV)	$k_{CS}$ (s <sup>-1</sup> )	$k_{CS,calc}^b$ (s <sup>-1</sup> )	$-\Delta G_{CR}$ (eV)	$\Delta G_{CR}^{\ddagger a}$ (eV)	$k_{CR}$ (s <sup>-1</sup> )	$k_{CR,calc}^c$ (s <sup>-1</sup> )
<b>1</b> PhCH <sub>3</sub> PhCH <sub>3</sub> <sup>d</sup> CHCl <sub>3</sub> PhCl THF ODCB PhCN	0.14	0.021	$2.7 \times 10^{11}$	$1.4 \times 10^{10}$	1.99	2.73	$< 8 \times 10^8$	$1.1 \times 10^8$
				$4.9 \times 10^{11}$				$5.7 \times 10^8$
	0.55	0.016	$2.2 \times 10^{11}$	$4.5 \times 10^{11}$	1.58	0.212	$2.1 \times 10^{10}$	$6.4 \times 10^9$
	0.61	0.006	$2.6 \times 10^{11}$	$5.2 \times 10^{11}$	1.52	0.204	$1.0 \times 10^{10}$	$1.1 \times 10^{10}$
	0.69	0.019	$3.9 \times 10^{11}$	$5.7 \times 10^{11}$	1.44	0.057	$3.4 \times 10^{10}$	$2.1 \times 10^{10}$
	0.76	0.003	$4.6 \times 10^{11}$	$5.8 \times 10^{11}$	1.37	0.078	$1.8 \times 10^{10}$	$3.5 \times 10^{10}$
	0.88	0.004	$2.5 \times 10^{11}$	$5.8 \times 10^{11}$	1.25	0.016	$5.5 \times 10^{10}$	$7.9 \times 10^{10}$
<b>2</b> PhCH <sub>3</sub> PhCH <sub>3</sub> <sup>d</sup> CHCl <sub>3</sub> PhCl THF ODCB PhCN	0.51	0.037	$1.6 \times 10^{12}$	$4.1 \times 10^{11}$	1.81	1.89	$3.0 \times 10^9$	$7.4 \times 10^9$
				$4.1 \times 10^{11}$				$3.9 \times 10^9$
	0.91	0.007	$1.5 \times 10^{12}$	$6.0 \times 10^{11}$	1.40	0.128	$6.6 \times 10^{10}$	$2.8 \times 10^{10}$
	0.98	0.020	$1.0 \times 10^{12}$	$6.6 \times 10^{11}$	1.34	0.120	$7.5 \times 10^{10}$	$4.3 \times 10^{10}$
	1.06	0.002	$1.5 \times 10^{12}$	$7.9 \times 10^{11}$	1.26	0.022	$8.9 \times 10^{10}$	$7.5 \times 10^{10}$
	1.13	0.022	$1.1 \times 10^{12}$	$9.1 \times 10^{11}$	1.19	0.033	$4.4 \times 10^{10}$	$1.1 \times 10^{11}$
	1.25	0.015	$1.3 \times 10^{12}$	$1.0 \times 10^{12}$	1.07	0.001	$9.3 \times 10^{10}$	$2.2 \times 10^{11}$
<b>3</b> PhCH <sub>3</sub> PhCH <sub>3</sub> <sup>d</sup> CHCl <sub>3</sub> PhCl THF ODCB PhCN	0.77	0.185	$1.5 \times 10^{12}$	$5.8 \times 10^{11}$	1.61	1.43	$1.6 \times 10^{10}$	$4.9 \times 10^9$
				$1.1 \times 10^{12}$				$2.5 \times 10^{10}$
	1.18	0.054	$1.0 \times 10^{12}$	$9.9 \times 10^{11}$	1.20	0.060	$1.2 \times 10^{11}$	$1.1 \times 10^{11}$
	1.24	0.085	$8.7 \times 10^{11}$	$1.0 \times 10^{12}$	1.14	0.053	$6.4 \times 10^{10}$	$1.5 \times 10^{11}$
	1.32	0.033	$1.0 \times 10^{12}$	$1.0 \times 10^{12}$	1.06	0.002	$2.6 \times 10^{11}$	$2.3 \times 10^{11}$
	1.39	0.082	$9.0 \times 10^{11}$	$9.7 \times 10^{11}$	0.99	0.006	$7.9 \times 10^{10}$	$3.1 \times 10^{11}$
	1.51	0.064	$5.8 \times 10^{11}$	$7.3 \times 10^{11}$	0.87	0.004	$1.9 \times 10^{11}$	$4.5 \times 10^{11}$

- a) Determined from the Marcus relation  $\Delta G^\ddagger = (\Delta G_0 + \lambda)^2 / 4\lambda$ , with  $\lambda = \lambda_i + \lambda_s$ ,  $\lambda_i = 0.25$  eV, and  $\lambda_s = (e^2 / 4\pi\epsilon_0)(1/(2r^+) + 1/(2r^-) - (1/R_{cc}))(1/n^2 - 1/\epsilon_s)$ .<sup>18</sup>
- b) Calculated for PERY(S<sub>1</sub>) → CSS and PERY(S<sub>1</sub>) → CSS\*<sup>\*</sup>; ( $k_{CS,calc} = k_{CSS} + k_{CSS^*}$ ) using  $\lambda_i = 0.25$  eV,  $\lambda_s = 0.5$  eV,  $V_{CSS} = 6$  meV,  $V_{CSS^*} = 8$  meV,  $\hbar\omega = 0.186$  eV ( $\omega = 1500$  cm<sup>-1</sup>) and  $T = 298$  K.
- c) Calculated for CSS → S<sub>1</sub>,  $\lambda_i = 0.25$  eV,  $\lambda_s = 0.5$  eV,  $V = 6$  meV,  $\hbar\omega = 0.186$  eV and  $T = 298$  K.
- d) Calculated using  $\lambda_s = 0.1$  eV instead of 0.5 eV (see text).

A semi-logarithmic plot of  $k_{CS}$  and  $k_{CR}$  vs.  $-\Delta G_0$  is given in Figure 5. The plot clearly shows that charge recombination (open symbols) takes place in the inverted region. The rates can be described using the non-adiabatic electron transfer theory proposed by Jortner *et al.*<sup>19,20</sup>

$$k_0 = \left( \frac{\pi}{\hbar^2 \lambda_s k_B T} \right)^{1/2} V^2 \sum_{n=0}^{\infty} e^{-S} \frac{S^n}{n!} \exp \left( - \frac{(\Delta G_0 + \lambda_s + n\hbar\omega)^2}{4\lambda_s k_B T} \right) \quad (2)$$

In equation 2,  $V$  describes the electronic coupling and  $S$  ( $= \lambda_i / \hbar\omega$ ) relates to the effective mode vibrational energy, while  $\lambda_i$  and  $\lambda_s$  are the internal and solvent reorganization energies, respectively. Taking  $\hbar\omega = 0.186$  eV (1500 cm<sup>-1</sup>) and  $T = 298$  K, a satisfactory fit could be obtained for  $\lambda_i = 0.25$  eV,



$\lambda_s = 0.5$  eV, and  $V = 6$  meV (Figure 5). This value of  $\lambda_s$  is in reasonable agreement with values calculated with the Born-Hush approximation for the more polar solvents.<sup>18</sup>

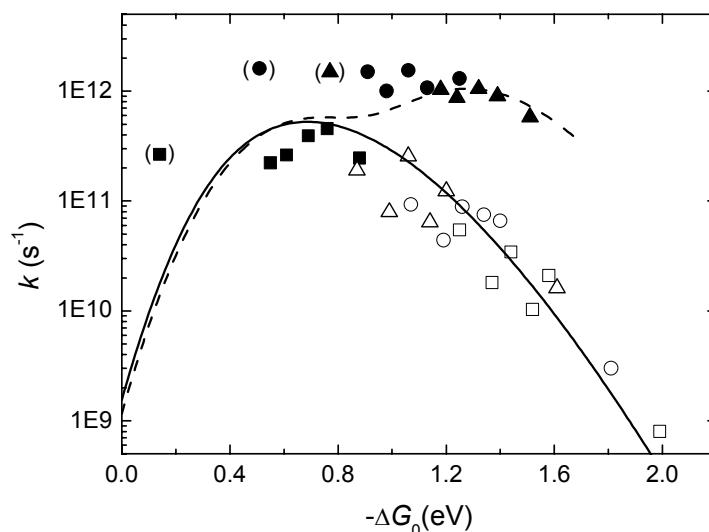


**Figure 5:** Rates for charge separation (solid markers) and recombination (open markers) versus  $-\Delta G_0$  for 1 (squares), 2 (circles), and 3 (triangles). The solid line represents  $k$  calculated from equation 1. The dashed line represents the calculated  $k$  for a combination of charge separation to CSS and CSS\*, taking into account a 0.6 eV lower driving force for the latter pathway. The data for charge separation in toluene (in parenthesis) were not used in the fitting because the solvent reorganization energy  $\lambda_s$  deviates significantly from that in the other solvents (see text).

Turning now to the rates for charge separation (Figure 5, solid markers), it appears that the  $k_{CS}$  data of 1 fall on the same curve as used to describe the charge recombination. Charge separation for 1 is close to the ‘optimal region’ ( $-\Delta G_0 \approx \lambda$ ). For 2 and 3, charge separation is more exergonic than for 1 and the rates for charge separation are expected to be lower because inverted behavior applies. In contrast, the experimental charge separation in 2 and 3 is significantly faster than in 1 (Figure 5). Nevertheless, a small reduction of  $k_{CS}$  (more pronounced for 3) with increasing  $-\Delta G_0$  indicates behavior close to the ‘inverted region’.

A possible explanation for the high  $k_{CS}$  of 2 and 3 is that charge transfer produces an excited-state of the charge-separated state (CSS\*) rather than the ground state (CSS, Figure 6).<sup>10</sup> The energy of CSS\* can be inferred from the absorption spectrum of OPV<sup>+</sup>, which exhibits a low-energy band with an onset at 0.6 eV (Figure 6).<sup>21</sup> Because  $-\Delta G_0$  (to CSS) exceeds 0.6 eV in solvents with  $\epsilon > 2.7$ , charge transfer from the PERY(S<sub>1</sub>) state to CSS\* is exergonic for 2 and 3. Non-radiative decay from CSS\* to CSS is expected to be fast and therefore charge recombination only occurs from CSS.

When  $-\Delta G_0$  is corrected for the 0.6 eV difference between CSS and CSS\*, the charge transfer will become less exergonic and is no longer expected to occur in the inverted region but rather in the optimal region. This rationalizes the moderate reduction of  $k_{CS}$  with increasing  $-\Delta G_0$  and explains (in part) the high values of  $k_{CS}$  for 2 and 3. By including the additional pathway to CSS\* with a 0.6 eV lower driving force, the experimental data for  $k_{CS}$  of 2 and 3 are in fair agreement with values obtained from equation 2 when the same parameters are used as before and the electronic coupling between

PERY( $S_1$ ) and CSS\* is set to  $V = 8$  meV, *i.e.* slightly higher than between PERY( $S_1$ ) and CSS ( $V = 6$  meV). For low values of  $-\Delta G_0$ , the rate constant does not change because the pathway to CSS\* is endergonic. For larger values of  $-\Delta G_0$ , charge separation is a combination of both pathways. The fit supports the presence of an additional charge separation pathway to CSS\* and reproduces the decrease of  $k_{CS}$  with increasing  $-\Delta G_0$  for 2 and 3.

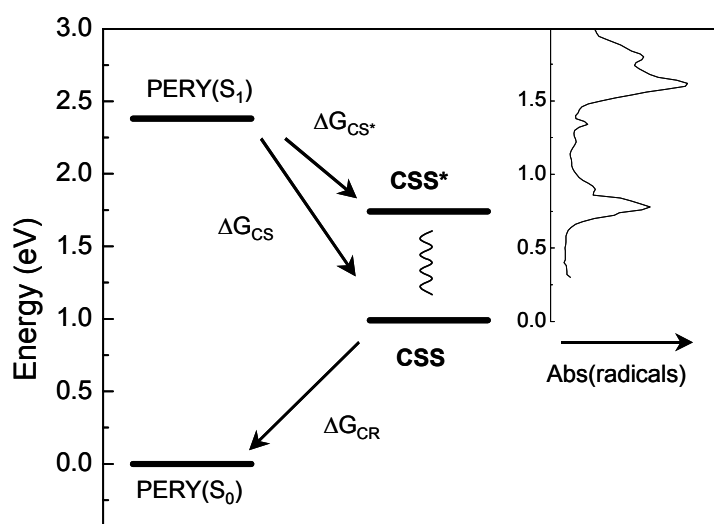


**Figure 6:** Energetic diagram for charge separation from PERY( $S_1$ ) to CSS and CSS\*. The inset shows the absorption spectrum of OPV-PERY<sup>-</sup>-OPV<sup>+</sup> relative to the energy level of CSS.

The three experimental rate constants for charge separation of 1-3 in toluene deviate from the calculated curve. This is primarily due to the fact that the solvent reorganization energy  $\lambda_s = 0.5$  eV, used to construct the curve, does not apply to apolar solvents like toluene. For toluene, the Born-Hush approximation gives  $\lambda_s = 0.1$  eV. Using the same parameters but setting  $\lambda_s = 0.1$  eV, brings the calculated rate constants for toluene closer to the experimental values (Table 1). The deviation of the toluene data might also be explained by the notion that the microscopic polarity, and hence  $-\Delta G_0$ , is not accurately described by  $\epsilon_s$  due to a substantial quadrupole moment of the solvent.<sup>22</sup>

### 3.3 Conclusions

The kinetics of photoinduced intramolecular charge separation and charge recombination in three homologous oligo(*p*-phenylene vinylene)-perylene bisimide-oligo(*p*-phenylene vinylene) arrays has been studied in solvents of different polarity. For the two molecules with the lowest reduction potentials, 2 and 3, the rates for charge separation and charge recombination decrease with increasing change in Gibbs-free energy, and hence represent an example of molecules in which charge separation and recombination occur close to, or in the Marcus inverted region. The presence of a low energy excited state of the charge separated state hampers detection of the Marcus inverted region. An

additional reaction to this CSS\* is favorable over electron transfer to the CSS state with high barriers in the inverted region.

### 3.4 Experimental Section

**Materials.** The synthesis of the studied compounds has been described previously.<sup>15,23</sup> The solvents for spectroscopic studies were of spectroscopic grade and used as received.

**Spectroscopic Techniques.** UV/Vis spectra were measured on a Perkin Elmer Lambda 40P and the steady state fluorescence spectra were measured on a Perkin Elmer LS-50B spectrofluorometer. A description of the transient photoinduced absorption setup can be found in chapter 2.

The specifications of the laser pulse were verified by measuring the optical Kerr-effect<sup>24</sup> (Figure 7) as signals with time constants below 1 ps were measured. This resulted in a cross-correlation with a full width at half maximum (FWHM) of 525 fs corresponding to a Gaussian-shaped pulse with a width  $\sigma$  of 223 fs. By taking into account that this is the width calculated for two convoluted pulses and assuming equal width for both of them, a pulse width of 158 fs is calculated, in agreement with the specification of 150 fs.

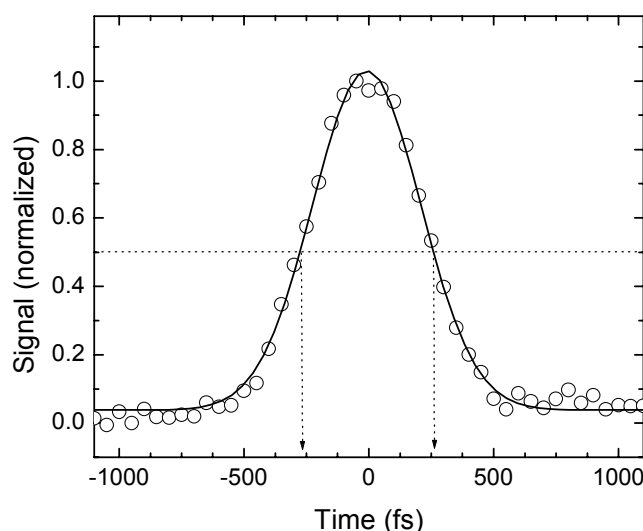


**Figure 7:** Determination of the pulse width of the used pump-probe transient absorption setup by measuring the Kerr-effect in heptane ( $\lambda_{\text{pump}} = 455 \text{ nm}$ ,  $\lambda_{\text{probe}} = 1450 \text{ nm}$ ).

By convoluting the instrument response ( $\sigma = 223 \text{ fs}$ ) and the expected rate constant for the charge separation reaction it is possible to analyze the expected photoinduced absorption signal mathematically. This revealed that rate constants of  $2 \times 10^{12} \text{ s}^{-1}$  or slower can be distinguished from the actual laser pulse width. For rate constants above  $5 \times 10^{12} \text{ s}^{-1}$  this is not possible anymore and a deconvolution procedure is necessary to obtain the true rate constant.

**Electrochemical Measurements.** Cyclic voltammetry was performed with an EG&G PAR 273 potentiostat in a three-electrode single-compartment cell using dichloromethane as solvent. Working electrode: platinum disk; counter electrode: platinum wire; reference electrode: Ag/AgCl. All potentials were internally referenced to the Fc/Fc<sup>+</sup> couple. The solutions were purged with argon gas prior to use. The supporting electrolyte was  $0.1 \text{ mol}\cdot\text{L}^{-1}$  tetrabutylammonium hexafluorophosphate (Fluka), which was recrystallized twice from ethanol / water and dried in a high vacuum.

**Parameters Used in the Calculations.** The parameters used in the calculation for the different driving forces and reorganization energies were as follows:

Solvent	$\epsilon_s$	$n$	$\lambda$
Toluene (PhCH <sub>3</sub> )	2.38	1.497	0.30
Chloroform (CHCl <sub>3</sub> )	4.81	1.446	0.77
Chlorobenzene (PhCl)	5.69	1.524	0.74
Tetrahydrofuran (THF)	7.52	1.407	0.97
o-Dichlorobenzene (ODCB)	9.93	1.552	0.86
Benzonitrile (PhCN)	25.3	1.528	1.00

$$\lambda = \lambda_i + \lambda_s, \lambda_i = 0.25 \text{ eV}$$

$$\lambda_s = (e^2 / 4\pi\epsilon_0) (1/(2r^+) + 1/(2r^-) - (1/R_{cc})) (1/n^2 - 1/\epsilon_s).$$

### 3.5 References and Notes

- 1 *Advances in Chemical Physics*, Jortner, J.; Bixon, M., Ed.; Wiley-Interscience, **1999**; Vols. 106 and 107.
- 2 *Electron Transfer in Chemistry*, Balzani, V., Ed.; Wiley-VCH: Weinheim, **2001**; Vols. 1-5.
- 3 Marcus, R. A. *J. Chem. Phys.* **1965**, *43*, 679.
- 4 Marcus, R. A.; Sutin, N. *Biochim. Biophys. Acta* **1985**, *811*, 265.
- 5 Marcus, R. A. *Rev. Mod. Phys.* **1993**, *65*, 599.
- 6 Miller, J. R.; Calcaterra, L. T.; Closs, G. L. *J. Am. Chem. Soc.* **1984**, *106*, 3047.
- 7 Closs, G. L.; Miller, J. R. *Science* **1988**, *240*, 440.
- 8 Closs, G. L.; Calcaterra, L. T.; Green, N. J.; Penfield, K. W.; Miller, J. R. *J. Phys. Chem.* **1986**, *90*, 3673.
- 9 Asahi, T.; Ohkohchi, M.; Matsusaka, R.; Mataga, N.; Zhang, R. P.; Osuka, A.; Maruyama, K. *J. Am. Chem. Soc.* **1993**, *115*, 5665.
- 10 Heitele, H.; Pöllinger, F.; Häberle, T.; Michel-Beyerle, M. E.; Staab, H. A. *J. Phys. Chem.* **1994**, *98*, 7402.
- 11 Macpherson, A. N.; Liddell, P. A.; Lin, S.; Noss, L.; Seely, G. R.; DeGraziano, J. M.; Moore, A. L.; Moore, T. A.; Gust, D. *J. Am. Chem. Soc.* **1995**, *117*, 7202.
- 12 Häberle, T.; Hirsch, J.; Pöllinger, F.; Heitele, H.; Michel-Beyerle, M. E.; Anders, C.; Döhling, A.; Krieger, C.; Rückemann, A.; Staab, H. A. *J. Phys. Chem.* **1996**, *100*, 18269.
- 13 Osuka, A.; Noya, G.; Taniguchi, S.; Okada, T.; Nishimura, Y.; Yamazaki, I.; Mataga, N. *Chem. Eur. J.* **2000**, *6*, 33.
- 14 Mataga, N.; Chosrowjan, H.; Taniguchi, S.; Shibata, Y.; Yoshida, N.; Osuka, A.; Kikuzawa, T.; Okada, T. *J. Phys. Chem. A* **2002**, *106*, 12191.
- 15 Peeters, E.; Van Hal, P.A.; Meskers, S. C. J.; Janssen, R. A. J.; Meijer, E. W. *Chem. Eur. J.* **2002**, *8*, 4470.
- 16 Weller, A. *Z. Phys. Chem.* **1982**, *133*, 93.
- 17 Neuteboom, E. E.; Meskers, S. C. J.; Van Hal, P. A.; van Duren, J. K. J.; Meijer, E. W.; Janssen, R. A. J.; Dupin, H.; Pourtois, G.; Cornil, J.; Lazzaroni, R.; Brédas, J.-L.; Beljonne, D. *J. Am. Chem. Soc.* **2003**, *125*, 8625.
- 18 Hush, N. S. *Trans. Faraday. Soc.* **1961**, *57*, 557.
- 19 Kestner, N. R.; Logan, J.; Jortner, J. *J. Phys. Chem.* **1974**, *78*, 2148.

- 20 Ulstrup, J.; Jortner, J. *J. Chem. Phys.* **1975**, *63*, 4358.
- 21 Van Hal, P. A.; Beckers, E. H. A.; Peeters, E.; Apperloo, J. J.; Janssen, R. A. J. *Chem. Phys. Lett.* **2000**, *328*, 403.
- 22 Würthner, F.; Yao, S.; Debaerdemaeker, T.; Wortmann, R. *J. Am. Chem. Soc.* **2002**, *124*, 9431.
- 23 Beckers, E. H. A.; Meskers, S. C. J.; Schenning, A. P. H. J.; Chen, Z.; Würthner, F.; Janssen, R. A. J. *J. Phys. Chem. A* **2004**, *108*, 6933.
- 24 *Femtosecond Laser Pulses*, Rullière, C.; Ed.; Springer, **1998**.

# Photoinduced Multistep Electron Transfer in an Oligoaniline–Oligo(*p*-phenylene vinylene) – Perylene Bisimide Molecular Array\*

### *Abstract*

*Photoinduced multistep electron transfer has been studied in two symmetrical oligoaniline–oligo(*p*-phenylene vinylene)–perylene bisimide–oligo(*p*-phenylene vinylene)–oligoaniline (OAn-OPV-PERY-OPV-OAn) multichromophore arrays with transient absorption spectroscopy in the femtosecond and nanosecond time domains. The arrays consist of a symmetrical donor(2)-donor(1)-acceptor-donor(1)-donor(2) arrangement, with two OAn-OPV segments coupled to a central PERY unit via a direct linkage (1) or a saturated spacer (2). Photoexcitation gives the OAn-OPV<sup>+</sup>-PERY<sup>-</sup>-OPV-OAn as the primary charge-separated state. For 1 the transfer is extremely fast ( $k_{CS} > 1 \text{ ps}^{-1}$ ) in polar and apolar solvents, while the rate constants for recombination differ and are significantly higher in polar solvents than in apolar solvents because recombination occurs in the Marcus inverted region. Charge separation and charge recombination are slower in 2, because the saturated spacer reduces the electronic coupling between OPV donor and PERY acceptor. The primary OAn-OPV<sup>+</sup>-PERY<sup>-</sup>-OPV-OAn charge-separated state can rearrange to the OAn<sup>+</sup>-OPV-PERY<sup>-</sup>-OPV-OAn state after a charge shift reaction. This charge shift is exergonic and competes with fast charge recombination. In polar solvents the efficiency of the charge shift is about 0.22 and 0.28 for 1 and 2, respectively, and only weakly dependent on the polarity. The OAn<sup>+</sup>-OPV-PERY<sup>-</sup>-OPV-OAn charge-separated state has a long lifetime as a result of the negligible interaction between the distant OAn<sup>+</sup> and PERY<sup>-</sup> redox sites, and can be observed up to several microseconds.*

---

\* Part of this work has been published: (a) Marcos Ramos, A.; Beckers, E. H. A.; Offermans, T.; Meskers, S. C. J.; Janssen, R. A. J. *Journal of Physical Chemistry A* **2004**, *108*, 8201-8211. (b) Marcos Ramos, A; Ph.D. Thesis, Eindhoven University of Technology, **2003**.

## 4.1 Introduction

For practical applications, it is often of interest to combine a high rate for charge separation with a low rate for charge recombination. For this purpose multichromophoric arrays have been designed in which the initial photoinduced charge separation is followed by charge migration reactions along a well-defined redox gradient that ultimately provides the spatial separation of the photogenerated charges that is essential to lower the rate for charge recombination. Various elegantly designed triads, tetrads, etc. have been synthesized and investigated in detail.<sup>1-29</sup>

Multistep electron transfer, or charge migration, is possibly also the origin of the longevity of charges in solid-state blends of donor and acceptor materials used in organic and polymer solar cells.<sup>30,31</sup> In these devices, excitons, created by the absorption of light, dissociate at the donor-acceptor interface forming an electron-hole pair. When this electron and hole escape from geminate recombination and diffuse away from the interface,<sup>32,33</sup> they can be collected at electrodes as a photocurrent.

Because of their high absorption coefficients in the visible region and their charge transport properties, OPV<sup>34-39</sup> and PERY<sup>40-46</sup> chromophores have also attracted interest for organic solar cells. Recent studies on covalently linked oligo(*p*-phenylene vinylene) (OPV) donors and perylene bisimide (PERY) acceptors in liquid crystalline OPV-PERY-OPV triads,<sup>47,48</sup>  $\pi$ -stacks of hydrogen-bonded OPV-PERY-OPV trimers,<sup>49</sup> and alternating (OPV-PERY)<sub>n</sub> copolymers,<sup>50</sup> have revealed that photoinduced electron transfer can be extremely fast in solution (< 1 ps), but that the lifetime is generally rather short (< 1 ns).

With the aim to extend the lifetime of the charge-separated state, two new multichromophoric molecular arrays incorporating a central OPV-PERY-OPV triad augmented with two *p*-oligoaniline (OAn) moieties as additional donors, have been designed (1 and 2, Figure 1). The two arrays differ in the connectivity between the central PERY segment and the OPV donors. In 1, the OPV and PERY units are directly connected providing a close proximity and possibly some conjugation, although the two chromophores are likely not coplanar. In 2, the OPV-PERY distances are longer and the conjugation is fully interrupted by saturated bonds. The redox potentials of the OAn, OPV, and PERY segments favor the OAn<sup>+</sup>-OPV-PERY<sup>-</sup>-OPV-OAn state as the lowest-energy charge-separated state after photoexcitation. Arrays 1 and 2 have been studied using transient absorption spectroscopy in solvents of different polarity to investigate the photoinduced multistep electron transfer. The kinetics of charge separation, migration, and recombination have been determined and are rationalized in terms of Marcus theory, using a continuum model to describe the free energy.

## 4.2 Results

**Absorption Spectroscopy.** The UV/Vis absorption spectrum of 1 in toluene (Figure 2a) exhibits two strong absorption bands, one centered at 327 nm and the other featuring vibronic fine structure with peaks at 464, 494 and 532 nm. For direct comparison, the absorption spectra of the OAn, OPV, and PERY reference compounds (Figure 1) are also plotted in Figure 2a. All chromophores contribute to the absorption of the UV region of 1, but the absorption in the visible region is dominated by the  $\pi$ - $\pi^*$

transitions of the OPV and PERY chromophores. The characteristic vibronic fine structure of the PERY chromophore is clearly present in the visible region.

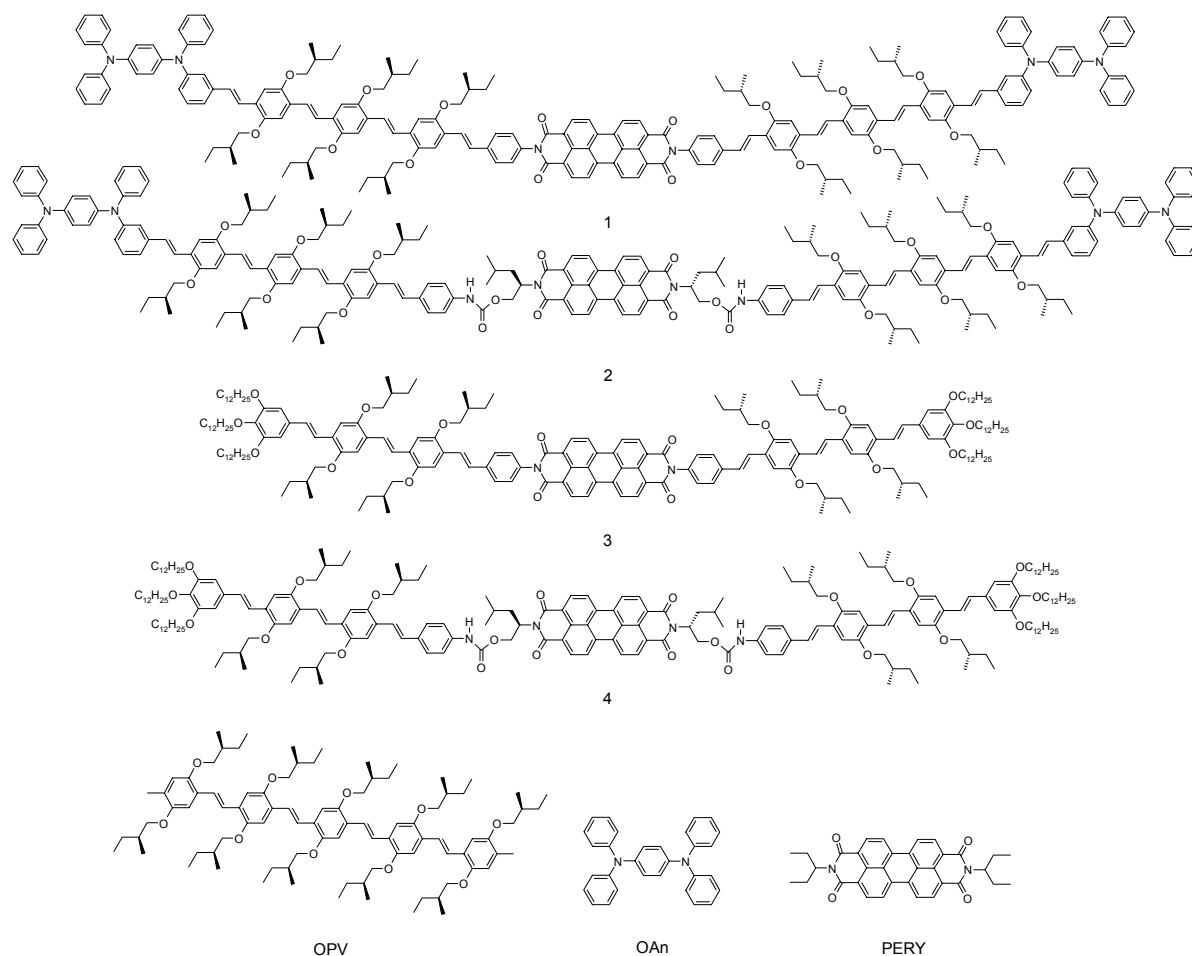


**Figure 1:** Chemical structures of D2-D1-A-D1-D2 arrays 1 and 2 and reference compounds 3, 4, OPV, OAn, and PERY.

The UV/Vis absorption spectrum of 2 (Figure 2b) recorded in THF also consists of the overlapping absorptions of the OAn, OPV and PERY chromophores. The low energy absorption band at 532 nm of the PERY chromophore exhibits a lower intensity for 2 than for 1. In *o*-dichlorobenzene, the spectrum is slightly shifted to higher wavelengths, but further rather similar.

In toluene (Figure 2b), the absorption spectrum of 2 shows a reduced intensity of the peak at 532 nm and a weak contribution above 550 nm, which indicates some aggregation as a consequence of intermolecular hydrogen bonding and  $\pi$ - $\pi$  interactions.<sup>48</sup>



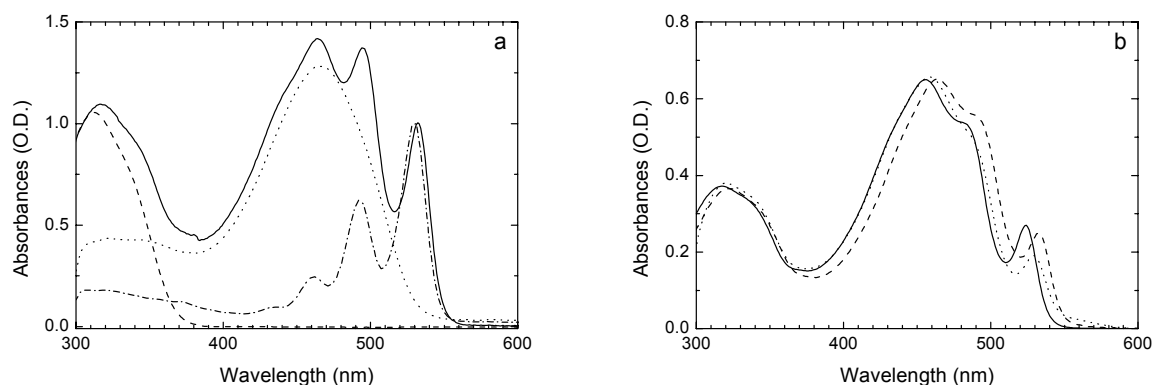


**Figure 2:** (a) UV/Vis absorption spectra of the OAn-OPV-PERY-OPV-OAn array 1 (solid) and model compounds OAn (dashed), OPV (dotted), and PERY (dash-dot) recorded in toluene solution. (b) UV/Vis absorption spectra of the OAn-OPV-PERY-OPV-OAn array 2 in tetrahydrofuran (solid line), ODCB (dashed line), and toluene (dotted line).

More proof for the presence of aggregates can be found by heating a solution of 2 in toluene (Figure 3). The band above 550 nm disappears and the characteristic absorption of molecularly dissolved perylene species appears at 532 nm indicating that indeed at room temperature aggregated structures are present.

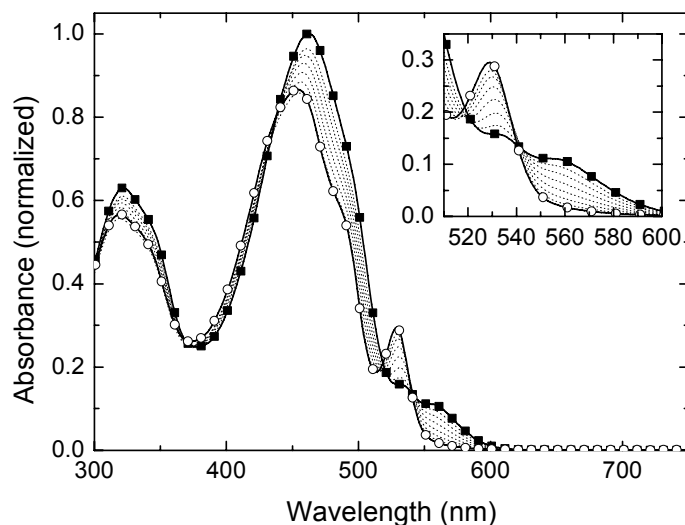


**Figure 3:** Absorption spectra of compound 2 in toluene ( $1 \times 10^{-4}M$ ) at different temperatures ranging from 20 °C (solid squares) to 90 °C (open circles).

**Electrochemistry.** The electrochemical properties of 1 and 2 and of the reference compounds OAn, OPV, and PERY were investigated by cyclic voltammetry in dichloromethane. The redox potentials are collected in Table 1. Reversible reduction of the PERY acceptor in 1 occurs at half-wave potentials of  $-0.53$  and  $-0.76$  V. Array 1 could be oxidized in four consecutive reversible oxidations at  $+0.53$  V and  $+1.03$  V corresponding to the OAn segment, and at  $+0.76$  and  $+0.96$  for the OPV moiety (Table 1). In dichloromethane, also four oxidation waves were observed for 2 at  $+0.53$  and  $+1.07$  V (OAn),

and at +0.74 and +0.90 V (OPV). In this solvent no reduction was observed for 2. We assume that the reduction of 2 in dichloromethane is hampered by aggregation. In accordance, the UV/Vis spectrum of 2 in dichloromethane is similar to that in toluene and indicative of aggregation. In THF, however, where aggregation is not observed, the cyclic voltammogram of 2 exhibits the two reduction waves at -0.60 and -0.89 V corresponding to the PERY moiety.

Comparison with the model compounds OPV, OAn, and PERY (Figure 1) reveals that the first and second oxidation potentials of 1 and 2 are not strongly affected by linking the OPV and OAn chromophores (Table 1). In contrast, the reduction potential of the PERY acceptor depends on the nature of the imide functionality. The reduction potentials of 1 and 2 are shifted by +0.12 and +0.05 V respectively with respect to that of the PERY reference compound (-0.65 V). For 2 the shift is less, owing to the similar alkyl substitution as in the PERY reference. In compound 1, some conjugation between the OPV and PERY chromophores is possible, although the first phenyl ring of the OPV moiety will not be coplanar with the PERY unit.

**Table 1:** One-electron half-wave redox potentials ( $E^0$ ) of OAn, OPV, PERY, and OAn-OPV-PERY-OPV-OAn (vs. SCE) calibrated with  $Fc/Fc^+$  (in dichloromethane with 0.1 M TBAPF<sub>6</sub>). The reduction potential of 2 is measured in THF.

Compound	$E^0_{\text{red}}$ (V)	$E^0_{\text{ox}}$ (V)
OAn	-	0.53 / 1.02
OPV	-	0.73 / 0.80
PERY	-0.65/-0.85	-
Array 1	-0.53/-0.76	0.53 / 0.76 / 0.96 / 1.07
Array 2	-0.60/-0.89	0.53 / 0.74 / 0.90 / 1.07

**Energetic Considerations.** Figure 4 shows the photophysical processes that can occur in these arrays upon illumination. Photoexcitation initially generates the localized singlet-excited states with energies at 3.40, 2.39 and 2.33 eV for <sup>1</sup>OAn\*, <sup>1</sup>OPV\*, and <sup>1</sup>PERY\* respectively, depending on the excitation energy used. In addition, a subsequent charge separation (CS) between adjacent chromophores would generate the OAn-OPV<sup>+</sup>-PERY<sup>-</sup>-OPV-OAn or OAn<sup>+</sup>-OPV<sup>-</sup>-PERY-OPV-OAn states. These charge-separated states can decay to the ground state via charge recombination (CR) or evolve to the more distant OAn<sup>+</sup>-OPV-PERY<sup>-</sup>-OPV-OAn state via a charge shift reaction (CSH).

In contrast to the localized singlet-excited states, the energy of the charged separated states is strongly influenced by the polarity of the medium. Equation 1 provides a means of estimating the driving force for charge separation as function of the polarity of the solvent and distance between chromophores.<sup>51</sup>

$$-\Delta G_0 = -e(E_{\text{ox}}(\text{D}) - E_{\text{red}}(\text{A})) + E_{00} + \frac{e^2}{4\pi\epsilon_0\epsilon_s R_{\text{cc}}} + \frac{e^2}{8\pi\epsilon_0} \left( \frac{1}{r^+} + \frac{1}{r^-} \right) \left( \frac{1}{\epsilon_{\text{ref}}} - \frac{1}{\epsilon_s} \right) \quad (1)$$

In this equation,  $E_{\text{ox}}(\text{D})$  and  $E_{\text{red}}(\text{A})$  are the oxidation and reduction potentials of the donor and acceptor molecules or moieties measured in a solvent with relative permittivity  $\epsilon_{\text{ref}}$ ,  $E_{00}$  is the energy of the excited state from which the electron transfer occurs, and  $R_{\text{cc}}$  is the center-to-center distance of the positive and negative charges in the charge separated state. The radii of the positive and negative ions



on the rates of formation (CS1 or CS2) and decay (CR1 and CSH1) of the OAn-OPV<sup>+</sup>-PERY<sup>-</sup>-OPV-OAn charge separated state. At 700 nm, the radical ions of all chromophores absorb, with molar absorption coefficients of  $7 \times 10^3$ ,  $15 \times 10^3$ , and  $\sim 80 \times 10^3 \text{ M}^{-1}\text{cm}^{-1}$  for OAn<sup>+</sup>,<sup>53</sup> OPV<sup>+</sup>,<sup>56</sup> and PERY<sup>-</sup><sup>57</sup> respectively. Therefore, the 700 nm absorption indicates the presence of both the OAn-OPV<sup>+</sup>-PERY<sup>-</sup>-OPV-OAn and OAn<sup>+</sup>-OPV-PERY<sup>-</sup>-OPV-OAn charge-separated states. Finally, at 900 nm the <sup>1</sup>OPV\* and <sup>1</sup>PERY\* singlet states dominate the transient absorption. At this wavelength the radical ions absorb as well, though with much lower molar absorption coefficients than at 700 nm.

**Table 2:** Change in free energy ( $\Delta G_0$ ) with reference to the lowest singlet excited state, reorganization energy ( $\lambda$ ), and barrier ( $\Delta G^\ddagger$ ) determined using equation 1-3.

Reaction (Figure 4)	Solvent	Array 1			Array 2		
		$\Delta G_0$ (eV)	$\lambda$ (eV)	$\Delta G^\ddagger$ (eV)	$\Delta G_0$ (eV)	$\lambda$ (eV)	$\Delta G^\ddagger$ (eV)
CS1	TOL	-0.59	0.35	0.043	-0.41	0.36	0.002
	CB	-1.04	0.77	0.024	-0.94	0.84	0.002
	THF	-1.12	0.84	0.022	-1.03	0.93	0.002
	ODCB	-1.18	0.87	0.026	-1.09	0.97	0.004
CR1	TOL	-1.74	0.35	1.389	-1.92	0.36	1.713
	CB	-1.29	0.77	0.090	-1.39	0.84	0.089
	THF	-1.21	0.84	0.041	-1.30	0.93	0.037
	ODCB	-1.15	0.87	0.023	-1.24	0.97	0.018
CSH1	TOL	+0.08	0.36	0.131	-0.01	0.36	0.086
	CB	-0.11	0.88	0.167	-0.14	0.88	0.158
	THF	-0.15	0.98	0.177	-0.16	0.88	0.148
	ODCB	-0.17	1.02	0.176	-0.18	1.02	0.174
CR2	TOL	-1.81	0.37	1.419	-1.91	0.37	1.605
	CB	-1.18	0.96	0.012	-1.26	0.98	0.020
	THF	-1.07	1.07	0.000	-1.14	1.09	0.001
	ODCB	-0.98	1.16	0.007	-1.06	0.98	0.002

**Array 1 in Toluene.** The transient differential transmission of 1 in toluene at 1450 nm (associated with the OPV<sup>+</sup> radical cation band of the OAn-OPV<sup>+</sup>-PERY<sup>-</sup>-OPV-OAn charge-separated state) of 1 in toluene exhibits a fast rise and a slow decrease after excitation at 450 nm (Figure 5). The rise occurs within 1 ps. The charge-separated state can evolve directly from the <sup>1</sup>OPV\* singlet excited state (CS2) or, via an intermediate energy transfer (ET2), from the <sup>1</sup>PERY\* singlet-excited state (CS1). Since the rate of formation of OPV<sup>+</sup> was independent of the excitation wavelength 450 nm (OPV) or 520 nm (PERY), we favor the latter interpretation. The slow decay of the 1450 nm absorption reveals that the OAn-OPV<sup>+</sup>-PERY<sup>-</sup>-OPV-OAn charge-separated state has a rather long lifetime ( $\sim 370$  ps) in toluene. The transient absorption of the PERY<sup>-</sup> radical anion in 1, recorded at 700 nm essentially superimposes with the temporal evolution of the band at 1450 nm (Figure 5). This confirms that both absorptions originate from the same charged species, *i.e.* OAn-OPV<sup>+</sup>-PERY<sup>-</sup>-OPV-OAn and that no charge shift occurs in toluene. The differential transmission at 900 nm (<sup>1</sup>OPV\* or <sup>1</sup>PERY\*) exhibits an abrupt rise and decay in the first picosecond, corresponding to the formation and decay of the <sup>1</sup>OPV\* (or <sup>1</sup>PERY\*) singlet-excited state (Figure 5). A similar signal is observed when the pump pulse is shifted from 450 to 520 nm to excite the PERY chromophore. The <sup>1</sup>OPV\* and <sup>1</sup>PERY\* states evolve within 1

ps into the OAn-OPV<sup>+</sup>-PERY<sup>-</sup>-OPV-OAn charge-separated state, as evidenced by the 1450 and 700 nm transient absorptions. In accordance, the signal at 900 nm exhibits the same temporal evolution as the 1450 and 700 nm differential transmissions after the initial transient singlet state feature has decayed.

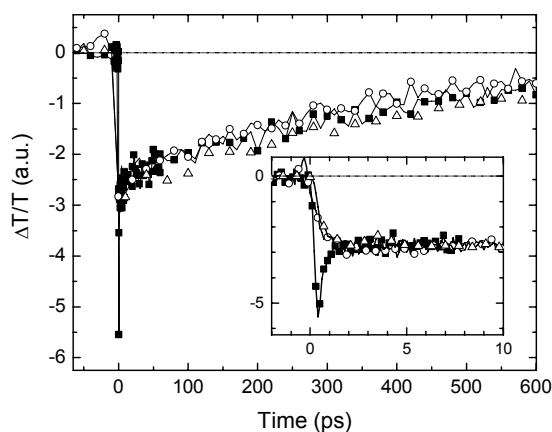


**Figure 5:** Differential transmission dynamics of **1** in toluene monitored at 1450 (open circles), 900 nm (closed squares), and 700 (open triangles) with excitation at 450 nm. The inset shows the differential transmissions at shorter time delays.

**Array 1 in Polar Solvents.** In more polar media than toluene, the OAn-OPV<sup>+</sup>-PERY<sup>-</sup>-OPV-OAn → OAn<sup>+</sup>-OPV-PERY<sup>-</sup>-OPV-OAn charge shift (CSH1) is exergonic for array 1 (Table 2). The differential transmission of the OPV<sup>+</sup> radical cation (at 1450 nm) shows that charge separation to the OAn-OPV<sup>+</sup>-PERY<sup>-</sup>-OPV-OAn state of **1** dissolved in THF also occurs with a high rate ( $k_{CS} > 1 \times 10^{12} \text{ s}^{-1}$ ) but that, compared to toluene, the lifetime of this state is dramatically reduced (12 ps vs. 370 ps) (Figure 6). The same kinetics was observed with excitation at 450 nm (OPV) or 520 nm (PERY). The differential transmission at 700 nm of the PERY<sup>-</sup> radical anion in array 1 in THF reveals the existence of two different time regimes (Figure 6). The first region exhibits a fast rise and decay during the first 30 ps. This initial feature is associated with the formation and decay of the OAn-OPV<sup>+</sup>-PERY<sup>-</sup>-OPV-OAn state and both OPV<sup>+</sup> and PERY<sup>-</sup> radical ions account for the transient absorption at 700 nm. After 30 ps most of the signal has decayed and a less intense, long-lived signal remains, which constitutes the second regime. Because the OPV<sup>+</sup> absorption at 1450 nm has disappeared after 30 ps, the long-lived signal at 700 nm is attributed to the OAn<sup>+</sup>-OPV-PERY<sup>-</sup>-OPV-OAn charge-separated state, formed by an intramolecular redox reaction of the primary charge-separated state. The differential transmission of **1** in THF at 900 nm exhibits the formation and decay of the singlet-excited state of the OPV and PERY chromophores (depending on which has been excited) in the first picosecond after photoexcitation (Figure 6). As in toluene, the singlet-excited state is quenched by charge separation to OAn-OPV<sup>+</sup>-PERY<sup>-</sup>-OPV-OAn.

Even though the rate for the charge shift (CSH1) cannot be extracted from the data, an efficiency of 0.22 in THF can be estimated from the transient absorption at 700 nm, using the molar absorption coefficients of the involved radical ions at this wavelength and assuming that the maximum intensity at 3 ps corresponds to the OAn-OPV<sup>+</sup>-PERY<sup>-</sup>-OPV-OAn state, while at 50 ps the remaining absorption

corresponds to the  $\text{OAn}^+\text{-OPV-PERY}^-\text{-OPV-OAn}$  state only. In chlorobenzene and *o*-dichlorobenzene, solvents of lower and higher polarity than THF, the differential transmissions at 1450, 900 and 700 nm of **1** exhibit similar time profiles as observed in THF. The efficiencies for charge shift are similar in all the polar solvents.

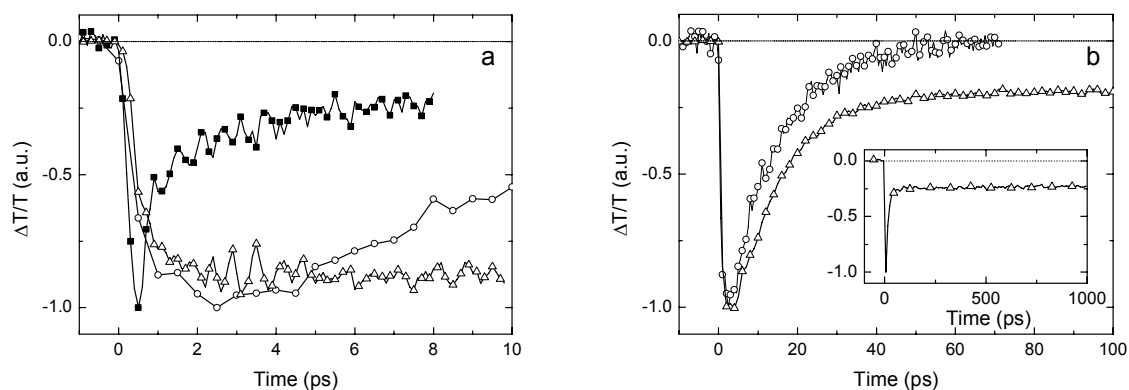


**Figure 6:** Differential transmission dynamics of **1** in THF monitored at 1450 (open circles), 900 (solid squares), and 700 nm (open triangles) with excitation at 450 nm, measured at different time delays. The inset shows the evolution of the 700 nm signal over the first nanosecond.

**Array 2 in Polar Solvents.** In THF, the rate for intramolecular photoinduced charge separation in **2** is ( $k_{\text{CS1}} = 2.9 \times 10^{11} \text{ s}^{-1}$ ) less than in **1** ( $k_{\text{CS1}} = 1 \times 10^{12} \text{ s}^{-1}$ ) as evidenced by the slower grow-in of the differential transmission at 1450 nm of the  $\text{OAn-OPV}^+\text{-PERY}^-\text{-OPV-OAn}$  state (Figure 7). The reduced rate constant for **2** is attributed to a smaller electronic coupling between OPV donor and PERY acceptor in the excited state for this compound in comparison with **1**.

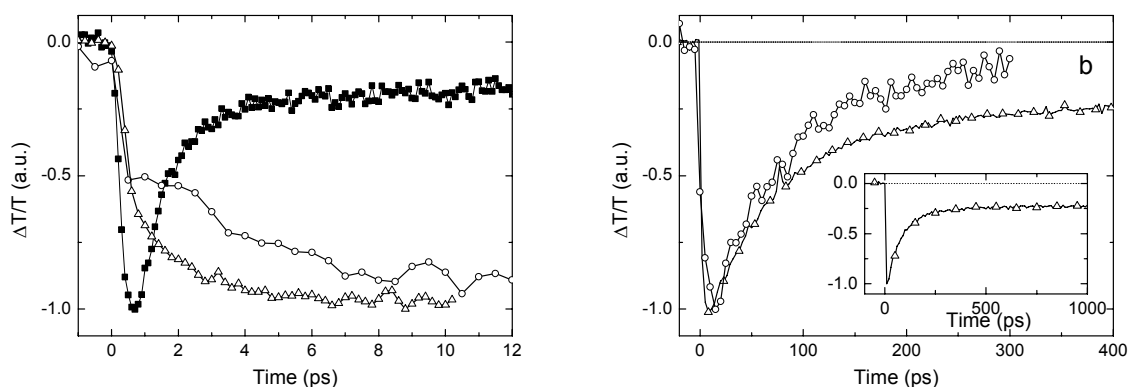


**Figure 7:** Differential transmission dynamics of **2** in THF monitored at 1450 (open circles), 900 (solid squares), and 700 nm (open triangles) with excitation at 455 nm, measured at different time delays. The inset shows the evolution of the 700 nm signal over the first nanosecond.

Likewise, the rate for charge recombination has decreased in **2**, giving the primary charge-separated state in **2** a longer lifetime (100 ps) than in **1** (12 ps). The efficiency of the intramolecular charge shift

generating the  $\text{OAn}^+\text{-OPV-PERY}^-\text{-OPV-OAn}$  state in 2 has increased to 0.28, as inferred from the transient absorption at 700 nm (Figure 7). Similar to 1, the efficiency for the charge shift in 2 is only weakly dependent on the solvent (THF, chlorobenzene, or *o*-dichlorobenzene).

Although the kinetics of the charge separation and recombination reaction are similar in all the studied polar solvent, a remarkable result is observed when array 2 is studied in the apolar solvent toluene (Figure 8). From the results obtained using absorption spectroscopy it is clear that array 2 is aggregated in toluene. Whereas the charge-separated state is expected to be higher in energy in apolar solvents, a considerable increase in the rate for both the charge separation ( $k_{\text{CS}} > 1 \times 10^{12} \text{ s}^{-1}$ ,  $\tau_{\text{CS}} < 1$  ps) and recombination ( $k_{\text{CR}} = 2.2 \times 10^{10} \text{ s}^{-1}$ ,  $\tau_{\text{CR}} = 46$  ps) reaction is observed in toluene. This remarkable difference can be a result of the aggregation of the OPV and PERY chromophores (Figure 3) in a face-to-face fashion. The influence of the chromophore packing will be discussed in more detail in Chapter 5.

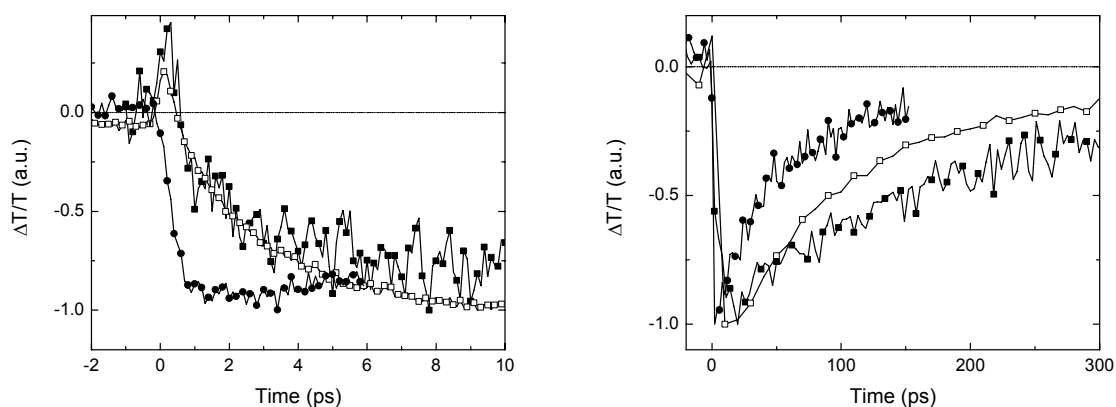


**Figure 8:** Transient photoinduced absorption traces for 2 in ODCB (solid squares), THF (open squares) and toluene (solid circles) recorded at 1450 nm.

Because the 700 nm signal of the  $\text{OAn}^+\text{-OPV-PERY}^-\text{-OPV-OAn}$  state does not decay within the first nanosecond, we used nanosecond transient spectroscopy to obtain information on the rate of charge recombination (CR2). Figure 9a shows the transient spectra in the 480-850 nm region obtained after exciting 1 in ODCB with a 4 ns pulse at 450 nm. The spectra show the well-defined absorption features corresponding to the  $\text{PERY}^-$  radical anion at 710 and 800 nm, and the associated bleaching in the visible range at 495 and 532 nm. The absorption of the  $\text{OAn}^+$  radical cation cannot be clearly distinguished because its electronic transitions overlap with those of the  $\text{PERY}^-$  radical anion and are less intense ( $\epsilon(860 \text{ nm}) \approx 15 \times 10^3 \text{ M}^{-1} \text{ cm}^{-1}$  for  $\text{OAn}^+$ , vs  $\epsilon(800 \text{ nm}) \approx 60 \times 10^3 \text{ M}^{-1} \text{ cm}^{-1}$  for  $\text{PERY}^-$ ). The signals can be observed into the microsecond time domain and demonstrate the longevity of the  $\text{OAn}^+\text{-OPV-PERY}^-\text{-OPV-OAn}$  state.

The decay of the signals under these conditions does not follow first-order kinetics and, hence, it is not possible to determine a monomolecular lifetime. This observation is consistent with the fact that at the used concentration ( $5 \times 10^{-5} \text{ M}$ ) the lifetime of the charge-separated state is much longer than the average time between diffusion limited collisions, which is on the order of  $\sim 40$  ns.

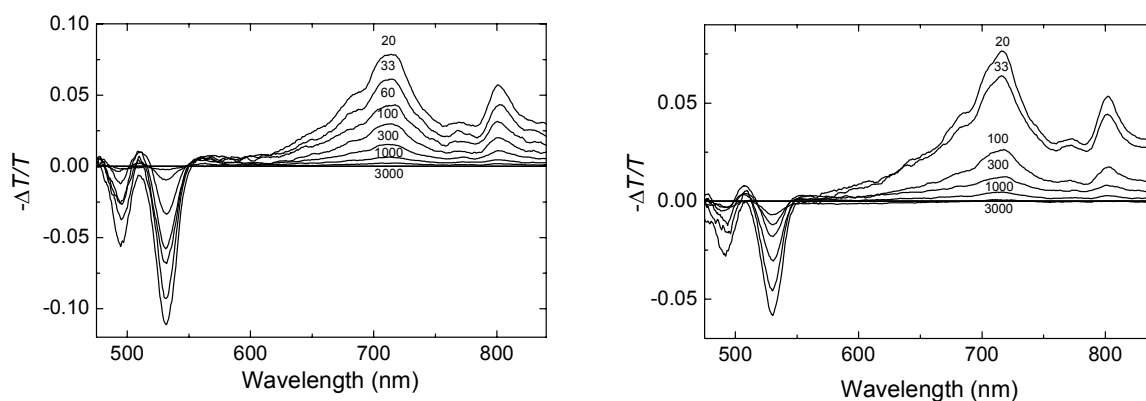


**Figure 9:** Differential transmission of 1 (left) and 2 (right) in *o*-dichlorobenzene solution ( $5 \times 10^{-5} M$ ), measured at room temperature with photoexcitation at 450 nm with 4 ns pulses. The absorption bands of the  $PERY^{\cdot-}$  radical anion can be observed at 710 and 800 nm. The numbers indicate the time delay in nanoseconds after the excitation pulse.

### 4.3 Discussion

Marcus theory provides an estimate for the free energy barrier ( $\Delta G^\ddagger$ ) for electron transfer based on the change in free energy ( $\Delta G_0$ ) and the reorganization energy ( $\lambda$ ) via:

$$\Delta G^\ddagger = \frac{(\Delta G_0 + \lambda)^2}{4\lambda} \quad (2)$$

The reorganization energy consists of an internal contribution ( $\lambda_i$ ) and a solvent term ( $\lambda_s$ ), which can be approximated via the Born-Hush approach to give after summation, with  $n$  the index of refraction:

$$\lambda = \lambda_i + \lambda_s = \lambda_i + \frac{e^2}{4\pi\epsilon_0} \left( \frac{1}{2} \left( \frac{1}{r^+} + \frac{1}{r^-} \right) - \frac{1}{R_{cc}} \right) \left( \frac{1}{n^2} - \frac{1}{\epsilon_s} \right) \quad (3)$$

The rate constants for the different processes, are not only a function of the energy barrier  $\Delta G^\ddagger$ , but also of the reorganization energy ( $\lambda$ ) and the electronic coupling ( $V$ ) between donor and acceptor in the excited state according to:

$$k = \left( \frac{4\pi^2}{h^2 \lambda k_B T} \right)^{1/2} V^2 \exp \left[ -\frac{(\Delta G_0 + \lambda)^2}{4\lambda k_B T} \right] \quad (4)$$

The values of  $\Delta G_0$ ,  $\lambda$ , and  $\Delta G^\ddagger$  calculated with equations 1 to 3 are collected in Table 2. The initial charge separation (CS1) occurs close to the Marcus optimal region because  $-\Delta G_0$  and  $\lambda$  are similar and, hence,  $\Delta G^\ddagger \approx 0$ . In such situation, the reaction rate is governed by the electronic coupling  $V$



between the donor and acceptor and the polarity of the solvent becomes less important. The electronic coupling depends on the nature of the spacer and on the separation of donor and acceptor via  $V^2 = V_0^2(R_0) \exp(-\beta(R_{cc} - R_0))$ , with  $R_0$  the contact distance. The electronic coupling in array 1 is likely high due to the semi-conjugated fashion by which the OPV and the PERY chromophores are linked, although the frontier molecular orbitals of the perylene bisimide have nodes at the imide nitrogen. The strong coupling explains the high rate constants for charge separation in 1 in all solvents ( $k_{CS1} > 1 \text{ ps}^{-1}$ ). In contrast, charge recombination (CR1) in OAn-OPV<sup>+</sup>-PERY<sup>-</sup>-OPV-OAn is in the Marcus inverted region ( $-\Delta G_0 > \lambda$ ) for all solvents (Table 2) and, consequently, the barrier for charge recombination is reduced with solvent polarity. In toluene, the most apolar solvent used, the energy barrier for the recombination is remarkably high and consistently a rather long lifetime (370 ps) of the OAn-OPV<sup>+</sup>-PERY<sup>-</sup>-OPV-OAn charge-separated state has been observed. In the more polar solvents, the calculated energy barrier is significantly less and recombination is expected to be much faster. This explains, to some extent, the 12 ps lifetime of the OAn-OPV<sup>+</sup>-PERY<sup>-</sup>-OPV-OAn charge-separated state in THF.

The charge shift occurs in the normal region ( $-\Delta G_0 < \lambda$ ) and is energetically less favorable than charge recombination (Table 2). Consequently, the energy barrier is higher. These two facts rationalize that the charge shift is slower than the charge recombination, although the actual rates will also strongly depend on the electronic coupling  $V$ , which is not accounted for in this analysis. In a study on a related system with C<sub>60</sub> as an acceptor instead of perylene bisimide, (OAn-OPV-C<sub>60</sub>),<sup>53</sup> it has been shown recently that increasing the lifetime of the primary charge-separated state is beneficial for the slower charge shift process to compete. In principle this condition is nicely fulfilled for array 1 in toluene but here the driving force for the charge shift is close to zero and the charge shift does not occur. Nevertheless, in polar solvents, where charge recombination is accelerated, the charge shift can be observed. The efficiency of the charge shift is similar in all polar solvents, consistent with the small variation in energy barriers for the charge shift (Table 2).

The rate for charge separation (CS1) is smaller for 2 than for 1, despite the similarly low energy barrier (Table 2). The reason for this difference is the type of linker between PERY and OPV units. In 2, electron transfer must occur over a longer distance, through space or through the saturated spacer by a superexchange mechanism, resulting in a reduced electronic coupling. The same effect occurs in the charge recombination and explains the longer lifetime of the OAn-OPV<sup>+</sup>-PERY<sup>-</sup>-OPV-OAn state of 2 in THF (100 ps) compared to that of 1 (12 ps). It can be assumed that slower charge recombination increases the efficiency for the charge shift in 2 with respect to 1.

Both for 1 and 2, the product of the charge-shift, OAn<sup>+</sup>-OPV-PERY<sup>-</sup>-OPV-OAn, has a long lifetime, even though the charge recombination from this state (CR2) is almost barrierless (Table 2). The explanation for the longevity is the large distance between the OAn<sup>+</sup> and the PERY<sup>-</sup> redox sites reduces their electronic coupling and hampers charge recombination (CR2) from the OAn<sup>+</sup>-OPV-PERY<sup>-</sup>-OPV-OAn state, resulting in a long lifetime.

#### 4.4 Conclusions

Two multichromophoric arrays 1 and 2 have been synthesized by covalently linking OAn, OPV, and PERY chromophores into a symmetrical OAn-OPV-PERY-OPV-OAn configuration. Sequential photoinduced intramolecular charge separation occurs in these multichromophoric arrays. The electron

transfer reactions start with forming the primary  $\text{OAn}^+\text{-OPV}^+\text{-PERY}^-\text{-OPV-OAn}$  charge-separated state. The rate for initial charge separation is independent of the chromophore (OPV or PERY) that is excited. This indicates that charge separation originates from the  $^1\text{PERY}^*$  state, *i.e.* CS1 rather than CS2 (Figure 4), and that it is preceded by an ultrafast  $^1\text{OPV} \rightarrow ^1\text{PERY}^*$  energy transfer (ET1) if the OPV is excited initially. The primary charge-separated state decays via charge recombination (CR1) or produces the secondary, more stable  $\text{OAn}^+\text{-OPV-PERY}^-\text{-OPV-OAn}$  charge-separated state via an intramolecular redox reaction, or charge shift (CSH1).

Regardless of the polarity of the solvent, the intramolecular charge separation is extremely fast in 1, because it occurs in the optimal region ( $-\Delta G_0 \sim \lambda$ ). Charge recombination occurs in the Marcus inverted region ( $-\Delta G_0 > \lambda$ ) and is fast in polar solvents, but remarkably slow in toluene. Both charge separation and recombination are slowed down in 2, because the saturated spacer reduces the electronic coupling between the OPV donor and PERY acceptor in the excited state. The charge shift that generates the  $\text{OAn}^+\text{-OPV-PERY}^-\text{-OPV-OAn}$  state competes with charge recombination and occurs in THF with an efficiency of 0.22 for 1 and 0.28 for 2. The higher efficiency for 2 is ascribed to the reduced rate constant for charge recombination from the primary charge-separated state in 2. However, the increase seems a bit small if the almost ten times slower recombination rate for compound 2 is taking into account. Compared to the lifetime of the  $\text{OPV}^+\text{-PERY}^-\text{-OPV}$  charge-separated state in triads (11 ps in THF),<sup>47</sup> the more stable  $\text{OAn}^+\text{-OPV-PERY}^-\text{-OPV-OAn}$  state has a lifetime that is many orders of magnitude longer as it can be observed into the microsecond domain in THF at room temperature.

## 4.5 Experimental Section

**Materials.** The synthesis of 1<sup>58</sup>, 2<sup>58</sup>, 3<sup>47</sup>, 4<sup>48</sup>, OPV<sup>59</sup>, OAn<sup>53</sup>, and PERY<sup>60</sup> has been reported previously.

**Spectroscopic Techniques.** The UV/Vis absorption spectra were recorded on a Perkin Elmer Lambda 900 spectrophotometer. Fluorescence spectra were recorded on an Edinburgh Instruments FS920 double-monochromator spectrometer equipped with a Peltier-cooled red-sensitive photomultiplier. Nanosecond pump-probe spectra were recorded by exciting the sample with pulses at 450 nm (pulse width 4 ns, repetition rate 10 Hz) obtained from an optical parametric oscillator (OPO), pumped by the third harmonic of a Nd-YAG laser. An intensified CCD camera was used to record the transmission of a tungsten-halogen probe light through the sample after dispersion by a spectrograph. The signal acquisition by the CCD camera was electronically gated at different time delays after the excitation pulse, using a gate width of about a tenth of the delay time. To obtain differential transmission spectra, the reference transmission was recorded at a 20 ms delay.

A detailed description of the setups used for electrochemical measurements and femtosecond transient absorption spectroscopy can be found in Chapter 2.

## 4.6 References

- 1 Wasielewski, M. R. *Chem. Rev.* **1992**, *92*, 435.
- 2 Gust, D.; Moore, T. A.; Moore, A. L. *Acc. Chem. Res.* **1993**, *26*, 198.
- 3 Gust, D.; Moore, T. A.; Moore, A. L. *Acc. Chem. Res.* **2001**, *34*, 40.
- 4 Guldi, D. M. *Chem. Soc. Rev.* **2002**, *31*, 22.

- 5 Imahori, H.; Mori, Y.; Matano, Y. *J. Photochem. Photobiol. C* **2003**, *4*, 51.
- 6 Gust, D.; Moore, T. A.; Makings, L. R.; Liddell, P. A.; Nemeth, G. A.; Moore, A. L. *J. Am. Chem. Soc.* **1986**, *108*, 8028.
- 7 Sakata, Y.; Tatemitsu, H.; Bienvenue, E.; Seta, P. *Chem. Lett.* **1988**, 1625.
- 8 Collin, J. P.; Guillerez, S.; Sauvage, J.-P.; Barigelletti, F.; De Cola, L.; Flamigni, L.; Balzani, V. *Inorg. Chem.* **1991**, *30*, 4230.
- 9 Osuka, A.; Najata, T.; Maruyama, K.; Mataga, N.; Asahi, T.; Yamazaki, I.; Nishimura, Y. *Chem. Phys. Lett.* **1991**, *185*, 88.
- 10 Mecklenburg, S. L.; Peek, B. M.; Erickson, B. W.; Meyer, T. J. *J. Am. Chem. Soc.* **1991**, *113*, 8540.
- 11 Larson, S. L.; Cooley, L. F.; Elliott, C. M.; Kelley, D. F. *J. Am. Chem. Soc.* **1992**, *114*, 9504.
- 12 Brouwer, A. M.; Mout, R. D.; Maassen, P. H.; Van den Brink, M.; van Ramesdonk, H. J.; Verhoeven, J. W.; Jonker, S. A.; Warman, J. M. *Chem. Phys. Lett.* **1991**, *186*, 481.
- 13 Brouwer, A. M.; Eijkelhoff, C.; Willemse, R. J.; Verhoeven, J. W.; Schuddeboom, W.; Warman, J. M. *J. Am. Chem. Soc.* **1993**, *115*, 2988.
- 14 Wasielewski, M. R.; Gaines, G. L., III; Wiederrecht, G. P.; Svec, W. A.; Niemczyk, M. P. *J. Am. Chem. Soc.* **1993**, *115*, 10442.
- 15 Gust, D.; Moore, T. A.; Moore, A. L. *J. Am. Chem. Soc.* **1993**, *115*, 11141.
- 16 Ohkohchi, M.; Takahashi, A.; Mataga, N.; Okada, T.; Osuka, A.; Yamada, H.; Maruyama, K. *J. Am. Chem. Soc.* **1993**, *115*, 12137.
- 17 Osuka, A.; Zhang, R. P.; Maruyama, K.; Ohno, T.; Nozaki, K. *Bull. Chem. Soc. Jpn.* **1993**, *66*, 3773.
- 18 Willemse, R. J.; Verhoeven, J. W.; Brouwer, A. M. *J. Phys. Chem.* **1995**, *99*, 5753.
- 19 Liddell, P. A.; Kuciauskas, D.; Sumida, J. P.; Nash, B.; Nguyen, D.; Moore, A. L.; Moore, T. A.; Gust, D. *J. Am. Chem. Soc.* **1997**, *119*, 1400.
- 20 Imahori, H.; Yamada, K.; Hasegawa, M.; Taniguchi, S.; Okada, T.; Sakata, Y. *Angew. Chem., Int. Ed.* **1997**, *36*, 2626.
- 21 Gosztola, D.; Niemczyk, M. P.; Wasielewski, M. R. *J. Am. Chem. Soc.* **1998**, *120*, 5118.
- 22 Kuciauskas, D.; Liddell, P. A.; Lin, S.; Johnson, T. E.; Weghorn, S. J.; Lindsey, J. S.; Moore, A. L.; Moore, T. A.; Gust, D. *J. Am. Chem. Soc.* **1999**, *121*, 8604.
- 23 Imahori, H.; Yamada, H.; Nishimura, Y.; Yamazaki, I.; Sakata, Y. *J. Phys. Chem. B* **2000**, *104*, 2099.
- 24 Miller, M. A.; Lammi, R. K.; Prathapan, S.; Holten, D.; Lindsey, J. S. *J. Org. Chem.* **2000**, *65*, 6634.
- 25 Hayes, R. T.; Wasielewski, M. R.; Gosztola, D. *J. Am. Chem. Soc.* **2000**, *122*, 5563.
- 26 Imahori, H.; Guldi, D. M.; Tamaki, K.; Yoshida, Y.; Luo, C.; Sakata, Y.; Fukuzumi, S. *J. Am. Chem. Soc.* **2001**, *123*, 6617.
- 27 Ambroise, A.; Kirmaier, C.; Wagner, R. W.; Loewe, R. S.; Bocian, D. F.; Holten, D.; Lindsey, J. S. *J. Org. Chem.* **2002**, *67*, 3811.
- 28 Sánchez, L.; Pérez, I.; Martín, N.; Guldi, D. M. *Chem. Eur. J.* **2003**, *9*, 2457.
- 29 Andersson, M.; Sinks, L. E.; Hayes, R. T.; Zhao, Y.; Wasielewski, M. R. *Angew. Chem., Int. Ed.* **2003**, *42*, 3139.
- 30 Sariciftci, N. S.; Smilowitz, L.; Heeger, A. J.; Wudl, F. *Science* **1992**, *258*, 1474.
- 31 Janssen, R. A. J.; Christiaans, M. P. T.; Hare, C.; Martín, N.; Sariciftci, N. S.; Heeger, A. J.; Wudl, F. *J. Chem. Phys.* **1995**, *103*, 8840.
- 32 Nogueira, A. F.; Montanari, I.; Nogueira, A. F.; Nelson, J.; Durrant, J. R.; Winder, C.; Loi, M. A.; Sariciftci, N. S.; Brabec, C. *J. Phys. Chem. B* **2003**, *107*, 1567.
- 33 Offermans, T.; Meskers, S. C. J.; Janssen, R. A. J. *J. Chem. Phys.* **2003**, *119*, 10924.

- 34 Nierengarten, J.-F.; Eckert, J.-F.; Nicoud, J.-F.; Ouali, L.; Krasnikov, V.; Hadziioannou, G. *Chem. Commun.* **1999**, 617.
- 35 Eckert, J.-F.; Nicoud, J.-F.; Nierengarten, J.-F.; Liu, S.-G.; Echegoyen, L.; Barigelletti, F.; Armaroli, N.; Ouali, L.; Krasnikov, V.; Hadziioannou, G. *J. Am. Chem. Soc.* **2000**, *122*, 7467.
- 36 Peeters, E.; van Hal, P. A.; Knol, J.; Brabec, C. J.; Sariciftci, N. S.; Hummelen, J. C.; Janssen, R. A. J. *J. Phys. Chem. B* **2000**, *104*, 10174.
- 37 El-ghayoury, A.; Schenning, A. P. J. H.; van Hal, P. A.; Van Duren, J. K. J.; Janssen, R. A. J.; Meijer, E. W. *Angew. Chem., Int. Ed.* **2001**, *40*, 3660.
- 38 Marcos Ramos, A.; Rispens, M.T.; Van Duren, J. K. J.; Hummelen, J. C.; Janssen, R. A. J. *J. Am. Chem. Soc.* **2001**, *123*, 6714.
- 39 De Boer, B.; Stalmach, U.; Van Hutten, P. F.; Melzer, C.; Krasnikov, V. V.; Hadziioannou, G. *Polymer* **2001**, *42*, 9097.
- 40 Wöhrle, D.; Meissner, D. *Adv. Mater.* **1991**, *3*, 129.
- 41 Schlettwein, D.; Wöhrle, D.; Karmann, E.; Melville, U. *Chem. Mater.* **1994**, *6*, 3.
- 42 Ferrere, S.; Zaban, A.; Gregg, B. A. *J. Phys. Chem. B* **1997**, *101*, 4490.
- 43 Schmidt-Mende, L.; Fechtenkötter, A.; Müllen, K.; Moons, E.; Friend, R. H.; MacKenzie, J. D. *Science* **2001**, *293*, 1119.
- 44 Dittmer, J. J.; Marseglia, E. A.; Friend, R. H. *Adv. Mater.* **2000**, *12*, 1270.
- 45 Dittmer, J. J.; Petritsch, K.; Marseglia, E. A.; Friend, R. H.; Rost, H.; Holmes, A. B. *Synth. Met.* **1999**, *102*, 879.
- 46 Angadi, M. A.; Gosztola, D.; Wasielewski, M. R. *J. Appl. Phys.* **1998**, *83*, 6187.
- 47 Peeters, E.; Van Hal, P. A.; Meskers, S. C. J.; Janssen, R. A. J.; Meijer, E. W. *Chem. Eur. J.* **2002**, *8*, 4470.
- 48 Asha, S.; Schenning, A. P. H. J.; Meijer, E. W. *Chem. Eur. J.* **2002**, *8*, 3353.
- 49 Schenning, A. P. H. J.; Van Herrikhuyzen, J.; Jonkheijm, P.; Chen, Z.; Würthner, F.; Meijer, E. W. *J. Am. Chem. Soc.* **2002**, *124*, 10252.
- 50 Neuteboom, E. E.; Meskers, S. C. J.; Van Hal, P. A.; Van Duren, J. K. J.; Meijer, E. W.; Dupin, H.; Pourtois, G.; Cornil, J.; Lazzaroni, R.; Brédas, J.-L.; Beljonne, D.; Janssen, R. A. J. *J. Am. Chem. Soc.* **2003**, *125*, 8625
- 51 Weller, A. *Z. Phys. Chem. Neue Folge* **1982**, *133*, 93.
- 52 Van Hal, P. A.; Beckers, E. H. A.; Peeters, E.; Apperloo, J. J.; Janssen, R. A. J. *Chem. Phys. Lett.* **2000**, *328*, 403.
- 53 Marcos Ramos, A.; Meskers, S. C. J.; Van Hal, P. A.; Knol, J.; Hummelen, J. C.; Janssen, R. A. J. *J. Phys. Chem. A* **2003**, *107*, 9269.
- 54 The positive charge is assumed to be located on the phenyl ring closest to the PERY moiety for the calculation of the OAn-OPV<sup>+</sup>-PERY<sup>-</sup> charge-separated state. See reference 36 for more details.
- 55 The assumption that charges are located at the centers of the chromophores is of course a simplification of the actual situation in which charges are likely to be strongly delocalized.
- 56 The molar absorption coefficients of the OPV chromophore at 700 and 900 nm have been extracted from the photoinduced absorption spectrum of a OPV/MP-C<sub>60</sub> (1:1) mixture in *o*-dichlorobenzene reported in reference 52, using the extinction coefficients of the MP-C<sub>60</sub> reported in Guldi, D. M.; Prato, M. *Acc. Chem. Res.* **2000**, *33*, 695.
- 57 Salbeck, J. *J. Electroanal. Chem.* **1992**, *340*, 169.

- 58 Marcos Ramos, A.; Beckers, E. H. A.; Offermans, T.; Meskers, S. C. J.; Janssen, R. A. J. *J. Phys. Chem. A* **2004**, *108*, 8201.
- 59 Peeters, E.; Janssen, R. A. J.; Meskers, S. C. J.; Meijer, E. W. *Polym. Prepr.* **1999**, *40*, 519.
- 60 Demmig, S.; Langhals, H. *Chem. Ber.* **1988**, *121*, 225.

# The Influence of Intermolecular Orientation on the Charge Transfer Kinetics in Self-assembled Oligo(*p*-phenylene vinylene) – Perylenebisimide Arrays\*

### *Abstract*

*The kinetics of photoinduced charge transfer reactions in covalently linked donor-acceptor molecules often undergo dramatic changes when these molecules self assemble from a molecular dissolved state into a nanoaggregate. Frequently, the origin of these changes is only partially understood. In this chapter the intermolecular spatial organization of three homologous arrays, consisting of a central perylene bisimide (PERY) acceptor moiety and two oligo(*p*-phenylene vinylene) (OPV) donor units is described. In these nanoaggregates both the face-to-face (H-type) and the slipped (J-type) stacking of the OPV and PERY chromophores can be identified. For the J-type aggregates, short intermolecular OPV-PERY distances are created that give rise to a charge-transfer absorption band. The proximity of the donor and acceptor groups in the J-type aggregates enables a highly efficient photoinduced charge separation with a rate ( $k_{cs} > 10^{12} \text{ s}^{-1}$ ) that significantly exceeds the rate of the intramolecular charge transfer of the same compounds when molecularly dissolved, even in the most polar media. In the H-type aggregates, on the other hand, the intermolecular OPV-PERY distance is not reduced compared to the intramolecular separation and, hence, the rates of the electron transfer reactions are not significantly affected compared to the molecular dissolved state. Similar to the forward electron transfer, the kinetics of the charge recombination in the aggregated state can be understood by considering the different inter-chromophoric distances that occur in the H and J-type aggregates. These results provide a first consistent rationalization of the remarkable differences that are observed for photoinduced charge transfer reactions of donor-acceptor compounds in molecularly-dissolved versus aggregated states.*

---

\* Beckers, E. H. A.; Meskers, S. C. J.; Schenning, A. P. H. J.; Chen, Z.; Würthner, F.; Marsal, P.; Beljonne, D.; Cornil, J.; Janssen, R. A. J. *Journal of the American Chemical Society*, in press.

## 5.1 Introduction

Photoinduced charge-transfer in donor-acceptor molecules is fairly well understood, in particular for covalently linked dyads in solution.<sup>1,2</sup> In molecular dyads, triads, tetrads, and more extended arrays containing different photo- and redox-active chromophores, photoinduced charge separation can result in long-lived charge-separated states. Various carefully designed energy and electron transfer cascades that mimic the steps occurring in natural photosynthesis have been synthesized and investigated in great detail.<sup>3,4</sup> In general, the energetics and kinetics of the formation of these charge-separated states can be adequately described by theories of Marcus and Jortner when taking into account the orientation, distance, and nature of the linker between the donor and acceptor chromophores.<sup>5,6</sup>

In contrast, characterization and insight into photoinduced electron transfer in self-assembled nanoscale (10-100 nm) architectures is only at its beginning. Of course it is well established that chlorophylls work in concert in photosynthesis to funnel light energy to the reaction center prior to a cascade of electron transfer reactions. However, collective behavior of chromophores related to photoinduced electron transfer has not received much attention in artificial systems. It is therefore interesting to study photoinduced charge transfer and recombination in donor-acceptor molecules that are able to self-organize into nanoaggregates or stacks in solution, either by lowering the temperature or by changing the polarity of the solvent. The self-assembly enables the controlled growth of nanoaggregates and provides a unique approach to gain insight in the transition in photophysical properties when single dyad molecules are transformed into a material. Ultimately, these insights may provide new routes towards charge separation, energy conversion, and storage assemblies.

Various recent results indicate that the photophysics of nanoassemblies, in which multiple covalently linked donor and acceptor systems are interacting with each other, can be dramatically different when compared to those of isolated compounds, however, the reasons for these differences are not always well understood. Wasielewski *et al.* reported ordered nanoparticles of tetrakis(peryene bisimide)-porphyrins in which donors and acceptors are stacked.<sup>7</sup> The forward electron transfer in these photofunctional nanoparticles is faster and the recombination slower compared to model compounds that do not form these aggregates under similar conditions. In this system, the stabilization of the charge-separated state occurs via migration of charges between closely coupled redoxactive groups. Another example shows the forward electron transfer in oligo(*p*-phenylene vinylene)-fullerene dyads can be up to an order of magnitude faster in thin films than the same reaction in the most polar solvents.<sup>8</sup> Taking into account that organic solids have a much lower relative dielectric constant (typically  $\epsilon_r = 3$  to 4) compared to the most polar solvents used ( $\epsilon_r = 25$ ), the increased transfer speed cannot be explained by the polarity. A similar order of magnitude increase was found in fine particles of oligothiophene-fullerene dyads when compared to benzonitrile solution.<sup>9</sup> For perylene bisimide systems rate constants for charge separation exceeding  $10^{12} \text{ s}^{-1}$  have been observed in aggregated structures where the formation of a charge separated state is not energetically favorable in the molecularly dissolved state.<sup>10-12</sup> Each of these examples demonstrates that aggregate formation leads to unexpected kinetics for photoinduced charge separation.

In order to rationalize some of the dramatic changes that occur in the photophysics of covalently-linked donor-acceptor molecules upon aggregation, the intermolecular distance between the donor and

acceptor chromophores in self-assembled aggregates is correlated with the kinetics of the photoinduced charge separation and recombination reactions. The comparison of molecular dissolved and aggregated solutions offers the opportunity to directly differentiate between intramolecular and intermolecular effects. For this purpose, three related covalently linked oligo(*p*-phenylene vinylene) (OPV) – perylene bisimide (PERY) arrays are studied here (Figure 1). These arrays were considered as an appropriate starting point for this study because the photoinduced charge transfer between these chromophores in solution has been extensively studied,<sup>13-17</sup> and the individual chromophores are known to form supramolecular aggregates in a variety of apolar solvents.<sup>12,18,19</sup> Previous studies on aggregates containing OPV<sup>20,21</sup> or PERY<sup>7,22,23</sup> moieties have revealed that stacking provides the possibility for excitations to hop to different sites within the same supramolecular structure or to delocalize over several chromophores.

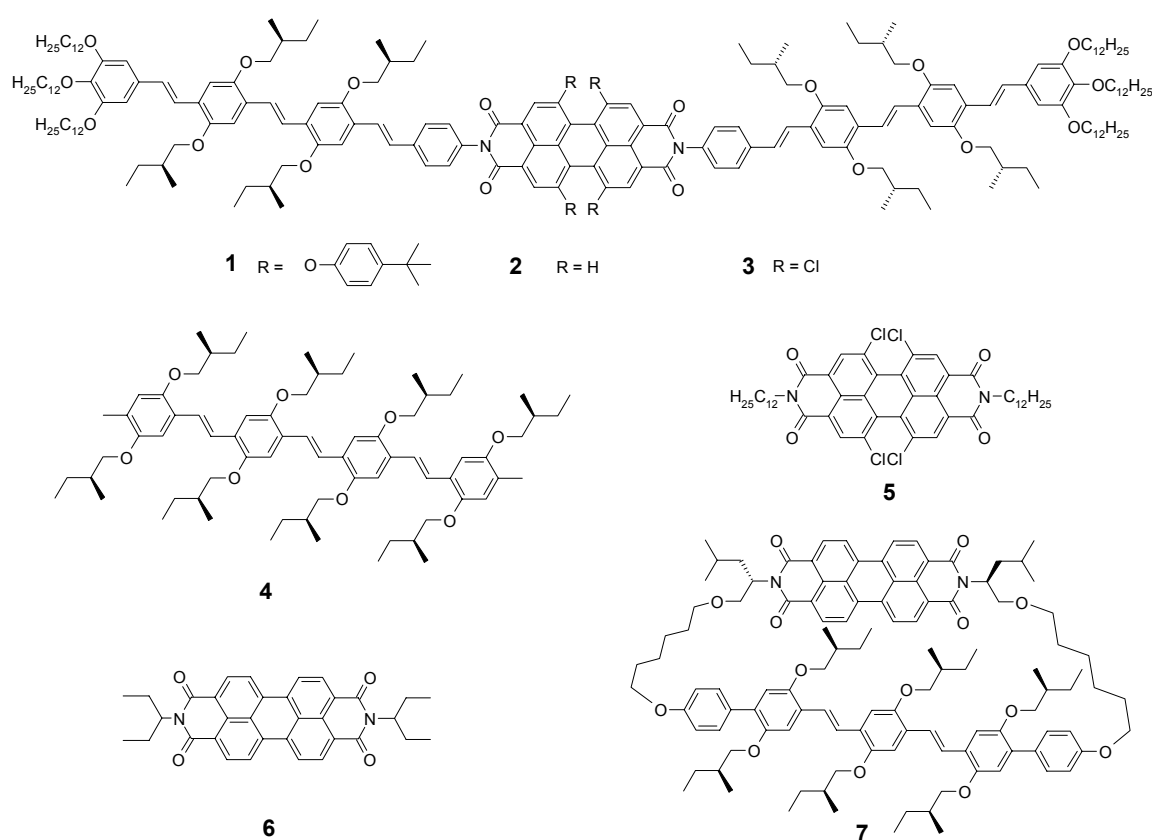


**Figure 1:** Studied OPV-PERY-OPV arrays 1, 2, 3 together with the OPV (4) and perylene bisimide (5, 6) reference compounds and the cyclic OPV-PERY dimer 7.

The three homologous OPV-PERY-OPV arrays used in this study consist of the same donor and acceptor building blocks, the only difference being the four substituents on the bay position of the perylene bisimide moiety. For compound 1,<sup>12</sup> these are *tert*-butylphenoxy substituents, whereas for compounds 2<sup>13</sup> and 3<sup>15</sup> the substituents are respectively hydrogen and chlorine. The different substituents influence the acceptor part of the system.<sup>15</sup> Moreover, the planarity of the perylene bisimide changes with the bay substituents. An almost flat conformation is expected for the hydrogen-substituted perylene bisimide moiety while torsion angles of 25° and 37° have been observed for



phenoxy and chlorine substituted perylene bisimides as a result of the increased steric hindrance.<sup>24-27</sup> This twisting is expected to affect the packing of the compounds in aggregates, while the differences in acceptor strength influence intermolecular donor-acceptor interactions.

The insights into the supramolecular organization, as inferred from optical absorption spectra and Molecular Mechanics calculations, provide a consistent description of the remarkable differences between the picosecond charge transfer kinetics in OPV-PERY-OPV arrays in molecularly-dissolved versus aggregated states when the distance between chromophores is the essential parameter.

## 5.2 Results and Discussion

**Intermolecular Organization in the Aggregates from Absorption Spectroscopy.** To understand the differences in photophysics between isolated molecules and molecules in nanoaggregates or thin films, knowledge and control over the mesoscopic ordering of the molecules is crucial, but in general difficult to obtain.<sup>4,26,28-30</sup> Although in favorable cases, techniques like x-ray diffraction (XRD), small angle neutron scattering (SANS), transmission electron microscopy (TEM), or atomic force microscopy (AFM) can be used to determine the supramolecular structure of aggregates,<sup>7,31-33</sup> this proved to be cumbersome for the present compounds. Among others, the concentration, surface interaction, temperature, and processing conditions often have an extremely large influence on the structures obtained. To enable a direct comparison of the structural information and the photophysics, both should preferably be studied under identical conditions. Therefore, structural analysis focuses on to the detailed analysis of the absorption spectra of the aggregated OPV-PERY-OPV arrays as dilute solutions in methylcyclohexane (MCH).

The UV/Vis absorption spectra of the arrays 1-3 in MCH are characterized by a strong band of the OPV units centered at ~425 nm and one or more vibronic transitions of the PERY core at higher wavelengths. The distinct changes that can be observed in the spectra recorded at 20 °C and 90 °C are consistent with the presence of aggregates at low temperature (Figure 2). Upon heating a solution of 1 in MCH from 20 °C to 90 °C a shift of the perylene bisimide maximum from 580 nm to 565 nm is observed. This shift is typical of the dissociation of the supramolecular structure as a result of the increased temperature.<sup>12</sup> Based on the red shift of the perylene bisimide absorption maximum of 1 upon aggregation, it is here proposed that a J-type aggregate (Figure 3) is obtained.<sup>34,35</sup> The OPV absorption shows a small (424 to 432 nm) red shift in the same temperature range.

For 3 similar red shifts are observed; the perylene bisimide absorption maximum shifts from 513 nm for molecularly dissolved species at elevated temperature to 528 nm for the aggregated species at room temperature, while the OPV unit shifts from 428 to 446 nm. This implies that for 3 a J-type structure may also exist. For 2, the changes in the spectra seem slightly more complex. Compared to the sharp perylene bisimide vibronic at 515 nm, a new (weak) band appears at ~550 nm upon aggregation while at the same time the intensity at ~470 nm is increased. Such a blue shift of the absorption maximum and an accompanying low-intensity band at lower energy is typical for the formation of H-type aggregates formed. In agreement with previous observations, the differences in aggregation observed for 1 and 3 versus 2 are consistent with the fact that the expected increased bulkiness and twist induced by the *tert*-butylphenoxy and chlorine substituents for 1 and 3,<sup>24-27,35</sup> hamper a face-to-face packing of

these chromophores, as required for H-type aggregation. It should be noted that for all aggregates some degree of rotational displacement may also be present.

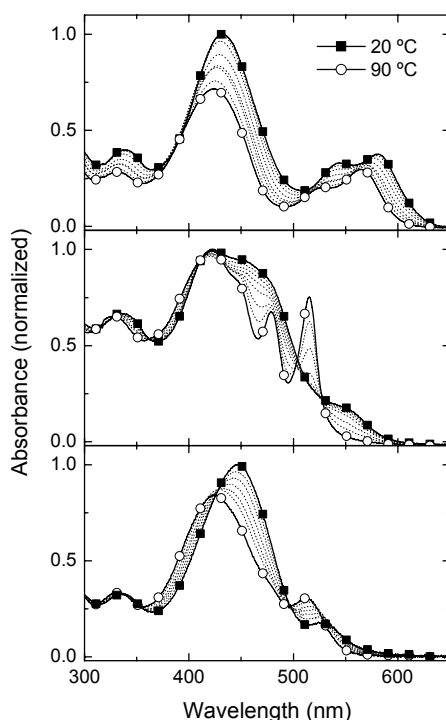


**Figure 2:** Absorption spectra of 1 (top,  $5 \times 10^{-5}$  M), 2 (middle,  $2 \times 10^{-6}$  M) and 3 (bottom,  $1.3 \times 10^{-6}$  M) measured in MCH. The solid squares show the absorption spectra recorded at 20 °C, whereas the open circles indicate the results obtained at 90 °C.

A study on the concentration dependence of the aggregation behavior at room temperature indicated that for concentrations above  $1 \times 10^{-5}$  M in MCH all three compounds are only present as aggregated species. For 1 only 50 percents of the molecules is aggregated in MCH at a concentration of  $4 \times 10^{-7}$  M, whereas this occurs at a concentration of  $5 \times 10^{-8}$  M for 3. At the lowest concentration where an absorption signal is detectable ( $1 \times 10^{-8}$  M), compound 2 is still completely aggregated.

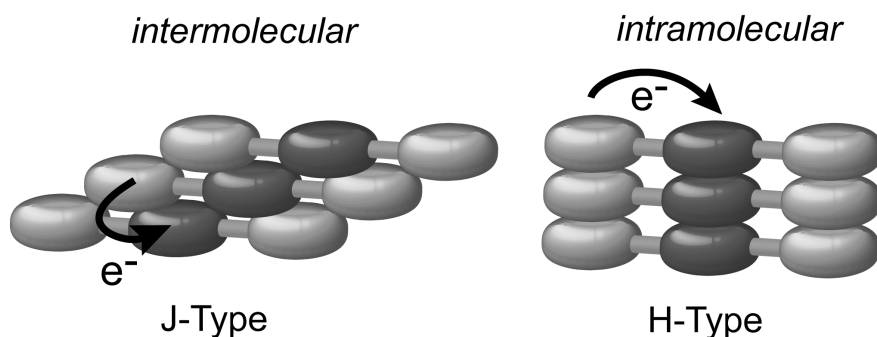


**Figure 3:** Cartoon of the two limiting situations for the one-dimensional packing of OPV-PERY-OPV arrays to give H-type (right) and J-type (left) aggregates.

Compounds 1-3 bear eight enantiomerically pure (*S*)-2-methylbutoxy substituents. This side-chain chirality can result in a circular dichroism of the  $\pi$ - $\pi^*$  transitions of the OPV and PERY chromophores when the molecules aggregate in a helical fashion. Small circular dichroism signals, originating from interchromophoric coupling, are indeed observed for 1-3 in MCH and disappear upon heating (Figure 4). The CD signal evidences some rotational displacement in the aggregates.

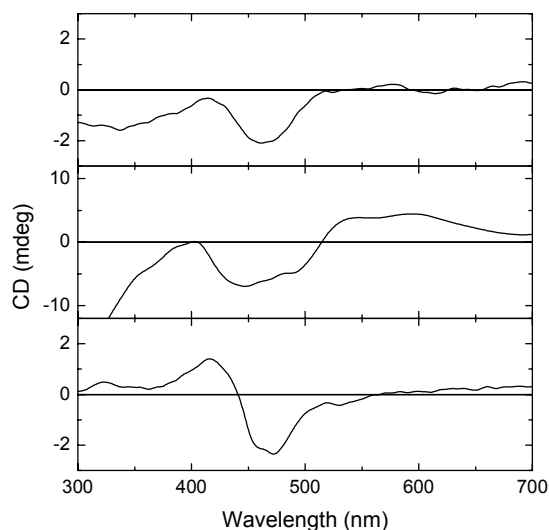


**Figure 4:** Circular dichroism spectra of  $5 \times 10^{-5} M$  solutions of 1 (top), 2 (middle) and 3 (bottom) in MCH recorded at 20 °C.

More evidence for the presence of a J-type aggregate structure for 3 in MCH has been obtained by analyzing the absorption spectra at higher concentration (Figure 5). Under these conditions and at the same concentrations, an absorption band that is not present for the separate reference compounds 4 and 5, can be observed for 3 in the region from 700 to 1000 nm. This band points to the occurrence of charge transfer (CT) between the two *different* chromophores in the ground state. In addition, the onset of the PERY( $S_1 \leftarrow S_0$ ) transition has slightly shifted to longer wavelengths as compared to the reference compounds. This shift is due to the dipole-allowed low-energy absorption that is characteristic for transition dipoles in a head-to-tail configuration in a J-type aggregate. The observed CT band is only expected when the OPV and perylene bisimide chromophores are in a face-to-face orientation. Because all molecules are aggregated at the concentrations used, a value of  $800 \text{ L}\cdot\text{mol}^{-1}\cdot\text{cm}^{-1}$  can be calculated as a lower limit for the molar absorption coefficient of this transition, based on the assumption that all present molecules will participate in forming such face-to-face aggregates.

Previously, it has been observed that the introduction of chlorine substituents on the bay position increases the tendency of perylene bisimide molecules to form intermolecular charge complexes with other aromatic molecules.<sup>36</sup> Therefore, a mixture of 4 and 5 is studied in order to see if a face-to-face OPV-PERY complex can be obtained when the OPV and PERY moieties are not covalently linked. As can be seen in Figure 5, the 1:1 mixture of 4 and 5 in MCH at  $10^{-4} M$  gives rise to the CT absorption band, demonstrating that the OPV and PERY compounds also have a tendency to stack on top of each

other when they are not covalently linked. This implies that the mixed system gains energy by forming a charge transfer complex in the ground state in which the  $\pi$ -electron systems of both compounds are in a sandwich-type configuration. Although the concentrations used in the experiment are similar for array 3 and the mixture of 4 and 5, the intensity of the CT absorption band is lower for the mixture, while the spectral positions are the same. This indicates that in the mixture not all molecules are forming a donor-acceptor aggregate; as can be expected the intensity of the CT band decreases with temperature as a result of a shift in this equilibrium. A semi-logarithmic plot of the intensity of the absorption band at 790 nm versus reciprocal temperature provided a binding enthalpy of -110 meV for the association of the complex containing 4 and 5.

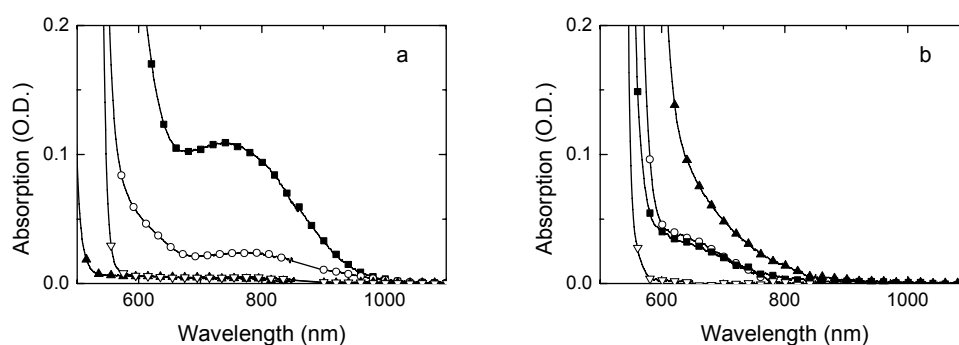


**Figure 5:** (a) Absorption spectra of 3 (solid squares,  $1.3 \times 10^{-4}$  M), 4 (solid triangles,  $10^{-4}$  M), 5 (open triangles,  $10^{-4}$  M), and a 1:1 mixture of 4 and 5 (open circles,  $10^{-4}$  M) in MCH at 20 °C. (b) Absorption spectra of 7 in MCH (solid squares,  $2 \times 10^{-4}$  M) and THF (open circles,  $2 \times 10^{-4}$  M), 2 in MCH (solid triangles,  $2 \times 10^{-4}$  M), and a 1:1 mixture of 4 and 6 in THF (open triangles,  $2 \times 10^{-4}$  M).

In addition to the chlorine substituted perylene bisimide compounds, the presence of a charge transfer absorption in the ground state was also studied for the OPV-PERY array 2. This is, however, less straightforward because 2 is believed not to form aggregates composed of two *different* chromophores in a face-to-face orientation.<sup>37</sup> By looking at the absorption spectrum it is therefore not surprising that for 2 the only visible difference with respect to the reference compounds 4 and 6 is a slight red shift of the absorption onset, caused by the presence of H-aggregates (Figure 5). Unfortunately it proved not possible to study the mixture of 4 and 6 because of the limited solubility of 6 in MCH. Therefore, the cyclic OPV-PERY dimer 7 was used as a model compound. As a result of the strained geometry within 7, the donor and acceptor moieties are always positioned on top of each other. As a consequence, an extra absorption is observed between 600 and 800 nm in MCH. In addition, this band is also observed in THF, a solvent in which aggregation of OPV and PERY compounds is generally not observed. Due to the strained geometry of 7, the polarity of the solvent does not influence the formation of a face-to-face complex, and therefore the CT-absorption is also observed in THF. As expected from the different reduction potentials ( $E_{\text{red}} = -1.02$  and  $-0.80$  V, vs.  $\text{Fc}/\text{Fc}^+$  in  $\text{CH}_2\text{Cl}_2$  for 2 and 3, respectively),<sup>15</sup> the position of the CT-absorption for unsubstituted perylene bisimide derivatives is already at considerably higher energies compared to the chlorine substituted analogs.<sup>38</sup> Therefore no attempt was made to monitor the CT-absorption for 1, because the CT state is even higher in energy as a result of the more negative reduction potential ( $E_{\text{red}} = -1.17$  V) and because the

ground-state absorption is considerably red-shifted due to the electron donating character of the *tert*-butylphenoxy substituents. As a result the CT-absorption is expected to be undetectable for the phenoxy-substituted OPV-PERY arrays, taking into account the spectral overlap and high molar absorption coefficient of the PERY( $S_1 \leftarrow S_0$ ) transition with respect to the CT-transition.

**Molecular Mechanics Calculations.** Researchers of the Laboratory for Chemistry of Novel Materials of the University of Mons-Hainaut have performed Molecular Mechanics (MM) calculations to gain a deeper insight into the packing of molecules 1, 2, and 3. These calculations provide, on a qualitative basis, the probability of H-type versus J-type aggregate formation among the three derivatives. To do so, the change in total energy as one molecule is slid with respect to the other is followed in a simple dimer model. The geometry of the isolated chains has first been optimized at the semi-empirical Hartree-Fock Austin Model 1 (AM1) level,<sup>39</sup> while constraining the OPV backbones to be fully planar and replacing the long saturated chains attached to the terminal phenylene rings by methoxy groups. The results indicate that the perylene bisimide molecule is fully planar in 2 and distorted into a cross-like geometry in 1 and 3 (Figure 6). The AM1 calculations tend to position the phenoxy groups of 1 oriented along the *z*-direction above and below the perylene bisimide plane.<sup>25</sup> Since crystallographic data<sup>24,40</sup> indicate that such a conformation is unlikely in a densely packed assembly, an extended structure where the phenoxy groups are predominantly oriented along the *y*-axis to provide a more flat molecule is considered in the following (Figure 6).<sup>41</sup>

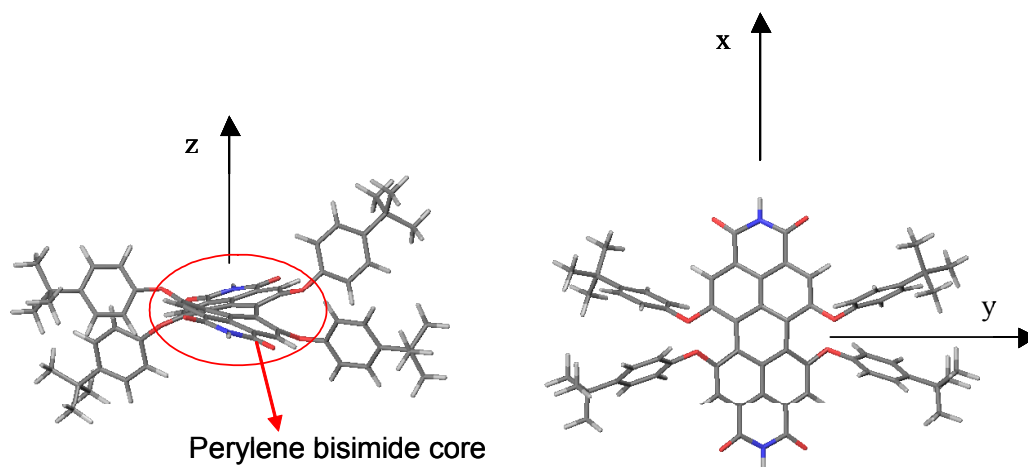


**Figure 6:** Illustration of the bending of the perylene bisimide core in 1 (left) and of the extended structure used in the MM calculations (right). The stacking axis *z* and the translational axis *x* are also defined.

The potential energy curve has been generated using the UFF (Universal Force Field) force field by calculating the energy of a stacked dimer, built from the isolated structure obtained at the AM1 level. The applicability of UFF to describe packing in molecular stacks has been validated in previous studies.<sup>42</sup> Non-bonding effects (van der Waals and Coulomb terms) in such long molecules have to be described with a long cut-off distance to provide a reliable stabilization energy upon packing. The spline method with a spline-on and -off parameter set respectively to 200 Å and 300 Å is used. The convergence criterion for the optimization has been set at  $10^{-5}$  kcal/mol and the charges are computed

by the default method. In the simulations, the stacking axis  $z$  is perpendicular to the perylene bisimide backbone in 2 and to its average molecular plane in 1 and 3; the translation axis  $x$  is set parallel to the axis connecting the nitrogen atoms of the perylene bisimide moiety, as illustrated in Figure 6. Thirteen initial structures that differ by the magnitude of the translation along  $x$  were generated by positioning the two molecules at an intermolecular separation along  $z$  larger than the equilibrium distance (initial distances of 4.0 Å for molecule 2, 5.0 Å for molecule 3, and in the range 7–9 Å for molecule 1). A full MM optimization is then achieved on the basis of these starting geometric configurations to yield optimized structures corresponding to local minima on the potential energy curve.

Figure 7 displays the total relative energy (with respect to the global minimum) versus translation along  $x$  (measured by the average distance between the perylene bisimide nitrogen atoms in the two interacting molecules), as calculated at the UFF level for the three molecules (see experimental section for the absolute energies and shifts). The analysis of the results shows that the fully cofacial geometry (zero displacement along  $x$ ) does not correspond to a stable configuration in any of the three compounds. This is mostly due to steric effects between the substituents in 1, Coulomb repulsion between the negatively charged nitrogen atoms in 2, and Coulomb repulsion between the chlorine atoms in 3. The latter effect leads to the largest intermolecular spacing for 3 (5.14 Å) compared to 1 (4.48 Å) and 2 (3.83 Å). The global minimum is obtained for a slightly displaced H-type configuration, corresponding to a shift along  $x$  of  $\sim 4.2$  Å in 1,  $\sim 2.8$  Å in 2 and  $\sim 4.2$  Å in 3. A local minimum is observed for the three compounds with displacements along the  $x$  direction of around 12 Å, which corresponds to a J-like architecture (the distance between the two nitrogen atoms of a perylene bisimide molecule is indeed  $\sim 11.3$  Å). However, this structure is found to be significantly more stable in 1 and 3 with respect to 2. This can be rationalized by the fact that the steric effects that destabilize the H-type aggregate in 1 and 3 are progressively switched off when sliding the two molecules on top of one another, thereby allowing for bonding van der Waals interactions.

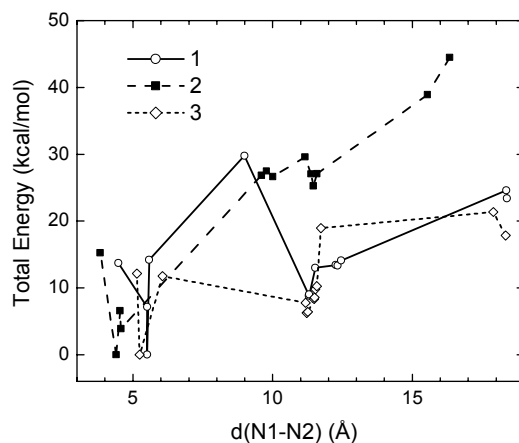


**Figure 7:** UFF-calculated evolution of the total energy of a dimer of 1, 2, and 3 as a function of the degree of translation represented by the average distance [ $d(N1-N2)$ ] between the perylene bisimide nitrogen atoms in the two interacting molecules. The energy of the global minimum is set equal to zero in all cases.

As similar steric effects are absent in 2, a monotonous decrease of the interaction energy as a function of translation along  $x$  is predicted in that case. It should be stressed here that the relative stability of J-

like vs. H-like architectures is underestimated in the dimer calculations due to the smaller interaction surface. Likely, J-aggregates will be further favored upon building a 3D model for the packing of 1 and 3. The calculations are thus consistent with the experimental data pointing to the fact that H-aggregates are observed only for 2, while for 1 and 3, steric repulsion between the substituted perylene bisimide cores drives the structures toward a J-type arrangement.

**Photoinduced Charge Separation and Recombination.** The dynamics of the photoinduced charge separation in MCH has been studied by transient photoinduced absorption spectroscopy (Figure 8), by monitoring the characteristic transient absorption of the OPV<sup>+</sup> radical cation at 1450 nm,<sup>13</sup> after excitation at 455 nm. These measurements reveal remarkable differences in the charge transfer kinetics for the aggregated state when compared to the same compounds in the molecularly dissolved state in *o*-dichlorobenzene (ODCB,  $\epsilon = 9.93$ ) and toluene ( $\epsilon = 2.38$ ), despite the fact that the polarity of the latter is similar to that of MCH ( $\epsilon = 2.02$ ). In a first approximation, the rate for charge separation is expected to be the lowest in MCH because the driving force ( $-\Delta G_{CS}$ ) decreases in less polar solvents (equation 1).<sup>43,44</sup>

$$-\Delta G_{CS} = -e[E_{ox}(D) - E_{red}(A)] + E(S_1) + \frac{e^2}{4\pi\epsilon_0\epsilon_s R_{cc}} + \frac{e^2}{8\pi\epsilon_0} \left( \frac{1}{r^+} + \frac{1}{r^-} \right) \left( \frac{1}{\epsilon_{ref}} - \frac{1}{\epsilon_s} \right) \quad (1)$$

Actually, an estimate of the energy of the intramolecular charge-separated state by means of equation 1 indicates that for compound 1 this state is degenerate with the first singlet-excited state of the perylene bisimide moiety ( $\Delta G_{CS} = 0.00$  eV). Because the driving force for the charge separation reaction for 1 is considerably smaller than the reorganization energy,<sup>15</sup> the charge transfer occurs in the normal Marcus region and, hence, the rate constant ( $k_{CS}$ ) increases with increasing driving force.<sup>45</sup> Therefore, if charge separation is present at all, the rate for charge separation for compound 1 in a molecularly dissolved state in MCH is expected to be slow. In contrast with these expectations, the charge separation reaction for 1 in MCH occurs at a considerably higher rate ( $k_{CS} = 1.2 \times 10^{12}$  s<sup>-1</sup>) than in ODCB ( $k_{CS} = 4.6 \times 10^{11}$  s<sup>-1</sup>) or in toluene ( $k_{CS} = 2.7 \times 10^{11}$  s<sup>-1</sup>). This difference can only be rationalized by the presence of aggregated species in MCH.

For 2 and 3, the photoinduced charge separation in MCH is equally fast and occurs with rate constants of  $k_{CS} = 2.2 \times 10^{12}$  and  $2.9 \times 10^{12}$  s<sup>-1</sup>, respectively.<sup>46</sup> Previous studies established that for 2 and 3, the forward charge transfer occurs close to Marcus optimal region.<sup>15</sup> Under these conditions it is difficult to predict how  $k_{CS}$  changes with solvent polarity and, hence, the high rate constants cannot directly be associated with the aggregated nature of the compounds.

An explanation for the fast forward electron transfer reaction in 1 in MCH, is that the formation of J-type aggregates enables charge separation to occur via an intermolecular process rather than intramolecularly, because the intermolecular distance between the OPV and PERY moieties is shorter than the intramolecular distance (Figure 3). This implies that the distance of 14 Å between the OPV and PERY chromophores<sup>15</sup> used for the calculation of the driving force is not applicable for 1 when it is in a J-type aggregate. The intermolecular distance of a typical  $\pi$ - $\pi$ -stacked system is approximately

4.0 Å and this introduces a considerable increase in the driving force for charge separation in MCH compared to calculations assuming a 14 Å distance (Figure 9).

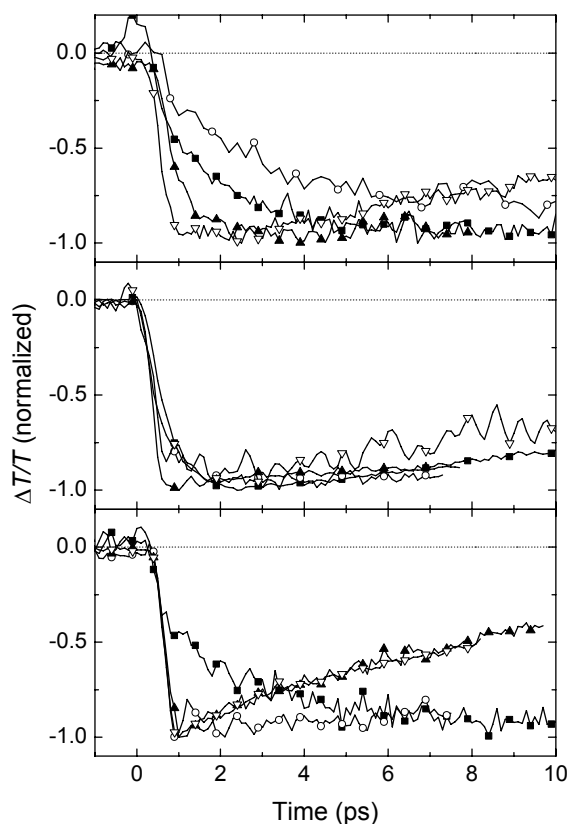


**Figure 8:** Transient photoinduced absorption dynamics probing charge separation of  $5 \times 10^{-5}$  M solutions of 1 (top), 2 (middle) and 3 (bottom) at room temperature in ODCB (solid squares), toluene (open circles), MCH (solid triangles) and in the solid state (open triangles). For all measurements an excitation wavelength of 455 nm was used with detection of the  $OPV^{+}$  absorption at 1450 nm.

For 1, the driving force, calculated from equation 1, increases from  $\sim 0$  eV at 14 Å to  $-1.27$  eV at a distance of 4 Å. Interestingly, the driving force for charge separation in MCH for distances around 4 Å is higher than in ODCB ( $\Delta G_{CS} = -0.76$  eV) and in toluene ( $\Delta G_{CS} = -0.14$  eV) at 14 Å, consistent with the observed decreasing rate constant for charge separation for 1 going from MCH to ODCB, and toluene.

However, this simple analysis ignores any changes in electronic coupling when going from an intramolecular to an intermolecular charge separation process. In these molecules the intramolecular coupling is fairly weak (see ref 15, 6 meV) due to the nodal plane in the frontier orbitals of the perylene bisimide core.<sup>14,41</sup> For compound 7, the electronic coupling for the face-to-face charge transfer has been calculated to be 8-9 meV when the electron transfer originates from the lowest singlet state in the dyad (PERY( $S_1$ )).<sup>14</sup> These numbers suggest that the electronic coupling is similar for the two processes, but the electronic coupling for intermolecular processes could vary strongly with the mutual orientation of the molecules.<sup>47</sup>



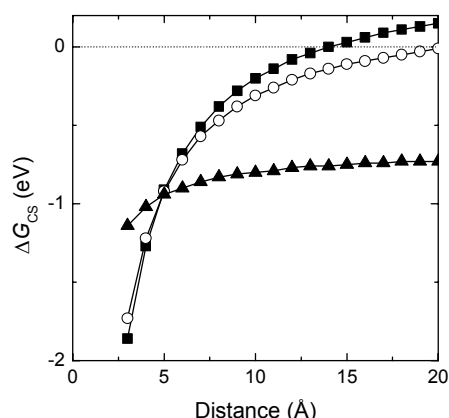


**Figure 9:** Calculated driving force for charge separation ( $\Delta G_{CS}$ ) for **1** at various interchromophoric distances in MCH (squares), toluene (circles) and ODCB (triangles).

Of course it is of interest to study if the changes in the rates for charge recombination ( $k_{CR}$ ) between the molecularly dissolved and aggregated states can also be rationalized by considering the shortest OPV-PERY distances as for charge separation. When the driving force for charge separation increases as a result of the shorter distance between the two chromophores, the driving force for charge recombination ( $-\Delta G_{CR}$ ) will diminish to satisfy that  $E(S_1) = -(\Delta G_{CS} + \Delta G_{CR})$ . Accordingly, Figure 10 shows that the driving force for charge recombination will increase for longer donor-acceptor distances. For the J-type aggregates of **1** in MCH the driving force for intermolecular charge recombination at 4 Å of  $\Delta G_{CR} = -0.86$  eV is therefore less than the value of  $-1.99$  eV for intramolecular recombination in toluene at 14 Å.

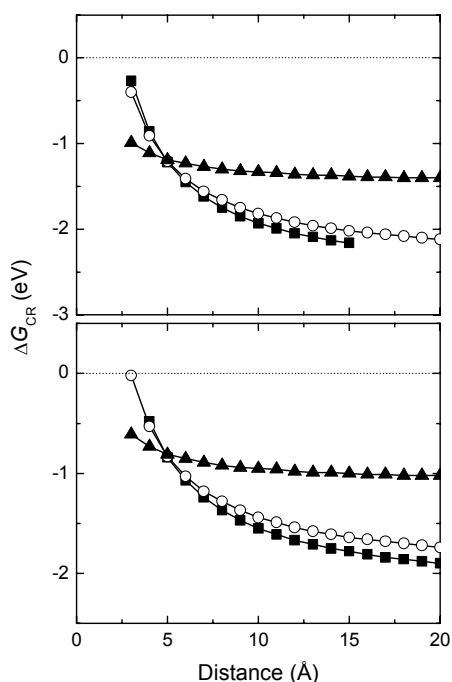


**Figure 10:** Calculated driving force for charge recombination ( $\Delta G_{CR}$ ) in **1** (top) and **3** (bottom) for different interchromophoric distances in MCH (squares), toluene (circles), and ODCB (triangles).

Charge recombination in arrays 1-3 is in the Marcus inverted region<sup>15</sup> and as a consequence the decrease in  $-\Delta G_{\text{CR}}$  leads to a faster charge recombination (*i.e.* a shorter lifetime of the charge-separated state). In agreement with this prediction the experimental results indicate that the rate for charge recombination for 1 in MCH ( $k_{\text{CR}} = 2 \times 10^9 \text{ s}^{-1}$ ) (Figure 11) is higher than in toluene ( $k_{\text{CR}} < 8 \times 10^8 \text{ s}^{-1}$ ). The photoinduced absorption of 1 in MCH at elevated temperatures, where this compound is in its molecularly dissolved state, leads to the same kinetics as that observed in toluene at room temperature.<sup>12</sup> This demonstrates that the arrangement of the supramolecular structure in the aggregated state causes the higher recombination rate.

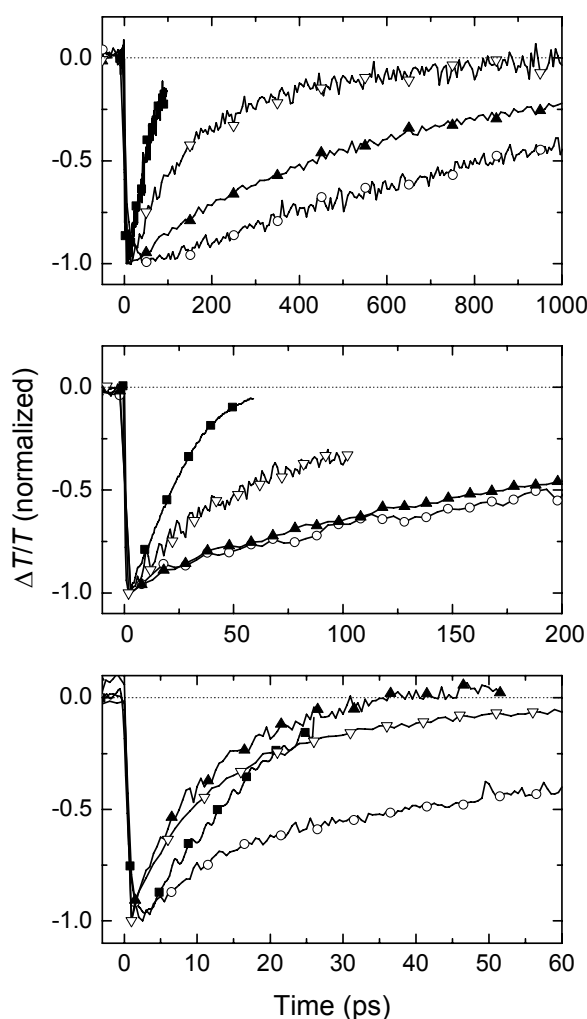


**Figure 11:** Transient photoinduced absorption dynamics probing charge recombination of  $5 \times 10^{-5} \text{ M}$  solutions of 1 (top), 2 (middle) and 3 (bottom) at room temperature in ODCB (solid squares), toluene (open circles), MCH (solid triangles) and the solid state (open triangles). For all measurements an excitation wavelength of 455 nm is used, with detection of the  $\text{OPV}^{+\bullet}$  absorption at 1450 nm.

For 3, the donor-acceptor distance would be similarly reduced from 14 Å to about 4 Å when it forms J-type aggregates and as a consequence charge recombination should be faster in the aggregated state

than in a molecularly dissolved state when solvents of similar polarity are used. The rate of charge recombination observed experimentally in MCH ( $k_{\text{CR}} = 8.3 \times 10^{10} \text{ s}^{-1}$ ) is indeed considerably higher than the rate measured in toluene ( $k_{\text{CR}} = 1.6 \times 10^{10} \text{ s}^{-1}$ ) and even slightly higher than in ODCB ( $k_{\text{CR}} = 7.9 \times 10^{10} \text{ s}^{-1}$ ). This is in full agreement with the lower energy of the charge-separated state for 3 as a result of its intermolecular nature and parallels the results obtained for 1. Moreover, the rate found for 3 in MCH is identical to the rate obtained for thin films of the same molecule. This suggests that in the solid state the donor and acceptor moieties also pack in a face-to-face configuration, similar to the J-type structure and is further confirmed by the nearly identical UV/Vis absorption in the film and in the aggregates. This is in accordance with the proposed morphologies for other OPV-PERY systems<sup>14</sup> and is a frequently observed packing motif for covalent donor-acceptor polymers.<sup>48-51</sup>

The formation of the complex of 4 and 5 implies that the donor and acceptor molecules are in very close proximity and therefore a photoinduced charge separation can be expected. The transient photoinduced absorption time trace of a 1:1 mixture of 4 and 5 recorded after exciting the sample at 455 nm and detecting at the OPV<sup>+</sup> absorption at 1450 nm confirms the intermolecular electron transfer between 4 and 5 in the mixed aggregate (Figure 12). The rapid rising of the signal ( $< 1 \text{ ps}$ ) indicates that charge separation occurs at a much faster rate than expected for a diffusion limited reaction between two molecularly dissolved molecules. Strikingly, the transients for 3 and the mixture of 4 and 5 are identical. Since the molecules 4 and 5 stack in a sandwich-type structure, this geometry is most likely also present for 3, in full agreement with the previous observations. This indicates that the CT and  $\pi$ - $\pi$  interactions between the OPV and PERY moieties determine to a large extent the structure of the complex in the solid state and in the aggregate.

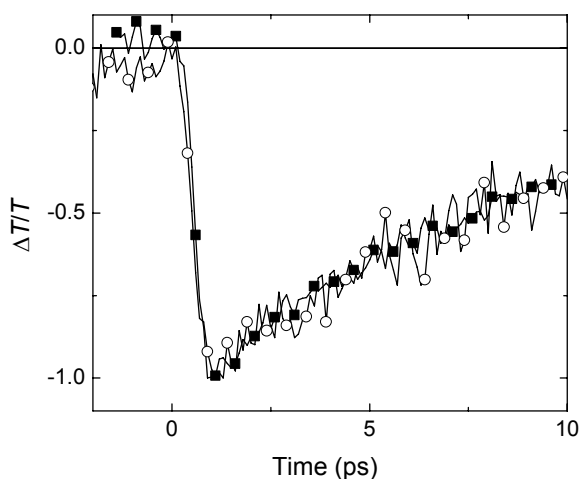


**Figure 12:** Transient photoinduced absorption dynamics in MCH of 3 (solid squares,  $5 \times 10^{-5} \text{ M}$ ) and a 1:1 mixture of compounds 4 and 5 (open circles,  $10^{-4} \text{ M}$ ). For both measurements an excitation wavelength of 455 nm is used, with detection of the OPV<sup>+</sup> absorption at 1450 nm.

Charge separation in 2 is equally fast in all solvents and not strongly affected by polarity or aggregation (Figure 8) and, hence differs strongly from the behaviors of 1 and 3. Charge recombination in 2, however, varies more strongly, and is faster in ODCB (Figure 11). In strong contrast with the results for 1 and 3, the rate for charge recombination of 2 dissolved in toluene or as

aggregates in MCH are identical ( $k_{CR} = 3.0 \times 10^9 \text{ s}^{-1}$ ). Apparently, the intermolecular effects that arise when 2 forms aggregates do not enhance the recombination rate, in contrast to the results observed for 1 and 3. This is in full agreement with the proposed molecular picture of an H-type aggregate, where the intramolecular distance between the OPV and PERY moieties remains the shortest distance between the chromophores. At the same time it can be concluded that delocalization of positive or negative charges in the H-type aggregates along a stack of chromophores does not enhance the lifetime or does not occur. In agreement with recent work by Wasielewski *et al.*,<sup>52</sup> the influence of aggregation is small and the photophysical properties of the aggregate resemble that of the molecular dissolved state in aggregates of donor-acceptor compounds where the donors stack on donors and the acceptors on acceptors (H-type).

### 5.3 Conclusions

The supramolecular structures of aggregates of three different OPV-PERY-OPV arrays 1-3 in MCH have been characterized in terms of H and J-type aggregates using absorption spectroscopy and Molecular Mechanics calculations. In these aggregates highly efficient and fast photoinduced charge separation occurs. For the H-type aggregates of 2, only minor differences are found for the kinetics of charge separation and recombination when the aggregates are compared to a non-aggregated, molecularly dissolved state in an apolar solvent. In contrast, the forward and backward electron transfer rates are considerably faster in J-type aggregates (1 and 3) than in solution, even for a polar solvent. These results can consistently be rationalized by considering the new close contacts of OPV and PERY chromophores that are created in J-type aggregates but are absent in H-type aggregates of the OPV-PERY-OPV arrays. For the bay-substituted derivatives 1 and 3, which are twisted in the middle of the PERY chromophore, a shift in the direction of the long axis of the molecule is triggered by steric effects and is fully supported by the spectroscopic data. The shortest donor-acceptor distance is identified as the most important parameter in accelerating charge transfer reactions, both separation and recombination, under conditions of J-type aggregation in an apolar medium. Ultimately, supramolecular interactions like hydrogen bonding, charge transfer interactions, and  $\pi$ - $\pi$  stacking of functional  $\pi$ -conjugated systems<sup>33,41,53,54</sup> may be used to create artificial systems with pre-defined photophysical properties that convert, store, or use photon energy. The results presented here demonstrate that a balance between molecular properties and intermolecular interactions is crucial to the photophysics of self-assembled architectures of functional molecules and that distance is a simple, but very important parameter.

### 5.4 Experimental Section

UV/Vis/near-IR absorption and fluorescence spectra were recorded on a Perkin Elmer Lambda 900 spectrometer whereas circular dichroism measurements were performed on a Jasco J-600 spectropolarimeter. The solvents MCH, toluene and ODCB were of spectroscopic grade and used as received. The synthesis of compounds 1,<sup>12</sup> 2,<sup>13</sup> 3,<sup>15</sup> 4,<sup>55</sup> 5,<sup>25</sup> 6,<sup>56</sup> and 7<sup>14</sup> has been published elsewhere. Detailed information on the parameters used for the calculation of the driving force for charge separation and recombination can be found in reference 15. All experiments are performed at room

temperature unless stated otherwise. A detailed description of the femtosecond laser system used for transient pump-probe experiments can be found in Chapter 2.

The results of the evolution of the total energy of the dimer (in kcal/mol) as a function of the average distance between the perylene bisimide nitrogen atoms in the two interacting molecules for 1, 2 and 3, as calculated at the UFF level are shown in the table below.

1		2		3	
d(N1-N2)	Energy	d(N1-N2)	Energy	d(N1-N2)	Energy
4.48	568.44	3.83	685.06	5.14	621.87
5.58	568.93	4.40	669.82	5.24	609.73
5.51	561.86	4.57	673.71	6.06	621.48
5.51	554.72	4.54	676.40	11.73	628.68
11.53	567.72	9.60	696.68	11.18	617.50
8.99	584.50	9.78	697.31	11.26	616.13
12.26	568.15	10.01	696.46	11.22	615.98
12.33	568.07	11.59	696.91	11.53	619.53
12.45	568.81	11.46	695.10	11.58	619.97
11.31	563.72	11.37	696.88	11.50	618.29
11.30	563.57	11.16	699.41	11.48	618.06
18.39	578.10	15.54	708.74	17.90	631.09
18.37	579.33	16.34	714.32	18.34	627.56

## 5.5 References

- 1 *Advances in Chemical Physics*, Jortner, J.; Bixon, M., Ed.; Wiley-Interscience, **1999**; Vols. 106 and 107.
- 2 *Electron Transfer in Chemistry*, Balzani, V., Ed.; Wiley-VCH: Weinheim, **2001**; Vols. 1-5.
- 3 Gust, D.; Moore, T. A.; Moore, A. L. *Acc. Chem. Res.* **1993**, *26*, 198.
- 4 Gust, D.; Moore, T. A.; Moore, A. L. *Acc. Chem. Res.* **2001**, *34*, 40.
- 5 Paddon-Row, M. N. *Acc. Chem. Res.* **1994**, *27*, 18.
- 6 Guldi, D. M. *Chem. Soc. Rev.* **2002**, *31*, 22.
- 7 Van der Boom, T.; Hayes, R. T.; Zhao, Y.; Bushard, P. J.; Weiss, E. A.; Wasielewski, M. R. *J. Am. Chem. Soc.* **2002**, *124*, 9582.
- 8 Van Hal, P.A.; Meskers, S. C. J.; Janssen, R. A. J. *Appl. Phys. A* **2004**, *79*, 41.
- 9 Fujitsuka, M.; Masuhara, A.; Kasai, H.; Oikawa, H.; Nakanishi, H.; Ito, O.; Yamashiro, T.; Aso, Y.; Otsubo, T. *J. Phys. Chem. B* **2001**, *105*, 9930.
- 10 Fuller, M. J.; Sinks, L. E.; Rybtchinski, B.; Giaimo, J. M.; Li, X.; Wasielewski, M. R. *J. Phys. Chem. A* **2005**, *109*, 970.
- 11 Rybtchinski, B.; Sinks, L. E.; Wasielewski, M. R. *J. Am. Chem. Soc.* **2004**, *126*, 12268.
- 12 Würthner, F.; Chen, Z.; Hoeben, F. J. M.; Osswald, P.; You, C.-C.; Jonkheijm, P.; Van Herrikhuyzen, J.; Schenning, A. P. H. J.; van der Schoot, P. P. A. M.; Meijer, E. W.; Beckers, E. H. A.; Meskers, S. C. J.; Janssen, R. A. J. *J. Am. Chem. Soc.* **2004**, *126*, 10611.

- 13 Peeters, E.; Van Hal, P. A.; Meskers, S. C. J.; Janssen, R. A. J.; Meijer, E. W. *Chem.-Eur. J.* **2002**, *8*, 4470.
- 14 Neuteboom, E. E.; Meskers, S. C. J.; Van Hal, P. A.; van Duren, J. K. J.; Meijer, E. W.; Janssen, R. A. J.; Dupin, H.; Pourtois, G.; Cornil, J.; Lazzaroni, R.; Brédas, J.-L.; Beljonne, D. *J. Am. Chem. Soc.* **2003**, *125*, 8625.
- 15 Beckers, E. H. A.; Meskers, S. C. J.; Schenning, A. P. H. J.; Chen, Z.; Würthner, F.; Janssen, R. A. J. *J. Phys. Chem. A* **2004**, *108*, 6933.
- 16 Ramos, A. M.; Beckers, E. H. A.; Offermans, T.; Meskers, S. C. J.; Janssen, R. A. J. *J. Phys. Chem. A* **2004**, *108*, 8201.
- 17 Ramos, A. M.; Meskers, S. C. J.; Beckers, E. H. A.; Prince, R. B.; Brunsveld, L.; Janssen, R. A. J. *J. Am. Chem. Soc.* **2004**, *126*, 9630.
- 18 Schenning, A. P. H. J.; van Herrikhuyzen, J.; Jonkheijm, P.; Chen, Z.; Würthner, F.; Meijer, E. W. *J. Am. Chem. Soc.* **2002**, *124*, 10252.
- 19 Neuteboom, E. E.; Van Hal, P. A.; Janssen, R. A. J. *Chem.-Eur. J.* **2004**, *10*, 3907.
- 20 Herz, L. M.; Daniel, C.; Silva, C.; Hoeben, F. J. M.; Schenning, A. P. H. J.; Meijer, E. W.; Friend, R. H.; Phillips, R. T. *Phys. Rev. B* **2003**, *68*, 045203/1.
- 21 Hoeben, F. J. M.; Herz, L. M.; Daniel, C.; Jonkheijm, P.; Schenning, A. P. H. J.; Silva, C.; Meskers, S. C. J.; Beljonne, D.; Phillips, R. T.; Friend, R. H.; Meijer, E. W. *Angew. Chem., Int. Ed.* **2004**, *43*, 1976.
- 22 Herz, L. M.; Silva, C.; Friend, R. H.; Phillips, R. T.; Setayesh, S.; Becker, S.; Marsitsky, D.; Müllen, K. *Phys. Rev. B* **2001**, *64*, 195203/1.
- 23 Li, X.; Sinks, L. E.; Rybtchinski, B.; Wasielewski, M. R. *J. Am. Chem. Soc.* **2004**, *126*, 10810.
- 24 Würthner, F.; Sautter, A.; Thalacker, C. *Angew. Chem., Int. Ed.* **2000**, *39*, 1243.
- 25 Hofkens, J.; Vosch, T.; Maus, M.; Kohn, F.; Cotlet, M.; Weil, T.; Herrmann, A.; Müllen, K.; De Schryver, F. C. *Chem. Phys. Lett.* **2001**, *333*, 255.
- 26 Chen, Z.; Debije, M. G.; Debaerdemaeker, T.; Osswald, P.; Würthner, F. *ChemPhysChem* **2004**, *5*, 137.
- 27 Leroy-Lhez, S.; Baffreau, J.; Perrin, L.; Levillain, E.; Allain, M.; Blesa, M.-J.; Hudhomme, P. *J. Org. Chem.* **2005**, *70*, 6313.
- 28 Tributsch, H.; Pohlmann, L. *Science* **1998**, *279*, 1891.
- 29 Struijk, C. W.; Sieval, A. B.; Dakhorst, J. E. J.; van Dijk, M.; Kimkes, P.; Koehorst, R. B. M.; Donker, H.; Schaafsma, T. J.; Picken, S. J.; Van de Craats, A. M.; Warman, J. M.; Zuilhof, H.; Sudhölter, E. J. R. *J. Am. Chem. Soc.* **2000**, *122*, 11057.
- 30 Schmidt-Mende, L.; Fechtenkötter, A.; Müllen, K.; Moons, E.; Friend, R. H.; MacKenzie, J. D. *Science* **2001**, *293*, 1119.
- 31 Hudson, S. D.; Jung, H. T.; Percec, V.; Cho, W. D.; Johansson, G.; Ungar, G.; Balagurusamy, V. S. K. *Science* **1997**, *278*, 449.
- 32 Percec, V.; Glodde, M.; Bera, T. K.; Miura, Y.; Shiyonovskaya, I.; Singer, K. D.; Balagurusamy, V. S. K.; Heiney, P. A.; Schnell, I.; Rapp, A.; Spiess, H. W.; Hudson, S. D.; Duan, H. *Nature* **2002**, *419*, 384.
- 33 Hoeben, F. J. M.; Jonkheijm, P.; Meijer, E. W.; Schenning, A. P. H. J. *Chem. Rev.* **2005**, *105*, 1491.
- 34 Kasha, M. *Rad. Res.* **1963**, *20*, 55.
- 35 Würthner, F.; Thalacker, C.; Diele, S.; Tschierske, C. *Chem. Eur. J.* **2001**, *7*, 2245.
- 36 Sadrai, M.; Bird, G. R.; Potenza, J. A.; Schugar, H. J. *Acta Cryst. C* **1990**, *C46*, 637.
- 37 Van Herrikhuyzen, J.; Syamakumari, A.; Schenning, A. P. H. J.; Meijer, E. W. *J. Am. Chem. Soc.* **2004**, *126*, 10121.

- 38 For aggregates of 3, the CT band is at 740 nm (1.68 eV) while the CT band in 7 is found at 640 nm (1.94 eV). In a first approximation, the difference in the energy of the CT bands (0.26 eV) scales with the difference between reduction potentials of the acceptor units (0.22 eV). This allows to predict that the CT absorption in aggregates of 1 should be ~0.15 eV above that of 7, i.e. at ~2.1 eV or 590 nm, which overlaps with the normal absorption of aggregate.
- 39 Dewar, M. J. S.; Zoebisch, E. G.; Healy, E. F.; Stewart, J. J. P. *J. Am. Chem. Soc.* **1985**, *107*, 3902.
- 40 Osswald, P.; Leusser, D.; Stalke, D.; Würthner, F. *Angew. Chem., Int. Ed.* **2005**, *44*, 250.
- 41 Würthner, F. *Chem. Commun.* **2004**, 1564.
- 42 Leclère, Ph.; Hennebicq, E.; Calderone, A.; Brocorens, P.; Grimsdale, A. C.; Müllen, K.; Brédas, J. L.; Lazzaroni, R. *Prog. Polym. Sci.* **2003**, *28*, 55.
- 43 Weller, A. *Z. Phys. Chem.* **1982**, *133*, 93.
- 44 In this equation  $E_{\text{ox}}(\text{D})$  and  $E_{\text{red}}(\text{A})$  are the oxidation and reduction potentials of the donor and acceptor molecules or moieties measured in a solvent with relative permittivity  $\epsilon_{\text{ref}}$ .  $E(\text{S}_1)$  is the energy of the excited state from which the electron transfer occurs and  $R_{\text{cc}}$  is the center-to-center distance of the positive and negative charges in the charge-separated state. The radii of the positive and negative ions are given by  $r^+$  and  $r^-$ ,  $\epsilon_s$  is the relative permittivity of the solvent,  $-e$  is the electron charge and  $\epsilon_0$  is the vacuum permittivity.
- 45 Marcus, R. A. *Rev. Mod. Phys.* **1993**, *65*, 599.
- 46 It should be noted here that differences in rate constants for the charge separation and recombination rates between the three studied compounds in the same solvent cannot be directly related to the supramolecular structure. The observed differences originate from the different acceptor strength induced by the substituents on the bay position of the perylene bisimide moiety.
- 47 Lemaur, V.; Steel, M.; Beljonne, D.; Brédas, J.-L.; Cornil, J. *J. Am. Chem. Soc.* **2005**, *127*, 6077.
- 48 Lokey, R. S.; Iverson, B. L. *Nature* **1995**, *375*, 303.
- 49 Nguyen, J. Q.; Iverson, B. L. *J. Am. Chem. Soc.* **1999**, *121*, 2639.
- 50 Zych, A. J.; Iverson, B. L. *J. Am. Chem. Soc.* **2000**, *122*, 8898.
- 51 Ghosh, S.; Ramakrishnan, S. *Macromolecules* **2005**, *38*, 676.
- 52 Rybchinski, B.; Sinks, L. E.; Wasielewski, M. R. *J. Phys. Chem. A* **2004**, *108*, 7497.
- 53 Piotrowiak, P. *Chem. Soc. Rev.* **1999**, *28*, 143.
- 54 Schenning, A. P. H. J.; Jonkheijm, P.; Peeters, E.; Meijer, E. W. *J. Am. Chem. Soc.* **2001**, *123*, 409.
- 55 Peeters, E.; Ramos, A. M.; Meskers, S. C. J.; Janssen, R. A. J. *J. Chem. Phys.* **2000**, *112*, 9445.
- 56 Demmig, S.; Langhals, H. *Chem. Ber.* **1988**, *121*, 225.

# Supramolecular OPV-Fullerene Architectures by Using the Ureido-pyrimidinone Quadruple Hydrogen-bonding Unit\*

### *Abstract*

*Novel supramolecular arrays consisting of an oligo(p-phenylene vinylene) (OPV) donor and fullerene (C<sub>60</sub>) acceptor are created via quadruple hydrogen bonding using self-complementary 2-ureido-4[1H]-pyrimidinone units. In these supramolecular donor-acceptor dyads, singlet-energy transfer from the excited OPV unit to the fullerene causes a strong quenching of the OPV fluorescence. The high association constant of the 2-ureido-4[1H]-pyrimidinone quadruple hydrogen-bonding unit results in high quenching factors ( $Q_{max} \geq 90$ ). The lower limit obtained for the rate constant for energy transfer ( $k_{EN} \geq 6 \times 10^{10} \text{ s}^{-1}$ ) is rationalized in terms of the Förster mechanism. Photoinduced electron transfer does not occur in these hydrogen-bonded dimers, not even in polar solvents. The absence of charge separation is ascribed to a low electronic coupling between the donor and acceptor in the excited state as result of the long distance between the chromophores. Furthermore, the formation of hetero-dimers of bifunctional oligo(p-phenylenevinylene) and C<sub>60</sub> ureido-pyrimidinone derivatives has been observed by <sup>1</sup>H-NMR and fluorescence techniques.*

---

\* This work has been published: (a) Beckers, E. H. A.; Van Hal, P. A.; Schenning, A. P. H. J.; El-ghayoury, A.; Peeters, E.; Rispens, M. T.; Hummelen, J. C.; Meijer, E. W.; Janssen, R. A. J. *Journal of Materials Chemistry* **2002**, 12, 2054-2060 (b) Beckers, E. H. A.; Schenning, A. P. H. J.; Van Hal, P. A.; El-ghayoury, A.; Sánchez, L.; Hummelen, J. C.; Meijer, E. W.; Janssen, R. A. J. *Chemical Communications* **2002**, 23, 2888-2889 (c) Rispens, M. T.; Sánchez, L.; Beckers, E. H. A.; Van Hal, P. A.; Schenning, A. P. H. J.; El-Ghayoury, A.; Peeters, E.; Meijer, E. W.; Janssen, R. A. J.; Hummelen, J. C. *Synthetic Metals* **2003**, 135-136, 801-803.



## 6.1 Introduction

In nature, energy and electron transfer play a vital role in processes like *e.g.* photosynthesis<sup>1,2</sup> and respiratory oxidative phosphorylation.<sup>3,4</sup> The molecular interaction between the chromophores in these systems is based on supramolecular organization in which hydrogen bonding is often a key element.<sup>5</sup> To elucidate the influence of hydrogen bonding interaction on photophysical properties and mimic these biological superstructures, various studies were performed.<sup>6-9</sup> Systems containing multiple hydrogen bonds were designed to gain strength and directionality.<sup>10-12</sup> With respect to these multiple bonded assemblies, electron transfer has been reported in donor-acceptor systems linked by a two-fold hydrogen bonded salt<sup>13-15</sup> or acid<sup>16-19</sup> bridge as well as a two point binding via a hydroxyl/carbonyl interaction.<sup>20</sup> To create an even stronger binding between the chromophores, Sessler and co-workers used the triple hydrogen bonded Watson-Crick cytosine-guanine base pair in their studies.<sup>21-25</sup> In general, however, hydrogen-bonded donor-acceptor systems exhibit low association constants. Consequently, only a small fraction of the donor and acceptors remain associated, while the remaining molecules are free to diffuse in solution. The strongest hydrogen bonded donor-acceptor complex ( $K_{\text{ass}} = 10^6 \text{ M}^{-1}$ ) investigated in photoinduced electron transfer reactions has been reported by Hamilton and co-workers.<sup>26</sup>

The 2-ureido-4[1H]-pyrimidinone unit (Figure 1) is a self-complementary DDAA motif quadruple hydrogen-bonding unit that possesses a high association constant of  $6 \times 10^7 \text{ M}^{-1}$  in water-saturated chloroform.<sup>27,28</sup> In non-competitive solvents the association constant is believed to be even one order of magnitude higher. In addition to the quadruple hydrogen bonding, the dimerization benefits from an intramolecular hydrogen bond present in the molecule. Moreover, the high association constant enables the formation of supramolecular polymers based on bifunctional ureido-pyrimidinone systems.<sup>29,30</sup>

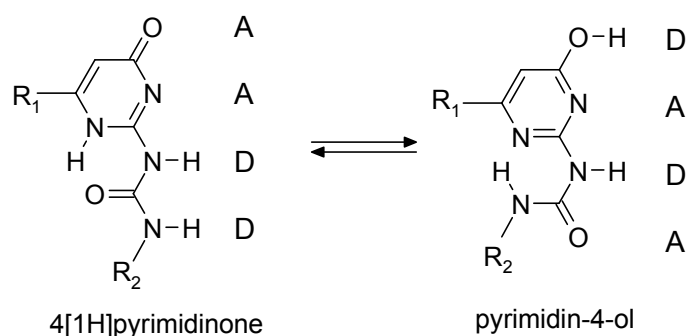


**Figure 1:** 2-ureido-4[1H]-pyrimidinone / pyrimidin-4-ol tautomerization. *D* and *A* indicate hydrogen bonding donors and acceptors. For clarity reasons, both tautomeric forms are displayed in their monomeric form.

Covalently linked dyads of oligo(*p*-phenylene vinylene)s (OPVs, Figure 2) and [60]fullerene ( $C_{60}$ ) exhibit interesting photophysical properties, among which energy and electron transfer reactions, and have been used to make photovoltaic devices.<sup>31-34</sup> Steady-state fluorescence spectroscopy and sub-

picosecond pump-probe spectroscopy established that photoexcitation of OPV4- $C_{60}$  (Figure 2) in apolar solvents, *e.g.* toluene, initiates an ultrafast ( $< 200$  fs) intramolecular singlet-energy transfer from the photoexcited OPV4 unit to  $C_{60}$ .<sup>35</sup> In polar solvents, *e.g.* *o*-dichlorobenzene (ODCB), a photoinduced electron transfer occurs in OPV4- $C_{60}$ , subsequent to the primary singlet-energy transfer, with a time constant of about 10 ps to yield a short-lived ( $\sim 50$ -90 ps) charge-separated state.<sup>35</sup>

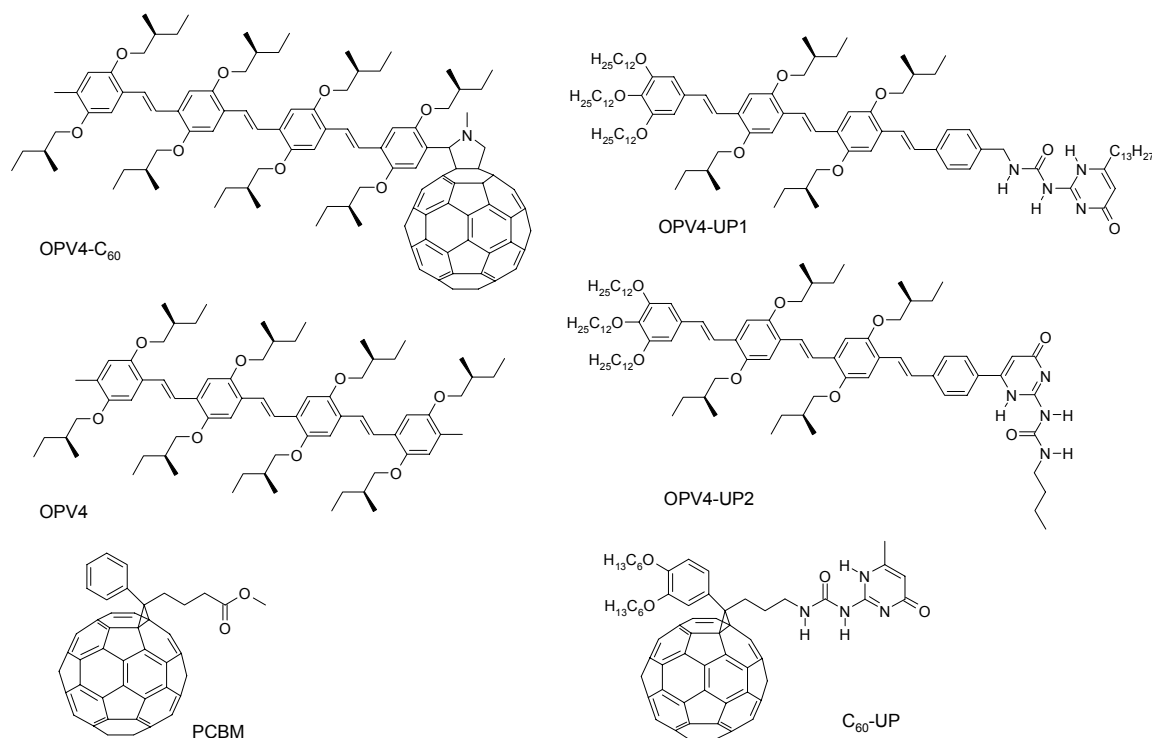


**Figure 2:** Structures of OPV4- $C_{60}$ , OPV4, and PCBM together with the 2-Ureido-4[1H]-pyrimidinone functionalized OPV4-UP1, OPV4-UP2, and  $C_{60}$ -UP compounds. For clarity reasons, all hydrogen bonding units are displayed in the monomeric keto form.

Supramolecular assembly of  $\pi$ -conjugated systems and fullerenes is a viable approach to create morphological organization in the active layer of photovoltaic cells or to advance towards the complexity of natural photoactive systems. Various alternatives exist for assembling donor and acceptor molecules by weak molecular interactions, like for example the well-studied non-covalently linked porphyrin-fullerene systems.<sup>36-42</sup>

## 6.2 Monofunctional OPV-Fullerene Ureido-Pyrimidinone Systems

The focus of this study is the investigation of the formation and excited-state behavior of a quadruple hydrogen bonded dyad involving an OPV4 donor and a  $C_{60}$  acceptor. As donor, two different OPV4 derivatives have been used (Figure 2). The first (OPV4-UP1) consists of an OPV4 unit linked to the R<sub>2</sub> position via a methylene spacer, while the second (OPV4-UP2) has an OPV4 unit directly linked to the

R<sub>1</sub> position of the ureido-pyrimidinone moiety.<sup>43</sup> The acceptor is a fullerene derivative, linked to the R<sub>2</sub> position via a butyl spacer.<sup>44</sup>

The high fluorescence quantum yield of the OPV4-UP (OPV4-UP1 and OPV4-UP2) molecules in solution, together with the strong quadruple hydrogen bond, allows us to investigate photoinduced energy and electron transfer reactions at extremely low concentrations. The combination of a high binding constant and low concentrations in the experiments, minimizes collisional donor-acceptor interactions and the interference of free molecules present in solutions in photophysical experiments. In addition, the lifetime of the formed hydrogen bonded complexes (>100 milliseconds<sup>28</sup>) is significantly larger than the timescale for the expected photophysical processes. As a result, the true (static) properties of the supramolecular donor-acceptor complex in energy or electron transfer can be studied.

**Optical Properties of OPV4-UP1 and OPV4-UP2.** The UV/Vis absorption spectra of OPV4-UP1 and OPV4-UP2 are dominated by the strong  $\pi$ - $\pi^*$  bands of the OPV4 unit in the 400-500 nm range (Figure 3). The wavelength of maximum absorption of OPV4-UP2 shows a small, but significant, red shift of 12 nm compared to the spectrum of OPV4-UP1. This difference is attributed to the direct attachment of the OPV4 moiety to the isocytosine of the ureido-pyrimidinone unit, resulting in a longer conjugation length.

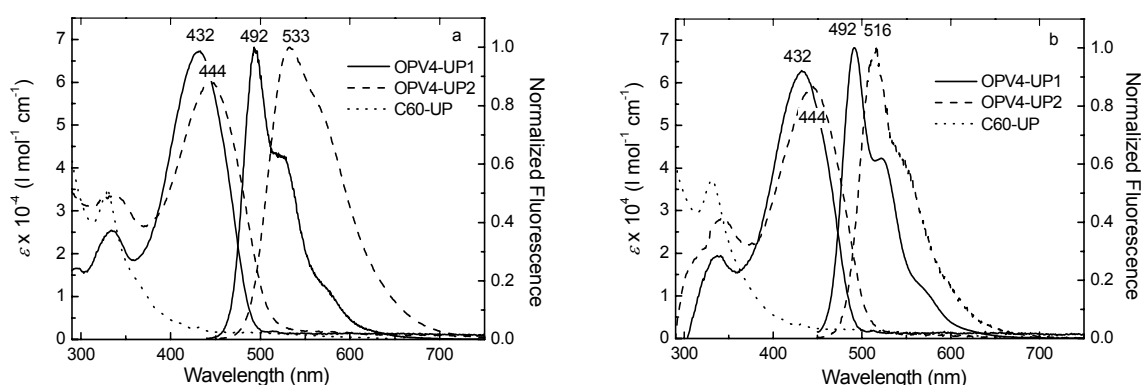


**Figure 3:** Absorption and fluorescence spectra of OPV4-UP1, OPV4-UP2, and C<sub>60</sub>-UP in chloroform (a) and toluene (b) (fluorescence of C<sub>60</sub>-UP is not shown).

Likewise, the fluorescence of OPV4-UP2 exhibits a red shift compared to that of OPV4-UP1 (Figure 3). Surprisingly, the magnitude of the shift of the fluorescence spectrum depends on the solvent; it is more than 15 nm larger for chloroform than for toluene. In addition, the characteristic OPV4 emission, consisting of a strong 0-0 transition and a vibronic shoulder at longer wavelengths, as seen in toluene is transformed into a broad band in chloroform.

To investigate whether interactions between the two OPV4-UP molecules in the OPV4-UP homodimers, which are present under these conditions, may cause this effect, a titration with dimethylsulfoxide (DMSO) was performed. DMSO is well known for its strong hydrogen bond accepting properties and addition of only a few percent DMSO will break up any dimers and result in the sole presence of monomeric ureido-pyrimidinone units. The fluorescence spectra of OPV4-UP1 in

chloroform and toluene do not change upon addition of a small amount of DMSO (Figure 4). This indicates that the absorption and fluorescence of monomeric and dimeric OPV4-UP1 are virtually identical. In contrast, when DMSO is added to an OPV4-UP2 solution, the fluorescence spectrum changes (Figure 4). The spectrum in chloroform containing 0.2 % (by volume) DMSO has shifted 10 nm to the blue and there is a small increase in fluorescence intensity. In toluene, both a shift and an increase in intensity were observed for OPV4-UP2, yet less pronounced than in the chloroform spectrum.<sup>45</sup> A tentative explanation for these effects is the formation of supramolecular assemblies of the homo-dimers as a result of  $\pi$ -stacking.<sup>46</sup> These supramolecular aggregates break up as soon as the quadruple hydrogen bonded homo-dimer dissociates by the addition of some DMSO.

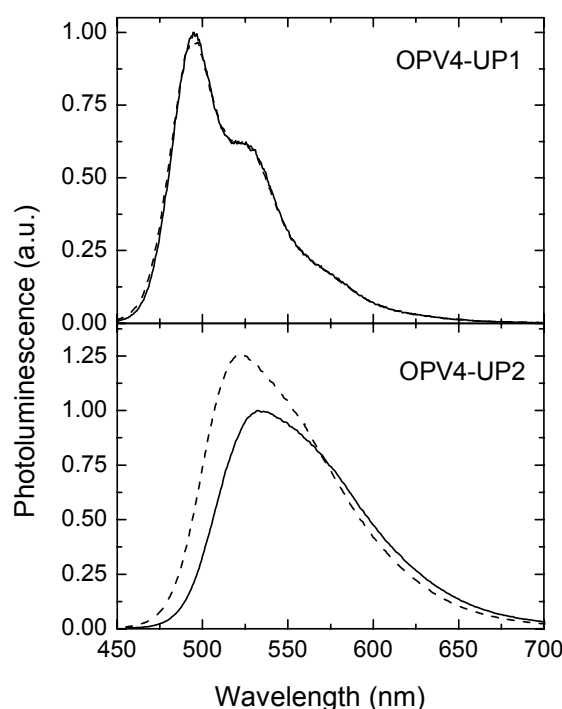


**Figure 4:** Fluorescence of OPV4-UP in chloroform (solid line) and in chloroform with 0.2 % DMSO (dashed lines), normalized to the concentration of the pure chloroform solutions.

The fluorescence quantum yield  $\phi$  and lifetime  $\tau$  of OPV4-UP1 and OPV4-UP2 were determined in the two solvents relative to fluorescein ( $\phi = 0.92$ ).<sup>47</sup> The quantum yield of OPV4-UP1 is slightly higher than that of OPV4-UP2, especially in chloroform (Table 1). The fluorescence quantum yield of OPV4-UP1, is similar to that of methyl end-capped OPV4 (Figure 2) that is 0.80 and 0.74 in chloroform and toluene, respectively. Apparently the conjugation of the OPV4 moiety to the isocytosine of the ureido-pyrimidinone unit in OPV-UP2, results in a small decrease of the quantum yield. Fluorescence lifetimes, measured with time-correlated single photon counting are in the range of 1.23-1.58 ns and only slightly dependent on the solvent (Table 1).

**Keto-Enol Equilibrium.** Besides the 2-ureido-4[1H]-pyrimidinone, also referred to as *keto* form, the pyrimidin-4-ol or *enol* tautomer can be present (Figure 1). In case the  $R_1$  substituent of the isocytosine

moiety is a (substituted) phenyl group, the equilibrium shifts to the *enol* tautomer, especially in more apolar solvents like toluene.<sup>27</sup> An electron withdrawing R<sub>1</sub> substituent stabilizes the *enol* form because a proton on the nitrogen in the isocytosine is more acidic than a proton on the oxygen attached to the isocytosine.<sup>48</sup> The pyridin-4-ol tautomer represents a DADA motif, which has a lower association constant ( $\sim 10^4$  to  $10^5$  M<sup>-1</sup>) due to less favourable secondary interaction in the hydrogen-bonding array.<sup>27,49,50</sup>

The DDAA and DADA motifs are not complementary and, hence, the equilibrium will affect the formation of the homo- and hetero-dimers. Therefore, it is important to determine the relative amount of both tautomeric forms present in solution. When both tautomers are present, the <sup>1</sup>H-NMR spectra give two sets of three N-H protons.<sup>27</sup> In addition, the aromatic proton signal of the pyrimidin-4-ol tautomer is found 0.3–0.5 ppm downfield to the alkylidene proton signal of the 4[1H]pyrimidinone tautomer.<sup>27</sup> By integration of the respective peak areas in the <sup>1</sup>H-NMR spectra it is possible to determine the relative amounts of *keto* and *enol*. We found that in chloroform, OPV4-UP1 is solely present in the DDAA tautomeric form, while OPV4-UP2 contains some (10–15 %) of the *enol* (Table 1). In toluene, the amounts of *keto* are less. OPV4-UP1 is for 90 % in the DDAA form in toluene, while the amount of 4[1H]-pyrimidinone in OPV4-UP2 has dropped to 50 %. The <sup>1</sup>H-NMR spectrum of C<sub>60</sub>-UP in toluene indicates that only the *keto* form is present. This is consistent with the fact that derivatives with *n*-alkyl substituents at both the R<sub>1</sub> and R<sub>2</sub> position are exclusively present as 4[1H]pyrimidinone tautomers.<sup>27</sup> We have no indications that in the present case the *keto-enol* equilibrium depends on the concentration (at the concentrations measured by NMR), but previously the ratio of the two tautomers was found to be concentration-dependent, with the *enol* favored at lower concentrations.<sup>27</sup> Hence, at lower concentrations, the actual ratios might differ from those collected in Table 1.

**Table 1:** Percentage of 4[1H]-pyrimidinone (% *keto*) determined from <sup>1</sup>H-NMR spectroscopy, the fluorescence lifetime ( $\tau$ ) and the fluorescence quantum yield ( $\phi$ ) in chloroform and toluene of OPV4-UP1, OPV4-UP2, and C<sub>60</sub>-UP.

Compound	Solvent	% <i>keto</i>	$\tau$ (ns)	$\phi$
OPV4-UP1	CHCl <sub>3</sub>	> 99	1.54	0.88
	toluene	90	1.23	0.84
OPV4-UP2	CHCl <sub>3</sub>	85-90	1.58	0.59
	toluene	~50	1.42	0.69
C <sub>60</sub> -UP	CHCl <sub>3</sub>	> 99	-	-
	toluene	> 99	-	-

**Fluorescence Quenching.** Fluorescence spectroscopy has been used to investigate the photophysical processes within the hydrogen bonded OPV4-UP/C<sub>60</sub>-UP hetero-dimers after photoexcitation. Information on the rate for energy or electron transfer within a hetero-dimer can be obtained by monitoring the quenching of the photoluminescence of the OPV4-UP moiety upon addition of C<sub>60</sub>-UP to an OPV4-UP solution. The reduction in photoluminescence is quantified by a quenching factor  $Q$ , defined as the ratio of the OPV4-UP fluorescence of the initial solution ( $I_0$ ) and the OPV4-UP fluorescence of the OPV4-UP/C<sub>60</sub>-UP mixture ( $I$ ). The results are depicted in a modified Stern-Volmer<sup>51</sup> plot (Figure 5), where the fluorescence quenching  $I_0/I$  is plotted as a function of the ratio of

C<sub>60</sub>-UP/OPV4-UP. Because an ultrafast singlet-energy transfer always precedes the electron transfer reaction in a covalently bound OPV4-C<sub>60</sub> dyad in solution,<sup>35</sup> we focused on the energy transfer process first.

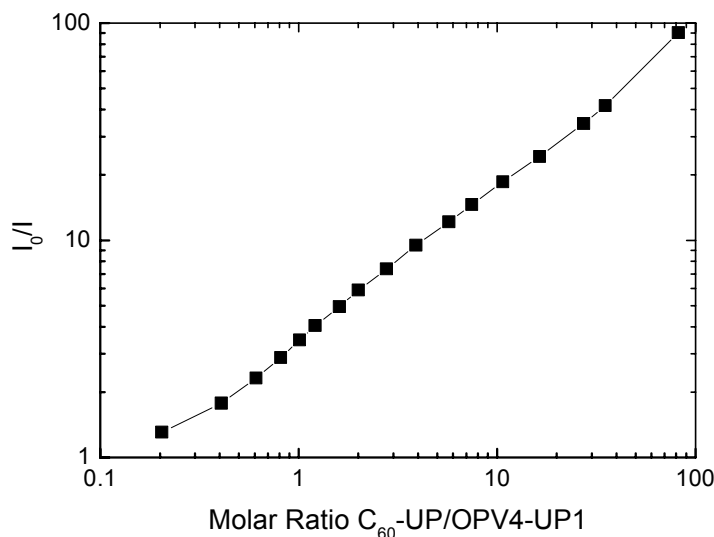


**Figure 5:** Modified Stern-Volmer plot for the fluorescence quenching of OPV4-UP1 ( $10^{-6}$  M) in chloroform upon addition of C<sub>60</sub>-UP.  $I_0$  is the fluorescence signal of the pure OPV4-UP1 solution. The excitation wavelength is 432 nm; the fluorescence intensity ( $I$ ) is determined at 492 nm.

To ensure that only *energy* transfer occurs from OPV4-UP to C<sub>60</sub>-UP, rather apolar solvents as toluene ( $\epsilon = 2.38$ ) and chloroform ( $\epsilon = 4.81$ ) were used. To avoid contributions of OPV4-UP fluorescence quenching via dynamic processes (collisional quenching) and to minimize additional fluorescence from free OPV4-UP units (that are not bonded in a homo- or hetero-dimer), the total concentration of UP units was kept between  $10^{-3}$  and  $10^{-6}$  M. A control experiment using OPV4-UP2 and a soluble C<sub>60</sub> derivative (PCBM, Figure 2) that is not able to form hydrogen bonds, reveals that no quenching occurs under the experimental conditions (Figure 6) and that dynamic (also referred to as collisional) quenching is not important. Consequently, the observed OPV4-UP photoluminescence only results from OPV4-UP/OPV4-UP homo-dimers and OPV4-UP/C<sub>60</sub>-UP hetero-dimers. Hence, any quenching ( $Q$ ) observed results from energy transfer in hetero-dimers only. It can be noted that a direct sensitization of the fullerene fluorescence is not observable experimentally owing to the large excess of C<sub>60</sub>-UP relative to the OPV4-UP donor.

Figure 5 shows that indeed a pronounced quenching of the OPV4-UP1 fluorescence occurs upon addition of C<sub>60</sub>-UP to OPV4-UP1 in chloroform due to the supramolecular association of donor (OPV4-UP1) and acceptor (C<sub>60</sub>-UP) moieties.<sup>52</sup> In the case of OPV4-UP1/C<sub>60</sub>-UP in chloroform, a fluorescence quenching of  $\geq 98.9\%$  is obtained at the highest C<sub>60</sub>-UP/OPV4-UP ratios investigated.<sup>53</sup> Interestingly, the  $Q$  value already exceeds the value of 2 at a C<sub>60</sub>-UP:OPV4-UP1 ratio of 1:1. This indicates that there is a preference for the hetero-dimer, rather than a statistical distribution (1:2:1) of OPV4-UP homo-dimer:OPV4-UP/C<sub>60</sub>-UP hetero-dimer:C<sub>60</sub>-UP homo-dimer.<sup>54</sup> Without knowing the exact amounts present, the non-statistical distribution prevents an accurate estimate of the limiting

quenching factor  $Q_{\max}$  of a hetero-dimer. A lower limit of  $Q_{\max}$ , however, can be obtained from the amount of fluorescence quenching at large  $C_{60}$ -UP/OPV4-UP ratios ( $> 50$ ), where the excess of  $C_{60}$ -UP causes most OPV4-UP molecules to be attached to a  $C_{60}$ -UP molecule. In the case of OPV4-UP1/ $C_{60}$ -UP in chloroform, this results in  $Q_{\max} \geq 90$ . Since no limiting value of  $Q$  is reached upon addition of  $C_{60}$ -UP at large  $C_{60}$ -UP/OPV4-UP ratios (Figure 5), the remaining fluorescence is predominated by the fluorescence of the OPV4-UP1/OPV4-UP1 homo-dimer rather than that of the OPV4-UP1/ $C_{60}$ -UP hetero-dimer. This lower estimate for  $Q_{\max}$  is more than one order of magnitude larger than quenching factors previously reported for hydrogen-bonded donor-acceptor dyads.<sup>13-26</sup>

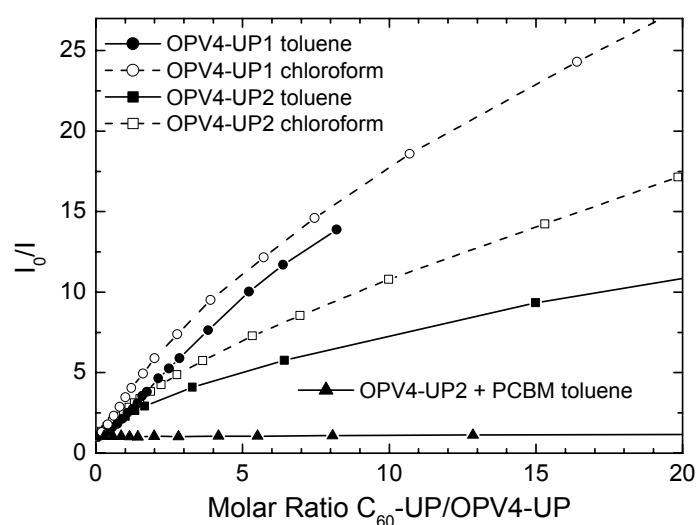


**Figure 6:** Modified Stern-Volmer plot of fluorescence quenching in toluene and chloroform. Concentrations of OPV4-UP are constant at  $10^{-6}$  M during the experiments.  $I_0$  is the fluorescence signal of the pure OPV4-UP solution. The excitation wavelength is 432 nm; the fluorescence intensity ( $I$ ) is determined at the emission maximum.

The fluorescence quenching of OPV4-UP1 upon addition of  $C_{60}$ -UP is less in toluene than in chloroform (Figure 6). This solvent effect can be ascribed to the *keto-enol* equilibrium discussed above. In chloroform, the amount of 4[1H]-pyrimidinone tautomer is higher than in toluene (Table 1). Because dimerization is favored for the *keto* form, the larger amount of 4[1H]-pyrimidinone in chloroform leads to a better coupling with the  $C_{60}$ -UP moiety and, hence, a more efficient quenching of the fluorescence.

The rationale that the amount of quenching is proportional to the amount of *keto* form present, is supported by the fluorescence quenching experiments on OPV4-UP2 in chloroform and toluene upon addition of  $C_{60}$ -UP. For OPV4-UP2 the amount of *keto* is much less in toluene (50 %) than in chloroform (85-90 %, Table 1). Accordingly, the quenching of the OPV4-UP2 fluorescence in chloroform is almost double to that in toluene.

Nevertheless, there is a remarkable difference in the amount of quenching of OPV4-UP1 and OPV4-UP2 in both solvents (Figure 6). Even in chloroform, where the *keto* form is the dominant tautomer, the fluorescence of OPV4-UP1 is quenched to a significantly larger extent than that of OPV4-UP2

upon adding C<sub>60</sub>-UP. While it is clear that the difference must originate from difference in molecular structure, the remarkable observation is that the distance between donor and acceptor is larger in the OPV4-UP1/C<sub>60</sub>-UP dimer than in the OPV4-UP2/C<sub>60</sub>-UP dimer, while the latter has a lower quenching factor.

The fluorescence quenching experiments of the OPV4-UP1 and OPV4-UP2 using C<sub>60</sub>-UP afford the quenching factors at different ratios of quencher versus fluorophore. The results presented above show that these values are directly related to the dimerization equilibrium of the hydrogen bonding molecules, their tendency to form hetero- or homo-couples and the *keto-enol* equilibrium of the individual chromophores. Although in principle it is possible to extract equilibrium constants and  $Q_{\max}$  from the Stern-Volmer plots, the complex nature of the system caused by the great variety of species present, hampered to achieve this goal.

**Förster Energy Transfer.** With the values of  $\phi$  and  $\tau$  the rate for singlet-energy transfer between a donor and acceptor can be estimated according using the Förster equation.<sup>55</sup>

$$k_{EN} = \frac{1}{\tau} \cdot \frac{9000(\ln 10)^{\frac{2}{3}} \phi}{128\pi^5 N_{av} n^4 d^6} J_F \quad (1)$$

In (1), the parameters  $N_{av}$  and  $n$  represent Avogadro's number and the refractive index of the solvent. The value of  $d$  is the center-to-center distance of the two chromophores involved in the energy transfer. This calculation uses the overlap ( $J_F$ ) between the absorption ( $\varepsilon(\bar{\nu})$ ) of the acceptor (C<sub>60</sub>-UP) and the fluorescence ( $F(\bar{\nu})$ ) of the donor (OPV4-UP) on an energy scale (cm<sup>-1</sup>) defined as:

$$J_F = \frac{\int \left( \frac{F(\bar{\nu})\varepsilon(\bar{\nu})}{\bar{\nu}^4} \right) d\bar{\nu}}{\int F(\bar{\nu}) d\bar{\nu}} \quad (2)$$

In addition, the rate for singlet-energy transfer can be obtained experimentally from the lifetime  $\tau$  and  $Q_{\max}$  via:

$$k_{EN} = \frac{Q_{\max} - 1}{\tau} \quad (3)$$

Using the lower estimate of  $Q_{\max} \geq 90$  obtained for the OPV4-UP1/C<sub>60</sub>-UP hetero-dimer, a rate constant for singlet-energy transfer of  $k_{EN} \geq 6 \times 10^{10} \text{ s}^{-1}$  is obtained from (3), which according to (1) corresponds to  $d \leq 17 \text{ \AA}$ . Using molecular modelling a distance of 18–19 Å has been estimated between the center of the fullerene and the center of the first phenyl ring of the OPV unit, *i.e.* close to the estimate of 17 Å based on the Förster model. It is interesting to note that in a previous study on OPV4-C<sub>60</sub> (Figure 2) a similar conclusion was reached.<sup>35</sup> For covalently linked OPV4-C<sub>60</sub> we established that delocalization of the singlet-excited state onto the first benzene ring of the OPV4 unit



is indeed a requirement to explain the high rate for singlet-energy transfer of  $k_{EN} = 5.3 \times 10^{12} \text{ s}^{-1}$  in this dyad by the Förster mechanism.<sup>35</sup>

**Electron Transfer.** After having assessed the occurrence of *energy* transfer within the two OPV4-UP/C<sub>60</sub>-UP hetero-dimers, it is of interest to see if photoinduced *electron* transfer occurs in these hydrogen-bonded dyads. For OPV4-C<sub>60</sub>, the occurrence of an electron transfer reaction depends strongly on the polarity of the solvent.<sup>33,35</sup> This solvent dependence could be explained quantitatively by the Weller equation, which relates the energy level of the charge separated state ( $G_{CS}$ ) to the polarity ( $\epsilon_s$ ) of the solvent:<sup>56</sup>

$$G_{cs} = e(E_{ox}(D) - E_{red}(A)) - \frac{e^2}{4\pi\epsilon_0\epsilon_s R_{cc}} - \frac{e^2}{8\pi\epsilon_0} \left( \frac{1}{r^+} + \frac{1}{r^-} \right) \left( \frac{1}{\epsilon_{ref}} - \frac{1}{\epsilon_s} \right) \quad (4)$$

Here  $-e$  is the electron charge,  $\epsilon_0$  is the vacuum permittivity,  $\epsilon_{ref}$  the polarity of the solvent used to determine the redox potentials  $E_{ox}(D)$  and  $E_{red}(A)$ ,  $R_{cc}$  the center-to-center distance of positive and negative charges, and  $r^+$  and  $r^-$  the radii of the positive and negative ions.<sup>31</sup> Using (4),  $G_{CS}$  was determined for the OPV4-UP1 ( $E_{ox}(D) = 0.71 \text{ V vs. SCE}$ ) and C<sub>60</sub>-UP ( $E_{red}(A) = -0.67 \text{ V vs. SCE}$ ) combination (Figure 7). In this calculation, the center-to-center distance between donor and acceptor was set at the minimum value possible for hydrogen-bonded hetero-dimer ( $R_{cc} = 17 \text{ \AA}$ ) and at infinity (energetically most unfavorable). The decrease of  $G_{CS}$  with increasing polarity of the solvent results in a negative value for  $\Delta G_{CS}$  for charge separation relative to the singlet and triplet excited state of C<sub>60</sub>-UP in polar solvents like ODCB and benzonitrile, irrespective of  $R_{cc}$ . Hence, from a free-energy point of view, electron transfer is possible in ODCB, but the actual rate will depend on the electronic coupling between the donor and acceptor in the excited state.

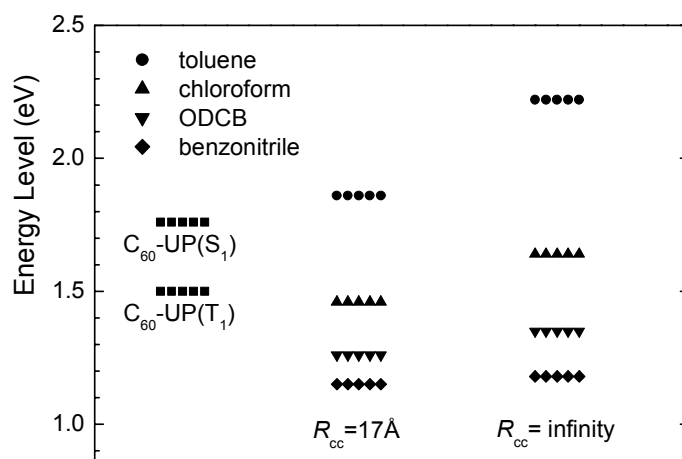


**Figure 7:** Energy level of the charge-separated state of the OPV4-UP1/C<sub>60</sub>-UP couple in solvents of different polarity, calculated using equation 4, assuming a center-to-center distance between positive and negative charges of  $17 \text{ \AA}$  (in the hydrogen bonded dimer) and infinity (upper limit). At the left side the singlet ( $S_1$ ) and triplet ( $T_1$ ) levels of C<sub>60</sub>-UP are shown.

The formation of a charge-separated state can be identified experimentally from a quenching of the acceptor fluorescence. When C<sub>60</sub>-UP is excited in the presence of OPV4-UP1, electron transfer should result in a quenching of the fullerene fluorescence, relative to the signal of a solution containing only C<sub>60</sub>-UP.

In the hydrogen bonded OPV4-UP1/C<sub>60</sub>-UP system in ODCB, this quenching of the C<sub>60</sub>-UP emission is not detected (Figure 8, left). A small blue shift of the C<sub>60</sub>-UP emission is observed, probably due to an unknown impurity. A titration experiment (Figure 8, right), monitoring the OPV4-UP1 fluorescence, resulted in a similar quenching as in apolar solvents, indicating that the hydrogen bonded hetero-dimer is formed in ODCB and undergoes singlet-energy transfer after photoexcitation. The OPV4-UP1 fluorescence quenching in ODCB occurs to the same extent as in toluene and chloroform. An explanation for the possible absence of charge transfer between OPV4-UP1 and C<sub>60</sub>-UP can be found in the larger distance over which the transfer must take place compared to OPV4-C<sub>60</sub>. The large distance between the donor and the acceptor induced by the two ureido-pyrimidinone units and the exponential decay of electron transfer rates with increasing distance,<sup>57</sup> results in a reduced tendency for charge transfer.<sup>58</sup>

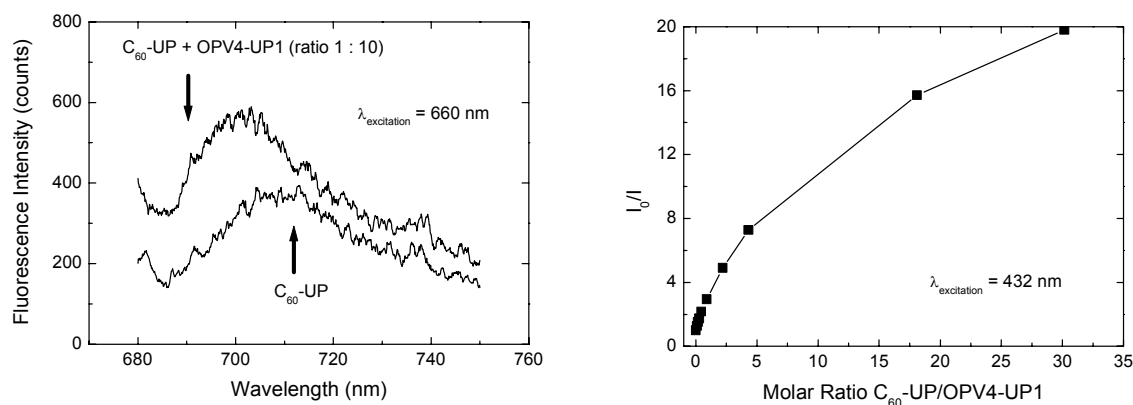


**Figure 8:** Fluorescence quenching for OPV4-UP1/C<sub>60</sub>-UP solutions in ODCB. The C<sub>60</sub>-UP concentration is  $4 \times 10^{-5}$  M for the top graph. The OPV4-UP1 concentration for the experiment shown in the bottom graph is  $10^{-6}$  M.

### 6.3 Bifunctional OPV-Fullerene Ureido-Pyrimidinone Systems

By using molecules that are functionalized with more than one ureido-pyrimidinone unit, it is possible to obtain more complex supramolecular architectures such as polymers and cycles.<sup>59-61</sup> Previous studies concerning this hydrogen-bonding unit have shown the formation of very stable structures<sup>62</sup> and the possibility to tune the equilibrium between polymers and cycles.<sup>61,63</sup> To study this behavior for systems containing a donor and acceptor moiety, an OPV and a fullerene derivative containing two ureido-pyrimidinones have been studied (Figure 9). The OPV derivative (OPV<sub>2</sub>-UP<sub>2</sub>) consists of two OPV-ureido-pyrimidinone units linked by a C<sub>12</sub> spacer at the 6-position of the isocytosine rings.<sup>64</sup> The fullerene derivative (C<sub>60</sub>-UP<sub>2</sub>) has a single C<sub>60</sub> molecule attached to two ureido-pyrimidinone units.<sup>65</sup>

In general, mixing of different species always leads to a statistical mixture of homo- and hetero-dimers due to the self-complementary nature of the system,<sup>66</sup> although in few cases specific dimerization is observed.<sup>63</sup> A <sup>1</sup>H-NMR spectrum of an equimolar mixture of OPV<sub>2</sub>-UP<sub>2</sub> and C<sub>60</sub>-UP<sub>2</sub> in CDCl<sub>3</sub> displays five peaks at low field (Figure 9) that are ascribed to the OPV<sub>2</sub>-UP<sub>2</sub>/C<sub>60</sub>-UP<sub>2</sub> hetero-dimer (Figure 10). These peaks are observed at chemical shifts significantly differing in position as compared to the spectra of the separate OPV<sub>2</sub>-UP<sub>2</sub> ( $\delta = 13.1, 12.1, \text{ and } 10.9$ )<sup>64</sup> and C<sub>60</sub>-UP<sub>2</sub> ( $\delta = 12.9, 11.6, \text{ and } 10.7$ )<sup>65</sup> homo-polymers.

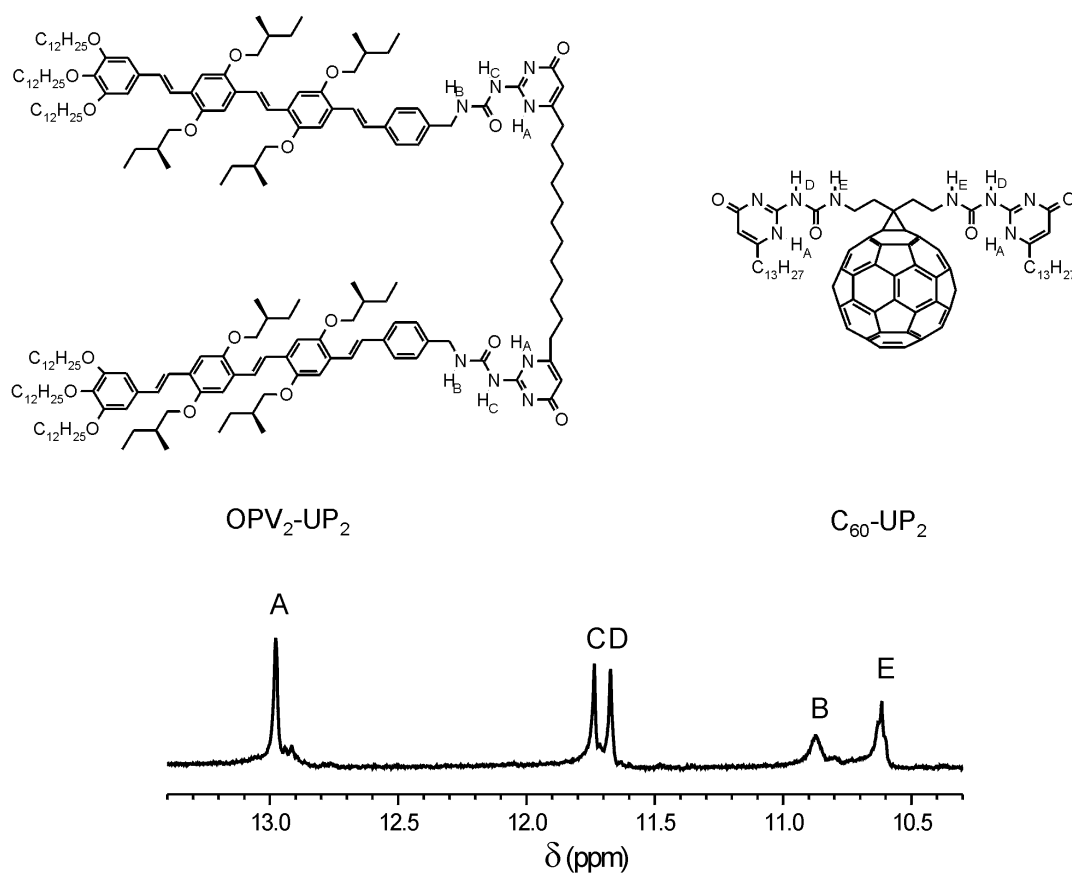


**Figure 9:** Bifunctional 2-ureido-4[1H]-pyrimidinone OPV<sub>2</sub>-UP<sub>2</sub> and C<sub>60</sub>-UP<sub>2</sub> compounds. <sup>1</sup>H-NMR in CDCl<sub>3</sub> of a 1:1 OPV<sub>2</sub>-UP<sub>2</sub>:C<sub>60</sub>-UP<sub>2</sub> mixture.

The assignment shown in Figure 9 is based on the typical resonances for UP dimers.<sup>64,65,67</sup> Therefore it can be concluded that the 1:1 mixture of the two compounds results in the selective formation of cyclic hetero-dimers and not a statistical mixture. The alternating OPV<sub>2</sub>-UP<sub>2</sub>/C<sub>60</sub>-UP<sub>2</sub> polymer (which results in an identical <sup>1</sup>H-NMR spectrum) is not assumed to be present as the viscosity of the solution is similar to that of pure chloroform. In addition, the concentration is too low to create polymeric structures.<sup>63</sup>

To investigate the properties of this unique assembly in more detail, the intensity of the OPV<sub>2</sub>-UP<sub>2</sub> fluorescence at  $\lambda_{em} = 494$  nm was monitored upon addition of C<sub>60</sub>-UP<sub>2</sub> in chloroform and toluene. During the addition the positions of the absorption bands remain unchanged, indicating a weak electronic interaction in the ground state.

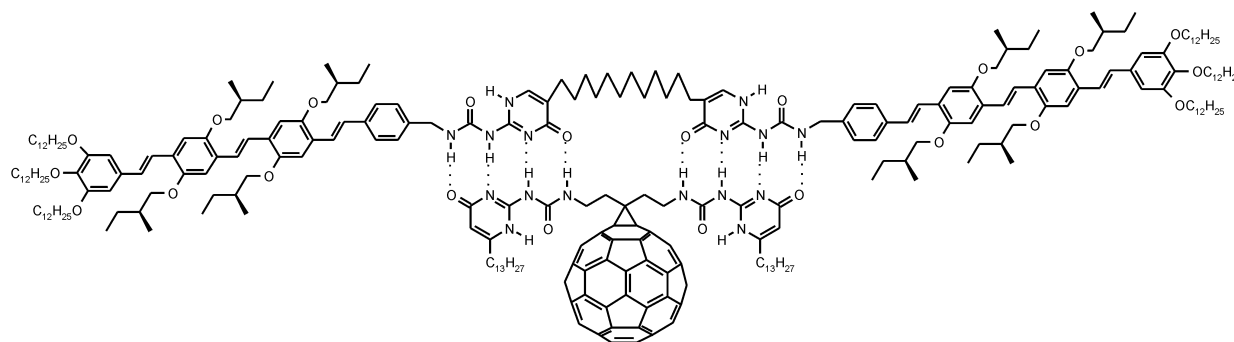


**Figure 10:** Structure of the  $OPV_2-UP_2/C_{60}-UP_2$  cyclic hetero-dimer as observed by  $^1H-NMR$  in chloroform of a 1:1  $OPV_2-UP_2:C_{60}-UP_2$  mixture.

However, this addition leads to a distinct quenching of the donor fluorescence, indicating the presence of singlet-energy transfer from the photoexcited OPV to the  $C_{60}$  moiety. The quenching rate in a 1:1 (equimolar mixture of molecules) and a 1:2 (equimolar mixture of chromophores)  $OPV_2UP_2:C_{60}-UP_2$  solution is monitored in time as the high stability of the species present, prevents an instantaneous equilibrium formation (Figure 11).

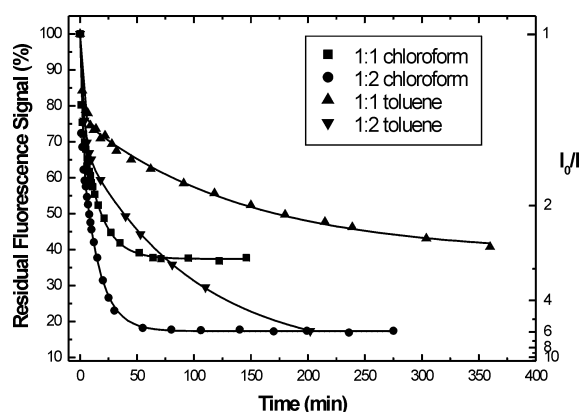


**Figure 11:** Fluorescence intensity of 1:1 and 1:2  $OPV_2-UP_2:C_{60}-UP_2$  mixtures in chloroform and toluene together with the exponential decay curves.  $I_0$  represents the fluorescence intensity of the pure  $OPV_2-UP_2$  solution, whereas  $I$  indicates the  $OPV_2-UP_2$  fluorescence in the indicated mixture. The concentration of  $OPV_2-UP_2$  is  $5 \times 10^{-7} M$ ,  $\lambda_{exc} = 435 nm$ ,  $\lambda_{em} = 494 nm$ ,  $T = 20^\circ C$ .

The mathematical fit of the experimental data with a double exponential decay results in time constants of 15 and 14 minutes in the case of respectively the 1:1 and 1:2 mixture in chloroform, whereas in toluene time constants of 180 and 86 minutes are calculated for the 1:1 and 1:2 mixture respectively. These time constants give an indication of the time to reach equilibrium, monitored by the formation of  $OPV_2-UP_2/C_{60}-UP_2$  couples. The second time constant ranges for all measurements from 1 to 3 minutes and is considered not to have any physical meaning as it is faster than the recording time of a single measurement.

To monitor the influence of temperature on the equilibrium, a solution of  $OPV_2-UP_2$  in toluene was heated, resulting in a slight decrease in fluorescence intensity. Subsequently, at  $80^\circ C$ ,  $C_{60}-UP_2$  was

added, resulting in an immediate quenching of the OPV fluorescence. The examined mixtures were then cooled. Reheating the solution resulted in similar intensities as obtained in the cooling run, demonstrating the reversibility of the interactions. The fluorescence intensities at 20 °C are the same as obtained by addition of the C<sub>60</sub> derivative at 20 °C. This indicates that the addition of C<sub>60</sub>-UP<sub>2</sub> at various temperatures does not influence the final state of the mixture. Furthermore, heating of a 1:1 mixture, which had been kept at room temperature equilibrium for one day, resulted in the same fluorescence intensities as in the case of adding C<sub>60</sub>-UP<sub>2</sub> at 80 °C.

A change in fluorescence results only from the breaking of an OPV<sub>2</sub>-UP<sub>2</sub>/OPV<sub>2</sub>-UP<sub>2</sub> couple followed by the formation of an OPV<sub>2</sub>-UP<sub>2</sub>/C<sub>60</sub>-UP<sub>2</sub> couple. Therefore, the calculated equilibrium time constant holds the sum of various processes *i.e.* the opening and closing of the hydrogen bond and the chance of two different non-bonded units colliding. This is in full agreement with the doubling of the time constant in toluene when only half the amount of the C<sub>60</sub>-UP<sub>2</sub> is present. The time constants indicate that the homo-polymeric species are highly stable in toluene because the exchange between different species proceeds very slow. The increase in time constants going from chloroform to toluene, can be rationalized by the one order of magnitude increase of the dimerization constant of the UP unit. This accounts for an increased thermodynamic penalty for the presence of non-bonded hydrogen bonding moieties, inducing a considerably lower concentration of free end groups that have the possibility to form new hetero-dimers. Therefore the time needed to reach equilibrium rises in toluene and can be adjusted by increasing the driving force to form equilibrium by enhancing the concentration of one of the compounds. Important is the fact that even though the dynamics of the equilibrium change with solvent, this does not influence the final composition of the mixture. Moreover, the amount of quenching ( $I_0/I > 2$  at ratio 1:1) reveals that the formation of OPV<sub>2</sub>-UP<sub>2</sub>/C<sub>60</sub>-UP<sub>2</sub> hetero-couples is favourable as compared to the formation of the respective homo-couples, consistent with the <sup>1</sup>H-NMR results.

Although the  $I_0/I$  value obtained by fluorescence studies for the ratio of 1:1 of OPV<sub>2</sub>-UP<sub>2</sub>:C<sub>60</sub>-UP<sub>2</sub> is larger than the estimated value of 2, the selectivity for the formation of hetero-dimers is less than was indicated by <sup>1</sup>H-NMR measurements. In the case of an exclusive presence of hetero-dimers, fluorescence quenching is expected to its full extent for the equimolar ratio of OPV<sub>2</sub>-UP<sub>2</sub> to C<sub>60</sub>-UP<sub>2</sub>, however the addition of an extra amount of C<sub>60</sub>-UP<sub>2</sub> (e.g. a 1:2 ratio) leads here to an increase of the fluorescence quenching as the  $I_0/I$  value increases from 3 to 6. This difference between the fluorescence and <sup>1</sup>H-NMR results is likely to be caused by the large difference in experimental concentration between both techniques.

## 6.4 Conclusions

A photoinduced singlet-energy transfer reaction between OPV4 and C<sub>60</sub> derivatives is observed in 2-ureido-4[1H]-pyrimidinone hydrogen bonded hetero-dimers in apolar and polar solvents. The change in the equilibrium between 4[1H]-pyrimidinone and pyrimidin-4-ol tautomers of OPV4-UP by varying the solvent, results in a proportional change in the quenching factor of the OPV4-UP fluorescence because the *enol* form is not able to bind with the *keto* form of C<sub>60</sub>-UP. The lower limit of the maximum quenching ( $Q_{\max} \geq 90$ ) obtained for OPV4-UP1/C<sub>60</sub>-UP mixtures in chloroform is at least one order of magnitude higher than values reported so far for hydrogen-bonded dyads<sup>13-26</sup> and results

from the high association constant of the dimers.<sup>28</sup>  $Q_{\max} \geq 90$  corresponds to a rate constant for singlet-energy transfer of  $k_{EN} \geq 6 \times 10^{10} \text{ s}^{-1}$  which can be rationalized based on the Förster mechanism. Although energetically possible, photoinduced electron transfer does not occur in these hydrogen-bonded dimers. The absence of charge separation in polar solvents is most likely due to the significant distance between donor and acceptor in the quadruple hydrogen-bonded hetero-dimers that causes an exponential decrease in the electronic coupling between the two units in the excited state.

In addition, the preferential formation of dimeric OPV<sub>2</sub>-UP<sub>2</sub>/C<sub>60</sub>-UP<sub>2</sub> hetero-cyclic structures based on the self-complementary UP quadruple hydrogen bonding unit has been inferred from <sup>1</sup>H-NMR studies in chloroform. Fluorescence studies confirm the occurrence of preferential formation of hetero-dimers, although the selectivity is less at lower concentrations (10<sup>-6</sup> M). The time for the equilibrium to settle is on the scale of minutes and temperature or solvent type has no effect on the final equilibrium state of the mixture. However, an increase in dimerization constant by varying the solvent, leads to an enhancement of the stability of the formed species.

## 6.5 Experimental Section

**General.** Solvents were of AR (toluene, chloroform) or HPLC (ODCB) grade and were used as received. Proton NMR spectra were recorded on Varian 400 or 500 MHz spectrometers with TMS as an internal standard. UV/Vis absorption spectra were recorded on a Perkin Elmer Lambda 40P spectrometer. A detailed description of the equipment used for the time-correlated single photon counting and cyclic voltammetry measurements can be found in Chapter 2.

**Materials.** The synthesis of the three ureido-pyrimidinone compounds (OPV4-UP1, OPV4-UP2, and C<sub>60</sub>-UP) used in this study has been described elsewhere.<sup>43,44</sup> OPV4<sup>31</sup> and PCBM<sup>68</sup> were used as reference compounds and were available from previous studies.

**Fluorescence Spectroscopy.** Fluorescence spectra were recorded on a Perkin Elmer LS50B or an Edinburgh Instruments FS920 luminescence spectrometer. In the fluorescence quenching experiments, a stock solution of 10 ml 10<sup>-6</sup> M OPV4-UP1 or OPV4-UP2 was used. To circumvent concentration corrections, 5 ml of this solution was used to dissolve the C<sub>60</sub>-UP to give a 10<sup>-4</sup> M C<sub>60</sub>-UP solution with 10<sup>-6</sup> M OPV4-UP. The first measurement to determine the  $I_0$  fluorescence was measured on 2 ml of the OPV4-UP stock solution. The fluorescence signal  $I$  of OPV4-UP was then monitored upon addition of the OPV4-UP/C<sub>60</sub>-UP solution in steps of first a few microliters and later steps of 100 to 250  $\mu\text{l}$ . Finally the OPV4-UP/C<sub>60</sub>-UP stock solution was measured in a separate experiment, providing the quenching in a 100:1 C<sub>60</sub>-UP:OPV4-UP ratio. A cut-off filter of 665 nm was used in the emission beam to prevent stray light in the fluorescence experiments for detecting electron transfer. For fluorescence quantum yield determination, solutions with an optical density of 0.1 at the excitation wavelength ( $\lambda = 430 \text{ nm}$ ) were used and the spectra were corrected for the wavelength dependence of the detection system. The fluorescence spectra were integrated on an energy scale and the area was compared to that of a reference of fluorescein in 0.1 N aqueous NaOH with a quantum yield of 0.92.<sup>47</sup>

## 6.6 References and Notes

- 1 Moser, C. C.; Keske, J. M.; Warnecke, K.; Farid R. S.; Dutton, P. L. *Nature* **1992**, 355, 796.
- 2 Wasielewski, M. R. *Chem. Rev.* **1992**, 92, 435.
- 3 Pelletier, H.; Kraut J. *Science* **1992**, 258, 1748.

- 4 Hayashi, T.; Ogoshi, H. *Chem. Soc. Rev.* **1997**, *26*, 355.
- 5 *Supramolecular Chemistry*, Lehn, J.-M. VCH, Weinheim, **1995**.
- 6 *Supramolecular Photochemistry*, Balzani, V.; Scandola, F. Ellis Horwood, Chichester, **1991**.
- 7 Piotrowiak, P.; *Chem. Soc. Rev.* **1999**, *28*, 143.
- 8 Sessler, J. L.; Wang, B.; Springs, S. L.; Brown, C. T. in *Comprehensive Supramolecular Chemistry*, ed. Atwood, J. L.; Davies, J. E. D.; MacNicol, D. D.; Vögtle F.; Murakami, Y. Pergamon, Oxford, **1996**, Vol. 4, p. 311.
- 9 Hoeben, F. J. M.; Jonkheijm, P.; Meijer, E. W.; Schenning, A. P. H. J. *Chem. Rev.* **2005**, *105*, 1491.
- 10 Corbin, P. S.; Zimmermann, S. C. *J. Am. Chem. Soc.* **1998**, *120*, 9710.
- 11 Sessler, J. L.; Wang, R. *Angew. Chem. Int. Ed.* **1998**, *37*, 1726.
- 12 Sherrington, D. C.; Taskinen, K. A. *Chem. Soc. Rev.* **2001**, *30*, 83.
- 13 Roberts, J. A.; Kirby, J. P.; Nocera, D. G. *J. Am. Chem. Soc.* **1995**, *117*, 8051.
- 14 Kirby, J. P.; Roberts, J. A.; Nocera, D. G. *J. Am. Chem. Soc.* **1997**, *119*, 9230.
- 15 Myles, A. J.; Branda, N. R. *J. Am. Chem. Soc.* **2001**, *123*, 177.
- 16 Turro, C.; Chang, C. K.; Leroy, G. E.; Cukier, R. I.; Nocera, D. G. *J. Am. Chem. Soc.* **1992**, *114*, 4013.
- 17 Prasad, E.; Gopidas, K. R. *J. Am. Chem. Soc.* **2000**, *122*, 3191.
- 18 Smitha, M. A.; Prasad, E.; Gopidas, K. R. *J. Am. Chem. Soc.* **2001**, *123*, 1159.
- 19 Smitha, M. A.; Gopidas, K. R. *Chem. Phys. Lett.* **2001**, *350*, 86.
- 20 Aoyama, Y.; Asakawa, M.; Matsui, Y.; Ogoshi, H. *J. Am. Chem. Soc.* **1991**, *113*, 6233.
- 21 Furuta, H.; Magda, D. J.; Sessler, J. L. *J. Am. Chem. Soc.* **1991**, *113*, 978.
- 22 Harriman, A.; Magda, D. J.; Sessler, J. L. *J. Phys. Chem.* **1991**, *95*, 1530.
- 23 Harriman, A.; Kubo, Y.; Sessler, J. L. *J. Am. Chem. Soc.* **1992**, *114*, 388.
- 24 Sessler, J. L.; Wang, B.; Harriman, A. *J. Am. Chem. Soc.* **1993**, *115*, 10418.
- 25 Sessler, J. L.; Sathiosatham, M.; Brown, C. T.; Rhodes, T. A.; Wiederrecht, G. *J. Am. Chem. Soc.* **2001**, *123*, 3655.
- 26 Tecilla, P.; Dixon, R. P.; Slobodkin, G.; Alavi, D. S.; Waldeck, D. H.; Hamilton, A. D. *J. Am. Chem. Soc.* **1990**, *112*, 9408.
- 27 Beijer, F. H.; Kooijman, H.; Spek, A. L.; Sijbesma, R. P.; Meijer, E. W. *J. Am. Chem. Soc.* **1998**, *37*, 75.
- 28 Söntjens, S. H. M.; Sijbesma, R. P.; Van Genderen, M. H. P.; Meijer, E. W. *J. Am. Chem. Soc.* **2000**, *122*, 7487.
- 29 Sijbesma, R. P.; Beijer, F. H.; Brunsveld, L.; Folmer, B. J. B.; Hirschberg, J. H. K. K.; Lange, R. F. M.; Lowe, J. K. L.; Meijer, E. W. *Science* **1997**, *278*, 1601.
- 30 Brunsveld, L.; Folmer, B. J. B.; Meijer, E. W.; Sijbesma, R. P. *Chem. Rev.* **2001**, *101*, 4071.
- 31 Nierengarten, J.-F.; Eckert, J.-F.; Nicoud, J.-F.; Ouali, L.; Krasnikov, V.; Hadziioannou, G. *Chem. Commun.* **1999**, 617.
- 32 Eckert, J.-F.; Nicoud, J.-F.; Nierengarten, J.-F.; Liu, S.-G.; Echegoyen, L.; Barigelletti, F.; Armaroli, N.; Ouali, L.; Krasnikov, V.; Hadziioannou, G. *J. Am. Chem. Soc.* **2000**, *122*, 7467.
- 33 Armaroli, N.; Barigelletti, F.; Ceroni, P.; Eckert, J.-F.; Nicoud, J.-F.; Nierengarten, J.-F. *Chem. Commun.* **2000**, 599.
- 34 Peeters, E.; Van Hal, P. A.; Knol, J.; Brabec, C. J.; Sariciftci, N. S.; Hummelen, J. C.; Janssen, R. A. J. *J. Phys. Chem. B.* **2000**, *104*, 10174.
- 35 Van Hal, P. A.; Janssen, R. A. J.; Lanzani, G.; Cerullo, G.; Zavelani-Rossi, M.; De Silvestri, S. *Phys. Rev. B* **2001**, *64*, 075206.

- 36 Armaroli, N.; Diederich, F.; Echegoyen, L.; Habicher, T.; Flamigni, L.; Marconi, G.; Nierengarten, J.-F. *New. J. Chem.* **1999**, *23*, 77.
- 37 Dsouza, F.; Deviprasad, G. R.; Rahman, M. S.; Choi, J. P. *Inorg. Chem.* **1999**, *38*, 2157.
- 38 Da Ros, T.; Prato, M.; Guldi, D.; Alessio, E.; Ruzzi, M.; Pasimeni, L. *Chem. Commun.* **1999**, 635.
- 39 Guldi, D.; Luo, C.; Da Ros, T.; Prato, M.; Dietel, E.; Hirsch, A. *Chem. Commun.* **2000**, 375.
- 40 Sun, D.; Tham, F. S.; Reed, C. A.; Chaker, L.; Burgess, M.; Boyd, P. D. W. *J. Am. Chem. Soc.* **2000**, *122*, 10704.
- 41 Yamaguchi, T.; Ishii, N.; Tashiro, K.; Aida, T. *J. Am. Chem. Soc.* **2003**, *125*, 13934.
- 42 Shoji, Y.; Tashiro, K.; Aida, T. *J. Am. Chem. Soc.* **2004**, *126*, 6570.
- 43 El-ghayoury, A.; Peeters, E.; Schenning, A. P. H. J.; Meijer, E. W. *Chem. Commun.* **2000**, 1969.
- 44 Rispens, M. T.; Sánchez, L.; Knol, J.; Hummelen, J. C. *Chem. Commun.* **2001**, 161.
- 45 All spectra shown are 0.2 % DMSO solutions by volume. Spectra of solutions containing 0.1 % to 0.5 % are similar, above 1 % DMSO the spectra change due to polarity increase of the solvent mixture and a possible presence of a non-hydrogen bonding *keto* believed to exist in DMSO, see Beijer, F. H. *Ph.D. Thesis*, Eindhoven University of Technology, **1998**.
- 46 Schenning, A. P. H. J.; Jonkheijm, P.; Peeters, E.; Meijer, E. W. *J. Am. Chem. Soc.* **2001**, *123*, 409.
- 47 Demas, J. N.; Crosby, G. A. *J. Phys. Chem.* **1971**, *75*, 991.
- 48 *Advances in Heterocyclic Chemistry, the Tautomerism of Heterocycles*, Elguero, J.; Marzin, C.; Katritzky, A. R.; Linda, P. Academic Press, New York, **1976**.
- 49 Jorgensen, W. L.; Pranata, J. *J. Am. Chem. Soc.* **1990**, *112*, 2008.
- 50 Pranata, J.; Wierschke, S. G.; Jorgensen, W. L. *J. Am. Chem. Soc.* **1991**, *113*, 2810.
- 51 Stern, O.; Volmer, M. *Phys. Z.* **1919**, *20*, 183.
- 52 The supramolecular association of the donor and acceptor was also observed in a <sup>1</sup>H-NMR spectrum of a mixture of both chromophores.
- 53 At the highest C<sub>60</sub>-UP concentration, the OPV4-UP1 quenching might be overestimated somewhat because the excitation (432 nm) also excites C<sub>60</sub>-UP.
- 54 In a 1:1 mixture of two compounds A and B, the statistical ratio for the formation of dimers is 1:2:1 for A-A:A-B:B-B.
- 55 Förster, T. *Discuss. Faraday Soc.* **1959**, *27*, 7.
- 56 Weller, A. Z. *Phys. Chem. Neue Folge* **1982**, *133*, 93.
- 57 Wasielewski, M. R. in *Photoinduced Electron Transfer*, ed. Fox, M. A.; Chanon, M. **1988**, Vol 1, pp 161-206.
- 58 Pati, R.; Karna, S. P. *Chem. Phys. Lett.* **2002**, *351*, 302.
- 59 Sijbesma, R. P.; Beijer, F. H.; Brunsveld, L.; Folmer, B. J.; Hirschberg, J. H.; Lange, R. F.; Lowe, J. K.; Meijer, E. W. *Science* **1997**, *278*, 1601.
- 60 Brunsveld, L.; Folmer, B. J. B.; Meijer, E. W.; Sijbesma, R. P. *Chem. Rev.* **2001**, *101*, 4071.
- 61 Ten Cate, A. T.; Sijbesma, R. P. *Macromol. Rapid Commun.* **2002**, *23*, 1094.
- 62 Folmer, B. J. B.; Sijbesma, R. P.; Kooijman, H.; Spek, A. L.; Meijer, E. W. *J. Am. Chem. Soc.* **1999**, *121*, 9001.
- 63 Söntjens, S. H. M.; Sijbesma, R. P.; Van Genderen, M. H. P.; Meijer, E. W. *Macromolecules* **2001**, *34*, 3815.
- 64 El-ghayoury, A.; Schenning, A. P. H. J.; Van Hal, P. A.; Van Duren, J. K. J.; Janssen, R. A. J.; Meijer, E. W. *Angew. Chem., Int. Ed.* **2001**, *40*, 3660.
- 65 Sánchez, L.; Rispens, M. T.; Hummelen, J. C. *Angew. Chem., Int. Ed.* **2002**, *41*, 838.



- 66 Beckers, E. H. A.; Van Hal, P. A.; Schenning, A. P. H. J.; El-ghayoury, A.; Peeters, E.; Rispens, M. T.; Hummelen, J. C.; Meijer, E. W.; Janssen, R. A. J. *J. Mater. Chem.* **2002**, *12*, 2054.
- 67 Beijer, F. H.; Sijbesma, R. P.; Kooijman, H.; Spek, A. L.; Meijer, E. W. *J. Am. Chem. Soc.* **1998**, *120*, 6761.
- 68 Hummelen, J. C.; Knight, B. W.; LePeq, F.; Wudl, F.; Yao, J.; Wilkins, C. L. *J. Org. Chem.* **1995**, *60*, 532.

# Hydrogen-bonded Oligo(*p*-phenylene vinylene) – Perylene Bisimide Arrays\*

### *Abstract*

*The photophysical properties of dissolved ureido-pyrimidinone coupled OPV-PERY heterodimers are described in the first part of this chapter. A photoinduced energy transfer reaction takes place in this heterodimer with a rate of  $2 \times 10^{11} \text{ s}^{-1}$ . Although energetically favorable, a photoinduced electron transfer reaction could not be observed for this hydrogen-bonded system. In the second part, aggregated complexes of diaminotriazine oligo(*p*-phenylene vinylene) (OPV) units hydrogen-bonded to different perylene bisimide (PERY) compounds have been investigated by means of absorption, circular dichroism, and photoinduced absorption spectroscopy. These studies reveal that in the aggregated state a fast charge separation occurs, likely via an intermolecular pathway in the J-type structure of the stacked hydrogen-bonded OPV-PERY arrays. The subsequent charge recombination reaction depends strongly on the nanoscopic differences within the J-type geometry as revealed by comparison of stacked supramolecular dimers, trimers, and covalently linked systems. A coupled oscillator model is used to propose the intermolecular arrangements that are consistent with the absorption and circular dichroism spectra.*

---

\* Parts of this work have been published: (a) Neuteboom, E. E.; Beckers, E. H. A.; Meskers, S. C. J.; Meijer, E. W.; Janssen, R. A. J. *Organic and Biomolecular Chemistry* **2003**, *1*, 198-203 (b) Würthner, F.; Chen, Z.; Hoeben, F. J. M.; Osswald, P.; You, C.-C.; Jonkheijm, P.; Van Herrikhuyzen, J.; Schenning, A. P. H. J.; Van der Schoot, P. P. A. M.; Meijer, E. W.; Beckers, E. H. A.; Meskers, S. C. J.; Janssen, R. A. J. *Journal of the American Chemical Society* **2004**, *126*, 10611-10618 (c) Beckers, E. H. A.; Meskers, S. C. J.; Jonkheijm, P.; Schenning, A. P. H. J.; Chen, Z.; Würthner, F.; Janssen, R. A. J. *manuscript in preparation*.

## 7.1 Introduction

The study of photoinduced energy and electron transfer reactions between donors and acceptors assembled via hydrogen-bonding interactions has attracted considerable interest in recent years because hydrogen bonding is often a key structural element in the natural photofunctional systems.<sup>1-20</sup> Therefore numerous artificial systems have been proposed in order to obtain a better understanding of the structure property relationships in donor-acceptor arrays. In this study, oligo(*p*-phenylene vinylene) (OPV) is used as a donor material because its characteristics have been well-studied in combination with various acceptor materials.<sup>21-27</sup> As a counterpart, perylene bisimides (PERY) are chosen as acceptor material.<sup>26,28,29</sup> In all cases, the OPV and PERY units are connected via multiple hydrogen bonding. In first part of this chapter, the photophysical processes in molecularly dissolved ureido-pyrimidinone coupled dimers are studied. In the second part, charge transfer reactions in aggregated structures of diaminotriazine coupled OPV-PERY arrays are investigated

## 7.2 Ureido-Pyrimidinone Coupled OPV-PERY Arrays

The influence of a supramolecular linkage on the energy and electron transfer reaction is studied in a hydrogen bonded OPV-PERY dimer. The strong hydrogen-bonding properties of the quadruple hydrogen bonding ureido-pyrimidinone unit<sup>30,31</sup> enable the study of photophysical processes in donor-acceptor systems even at dilute concentrations.<sup>32</sup> The studied compounds OPV-UP<sup>33</sup> and PERY-UP<sup>34</sup> are shown in Figure 1. The OPV-UP consists of an OPV tetramer with on one side three dodecyloxy chains and the other side connected to the ureido-pyrimidinone unit via a methyl linker. The perylene bisimide moiety of PERY-UP is connected to the ureido-pyrimidinone unit via a di-*tert*-butylphenyl linker.

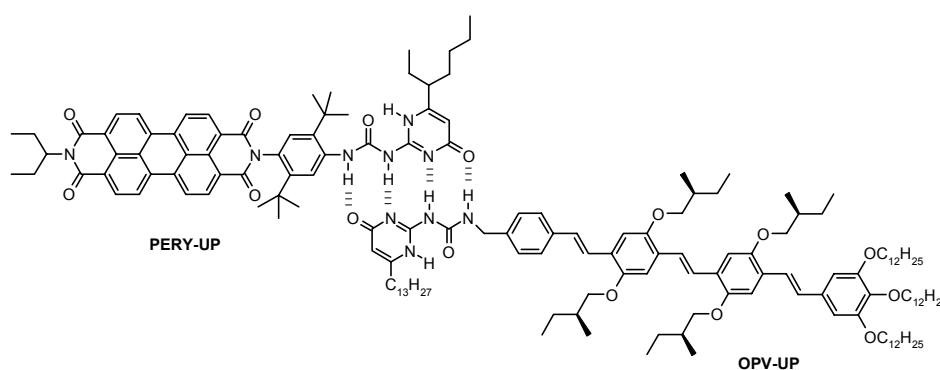


**Figure 1:** Heterodimer of PERY-UP and OPV-UP, bound by the ureido-pyrimidinone quadruple hydrogen-bonding unit.

**Optical Properties.** The absorption and photoluminescence spectra of PERY-UP, OPV-UP are shown in Figure 2. The characteristic absorption peaks of the molecularly dissolved perylene bisimide are at 459, 490, and 527 nm for PERY-UP. The absorption spectrum of OPV-UP is not structured and

maximizes at 432 nm. The fluorescence spectra reveal that the singlet-excited state ( $S_1$ ) of OPV-UP ( $E(S_1) = 2.52$  eV) is higher in energy than the singlet-excited state of PERY-UP ( $E(S_1) = 2.32$  eV).

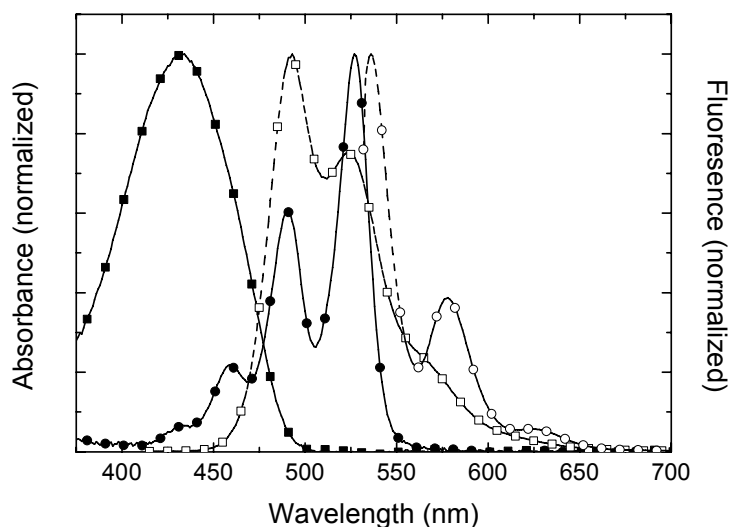


**Figure 2:** Normalized absorption (solid symbols) and fluorescence (open symbols) spectra of OPV-UP (squares) and PERY-UP (circles) in toluene. The excitation wavelength is 410 nm for OPV-UP and 527 nm for PERY-UP.

**Transient Photoinduced Absorption (PIA).** Sub-picosecond transient pump-probe spectroscopy was performed at room temperature on OPV-UP/PERY-UP solutions to assess the temporal evolution of the singlet-energy transfer on short timescales (Figure 3). At 900 nm the  $S_n \leftarrow S_1$  photoinduced absorption of OPV chromophore is present,<sup>25</sup> providing information on the decay kinetics of the OPV-UP( $S_1$ ) state.

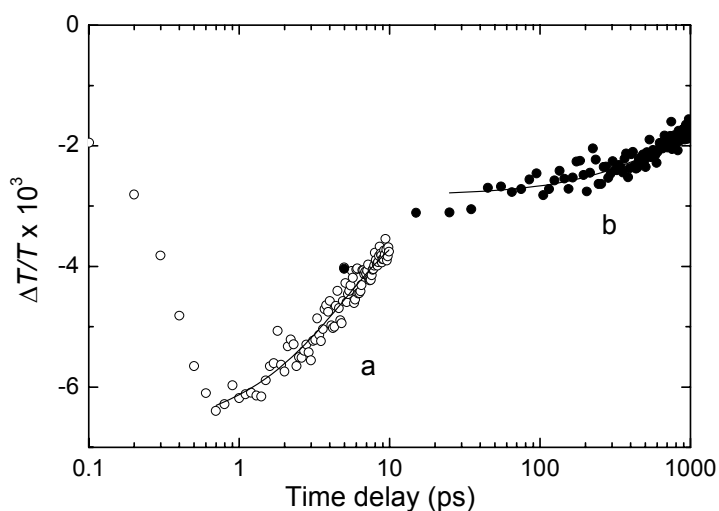


**Figure 3:** Differential transmission dynamics of the OPV ( $S_n \leftarrow S_1$ ) absorption at 900 nm as a function of the pump-probe time delay after photoexcitation at 450 nm. The concentration PERY-UP is  $2 \times 10^{-4}$  M and the concentration OPV-UP is  $4 \times 10^{-5}$  M in toluene. Solid lines are fits to decays with time constant of 5 ps (a) and 1100 ps (b).

Upon preferential photoexcitation of the OPV-UP moiety at 450 nm in a mixture of  $4 \times 10^{-5}$  M OPV-UP and  $2 \times 10^{-4}$  M PERY-UP in toluene, a negative differential transmission was observed by probing at 900 nm. The dynamics in the low picosecond time range (Figure 3, open circles) show a rapid decay which can be fitted to a mono-exponential decay with a time constant of 5 ps, *i.e.* a rate of  $k = 2 \times 10^{11}$  s<sup>-1</sup>. On longer time scales (Figure 3, closed circles) a much slower decay is visible with a mono-exponential time constant of 1.1 ns.

The two different decay times account for the fact that under these conditions both OPV-UP/PERY-UP heterodimers and OPV-UP/OPV-UP homodimers are present. It is important to note that a control experiment confirmed that the  $S_n \leftarrow S_1$  photoinduced absorption of the PERY chromophore has only a small (~10 %) contribution to the photoinduced absorption at 900 nm. The fast (5 ps) decay is attributed to the singlet-energy transfer reaction from OPV-UP( $S_1$ ) to PERY-UP in the heterodimer, while the slow (1.1 ns) decay represents the intrinsic relaxation of OPV-UP( $S_1$ ) in the homodimer. The lifetime of the latter process is close to the photoluminescence lifetime of 1.23 ns of OPV-UP homodimers.<sup>32</sup>

**Electron Transfer.** In previous chapters it has been shown that these OPV and PERY chromophore can also engage in a photoinduced electron transfer reaction. For charge transfer to occur, the combination of OPV-UP and PERY-UP should have a charge separated state energy level that is lower than the singlet-excited state of the PERY-UP. The free energy for this charge separation reaction can be calculated by using the Weller equation:<sup>35,36</sup>

$$\Delta G_{CS} = e(E_{ox}(D) - E_{red}(A)) - E_{00} - \frac{e^2}{4\pi\epsilon_0\epsilon_s R_{cc}} - \frac{e^2}{8\pi\epsilon_0} \left( \frac{1}{r^+} + \frac{1}{r^-} \right) \left( \frac{1}{\epsilon_{ref}} - \frac{1}{\epsilon_s} \right) \quad (1)$$

Table 1, shows that according to equation 1 a photoinduced electron transfer reaction is energetically possible for the OPV-UP/PERY-UP heterodimer in solvents of varying polarity from either the OPV-UP or the PERY-UP singlet-excited states.

**Table 1:** Change in free energy for charge separation  $\Delta G_{CS}$  (eV) from OPV( $S_1$ ) and PERY( $S_1$ ) together with the solvent reorganization energy  $\lambda_s$  (eV) for OPV-UP/PERY-UP heterodimers in different solvents as calculated from equations 1 and 3. The oxidation potential for OPV-UP is 0.71 V whereas the reduction potential of PERY-UP is -0.61 V, both measured in dichloromethane ( $\epsilon = 8.93$ ).

$\Delta G_{CS}^{OPV}$  uses  $E_{00} = 2.52$  eV;  $\Delta G_{CS}^{PERY}$  uses  $E_{00} = 2.32$  eV;  $R_{cc} = 33$  Å;  $r^+ = 5.05$  Å;  $r^- = 4.71$  Å.

	$\Delta G_{CS}^{OPV}$	$\Delta G_{CS}^{PERY}$	$\lambda_s$
toluene	-0.47	-0.27	0.07
ODCB	-1.28	-1.08	0.79
benzonitrile	-1.43	-1.23	0.98

To investigate the possibility for electron transfer in the heterodimer in more detail, the fluorescence signal of PERY-UP at 578 nm was monitored after selective photoexcitation of PERY-UP at 527 nm

as a function of an increasing amount of OPV-UP. For this purpose, a solution of  $2 \times 10^{-5}$  M OPV-UP and  $1 \times 10^{-6}$  M PERY-UP was added in steps to a  $1 \times 10^{-6}$  M solution of PERY-UP. Irrespective of the polarity of the solvent (toluene,  $\epsilon = 2.38$ ; *o*-dichlorobenzene (ODCB),  $\epsilon = 9.93$ ; benzonitrile,  $\epsilon = 25.18$ ) the PERY-UP fluorescence signal remained constant. From this experiment it can be concluded that photoinduced electron transfer does not occur in the heterodimer from the PERY-UP( $S_1$ ) state.

If electron transfer is absent but thermodynamically feasible, it is likely hampered kinetically. The expression for the rate constant for non-adiabatic charge separation can be expressed as follows:

$$k_{cs} = \left( \frac{4\pi^3}{h^2 \lambda k_B T} \right)^{1/2} V^2 \exp \left[ \frac{-\Delta G_{cs}^\ddagger}{k_B T} \right] \quad (2)$$

This shows that  $k_{cs}$  is determined by the coupling ( $V$ ) between donor and acceptor in the excited state, the reorganization energy  $\lambda$  and the barrier for charge separation ( $\Delta G_{cs}^\ddagger = (\Delta G_{cs} + \lambda)^2 / 4\lambda$ ). The reorganization energy is the sum of internal ( $\lambda_i$ ) and solvent ( $\lambda_s$ ) contributions. The latter can be estimated from:<sup>37</sup>

$$\lambda_s = \frac{e^2}{4\pi\epsilon_0} \left[ \frac{1}{2} \left( \frac{1}{r^+} + \frac{1}{r^-} \right) - \frac{1}{R_{cc}} \right] \left( \frac{1}{n^2} - \frac{1}{\epsilon_s} \right) \quad (3)$$

The internal reorganization energy  $\lambda_i$  is probably not very high for these extended conjugated systems and estimated to be in the range of 0.2 to 0.5 eV. Within these limits the barrier  $\Delta G_{cs}^\ddagger$  for charge separation from PERY-UP( $S_1$ ) remains less than 0.01 eV in ODCB and benzonitrile, and is only slightly higher in toluene ( $< 0.04$  eV). The absence of electron transfer in each of these solvents is therefore ascribed to a very weak electronic coupling ( $V$ ) of donor and acceptor in the excited state, rather than a high barrier.  $V$  is known to be exponentially dependent on the distance between donor and acceptor. Molecular modelling indicates an appreciable distance between OPV-UP and PERY-UP units in the heterodimer, causing a low  $V$ . In agreement with this proposition, photoinduced electron transfer reaction does occur between OPV and PERY chromophores in systems where the two redox-active chromophores are at a much shorter distance.<sup>26,27,38,39</sup>

### 7.3 Diaminotriazine Coupled OPV-PERY Arrays

For the covalently linked OPV-PERY-OPV arrays it has already been shown that the type of packing can have tremendous consequences for the kinetics of the charge separation and recombination reaction, especially in J-type configurations (Chapter 5). However, a more detailed investigation of the influence of intermolecular orientation on charge transfer kinetics was hampered by the fact that in these covalent donor-acceptor-donor arrays the acceptor strength also changed. One could envision situations where a low intramolecular driving force for charge separation is expected to result in slow kinetics, whereas the intermolecular pathway in J-type aggregates can have a significantly enhanced rate for charge separation.<sup>40</sup> In this chapter, aggregates of various OPV-PERY complexes containing *tert*-butylphenoxy and chlorine substituents on the bay position of the PERY units are studied. These

bay substituents introduce torsion along the molecular axis, leading to packing in a J-type fashion. This facilitates a comparison of the supramolecular arrays with their covalent analogues and allows studying the effects of subtle differences in aggregation geometry within the J-type packing for arrays with the same (intramolecular) driving force for charge separation and recombination.

The hydrogen-bonding array that is used to study supramolecularly coupled OPV-PERY systems is the diaminotriazine unit (Figure 4).<sup>41-45</sup> This unit has a DAD motif, complementary with the ADA motif of the imides of the used PERY chromophore. A key advantage of this motif is that it is not self-complementary; hence the formation of homodimers is prevented, leaving the OPV-PERY couples as the only possible hydrogen-bonded structure.

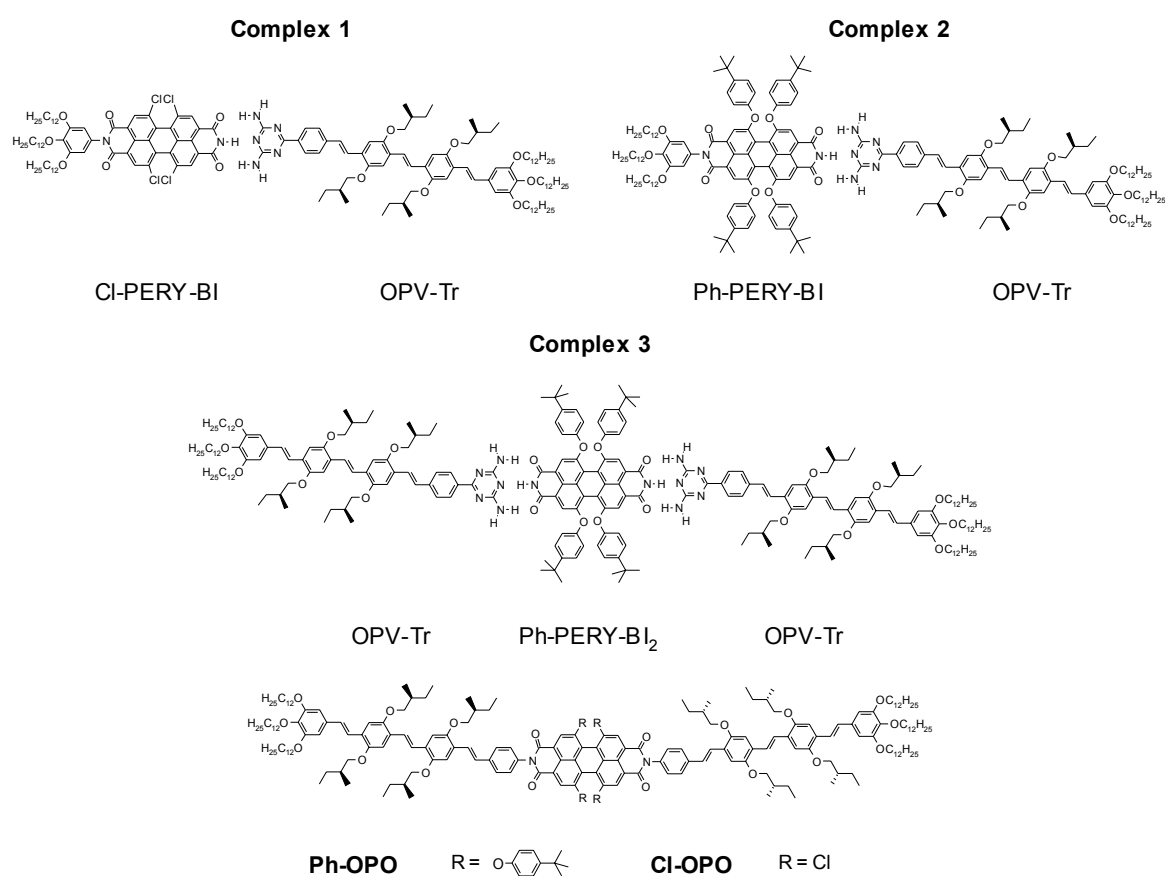


**Figure 4:** Studied diamino-triazine OPV-PERY complexes 1, 2 and 3 together with the covalent OPV-PERY-OPV triads Ph-OPO and Cl-OPO.

**Chlorine-substituted OPV-PERY Systems.** The first complex that is studied (complex 1, Figure 4) consists of a perylene bisimide unit with four chlorine substituents on the bay position and on one side a trialkoxyphenyl unit (Cl-PERY-BI), leaving only one side of the molecule available for complexation with the OPV-diaminotriazine compound (OPV-Tr). The absorption and circular dichroism spectra recorded in methylcyclohexane (MCH) indicate that at a concentration of  $10^{-4}$  M the molecules are aggregated at room temperature (Figure 5). Upon increasing the temperature, the absorption maximum shifts to the blue indicating that the aggregates are ordered in a J-type structure.

Although the circular dichroism gives strong evidence for a helically organized aggregated structure, it is difficult to explain the precise origin of the bisignate signal because the absorption bands of the OPV and PERY chromophore overlap in this wavelength region.

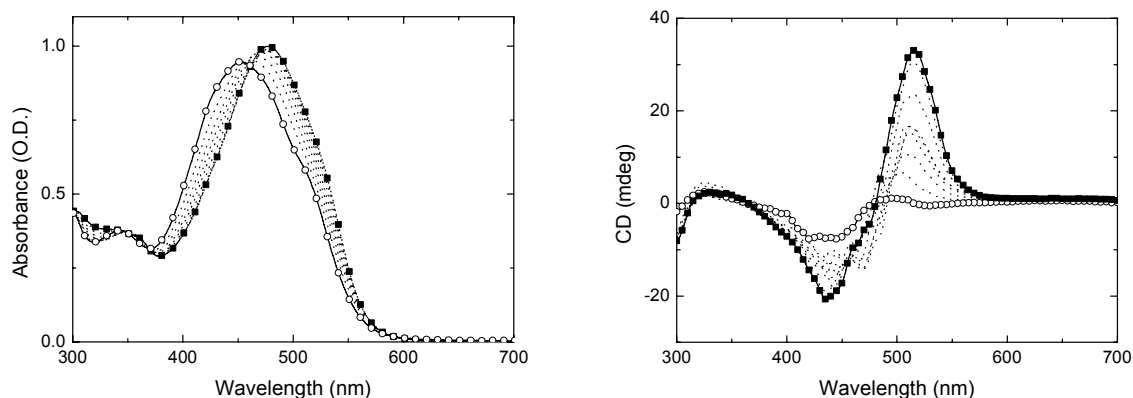


**Figure 5:** Absorption (left) and circular dichroism (right) spectra of a  $1 \times 10^{-4}$  M solution of complex 1 in MCH at temperatures ranging from 10 °C (solid squares) to 90 °C (open circles).

The use of OPV-Tr as donor material in combination with the strong acceptor Cl-PERY-BI (Table 2) creates a considerable driving force for electron transfer even in solvents of low polarity like MCH. Indeed, the transient photoinduced absorption (PIA) trace recorded at 1450 nm indicates that at room temperature OPV radical cations are created after photoexcitation (Figure 6).<sup>46</sup> The rise of the signal occurs within 1 ps, indicating that the rate for charge separation ( $k_{CS}$ ) is faster than  $10^{12}$  s<sup>-1</sup>. The decay of the signal can be fitted with an exponential decay having a time constant of 2 ps, equivalent to a charge recombination rate ( $k_{CR}$ ) of  $5 \times 10^{11}$  s<sup>-1</sup>.

**Table 2:** Redox potentials of the studied compounds and the PERY( $S_1$ ) energy levels. The PERY( $S_1$ ) energy is calculated from the absorption maximum in  $CH_2Cl_2$ . The redox potentials are referenced to the  $Fc/Fc^+$  redox couple and were measured in  $CH_2Cl_2$  with 0.1 M  $NBu_4PF_6$  as supporting electrolyte.

Compound	$E_{ox}(OPV)$ (V)	$E_{red}(PERY)$ (V)	PERY( $S_1$ ) (eV)
OPV-Tr	+0.33	-	-
Cl-PERY-BI	-	-0.81	2.38
Ph-PERY-BI	-	-1.17	2.12
Ph-PERY-BI <sub>2</sub>	-	-1.16	2.13
Ph-OPO	+0.34	-1.17	2.13
Cl-OPO	+0.33	-0.80	2.38

A comparison of the charge transfer kinetics with the related covalent Cl-OPO triad shows a remarkable difference in the rate constants for the recombination reaction. Although the chromophores and intramolecular donor-acceptor distance are similar for complex 1 and Cl-OPO, the recombination rate for complex 1 ( $5 \times 10^{11}$  s<sup>-1</sup>, 2 ps) is much higher than the rate of  $8.3 \times 10^{10}$  s<sup>-1</sup> (12 ps) for Cl-OPO in MCH. Since both the hydrogen-bonding complex and the triad are in a J-type configuration, this



implies that small conformational changes on the nanoscopic level in the aggregate are important for the charge transfer kinetics. An analysis of the circular dichroism effects emphasizes that a subtle difference in packing exists as complex 1 shows a clear bisignate signal and hardly any signal is observed for the Cl-OPO triad (Chapter 5). This indicates that intermolecular effects within a J-type structure influence the kinetics of the charge transfer reaction.

At an elevated temperature of 50 °C, a large amount of molecules is still aggregated (Figure 5), in agreement with the observation of unchanged kinetics of the transient absorption trace of the OPV radical cation. However, when the sample was heated to 90 °C, the circular dichroism almost disappeared and the absorption spectrum showed a considerable shift of the PERY maximum compared to the spectrum recorded at room temperature. This implies that the aggregates are broken at 90 °C and likely the hydrogen bond between the OPV and PERY chromophores is disrupted as well.<sup>47</sup> In accordance, Figure 6 shows that no OPV radical cation signal can be detected on a picosecond timescale at 90 °C because the loss of connectivity between the OPV and PERY chromophores in the molecularly dissolved state inhibits the electron transfer.

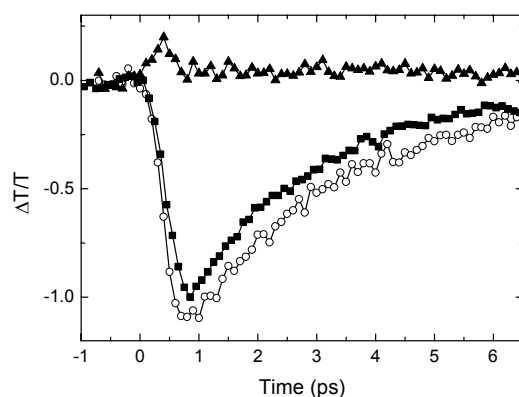


**Figure 6:** Transient photoinduced absorption spectra of a  $1 \times 10^{-4}$  M solution of complex 1 in MCH at 20 °C (squares), 50 °C (circles) and 90 °C (triangles) with  $\lambda_{exc} = 460$  nm and  $\lambda_{det} = 1450$  nm.

**Phenoxy-substituted OPV-PERY Systems.** Complex 2 contains a *tert*-butylphenoxy substituted perylene bisimide, but is otherwise identical to complex 1. The absorption and circular dichroism spectra at various temperatures indicate that at room temperature complex 2 aggregates in MCH (Figure 7a). At room temperature the absorption maximum of both the OPV and PERY moiety is red shifted compared to the spectra at elevated temperatures in agreement with packing in a J-type fashion. The circular dichroism signal at 5 °C shows a double bisignate signal (-/+/-/+) in the OPV and PERY absorption range. This signal disappears upon heating and is not detected above 25 °C. It should be noted that the intensity of the circular dichroism signal decreases more rapidly with increasing temperature than the shift of the absorption spectrum. This indicates that at elevated temperatures only small aggregates exist or that the present aggregates contain significantly less helically ordered domains.

Analogous to the dimeric structure of complex 2, it is possible to create a supramolecular triad consisting of two OPV-Tr units and one PERY moiety by using a symmetric perylene bisimide (Ph-PERY-BI<sub>2</sub>) instead of the asymmetric monoimide (Ph-PERY-BI) as shown in Figure 4 (complex 3).

With the  $\pi$ -system significantly enlarged, it can be expected that aggregates of complex 3 are more stable than the ones created with the dimeric complex 2. At a concentration of  $5 \times 10^{-5}$  M of complex 3 in MCH, a considerable blue shift of the PERY absorption maximum from 586 nm to 560 nm is observed upon heating the solution from 20 to 90 °C (Figure 7), indicative for a J-type packing at low temperatures. The most pronounced shift is detected between 70 and 80 °C, in accordance with the loss of the circular dichroism signal at 70 °C. The transition temperature between aggregated and non-aggregated species is at noticeably higher temperatures for complex 3, even at a lower concentration. It can therefore be concluded that the supramolecular structures created with complex 3 are more stable than those created with complex 2.

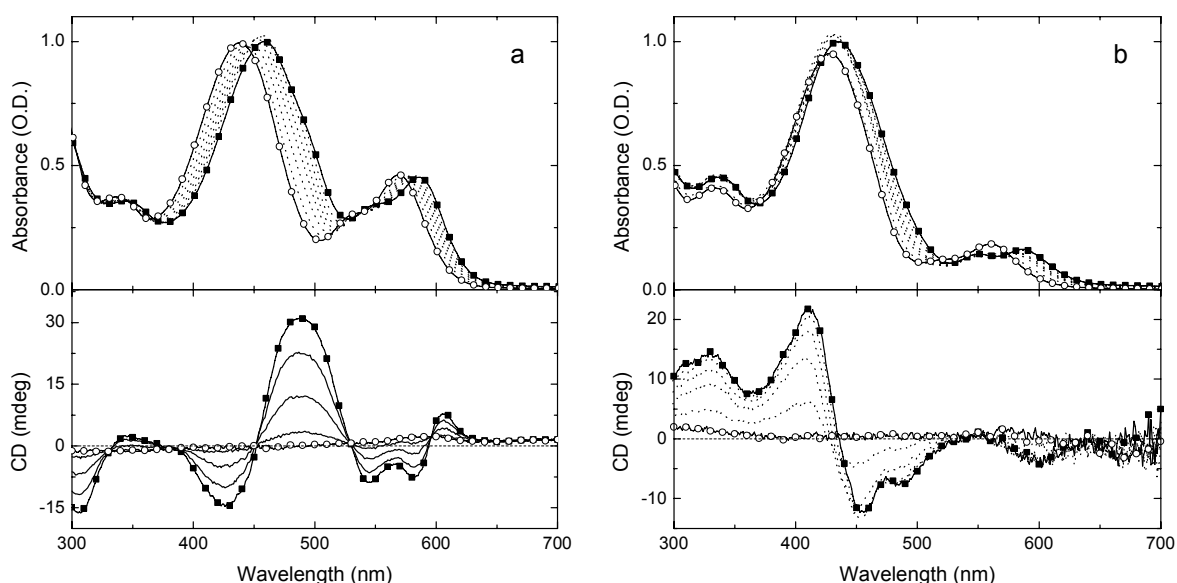


**Figure 7:** (a) Absorption spectra of a  $2 \times 10^{-4}$  M solution of complex 2 in MCH at temperatures ranging from 20 °C to 90 °C and circular dichroism spectra for complex 2 in MCH ( $2 \times 10^{-4}$  M) recorded at different temperatures ranging from 5 °C (squares) to 25 °C (circles). (b) Absorption spectra for complex 3 in MCH ( $5 \times 10^{-5}$  M) recorded at different temperatures ranging from 20 °C (squares) to 90 °C (circles) and circular dichroism spectra for complex 3 in MCH ( $5 \times 10^{-5}$  M) recorded at different temperatures ranging from 20 °C (squares) to 70 °C (circles).

A good indication for the presence of a charge transfer reaction can be obtained by monitoring the intensity of the acceptor luminescence. For complex 3, the photoluminescence intensity of the PERY moiety at 590 nm is monitored as a function of temperature (Figure 8). At elevated temperatures, the amount of luminescence is considerably higher than at room temperature, indicating that the luminescence is significantly quenched in the aggregated species. The observed transition temperature of 55 °C (at a concentration of  $5 \times 10^{-6}$  M) is similar to the observed transition in the absorption and circular dichroism experiments.<sup>48</sup> Aggregate formation can also lead to luminescence quenching, especially for H-type aggregates. However, J-type aggregation as observed for complex 3, generally does not result in a large luminescence quenching as the lowest exciton state is radiatively coupled to

the ground state. The almost quantitative quenching of the luminescence is therefore attributed to a charge transfer reaction in the supramolecular structure.

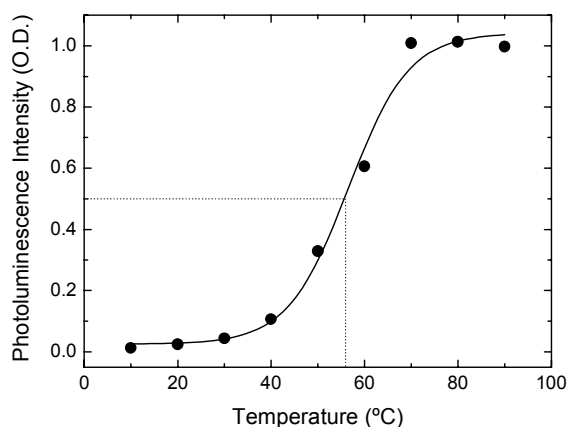


**Figure 8:** Normalized photoluminescence intensity at 590 nm for a  $5 \times 10^{-6}$  M solution of complex 3 in MCH recorded at different temperatures.

A key difference between the phenoxy and the chlorine substituted PERY species is the reduction potentials which are determined at  $-1.17$  V and  $-0.80$  V respectively, accompanied by a difference in energy of the PERY( $S_1$ ) state (Table 2). In addition, there is a considerable difference in  $S_1$  energy of Ph-PERY-BI (2.12 eV) and Cl-PERY-BI (2.38 eV). The sum of the 0.37 and 0.26 eV differences in reduction potential and singlet energy results in a 0.63 eV larger driving force for charge separation at the same distance for complex 1. The Weller equation predicts that the charge separated state will be 0.51 eV higher in energy than the PERY( $S_1$ ) if an infinite distance between the donor and acceptor is taken into account for complex 2 in MCH (equation 1). The energy of the charge separated state is only lower in energy than the PERY( $S_1$ ) state at distances shorter than 13 Å. The photoluminescence quenching in the aggregated state strongly suggests the occurrence of an electron transfer and therefore transient absorption spectroscopy was employed to see if a photoinduced charge transfer reaction occurs in the aggregated OPV-PERY complexes 2 and 3 (Figure 9). By taking into account the low driving force for a charge separation reaction it is surprising to see that for both complex 2 and 3 a signal can be detected if the OPV radical cation band is monitored at 1450 nm (Figure 9). Moreover, the measured charge separation occurs within 1 ps ( $k_{CS} > 1 \times 10^{12}$  s $^{-1}$ ). Hence, the electron transfer occurs within the time resolution of the used setup and the high rate constant makes it very efficient. The observation of these high rate constants supports the presence of a charge transfer reaction within a stacked OPV-PERY domain, facilitated by short OPV-PERY distances. The charge recombination rate is much slower; values of  $2.8 \times 10^{10}$  s $^{-1}$  (36 ps) and  $6.3 \times 10^{10}$  s $^{-1}$  (16 ps) are observed for respectively complex 2 and 3. The difference between the rate constants is only a factor 2. The difference between the rate constants is a factor 2, even though the driving force for charge recombination should be the same for both complexes because the oxidation and reduction potentials, and the interchromophore distances are identical in both complexes. Likely, the factor of 2 results from a slightly different arrangement of the chromophores. The absorption and circular dichroism spectra of

the complexes 2 and 3 together with Ph-OPO indicated that all three systems are aggregated in a J-type fashion but with a subtle difference in the packing geometry (Figure 7).

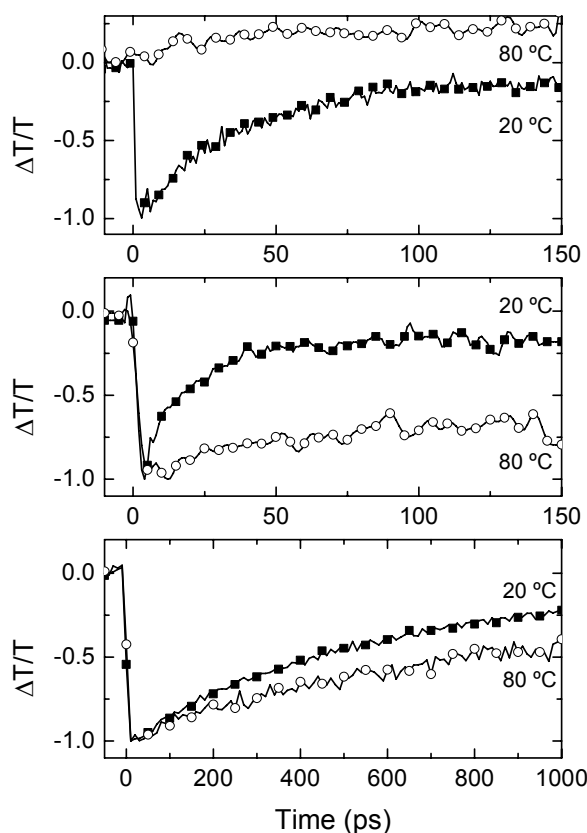


**Figure 9:** Transient photoinduced absorption traces for complex 2 (top,  $2 \times 10^{-4}$  M), complex 3 (middle,  $5 \times 10^{-5}$  M) and Ph-OPO (bottom,  $5 \times 10^{-5}$  M) in MCH. The solid squares indicate measurements at 20 °C while the open circles show spectra recorded at 80 °C. The excitation wavelength is 455 nm whereas the signal is detected at 1450 nm.

Even though a difference in charge separation rate for aggregated systems of complex 2 and 3 can be expected, it is not possible to distinguish between the observed rates for both complexes because the formation of charges occurs with time constants similar or faster than the time resolution of the used transient absorption setup. However the observation of these extremely fast rate constants supports the presence of a charge transfer reaction via an intermolecular reaction within a stacked OPV-PERY domain, facilitated by short OPV-PERY distances.

The absorption and circular dichroism spectra reveal that the aggregates break when heating solutions of complex 2 and 3 in MCH. Consequently, one expects a loss of the OPV radical cation signal in the transient absorption at elevated temperatures. For complex 2, indeed no cation signal is observed at 80 °C. In contrast, for complex 3 a clear signal can be detected at 80 °C with a grow-in time faster than 1 ps. The lifetime of the created charges increases from 16 ps at 20 °C to more than 200 ps at 80 °C for complex 3. This indicates that the photoinduced charge separation reaction occurs, but that the packing of the chromophores has changed significantly. The reduced rate for charge recombination must come from the molecularly dissolved hydrogen-bonded complexes or small aggregates present at higher

temperatures. This is in agreement with the absorption and circular dichroism results. These measurements show that indeed some aggregated species can be present at elevated temperatures because the maximum absorption spectrum is still shifting and a small circular dichroism signal can be detected (Figure 7). The distance between the redox centers in these complexes is larger than in the  $\pi$ - $\pi$  stacked assembly with close contact between OPV and perylene bisimide of neighboring triads resulting in a decrease of the rate for charge recombination.

Besides the comparison of the recombination rates for both hydrogen-bonded complexes, it is also possible to compare these results with the rates obtained for the covalently linked Ph-OPO compound in its aggregated state in MCH (Figure 9). Having a decay time of 500 ps ( $k_{CR} = 2.0 \times 10^9 \text{ s}^{-1}$ ), the charge recombination is much slower for Ph-OPO than for the complexes 2 and 3. A possible cause for this difference is the more coplanar arrangement of the OPV and perylene bisimide units in the hydrogen-bonded assembly. This creates a more tightly packed aggregate in which the OPV and perylene bisimide moieties of neighboring units approach more closely, leading to stronger electronic interactions. This is consistent with the recombination time of 200 ps for complex 3 at 80 °C, which approaches the 500 ps obtained for the weakly coupled Ph-OPO aggregates.

#### 7.4 Analysis of Aggregate Packing

Although the determination of the exact aggregate structure seems to be an unattainable goal for now, the observed strong dependence of charge transfer kinetics calls for a more elaborate study on the possible types of packing within the aggregates in order to improve the understanding of structure-property relation in aggregated structures. Therefore, the excited state levels of four proposed types of aggregates (Figure 10) are evaluated by means of calculations on a coupled oscillator model (see experimental section for more details). This model uses the classical dipole-dipole interaction between the transition dipoles  $\bar{\mu}_{0,1}^Q$  of all OPV and PERY chromophores ( $Q = A, B, \dots, N$ ) in the system:

$$V_{AB} = \frac{\bar{\mu}_{0,1}^A \cdot \bar{\mu}_{0,1}^B |\bar{R}_A - \bar{R}_B|^2 - 3(\bar{\mu}_{0,1}^A \cdot (\bar{R}_A - \bar{R}_B))(\bar{\mu}_{0,1}^B \cdot (\bar{R}_A - \bar{R}_B))}{|\bar{R}_A - \bar{R}_B|^5} \quad (4)$$

By solving the matrix Hamiltonian (see Experimental Section for more details), the energies and the electrical and magnetic transition dipole and moments  $\bar{\mu}_{0,i}$  and  $\bar{m}_{0,i}$  from the ground state to the collective states  $i$  are obtained for the coupled system:

$$\bar{\mu}_{0,i} = \sum_{Q=A}^N c_{i,Q} \bar{\mu}_{0,1}^Q \quad \text{and} \quad \bar{m}_{0,i} = i\alpha \sum_{Q=A}^N c_{i,Q} (\bar{R}_Q \times \bar{\mu}_{0,1}^Q) \quad (5)$$

The principal transition moments of the complex provide an estimate of the relative intensity of the transition ( $\bar{\mu}_{0,i} \cdot \bar{\mu}_{0,i}$ ) and relative sign and intensity of the circular dichroism ( $\text{Im}(\bar{\mu}_{0,i} \cdot \bar{m}_{0,i})$ ). The calculations provide a first order approximation of the relative shift of the energy levels and show whether a transition is allowed or forbidden. In addition, the shape of the circular dichroism signal can

be predicted. In this way the experimental absorption and circular dichroism spectra of complex 2 and 3 can be compared with structural models. The present analysis is by no means a quantitative and comprehensive investigation, but it might be used as an eye-opener to see how the contributions of small difference in packing influence the absorption and chiroptical properties of supramolecular structures.

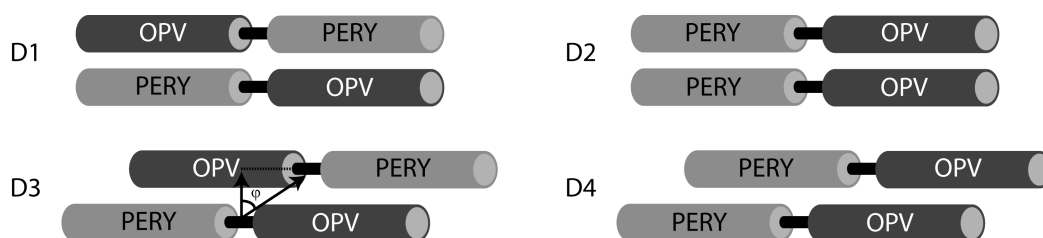


**Figure 10:** Suggested packing geometries for OPV-PERY dimers as used for the electronic interaction model to predict aggregate influence on the absorption and circular dichroism characteristics.

The first two structures (D1 and D2) propose a supramolecular aggregate where two coupled OPV-PERY dimers are stacked directly on top of each other without any longitudinal shift. For D1 the OPV and PERY chromophores are stacked on top of each other whereas in D2 OPV-OPV and PERY-PERY couples are formed. For D1, a small blue shift is expected for the OPV absorption band, whereas the PERY absorption will be red shifted (Figure 11). For D2 the typical strong blue shift of the H-type aggregate is expected for both chromophores. As a result, the presence of aggregated structures similar to D1 and D2 is excluded because the absorption spectrum of complex 2 (Figure 7) shows a red shift for both the OPV and PERY maximum. The packing should include a considerable longitudinal shift of one of the molecules (J-type fashion) as shown for both D3 and D4 in order to obtain a red shift for both absorption maxima (Figure 10).

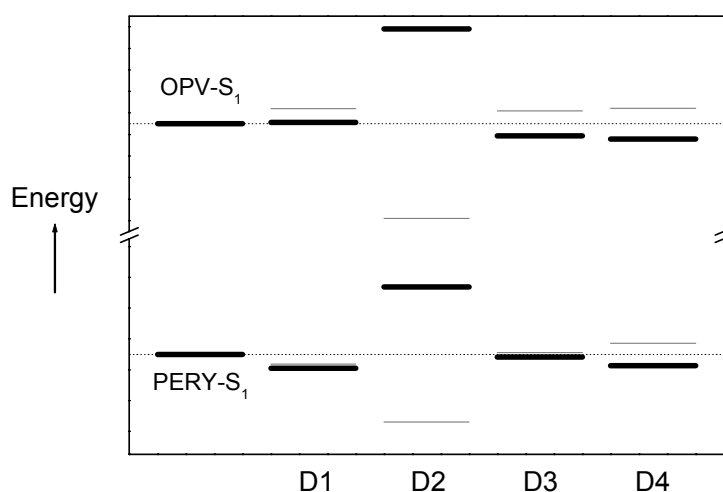


**Figure 11:** Excited state energy levels for OPV and PERY in the proposed structures D1, D2, D3 and D4 as calculated from the eigenvalues of the exciton coupling hamiltonian matrix. The black levels indicate energy levels that have an allowed transition from the ground state, whereas the gray lines represent the energy levels with a forbidden transition.

The absorption spectra indicate that all the studied aggregates are packed in a J-type fashion. The characteristics of the circular dichroism might add more information on the geometry in this type of aggregate. In addition to the electronic dipole, the magnetic dipole moment is calculated, providing an estimate of the strength and sign of the predicted circular dichroism spectrum. To model the chirality, the angles  $\alpha$  and  $\beta$  are included between the two dyad layers as shown in Figure 12. The parameter  $\alpha$  creates an angle between the two dyad molecules whereas  $\beta$  is introduced to create an angle between the OPV and PERY chromophore within a dyad molecule.

For structure D2A an angle  $\alpha = 25^\circ$  results in a bisignate circular dichroism signal for both the OPV and PERY chromophore with a positive sign at the high-energy side of both absorption bands (+/-/+/-; Figure 12). In the D4A structure, a longitudinal shift is introduced along the molecular axis creating an angle ( $\varphi$ ) of  $63^\circ$  between the two connection centers of the dyads. Together with  $\alpha = 25^\circ$  this results in a -/+/-/+ circular dichroism spectrum, exactly opposite to D2A, and nicely matching the experimental signs in the circular dichroism spectrum of complex 2 (Figure 7). Moreover, the absorption spectrum of D4A is red shifted for both chromophores.

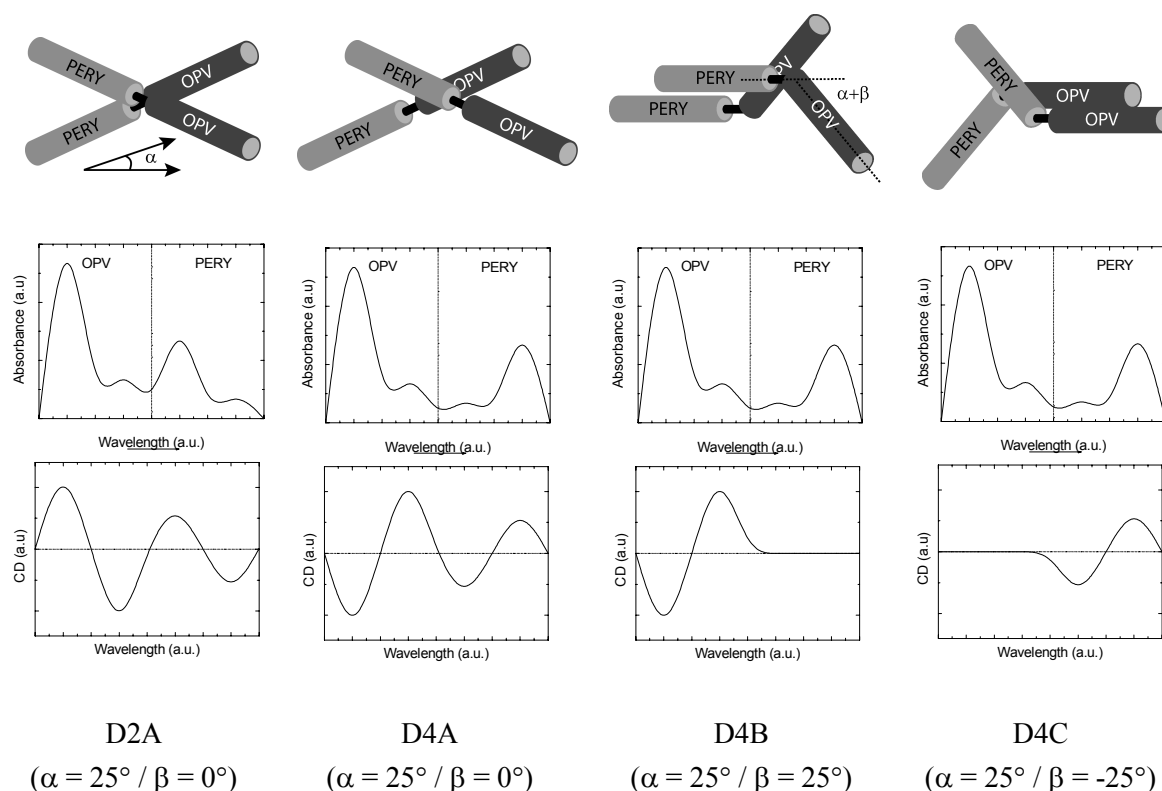


**Figure 12:** Cartoons illustrating the top-view of different geometries for the modeled OPV-PERY dyad systems D2A and D4A-C, together with their predicted absorption and circular dichroism spectra. The circular dichroism spectra of the D4A-C structures are calculated for  $\varphi = 63^\circ$ .

The features of the related circular dichroism change dramatically if an angle ( $\beta$ ) is created in the linkage between the OPV and PERY moieties. By bending the PERY part in the same direction as the rotation of the molecule, the circular dichroism signal of this chromophore is lost. A bend of the PERY

moiety in the opposite direction, results in the loss of the OPV signal as both OPV chromophores are placed parallel to each other in this way.

The effect of the shift was studied for D4A in more detail by varying the angle  $\varphi$ . This shows that for angles below  $\varphi = 50^\circ$  the circular dichroism spectrum is similar to that of D2A, also accompanied by an expected blue shift of both absorption maxima. Around the magic angle of  $\varphi = 54.7^\circ$  the circular dichroism signal of the PERY is lost, whereas the sign of the bisignate signal of the OPV changes. For angles larger than  $\varphi = 60^\circ$  a signal as shown in Figure 12 is expected.

Similar to D4, the absorption spectra of structure D3 should result in a red shift of both the OPV and PERY maximum, in agreement with the experimentally observed features. Furthermore, the calculations reveal that incorporation of chirality into D3 results in the experimentally observed -/+/-/+ circular dichroism spectrum for all three configurations tested (D3A, D3B and D3C; Figure 13). Actually, the same circular dichroism features are predicted for D1A, but the calculated blue shift of the OPV maximum excludes the presence of this structure. The extent of the longitudinal shift has no influence on the circular dichroism signal, except for D3B where the signal of the OPV changes sign for large shifts.

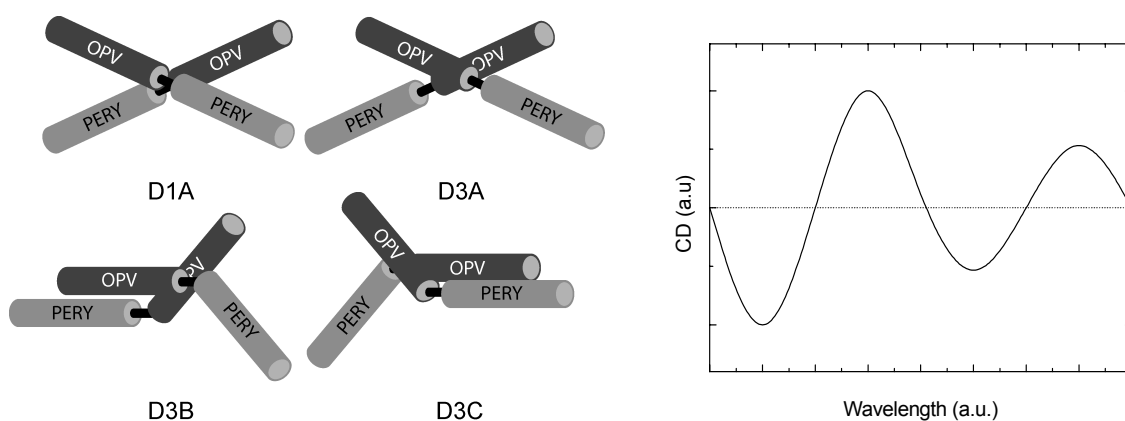


**Figure 13:** Cartoons illustrating the top-view of different geometries for the modeled OPV-PERY dyad systems D1A and D3A-C together with their predicted circular dichroism spectrum.

Although this analysis does not solve the precise structure of complex 2, the calculation of the circular dichroism and absorption spectra shed some light on the possible geometries that are present. Based on a comparison with the experimental spectra, a packing of the chromophores like D1 and D2 is improbable, just like a D4 structure with an angle between the OPV and PERY parts. On the other hand, the D3A-C structures and a D4A packing, *i.e.* without an angle  $\beta$ , but with a considerable longitudinal shift between the OPV and PERY parts, appear to be good candidates for the actual geometry of complex 2 in MCH. The necessity of introducing the longitudinal shift to explain both absorption and circular dichroism for complex 2 gives reason to believe that between the adjacent layers, the OPV and PERY chromophores are in close proximity.

A similar analysis (see experimental section for more details) can be performed for triads mimicking complex 3 (Figure 14). The difference between the suggested models is the longitudinal shift between the two packed triad systems, which is present for T2 but not for T1. For the H-type aggregate T1 both



the OPV and PERY absorption spectrum should shift to the blue, which is not observed experimentally for complex 3 (Figure 7). The T2 seems to be a better representation for complex 3 because the calculations predict a distinct red shift for both chromophores upon aggregation, in agreement with the experimentally observed absorption spectra.

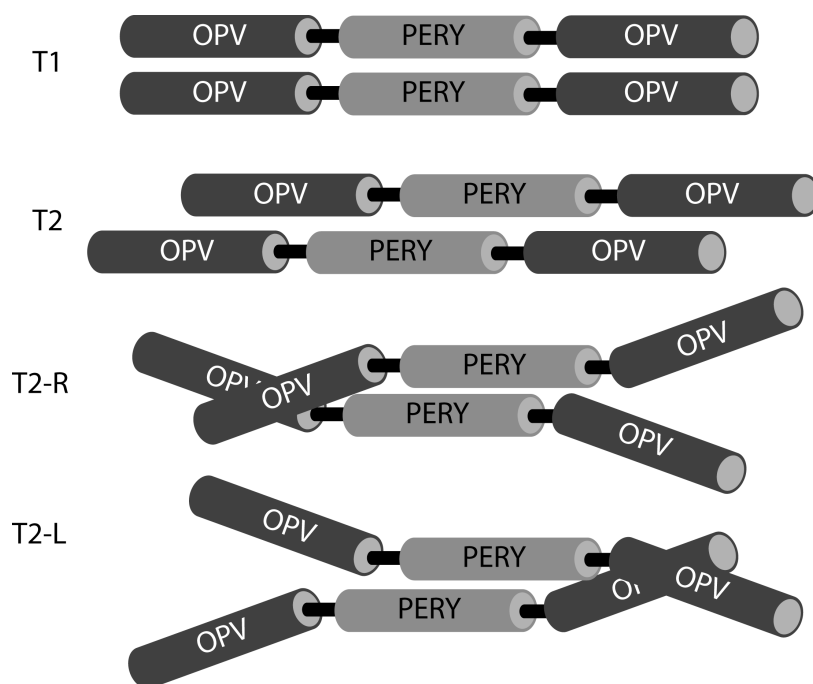


**Figure 14:** Structures T1 and T2 for complex 3. For T2-R and T2-L the shift between the two layers is accompanied by a twist along the molecular axis to create chirality in the structure.

By introducing a twist in the OPV-PERY-OPV triad as in T2-R or T2-L the absorption spectrum, the structure becomes chiral, which results in a circular dichroism signal. The circular dichroism spectra of T2-R and T2-L were calculated (Figure 15). The analysis again shows that a longitudinal shift between the two molecules is of significant importance for the circular dichroism spectra. For small shifts ( $\varphi < 40^\circ$ ) the T2-R structure gives a bisignate signal with a negative sign at the high-energy side of the OPV absorption, accompanied by a negative PERY signal.

By increasing the shift ( $\varphi > 50^\circ$ ) for T2-R, the signal at the OPV wavelengths changes sign, but the PERY signal remains negative. This is in complete agreement with the experimental data (Figure 7) and suggests that this type of geometry describes the packing of complex 3 in MCH. Importantly, the large longitudinal shift is in full agreement with the short intermolecular distance between OPV and PERY chromophores that explains the observed high rates for charge separation in aggregates of complex 3.

For the T2-L geometry the circular dichroism at the OPV absorption wavelengths matches nicely with the experimental results for small shifts ( $\varphi < 40^\circ$ ). However, a blue shift is expected for the OPV and

PERY unit in the absorption spectrum for these small angles of  $\varphi$ , whereas red shifts are observed in the experiments. Moreover, the circular dichroism signal at the PERY absorption wavelength is positive for all angles  $\varphi$ , thereby excluding that complex 3 is present in a similar geometry.

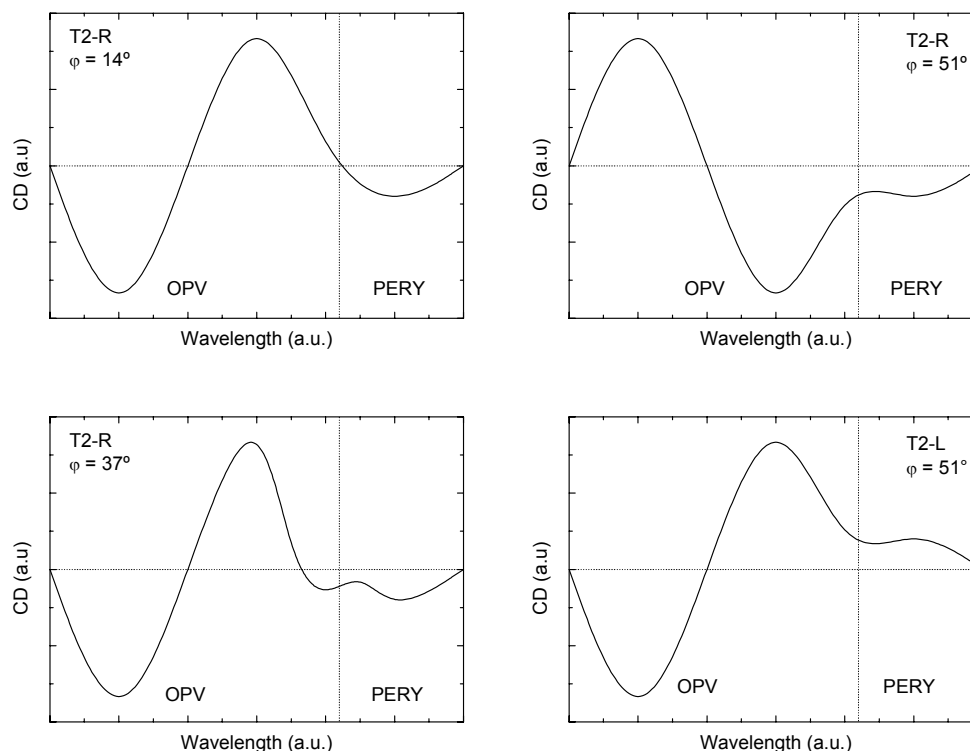


**Figure 15:** Circular dichroism spectra for the triad systems, calculated with the coupled oscillator model for orientations shown in Figure 14.

## 7.5 Conclusions

A ureido-pyrimidinone based OPV-PERY array was studied to investigate the effect of a hydrogen-bonding unit on the photophysical processes for a dissolved supramolecularly linked system. The temporal evolution of the singlet-energy transfer reaction by using sub-picosecond transient spectroscopy implied that a photoinduced energy transfer reaction takes place in the heterodimer with a rate of  $2 \times 10^{11} \text{ s}^{-1}$ . Although exergonic, electron transfer does not occur after photoexcitation as a result of a too weak electronic coupling between OPV and PERY chromophores in the excited state.

In contrast, a photoinduced charge transfer reaction was observed in MCH for aggregated OPV-PERY systems connected via a triazine-imide hydrogen bond. The reaction likely occurs intermolecularly between OPV and PERY chromophores of two different hydrogen bonded OPV-PERY arrays that are packed in a slipped, J-type fashion, thereby creating short OPV-PERY distances between adjacent layers in the stack. The absorption and circular dichroism spectra were used to assess the molecular orientation of the chromophores of the aggregates. The UV/Vis absorption spectra of all complexes are consistent with J-type aggregation. The circular dichroism spectra revealed that within the J-type packing, small structural differences exist. Although these variations seem subtle at first sight, they do

have a considerable influence on the charge recombination reaction as shown by comparing the ultrafast kinetics in stacked dimers, trimers and covalently linked systems. Invariably, charge recombination is faster for the hydrogen-bonded compounds compared to the covalently linked Ph-OPO and Cl-OPO derivatives. This explanation is consistent with larger CD effects observed for the hydrogen-bonded complexes.

To obtain more insight into the packing of supramolecular aggregates a coupled oscillator model was applied, which allowed evaluating different packing motifs qualitatively with the experimental absorption and circular dichroism spectra. Based on this model, several types of packing could definitely be excluded, whereas others nicely match the experimental observation. In general, a J-type packing with a large longitudinal shift provides the best correspondence of experiments and calculated spectra. The large shift is in full agreement with the strong dependence of the charge recombination on the packing since the large angle between two packed layers introduces the possibility of intermolecular charge transfer reactions.

The results presented here imply that the charge transfer kinetics are largely determined by subtle differences in the supramolecular organization of the chromophores, especially for packing in a J-type fashion. A comparison of the dissolved and aggregated OPV-PERY systems leads to the conclusion that ultimately the aggregation can even surpass parameters like the acceptor strength as the use of a weak but aggregated PERY chromophores results in the formation of a charge separated state, whereas a dissolved but stronger PERY unit only gives rise to an energy transfer reaction.

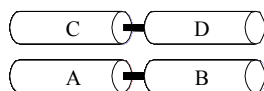
## 7.6 Experimental Section

**Materials.** The perylene bisimide molecules have been synthesized in the group of professor F. Würthner at the University of Würzburg, via procedures similar to previous PERY-triazine compounds.<sup>21,39,47</sup> The synthetic routes to obtain OPV-triazine<sup>48</sup>, Ph-OPO<sup>48</sup> and Cl-OPO<sup>27</sup> have also been reported before. The synthesis of the studied ureido-pyrimidinone compounds has been described previously.<sup>33,34,39</sup> The solvents for spectroscopic studies were of spectroscopic grade and used as received.

**Spectroscopic Techniques.** UV/Vis absorption spectra were recorded on a Perkin Elmer Lambda 900 spectrophotometer. Fluorescence spectra were recorded on an Edinburgh Instruments FS920 double-monochromator spectrometer and a Peltier-cooled red-sensitive photomultiplier whereas circular dichroism measurements were performed on a Jasco J-600 spectropolarimeter. A detailed description of the transient photoinduced absorption setup can be found in chapter 2.

**Electrochemical Measurements.** Cyclic voltammograms were measured in 0.1 M tetrabutylammonium hexafluorophosphate (TBAPF<sub>6</sub>) as a supporting electrolyte in dichloromethane using a Potentiostat Wenking POS73 potentiostat. The working electrode was a Pt disk (0.2 cm<sup>2</sup>), the counter electrode was a Pt plate (0.5 cm<sup>2</sup>), and a saturated calomel electrode (SCE) was used as reference electrode, calibrated against Fc/Fc<sup>+</sup>.

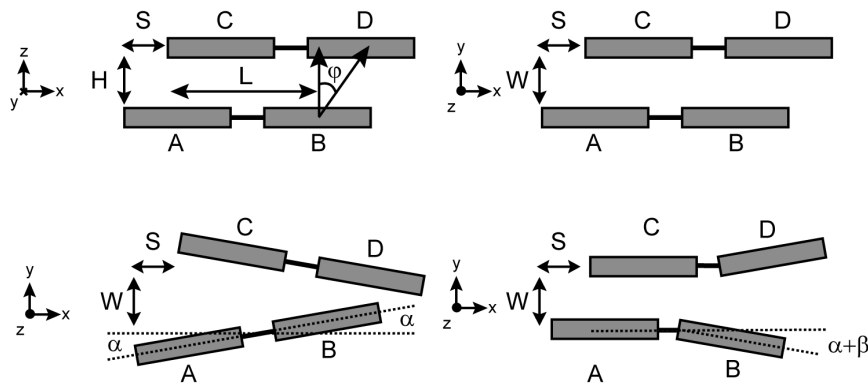
**Calculations on the Excited State Energies of Proposed Aggregated Structures – Dyad Systems.** The labels A, B, C and D for the chromophores within the stacked dyads are as follows:



The transition dipole moment ( $\mu$ ) for all parts is in the  $x$ -axis direction. The parameters used for the position ( $R$ ) of the chromophores are  $L = 3$ ,  $W = 0.3$ , and  $H = 1$ , where  $L$  indicates the distance between the OPV and PERY moiety,  $W$  indicates the shift along the  $y$ -axis, and  $H$  indicates the height difference of the two dyads in the  $z$ -direction. Varying the  $W$  parameter is not in the scope of this work, but it should be mentioned that a value of  $W = 0$  instead of  $W = 0.3$  has hardly any influence on the outcome of the calculations.

The longitudinal slip between the two dyads is represented by the  $S$ -parameter. A value of  $S = 0$  is used for the calculations of D1 and D2 whereas for D3 and D4 a value of 1 is used for this parameter. This introduces an angle ( $\varphi$ ) of  $45^\circ$  between the AB and CD dyad in the  $xz$ -plane.

Chirality is introduced into the model by creating angles between the two dyads instead of using only a fixed parallel orientation. The first angle ( $\alpha$ ) indicates the angle of the dyad system upon rotation in the  $xy$ -plane, whereas the second angle ( $\beta$ ) indicates the angle between the two chromophores within a linked dyad. A positive sign is chosen for a counterclockwise rotation of the AB-dyad, whereas the CD-dyad always rotates in the opposite direction. The indicated packing shown on the right bottom of the diagram shows the case of  $\alpha = \beta$ , thereby placing A and C in a parallel fashion.



The table below shows an example of the dipoles and positions for an OPV-PERY system with a D4 geometry. A prefactor of  $\sqrt{2}$  is incorporated in the dipole for OPV chromophores because its molar absorption coefficient is two times as large as that of the PERY unit. As a result of the fixed chromophore distance, the angle  $\alpha$  is incorporated in the position vectors  $R$  to compensate the position for rotation.

$$\mu_A := \begin{bmatrix} \cos(\alpha - \beta) \\ \sin(\alpha - \beta) \\ 0 \end{bmatrix} \quad \mu_B := \sqrt{2} \cdot \begin{bmatrix} \cos(\alpha + \beta) \\ \sin(\alpha + \beta) \\ 0 \end{bmatrix} \quad \mu_C := \begin{bmatrix} \cos(\alpha - \beta) \\ -\sin(\alpha - \beta) \\ 0 \end{bmatrix} \quad \mu_D := \sqrt{2} \cdot \begin{bmatrix} \cos(\alpha + \beta) \\ -\sin(\alpha + \beta) \\ 0 \end{bmatrix}$$

$$R_A := \begin{bmatrix} \left(-\frac{L}{2} - \frac{S}{2}\right) \cdot \cos(\alpha) \\ -\frac{W}{2} - \frac{L}{2} \cdot \sin(\alpha) \\ -\frac{H}{2} \end{bmatrix} \quad R_B := \begin{bmatrix} \left(\frac{L}{2} - \frac{S}{2}\right) \cdot \cos(\alpha) \\ -\frac{W}{2} + \frac{L}{2} \cdot \sin(\alpha) \\ -\frac{H}{2} \end{bmatrix} \quad R_C := \begin{bmatrix} \left(-\frac{L}{2} + \frac{S}{2}\right) \cdot \cos(\alpha) \\ \frac{W}{2} + \frac{L}{2} \cdot \sin(\alpha) \\ \frac{H}{2} \end{bmatrix} \quad R_D := \begin{bmatrix} \left(\frac{L}{2} + \frac{S}{2}\right) \cdot \cos(\alpha) \\ \frac{W}{2} - \frac{L}{2} \cdot \sin(\alpha) \\ \frac{H}{2} \end{bmatrix}$$

By combining the transition dipole moment and the positions of the chromophores the exciton coupling ( $I$ ) can be calculated using the following equation:

$$V(\mu_A, \mu_B, R_A, R_B) := \frac{\mu_A \cdot \mu_B \cdot (|(R_A - R_B)|)^2 - 3 \cdot (\mu_A \cdot (R_A - R_B)) \cdot (\mu_B \cdot (R_A - R_B))}{(|(R_A - R_B)|)^5}$$

By placing all interactions in a Hamiltonian determinant it is possible to extract the eigenvalues of the system, representing the respective energy levels. For this calculation an arbitrary value of 5 is used for the starting energy ( $E$ ). As indicated in the example for D4 below, a value of +5 is used for the OPV excited state, whereas for the PERY( $S_1$ ) state a value of  $-5$  is used.

$$H := \begin{bmatrix} -E & V(\mu A, \mu B, RA, RB) & V(\mu A, \mu C, RA, RC) & V(\mu A, \mu D, RA, RD) \\ V(\mu A, \mu B, RA, RB) & E & V(\mu B, \mu C, RB, RC) & V(\mu B, \mu D, RB, RD) \\ V(\mu A, \mu C, RA, RC) & V(\mu B, \mu C, RB, RC) & -E & V(\mu C, \mu D, RC, RD) \\ V(\mu A, \mu D, RA, RD) & V(\mu B, \mu D, RB, RD) & V(\mu C, \mu D, RC, RD) & E \end{bmatrix}$$

Solving the eigenvalue problem  $H\psi = E\psi$  yields eigenvalues  $E_i$  which are the energies of the collective excited states of the complex of chromophores ( $i = 1$  to  $N$  in the case of  $N$  interacting chromophoric groups). The corresponding eigenvectors  $\psi_i$  describe the contribution of each chromophore to the particular excited state:

$$\psi_i = \begin{bmatrix} c_{i,A} \\ c_{i,B} \\ c_{i,C} \\ c_{i,D} \end{bmatrix}$$

where the real coefficient  $c_{i,A}$  describes the weight of the  $S_1$  excited state of chromophore A in the collective excited state  $i$  of the complex. In the limiting case of  $c_{i,A}^2 = 1$  the excited state  $i$  is completely localized on chromophore A which is only possible if the excited state interactions of chromophore A with the others in the complex are zero. The transition dipole moment  $\mu_{0,i}$  for transition from the ground state to the collective state  $i$  can be expressed as:

$$\vec{\mu}_{0,i} = c_{i,A}\vec{\mu}_{0,1}^A + c_{i,B}\vec{\mu}_{0,1}^B + \dots = \sum_{Q=1}^N c_{i,Q}\vec{\mu}_{0,1}^Q$$

The scalar product  $\vec{\mu}_i \cdot \vec{\mu}_i$  gives information on the dipole strength, which is proportional to the transition probability ( $\alpha = 0$ ;  $\beta = 0$ ;  $S = 0$  (D1 and D2) or  $S = 1$  (D3 and D4)):

	Eigenvalues	Eigenvectors				Dipole strength
	$E_i$	$c_A$	$c_B$	$c_C$	$c_D$	$\mu_i \cdot \mu_i$
D1	5.024	0.079	0.703	0.703	0.078	4.606
	5.282	-0.092	0.701	-0.701	0.092	0
	-5.125	-0.701	-0.092	0.092	0.701	0
	-5.181	0.703	-0.079	-0.079	0.703	1.394
D2	6.76	-0.012	0.707	-0.012	0.707	3.907
	3.243	-0.002	0.707	0.002	-0.707	0
	-4.124	0.707	0.012	0.707	0.012	2.093
	-5.879	-0.707	-0.002	0.707	0.002	0
D3	5.237	0.007	0.707	-0.707	-0.007	0
	4.773	-0.022	0.707	0.707	-0.022	3.82
	-4.975	-0.707	0.007	-0.007	0.707	0
	-5.035	0.707	0.022	0.707	0.707	2.18
D4	5.289	-0.005	0.709	-0.004	-0.706	0
	4.717	-0.01	0.705	-0.02	0.709	3.881
	-4.856	0.71	-0.005	-0.704	-0.005	0
	-5.149	0.706	0.019	0.71	0.01	2.119

To calculate the chiroptical properties associated with the collective excited states we define the magnetic transition dipole moment  $m_{0,i}$  for transition from the ground state to collective state  $i$ :<sup>49</sup>

$$\vec{m}_{0,i} = i\alpha c_{i,A}(\vec{R}_A \times \vec{\mu}_{0,1}^A) + i\alpha c_{i,B}(\vec{R}_B \times \vec{\mu}_{0,1}^B) + \dots = i\alpha \sum_{Q=1}^N c_{i,Q}(\vec{R}_Q \times \vec{\mu}_{0,1}^Q)$$

Here the magnetic dipole moment is a purely imaginary quantity. This reflects the fact that in the optical cycle  $m_{0,i}$  lags 90° degrees behind in phase compared to the electrical transition dipole moment  $\mu_{0,i}$ . With the help of the magnetic transition dipole moments we can calculate the magnitude of the circular dichroism ( $\Delta A = A_L - A_R$  with  $A_L$  the absorbance of *left* circular polarized light) for the absorptive transition from the ground state to state  $i$ .

$$\begin{aligned} \Delta A_{0,i} &= \text{Im}(\vec{\mu}_{0,i} \cdot \vec{m}_{0,i}) \propto \left( \sum_{Q=1}^N c_{i,Q} \vec{\mu}_{0,1}^Q \right) \cdot \left( \sum_{P=1}^N c_{i,P} (\vec{R}_P \times \vec{\mu}_{0,1}^P) \right) \\ &\propto \sum_{Q=1}^N \sum_{\substack{P=1 \\ P>Q}}^N c_{i,Q} c_{i,P} \left[ \vec{\mu}_{0,1}^Q \cdot (\vec{R}_P \times \vec{\mu}_{0,1}^P) + \vec{\mu}_{0,1}^P \cdot (\vec{R}_Q \times \vec{\mu}_{0,1}^Q) \right] \\ \Delta A_{0,i} &\propto \sum_{Q=1}^N \sum_{\substack{P=1 \\ P>Q}}^N c_{i,Q} c_{i,P} (\vec{R}_P - \vec{R}_Q) \cdot (\vec{\mu}_{0,1}^Q \times \vec{\mu}_{0,1}^P) \end{aligned}$$

The scalar product of  $\mu_i$  with  $m_i$  then gives the relative intensity and sign of the circular dichroism signal. The influence of the angle  $\alpha$  and  $\beta$  on the circular dichroism is shown in the following table for dyad structure D4 (with  $S = 2$ ,  $\varphi = 63^\circ$ ):

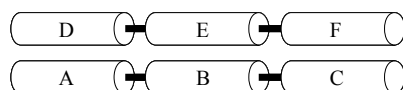
D2 $\alpha=25^\circ/\beta=0^\circ$		D4A $\alpha=25^\circ/\beta=0^\circ$		D4B $\alpha=25^\circ/\beta=25^\circ$		D4C $\alpha=25^\circ/\beta=-25^\circ$	
<i>Abs</i>	<i>CD</i>	<i>Abs</i>	<i>CD</i>	<i>Abs</i>	<i>CD</i>	<i>Abs</i>	<i>CD</i>
<b>5.673</b>	0.75	5.137	-0.77	<b>5.109</b>	-0.97	5.151	-0.01
4.331	-0.76	<b>4.870</b>	0.74	<b>4.894</b>	0.98	<b>4.859</b>	-0.03
<b>-4.844</b>	0.40	-4.98	-0.38	-4.975	-0.01	<b>-4.994</b>	-0.46
-5.159	-0.39	<b>-5.027</b>	0.41	<b>-5.027</b>	0.01	<b>-5.016</b>	0.49

The table displays the shift of the energy levels of the OPV and PERY chromophores and indicates if a transition is allowed (bold) or forbidden (normal). In addition, the relative magnitude and sign of the circular dichroism are indicated. Furthermore, the influence of the longitudinal shift  $S$  is investigated for D4A as shown in the table below.

D4A									
$S = 0.5$		$S = 1$		$S = 1.25$		$S = 1.5$		$S = 2$	
<i>Abs</i>	<i>CD</i>	<i>Abs</i>	<i>CD</i>	<i>Abs</i>	<i>CD</i>	<i>Abs</i>	<i>CD</i>	<i>Abs</i>	<i>CD</i>
<b>5.413</b>	0.75	<b>5.045</b>	0.74	5.064	-0.77	5.118	-0.77	5.137	-0.77
4.591	-0.76	4.961	-0.77	<b>4.943</b>	0.74	<b>4.891</b>	0.74	<b>4.87</b>	0.74
<b>-4.881</b>	0.40	<b>-4.951</b>	0.40	<b>-4.982</b>	0.41	<b>-5.001</b>	-0.03	-4.98	-0.38
-5.123	-0.38	-5.054	-0.38	-5.026	-0.38	<b>-5.007</b>	0.06	<b>-5.027</b>	0.41

**Calculations on the Excited State Energies of Proposed Aggregated Structures – Triad Systems.**

For complex 3, the same calculation can be done with all parameters kept the same as for the dyad system ( $S_{T1} = 0$ ;  $S_{T2} = 0.25, 0.75$  or  $1.25$ ) and the chromophore labels as follows:



Examples of the outcome of the calculations using the exciton-coupling model are given for T1, T2 ( $S = 1.25$ ) and T2-L ( $S = 1.25$ ,  $\varphi = 51^\circ$ ,  $\alpha = 25^\circ$ ) in the table below.

	Eigenvalues	Eigenvectors						Dipole strength
	$E_i$	$c_A$	$c_B$	$c_C$	$c_D$	$c_E$	$c_F$	$\mu_i \cdot \mu_i$
T1	6.296	-0.5	0	0.5	-0.5	0	0.5	0
	6.232	0.5	-0.017	0.5	0.5	-0.017	0.5	7.802
	3.738	-0.5	0.003	-0.5	0.5	-0.003	0.5	0
	3.72	0.5	0	-0.5	-0.5	0	0.5	0
	-4.006	0.012	0.707	0.012	0.012	0.707	0.012	2.198
	-6	-0.002	-0.707	-0.002	0.002	0.707	0.002	0
T2	5.245	0.487	0.002	0.513	-0.513	-0.002	-0.487	0
	5.24	0.508	0.008	-0.492	-0.492	0.008	0.508	0.004
	4.799	0.513	-0.009	-0.487	0.487	0.009	-0.513	0
	4.728	0.492	-0.022	0.507	0.507	-0.022	0.492	7.742
	-4.799	-0.005	-0.707	0.007	-0.007	0.707	-0.005	0
	-5.213	0.01	0.707	0.021	0.021	0.707	0.01	2.254
T2-L	5.241	0.506	0.009	-0.493	-0.493	0.009	0.506	0.003
	5.248	0.488	0.002	0.512	-0.512	-0.002	-0.488	1.428
	4.793	-0.512	0.01	0.488	-0.488	-0.01	0.512	0
	4.731	0.493	-0.022	0.506	0.506	-0.022	0.493	6.3
	-4.8	0.005	-0.707	-0.008	0.008	0.707	-0.005	0
	-5.213	0.01	0.707	0.022	0.022	0.707	0.01	2.23

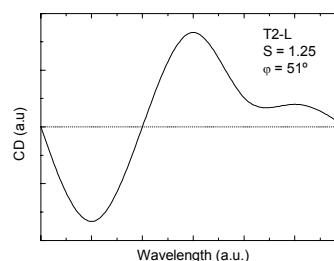
For the calculation of the circular dichroism effect, an angle  $\alpha$  has to be created between the chromophores similarly to the previously described dyad systems. Therefore the positions of the chromophores and their dipole vectors have been changed as indicated below.

$$\mu_A := \sqrt{2} \cdot \begin{bmatrix} \cos(\alpha) \\ \sin(\alpha) \\ 0 \end{bmatrix} \quad \mu_B := \begin{pmatrix} 1 \\ 0 \\ 0 \end{pmatrix} \quad \mu_C := \sqrt{2} \cdot \begin{bmatrix} \cos(\alpha) \\ \sin(\alpha) \\ 0 \end{bmatrix} \quad \mu_D := \sqrt{2} \cdot \begin{bmatrix} \cos(\alpha) \\ -\sin(\alpha) \\ 0 \end{bmatrix} \quad \mu_E := \begin{pmatrix} 1 \\ 0 \\ 0 \end{pmatrix} \quad \mu_F := \sqrt{2} \cdot \begin{bmatrix} \cos(\alpha) \\ -\sin(\alpha) \\ 0 \end{bmatrix}$$

$$R_A := \begin{pmatrix} -L \\ -W \\ -H \end{pmatrix} \quad R_B := \begin{pmatrix} 0 \\ 0 \\ -H \end{pmatrix} \quad R_C := \begin{pmatrix} L \\ W \\ -H \end{pmatrix} \quad R_D := \begin{pmatrix} S-L \\ W \\ H \end{pmatrix} \quad R_E := \begin{pmatrix} S \\ 0 \\ H \end{pmatrix} \quad R_F := \begin{pmatrix} S+L \\ -W \\ H \end{pmatrix}$$

An example of the expected circular dichroism spectrum for T2-L with a distance  $S = 1.25$  ( $\varphi = 51^\circ$ ),  $W = 0.3$  and  $\alpha = 25^\circ$  is given below.

Eigenvalues	Circular Dichroism
5.241	0
5.248	-1.534
4.793	0
4.731	1.504
-4.8	0.003
-5.213	0.028



This result leads to an expected circular dichroism spectrum where at the OPV absorption band a bisignate signal can be observed that is negative at lower wavelengths and positive at higher wavelengths. In addition, the prediction indicates a positive circular dichroism signal at absorption wavelengths of the PERY chromophore.

## 7.7 References and Notes

- 1 Tecilla, P.; Dixon, R. P.; Slobodkin, G.; Alavi, D. S.; Waldeck, D. H.; Hamilton, A. D. *J. Am. Chem. Soc.* **1990**, *112*, 9408.
- 2 Balzani, V.; Scandola, F. *Supramolecular Photochemistry*, Ellis Horwood, Chichester, **1991**.
- 3 Harriman, A.; Magda, D. J.; Sessler, J. L. *J. Phys. Chem.* **1991**, *95*, 1530.
- 4 Harriman, A.; Kubo, Y.; Sessler, J. L. *J. Am. Chem. Soc.* **1992**, *114*, 388.
- 5 Turro, C.; Chang, C. K.; Leroi, G. E.; Cukier, R. I.; Nocera, D. G. *J. Am. Chem. Soc.* **1992**, *114*, 4013.
- 6 Sessler, J. L.; Wang, B.; Harriman, A. *J. Am. Chem. Soc.* **1993**, *115*, 10418.
- 7 Sessler, J. L.; Wang, B.; Harriman, A. *J. Am. Chem. Soc.* **1995**, *117*, 704.
- 8 De Rege, P. J. F.; Williams, S. A.; Therien, M. J. *Science* **1995**, *269*, 1409.
- 9 Roberts, J. A.; Kirby, J. P.; Nocera, D. G. *J. Am. Chem. Soc.* **1995**, *117*, 8051.
- 10 Sessler, J. L.; Wang, B.; Springs, S. L.; Brown, C. T. in *Comprehensive Supramolecular Chemistry*, ed. Atwood, J. L.; Davies, J. E. D.; MacNicol, D. D.; Vögtle, F.; Murakami, Y. Pergamon, Oxford, **1996**, *Vol. 4*, 311.
- 11 Kirby, J. P.; Roberts, J. A.; Nocera, D. G. *J. Am. Chem. Soc.* **1997**, *119*, 9230.
- 12 Ward, M. D. *Chem. Soc. Rev.*, **1997**, *26*, 365.
- 13 Piotrowiak, P. *Chem. Soc. Rev.*, **1999**, *28*, 143.
- 14 Prasad, E.; Gopidas, K. R. *J. Am. Chem. Soc.*, **2000**, *122*, 3191.
- 15 Chang, C. J.; Brown, J. D.; Chang, M. C. Y.; Baker, E. A.; Nocera, D. G. in *Electron Transfer in Chemistry*, ed. Balzani, V. Wiley-VCH, Weinheim, **2001**, *Vol. 3*, 409.
- 16 Myles, A. J.; Branda, N. R. *J. Am. Chem. Soc.* **2001**, *123*, 177.
- 17 Smitha, M. A.; Prasad, E.; Gopidas, K. R. *J. Am. Chem. Soc.* **2001**, *123*, 1159.
- 18 Sessler, J. L.; Sathiosatham, M.; Brown, C. T.; Rhodes, T. A.; Wiederrecht, G. *J. Am. Chem. Soc.* **2001**, *123*, 3655.
- 19 Smitha, M. A.; Gopidas, K. R. *Chem. Phys. Lett.* **2001**, *350*, 86.
- 20 Hoeben, F. J. M.; Jonkheijm, P.; Meijer, E. W.; Schenning, A. P. H. J. *Chem. Rev.* **2005**, *105*, 1491.
- 21 Nierengarten, J.-F.; Eckert, J.-F.; Nicoud, J.-F.; Ouali, L.; Krasnikov, V.; Hadziioannou, G. *Chem. Commun.* **1999**, 617.
- 22 Eckert, J.-F.; Nicoud, J.-F.; Nierengarten, J.-F.; Liu, S.-G.; Echegoyen, L.; Barigelletti, F.; Armaroli, N.; Ouali, L.; Krasnikov, V.; Hadziioannou, G. *J. Am. Chem. Soc.* **2000**, *122*, 7467.



- 23 Armaroli, N.; Barigelletti, F.; Ceroni, P.; Eckert, J.-F.; Nicoud, J.-F.; Nierengarten, J.-F. *Chem. Commun.* **2000**, 599.
- 24 El-Ghayoury, A.; Schenning, A. P. H. J.; Van Hal, P. A.; Van Duren, J. K. J.; Janssen, R. A. J.; Meijer, E. W. *Angew. Chem., Int. Ed.* **2001**, *40*, 3660.
- 25 Van Hal, P. A.; Janssen, R. A. J.; Lanzani, G.; Cerullo, G.; Zavelani-Rossi, M.; De Silvestri, S. *Phys. Rev. B* **2001**, *64*, 075206/1.
- 26 Neuteboom, E. E.; Meskers, S. C. J.; Van Hal, P. A.; van Duren, J. K. J.; Meijer, E. W.; Janssen, R. A. J.; Dupin, H.; Pourtois, G.; Cornil, J.; Lazzaroni, R.; Bredas, J.-L.; Beljonne, D. *J. Am. Chem. Soc.* **2003**, *125*, 8625.
- 27 Beckers, E. H. A.; Meskers, S. C. J.; Schenning, A. P. H. J.; Chen, Z.; Würthner, F.; Janssen, R. A. J. *J. Phys. Chem. A* **2004**, *108*, 6933.
- 28 Schmidt-Mende, L.; Fechtenkötter, A.; Müllen, K.; Moons, E.; Friend, R. H.; MacKenzie, J. D. *Science* **2001**, *293*, 1119.
- 29 Muthukumar, K.; Loewe, R. S.; Kirmaier, C.; Hindin, E.; Schwartz, J. K.; Sazanovich, I. V.; Diers, J. R.; Bocian, D. F.; Holten, D.; Lindsey, J. S. *J. Phys. Chem. B* **2003**, *107*, 3431.
- 30 Beijer, F. H.; Kooijman, H.; Spek, A. L.; Sijbesma, R. P.; Meijer, E. W. *J. Am. Chem. Soc.* **1998**, *37*, 75.
- 31 Söntjens, S. H. M.; Sijbesma, R. P.; Van Genderen, M. H. P.; Meijer, E. W. *J. Am. Chem. Soc.* **2000**, *122*, 7487.
- 32 Beckers, E. H. A.; Van Hal, P. A.; Schenning, A. P. H. J.; El-Ghayoury, A.; Peeters, E.; Rispens, M. T.; Hummelen, J. C.; Meijer, E. W.; Janssen, R. A. J. *J. Mater. Chem.* **2002**, *12*, 2054.
- 33 El-Ghayoury, A.; Peeters, E.; Schenning, A. P. H. J.; Meijer, E. W. *Chem. Commun.* **2000**, 1969.
- 34 Neuteboom, E. E.; Beckers, E. H. A.; Meskers, S. C. J.; Meijer, E. W.; Janssen, R. A. J. *Org. Biomol. Chem.* **2003**, *1*, 198.
- 35 Weller, A.; *Z. Phys. Chem. Neue Folge* **1982**, *133*, 93.
- 36 In equation 4,  $-e$  is the electron charge,  $\epsilon_0$  the vacuum permittivity,  $\epsilon_s$  the polarity of the solvent,  $\epsilon_{ref}$  the polarity of the solvent used to determine the redox potentials  $E_{ox}(D)$  and  $E_{red}(A)$ ,  $R_{cc}$  the centre-to-centre distance of positive and negative charges and  $r^+$  and  $r^-$  the radii of the positive and negative ions.  $E_{00}$  is the energy of the excited state from which electron transfer occurs. For OPV-UP,  $r^+ = 5.05 \text{ \AA}$  (Ref. 25). For the perylene bisimide segment of PERY-UP,  $r^- = 4.71 \text{ \AA}$  was taken from the density ( $\rho = 1.59 \text{ g cm}^{-3}$ ) of *N,N'*-dimethylperylene-3,4:9,10-tetracarboxylic-bisimide derived from the X-ray crystallographic data (E. Hädicke and F. Graser, *Acta Cryst. C*, 1986, **42**, 189) via  $r^- = [3M/(4\pi\rho NA)]^{1/3}$ .  $R_{cc}$  was set to 33 Å.
- 37 Oevering, H.; Paddon-Row, M. N.; Heppener, M.; Oliver, A. M.; Cotsaris, E.; Verhoeven, J. W.; Hush, N. S. *J. Am. Chem. Soc.* **1987**, *109*, 3258.
- 38 Peeters, E.; Van Hal, P. A.; Meskers, S. C. J.; Janssen, R. A. J.; Meijer, E. W. *Chem. Eur. J.* **2002**, *8*, 4470.
- 39 Schenning, A. P. H. J.; Van Herrikhuyzen, J.; Jonkheijm, P.; Chen, Z.; Würthner, F.; Meijer, E. W. *J. Am. Chem. Soc.* **2002**, *124*, 10252.
- 40 Sinks, L. E.; Rybtchinski, B.; Imura, M.; Jones, B. A.; Goshe, A. J.; Zuo, X.; Tiede, D. M.; Li, X.; Wasielewski, M. R. *Chem. Mater.*, ASAP.
- 41 Würthner, F.; Thalacker, C.; Sautter, A.; Schartl, W.; Ibach, W.; Hollricher, O. *Chem. Eur. J.* **2000**, *6*, 3871.
- 42 Ilhan, F.; Gray, M.; Rotello, V. M. *Macromolecules* **2001**, *34*, 2597.
- 43 Kawasaki, T.; Tokuhira, M.; Kimizuka, N.; Kunitake, T. *J. Am. Chem. Soc.* **2001**, *123*, 6792.

- 44 Thalacker, C.; Würthner, F. *Adv. Funct. Mat.* **2002**, *12*, 209.
- 45 Schenning, A. P. H. J.; Jonkheijm, P.; Peeters, E.; Meijer, E. W. *J. Am. Chem. Soc.* **2001**, *123*, 409.
- 46 Van Hal, P. A.; Beckers, E. H. A.; Peeters, E.; Apperloo, J. J.; Janssen, R. A. J. *Chem. Phys. Lett.* **2000**, *328*, 403.
- 47 Würthner, F. *Chem. Commun.* **2004**, 1564.
- 48 Würthner, F.; Chen, Z.; Hoeben, F. J. M.; Osswald, P.; You, C.-C.; Jonkheijm, P.; Van Herrikhuyzen, J.; Schenning, A. P. H. J.; Van der Schoot, P. P. A. M.; Meijer, E. W.; Beckers, E. H. A.; Meskers, S. C. J.; Janssen, R. A. J. *J. Am. Chem. Soc.* **2004**, *126*, 10611.
- 49 *Circular Dichroism Spectroscopy*, Harada, N.; Nakanishi K. *Oxford University Press*, **1984**.



# Charge Transfer in Supramolecular Co-Aggregates of Oligo(p-phenylene vinylene) and Perylene Bisimide in Water\*

### *Abstract*

*Hydrophobic effects, in combination with the tendency of  $\pi$ -conjugated donor and acceptor chromophores to form a charge transfer complex, have been used to create co-aggregates of oligo(p-phenylene vinylene) and perylene bisimide molecules in water with an alternating face-to-face structure. A fast, sub-picosecond photoinduced electron transfer has been identified in these alternating stacks by pump-probe spectroscopy.*

---

\* This work has been published: Beckers, E. H. A.; Jonkheijm, P.; Schenning, A. P. H. J.; Meskers, S. C. J.; Janssen, R. A. J. *ChemPhysChem* **2005**, *6*, 2029-2031.

## 8.1 Introduction

The photophysical properties of mixed aggregates –*i.e.* those consisting of different chromophores that *co*-assemble in solution– have received remarkably little attention, even though the organization of alternating electron rich and electron deficient units has often been used to create supramolecular architectures.<sup>1-12</sup> Photoinduced *energy transfer* has been studied in mixed stacks such as supramolecular zinc chlorin assemblies *co*-aggregated with various energy traps,<sup>13</sup> oligo(*p*-phenylene vinylene)s (OPVs) of different conjugation length,<sup>14</sup> and in mixed organogels.<sup>15,16</sup> In a few examples, aggregates of covalently-linked and hydrogen-bonded donor-acceptor molecules in organic solvents have been considered for photoinduced *electron transfer* reactions in an attempt to provide new routes for light energy conversion and storage.<sup>17-19</sup> This chapter gives a first example of  $\pi$ -conjugated molecules with donor and acceptor character that form supramolecular *co*-aggregates in aqueous solution and give electron transfer upon illumination.

This design for supramolecular assemblies uses a combination of OPV (1)<sup>20</sup> and perylene bisimide (PERY) (2)<sup>21</sup> molecules (Figure 1). The large planar and hydrophobic  $\pi$ -systems of these molecules enable  $\pi$ - $\pi$  stacking interactions that result in formation of aggregates in polar solvents.<sup>18</sup> Similar to other water-soluble OPV<sup>22,23</sup> and PERY<sup>24-28</sup> derivatives, the hydrophobic nature of the  $\pi$ -conjugated system was compensated by introducing water-soluble substituents, *viz.* oligoethylene glycol side chains. As a result of the balance between these hydrophobic and hydrophilic interactions, each of the molecules can be dissolved in water in the form of small aggregates or stacks.

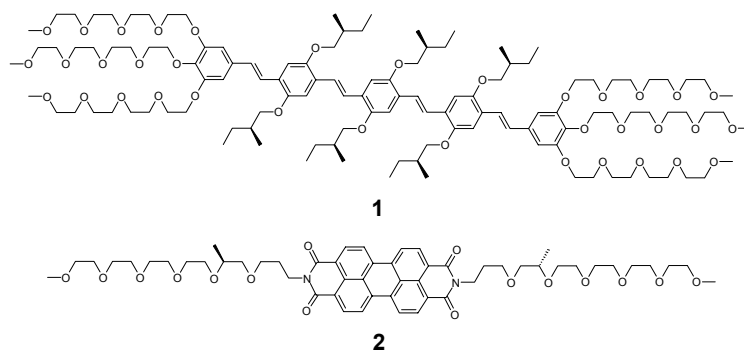


**Figure 1:** Structure of water-soluble OPV (1) and PERY (2) derivatives.

## 8.2 Results and Discussion

**UV/Vis Absorption Spectroscopy.** Aqueous solutions of 1, 2, and their mixtures were obtained by dissolving the compounds in tetrahydrofuran (THF) and injecting these solutions into water. THF was then removed by heating, providing clear aqueous solutions. When 1 is dissolved in water, the maximum of the  $\pi$ - $\pi^*$  transition in the optical absorption is significantly blue shifted and the fluorescence is strongly quenched as compared to the spectrum of a molecularly dissolved sample of 1 in chloroform (Figure 2a). The blue shift and fluorescence quenching observed in the spectra of 1 in

water have previously been studied in detail and are characteristic for the formation of aggregates.<sup>20</sup> Compound 2 exhibits a similar shift of the  $\pi$ - $\pi^*$  transition when dissolved in water compared to a chloroform solution, together with the loss of the distinct sharp vibronic transitions of molecularly dissolved PERY chromophores. For 1 and 2 the blue shift and the changes in the shape of the absorption spectrum are accompanied by a red shift of the onset of the absorption to longer wavelengths. Together, these features are typical of aggregated chromophores.

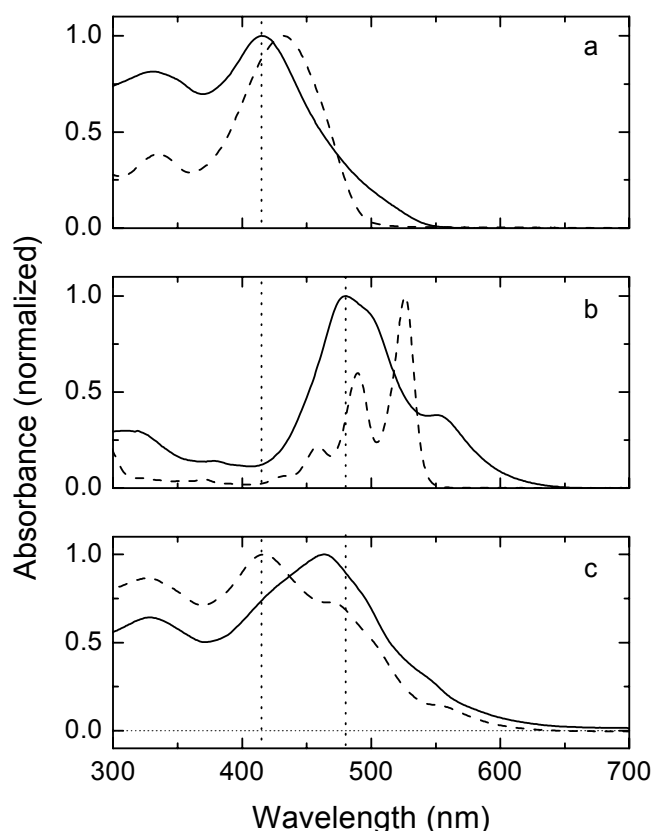


**Figure 2:** (a) Absorption spectra of 1 ( $1 \times 10^{-4}$  M) in water (solid line) and  $\text{CHCl}_3$  (dashed line). (b) Absorption spectra 2 ( $1 \times 10^{-4}$  M) in water (solid line) and  $\text{CHCl}_3$  (dashed line). (c) Measured absorption spectrum of a 1:1 mixture of 1 and 2 ( $1 \times 10^{-4}$  M) in water (solid line) and the linear superposition of the spectra of pure 1 and 2 at the same concentration (dashed line). The latter spectrum has been normalized after summation.

To study the formation of mixed aggregates, the absorption spectrum of a 1:1 ( $1 \times 10^{-4}$  M) mixture of 1 and 2 in water was recorded and compared to the linear superposition of the spectra of pure 1 and 2 in water at the same concentration (Figure 2c). These spectra should be identical if mixing does not result in direct interaction between 1 and 2. Figure 2c shows, however, that there is a clear difference between the absorption maximum of the linear superposition of the spectra of 1 and 2 (417 nm) and that of the experimentally obtained spectrum of their physical mixture (464 nm). This indicates that both molecules experience a strongly different micro-environment in the co-aggregates as compared to the aggregates of the pure compounds and that OPV-OPV and BPI-BPI interactions are lost.

Therefore, it can be concluded that OPV-BPI chromophore interactions are present in aggregated mixtures of 1 and 2 in water.

**Transient Photoinduced Absorption Spectroscopy.** Transient pump-probe spectroscopy allows the identification of the photophysical processes in the mixed aggregates and the temporal evolution of the excited states. The radical cation of the OPV chromophore ( $\text{OPV}^+$ ) has an absorption at 1450 nm that can be used to probe the formation of a charge-separated state.<sup>29</sup> The band at 1450 nm corresponds to the low-energy transition of the radical cation and is highly characteristic for  $\text{OPV}^+$  because it does not interfere with the OPV triplet bands at 750 nm eV.<sup>30</sup> After photoexcitation of a 1:1 ( $1 \times 10^{-4}$  M) assembly of 1 and 2 in water with 150 fs pulses at 455 nm, a strong transient differential absorption was observed at 1450 nm (Figure 3a) that gives direct spectral evidence of the formation of a charge-separated state.<sup>31</sup> The rapid rise of this signal indicates that charge separation is extremely fast ( $k_{\text{CS}} > 5 \times 10^{12} \text{ s}^{-1}$ ), likely faster than the response time of the equipment ( $\sim 200$  fs). Such fast kinetics implies that the OPV and PERY chromophores must be in very close proximity. If charge separation would take place in a molecularly dissolved system, it would be diffusion limited, and have a rate constant of  $\sim 10^6 \text{ s}^{-1}$  or less at the  $1 \times 10^{-4}$  M concentration used in the experiment. The decay of the 1450 nm signal (Figure 3b) shows that the charge recombination occurs with a rate constant of  $k_{\text{CR}} = 1.5 \times 10^{10} \text{ s}^{-1}$ .

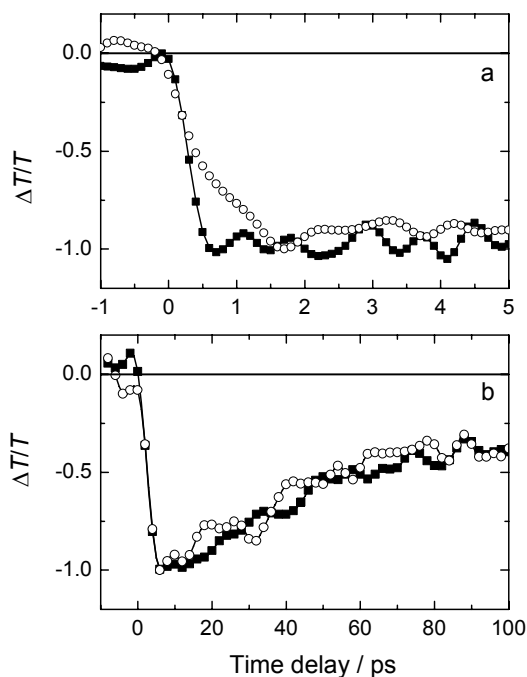


**Figure 3:** Differential transmission dynamics of mixed aggregates of 1 and 2 in water for two different compositions 1:1 (solid squares) and 1:0.67 (open circles) probed at 1450 nm ( $\text{OPV}^+$ ) following photoexcitation at 455 nm with 150 fs pulses. The two panels correspond to time domains revealing (a) formation and (b) recombination of the charge-separated state.

The charge transfer dynamics were also monitored for a 1:0.67 ratio of donor and acceptor chromophores. Figure 3a shows the transient signal at 1450 nm for an aggregate of 1 and 2 with a

1:0.67 ratio. By comparison with the trace for the 1:1 mixture, two distinctly different components can be identified for the rate of charge formation, one similarly fast as in the first experiment, and one with a reduced rate. The decreased rate of the second component is attributed to OPV domains in the aggregate. These domains make that some photoexcited OPV chromophores are not in close proximity with a PERY chromophore. As a result, such photoexcitations must first migrate within the OPV domain<sup>32</sup> to the interface with PERY moieties before they give rise to electron transfer. Interestingly, the charge recombination kinetics is not significantly affected by this change in composition (Figure 3b). The composition-independent recombination can be rationalized by considering that mainly geminate recombination will occur because charges will be created on OPV and PERY molecules that are in close proximity.

**Photoluminescence Quenching.** Additional insight into the charge transfer in mixed aggregates was obtained by monitoring the fluorescence intensity of aggregates of PERY derivative 2, incorporating increasing amounts of 1. The formation of PERY aggregates is known to result in a distinct red shift of the photoluminescence.<sup>33-35</sup> Correspondingly, a fluorescence maximum was found at 690 nm (Figure 4) for aggregates of 2 in water when they were excited at 600 nm, *i.e.* at photon energies below the optical band gap of the isolated PERY and OPV moieties (Figure 2). The intensity of the aggregate emission at 690 nm decreases considerably with increasing amounts of OPV molecules in the aggregate until it can no longer be measured quantitatively below a 0.5:1 ratio of compound 1 versus compound 2. The increased fluorescence quenching implies that OPV-PERY contacts rise in number with increasing OPV concentration. The loss in PERY aggregate emission (Figure 2c) is consistent with the photoinduced charge transfer reaction inferred from pump-probe spectroscopy experiments.

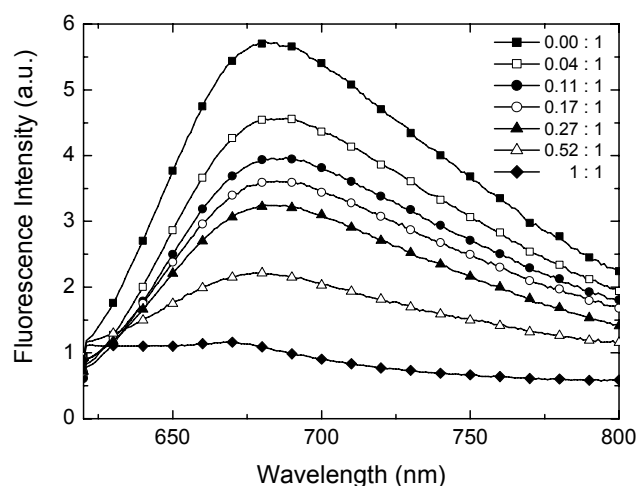


**Figure 4:** Fluorescence intensity of a  $1 \times 10^{-4}$  M solution of aggregates of 2 in water incorporating increasing amounts of 1 (specific ratios of compound 1 vs compound 2 are given in the legend). The fluorescence signal was measured with excitation at 600 nm.

Previous studies on covalently linked OPV and PERY derivatives show that they form a sandwich-like structure in the solid state in which the OPV and PERY moieties are packed on top of each other in a face-to-face orientation as a result of a ground state charge transfer interaction.<sup>36,37</sup> The typical rates for



charge separation and recombination in this type of face-to-face configuration are  $k_{CS} > 2 \times 10^{12} \text{ s}^{-1}$  and  $k_{CR} = 1.5 \times 10^{10} \text{ s}^{-1}$ , respectively.<sup>37</sup> These rates are virtually identical to the rate constants now observed for the 1:1 aggregated mixture in water and consistent with a supramolecular organization into a sandwich like structure of the present co-assemblies, similar to that in the covalently linked systems.

### 8.3 Conclusions

A photoinduced charge transfer reaction occurs in mixed  $\pi$ -conjugated OPV-PERY aggregates in water. Exciton diffusion preceding the electron transfer reaction was identified in the OPV domains for aggregates containing an excess of OPV. Hydrophobic effects in combination with the tendency of OPV and PERY chromophores to form a charge transfer complex in the ground state most likely lead to the formation of sandwich-like structure where OPV and PERY chromophores are positioned in a face-to-face configuration. Future studies on electron transfer dynamics on a nanoscale in weakly interacting molecular systems will aid in the future design of multifunctional architectures and nanostructured materials for artificial electronic and photonic devices.

### 8.4 Experimental Section

The synthesis of the OPV<sup>20</sup> and PERY<sup>21</sup> compounds has previously been reported. A detailed description of the used spectroscopic techniques can be found in Chapter 2.

### 8.5 References and Notes

- 1 Ringsdorf, H.; Wüstefeld, R.; Zerta, E.; Ebert, M.; Wendorff, J. H. *Angew. Chem., Int. Ed.* **1989**, *28*, 914.
- 2 Lokey, R. S.; Iverson, B. L. *Nature* **1995**, *375*, 303.
- 3 Shimomura, M.; Karthaus, O.; Ijro, K. *Synth. Met.* **1996**, *81*, 251.
- 4 Nguyen, J. Q.; Iverson, B. L. *J. Am. Chem. Soc.* **1999**, *121*, 2639.
- 5 Weck, M.; Dunn, A. R.; Matsumoto, K.; Coates, G. W.; Lobkovsky, E. B.; Grubbs, R. H. *Angew. Chem., Int. Ed.* **1999**, *38*, 2741.
- 6 Goldmann, D.; Janietz, D.; Schmidt, C.; Wendorff, J. H. *Angew. Chem., Int. Ed.* **2000**, *39*, 1851.
- 7 Feast, W. J.; Lövenich, P. W.; Puschmann, H.; Taliani, C. *Chem. Commun.* **2001**, 505.
- 8 Kilbinger, A. F. M.; Grubbs, R. H. *Angew. Chem., Int. Ed.* **2002**, *41*, 1563.
- 9 Gabriel, G. J.; Iverson, B. L. *J. Am. Chem. Soc.* **2002**, *124*, 15174.
- 10 Park, L. Y.; Hamilton, D. G.; McGehee, E. A.; McMenimen, K. A. *J. Am. Chem. Soc.* **2003**, *125*, 10586.
- 11 Ghosh, S.; Ramakrishnan, S. *Macromolecules* **2005**, *38*, 676.
- 12 Wang, Z.; Dötz, F.; Enkelmann, V.; Müllen, K. *Angew. Chem., Int. Ed.* **2005**, *44*, 1247.
- 13 Prokhorenko, V. I.; Holzwarth, A. R.; Müller, M. G.; Schaffner, K.; Miyatake, T.; Tamiaki, H. *J. Phys. Chem. B* **2002**, *106*, 5761.
- 14 Hoeben, F. J. M.; Herz, L. M.; Daniel, C.; Jonkheijm, P.; Schenning, A. P. H. J.; Silva, C.; Meskers, S. C. J.; Beljonne, D.; Phillips, R. T.; Friend, R. H.; Meijer, E. W. *Angew. Chem., Int. Ed.* **2004**, *43*, 1976.
- 15 Ajayaghosh, A.; George, S. J.; Praveen, V. K. *Angew. Chem., Int. Ed.* **2003**, *42*, 332,

- 16 Sugiyasu, K.; Fujita, N.; Shinkai, S. *Angew. Chem., Int. Ed.* **2004**, *43*, 1229.
- 17 Van der Boom, T.; Hayes, R. T.; Zhao, Y.; Bushard, P. J.; Weiss, E. A.; Wasielewski, M. R. *J. Am. Chem. Soc.* **2002**, *124*, 9582.
- 18 Schenning, A. P. H. J.; Van Herrikhuyzen, J.; Jonkheijm, P.; Chen, Z.; Würthner, F.; Meijer, E. W. *J. Am. Chem. Soc.* **2002**, *124*, 10252.
- 19 Würthner, F.; Chen, Z.; Hoeben, F. J. M.; Osswald, P.; You, C.-C.; Jonkheijm, P.; Van Herrikhuyzen, J.; Schenning, A. P. H. J.; Van der Schoot, P. P. A. M.; Meijer, E. W.; Beckers, E. H. A.; Meskers, S. C. J.; Janssen, R. A. J. *J. Am. Chem. Soc.* **2004**, *126*, 10611.
- 20 Jonkheijm, P.; Franssen, M.; Schenning, A. P. H. J.; Meijer, E. W. *J. Chem. Soc., Perkin Trans. 2* **2001**, 1280.
- 21 Van Herrikhuyzen, J.; Sayamakumari, A.; Schenning, A. P. H. J.; Meijer, E. W. *J. Am. Chem. Soc.* **2004**, *126*, 10021.
- 22 Li, H.; Li, Y.; Zhai, J.; Cui, G.; Liu, H.; Xiao, S.; Liu, Y.; Lu, F.; Jiang, L.; Zhu, D. *Chem. Eur. J.* **2003**, *9*, 6031.
- 23 Hulvat, J. F.; Sofos, M.; Tajima, K.; Stupp, S. I. *J. Am. Chem. Soc.* **2005**, *127*, 366.
- 24 Li, A. D. Q.; Wang, W.; Wang, L.-Q. *Chem. Eur. J.* **2003**, *9*, 4594.
- 25 Qu, J.; Kohl, C.; Pottek, M.; Müllen, K. *Angew. Chem., Int. Ed.* **2004**, *43*, 1528.
- 26 Arnaud, A.; Belleney, J.; Boue, F.; Bouteiller, L.; Carrot, G.; Wintgens, V. *Angew. Chem. Int. Ed.* **2004**, *43*, 1718.
- 27 Wang, W.; Han, J. J.; Wang, L.-Q.; Li, L.-S.; Shaw, W. J.; Li, A. D. Q. *Nano Lett.* **2003**, *3*, 455.
- 28 Kohl, C.; Weil, T.; Qu, J.; Müllen, K. *Chem. Eur. J.* **2004**, *10*, 5297.
- 29 Van Hal, P. A.; Beckers, E. H. A.; Peeters, E.; Apperloo, J. J.; Janssen, R. A. J. *Chem. Phys. Lett.* **2000**, **328**, 403.
- 30 Peeters, E.; Marcos Ramos, A.; Meskers, S. C. J.; Janssen, R. A. J. *J. Chem. Phys.* **2000**, *112*, 9445
- 31 In a control experiment the separate compounds were measured under further identical experimental conditions. For 2 no signal was observed. For 1, the observed signal at 1450 nm was less than 10% of the intensity measured for the 1:1 mixture, indicating that the contribution of the OPV ( $S_n \leftarrow S_1$ ) transition to the signal is small.
- 32 Herz, L. M.; Daniel, C.; Silva, C.; Hoeben, F. J. M.; Schenning, A. P. H. J.; Meijer, E. W.; Friend, R. H.; Phillips, R. T. *Phys. Rev. B* **2003**, *68*, 045203.
- 33 Gómez, U.; Leonhardt, M.; Port, H.; Wolf, H. C. *Chem. Phys. Lett.* **1997**, *268*, 1.
- 34 Puech, K.; Fröb, H.; Leo, K. *J. Lumin.* **1997**, *72-74*, 524.
- 35 Neuteboom, E. E.; Meskers, S. C. J.; Meijer, E. W.; Janssen, R. A. J. *Macromol. Chem. Phys.* **2004**, *205*, 217.
- 36 Neuteboom, E. E.; Meskers, S. C. J.; Van Hal, P. A.; Van Duren, J. K. J.; Meijer, E. W.; Janssen, R. A. J.; Dupin, H.; Pourtois, G.; Cornil, J.; Lazzaroni, R.; Brédas, J.-L.; Beljonne, D. *J. Am. Chem. Soc.* **2003**, *125*, 8625.
- 37 Neuteboom, E. E.; Van Hal, P. A.; Janssen, R. A. J. *Chem. Eur. J.* **2004**, *10*, 3907.



# Summary

The interplay between  $\pi$ -conjugated donor and acceptor molecules is crucial to the working principles of future organic semiconductor devices that convert light into solar fuels or solar electricity. The knowledge acquired from detailed studies on energy and electron transfer reactions on molecular donor-acceptor combinations that form the basis of these applications, is immense but still not complete. For covalently linked donor-acceptor systems, control over energy and electron reactions can be achieved, but extending these principles to understand and control the behavior in the solid state has proven to be cumbersome. More insight in the role of intermolecular effects within ensembles of donor-acceptor molecules as they occur in the solid state is essential in understanding the fundamental principles that rule charge transfer reactions in organic semiconductor systems comprising electron donors and acceptors. The aim of this thesis is to study photoinduced electron transfer mechanisms between donor and acceptor chromophores that are relevant to photovoltaic cells and to see how these processes evolve from molecule to material. As a result this thesis not only focuses on donor-acceptor arrays that are molecularly dissolved in solution but also on self-assembled nanoaggregates.

Chapter 2 describes the kinetics of photoinduced electron transfer reactions in fullerene-donor-fullerene triads containing an electron rich pyrrole ring in the donor moiety as investigated by photoluminescence and transient absorption spectroscopy. Depending on the solvent polarity and chromophore distance, the charge separation occurs at rates ranging from  $10^9 \text{ s}^{-1}$  to  $10^{10} \text{ s}^{-1}$ . The charge recombination could only be estimated to be faster than  $2 \times 10^{10} \text{ s}^{-1}$  as the large contribution of the  $S_n \leftarrow S_1$  absorption of the fullerene ( $C_{60}$ ) moiety hampers a more accurate determination.

The kinetics of photoinduced charge transfer reactions of three donor-acceptor systems based on oligo(*p*-phenylene vinylene) (OPV) and perylene bisimide (PERY) in a symmetrical OPV-PERY-OPV configuration are described in Chapter 3. The reduction potentials of three donor-acceptor-donor molecules differ strongly as a consequence of the four substituents on the bay-position of the PERY unit. The transient absorption experiments indicate that charge separation occurs from the excited singlet state of the PERY moiety to the charge-separated state (CSS) and to the lowest electronically excited-state level of the charge-separated state (CSS\*). At high driving forces achieved by changing the polarity of the solvent, the rates for charge separation and recombination decrease with increasing change in Gibbs-free energy. Hence these OPV-PERY-OPV arrays represent an exceptional example of molecules in which both charge separation and recombination occur close to or in the Marcus inverted region.

Chapter 4 focuses on the multistep photoinduced electron transfer in two symmetrical pentads consisting of two oligoaniline(OAn)-OPV segments coupled to a central PERY unit via a direct linkage (1) or a saturated spacer (2). Photoexcitation gives the OAn-OPV<sup>+</sup>-PERY<sup>-</sup>-OPV-OAn as the primary charge-separated state. Charge transfer is extremely fast ( $k_{CS} > 1 \text{ ps}^{-1}$ ) in all studied solvents for the system with the direct linker, while the rate constants for recombination occurs in the Marcus inverted region. Charge separation and charge recombination are slower in the array with the longer spacer as a result of the reduced electronic coupling between the donor and acceptor. The primary OAn-OPV<sup>+</sup>-PERY<sup>-</sup>-OPV-OAn charge-separated state rearranges to the OAn<sup>+</sup>-OPV-PERY<sup>-</sup>-OPV-OAn state after a charge shift reaction with efficiencies of about 0.22 and 0.28 for respectively 1 and 2, only weakly dependent on polarity. This state has a long

lifetime as a result of the negligible interaction between the distant redox sites, and can be observed up to several microseconds.

The OPV-PERY-OPV compounds studied in their molecularly dissolved state in Chapter 3 are subject of further investigation in Chapter 5 but now as self-assembled aggregates. This allows to determine the changes that occur as a result of intermolecular interactions that occur when molecules are in close proximity. The supramolecular organization of three arrays has been determined in methylcyclohexane using absorption and circular dichroism spectroscopy. Both face-to-face (H-type) and slipped (J-type) stacking of the OPV and PERY chromophores have been identified and molecular mechanics calculations confirm the tendency that bay-substitution of the PERY moiety results in J-type aggregation for the OPV-PERY-OPV arrays. For the J-type aggregates, the short intermolecular OPV-PERY distances enable a highly efficient charge transfer with a rate ( $k_{cs} > 10^{12} \text{ s}^{-1}$ ) that significantly exceeds the rate of the intramolecular reaction of the same compounds when molecularly dissolved. In the H-type aggregates the intermolecular OPV-PERY distance is not reduced compared to the intramolecular separation and, hence, the rates of the electron transfer reactions are not significantly affected. The different inter-chromophore distances that occur in the H and J-type aggregates can also rationalize the changes in the kinetics of the charge recombination upon aggregation.

Supramolecular arrays of OPV-donor and  $C_{60}$ -acceptor compounds, created via a quadruple hydrogen-bonding unit, are described in Chapter 6. In these dyads, singlet-energy transfer from the OPV unit to the fullerene causes a strong quenching of the OPV fluorescence ( $Q_{\text{max}} \geq 90$ ). The lower limit obtained for the rate constant for energy transfer ( $k_{\text{EN}} \geq 6 \times 10^{10} \text{ s}^{-1}$ ) is rationalized in terms of the Förster mechanism. Photoinduced electron transfer could not be observed in these hydrogen-bonded dimers. The absence of charge separation is ascribed to a small electronic coupling between the donor and acceptor in the excited state as a result of the long distance between the chromophores. Furthermore, the formation of heterodimers of bifunctional OPV and  $C_{60}$  ureido-pyrimidinone derivatives has been observed by  $^1\text{H-NMR}$  and fluorescence techniques.

Chapter 7 describes the photophysical properties of molecularly dissolved ureido-pyrimidinone coupled OPV-PERY heterodimers. Pump-probe spectroscopy allowed determining the rate for energy transfer in this hydrogen-bonded system in dilute solution. A photoinduced electron transfer reaction could not be observed for this hydrogen-bonded system. The second part of this chapter focuses on the effects of aggregation on the charge transfer kinetics of hydrogen-bonded OPV-PERY systems. In these aggregated hydrogen-bonded OPV-PERY systems a highly efficient charge separation occurs, likely via an intermolecular pathway in the J-type structure of the stacked OPV-PERY arrays. The charge recombination reaction depends strongly on the nanoscopic differences within the J-type geometry as revealed by comparison of a variety of stacked systems. An attempt is made to investigate the influence of these small differences by linking the absorption and circular dichroism to the photoinduced absorption spectroscopy results. A coupled oscillator model is used in an attempt to propose different molecular arrangements that are consistent with the experimental observations.

Chapter 8 describes the formation of alternating face-to-face co-aggregates of OPV and PERY molecules in water induced by the combination hydrophobic effects and the tendency of  $\pi$ -conjugated donor and acceptor chromophores to form a charge transfer complex. Pump-probe spectroscopy revealed a sub-picosecond photoinduced electron transfer in these alternating stacks.

# Samenvatting

Het samenspel tussen  $\pi$ -geconjugeerde donor en acceptor moleculen is cruciaal voor de werking van toekomstige organische halfgeleiders die licht omzetten in zonne-energie. De kennis opgedaan bij gedetailleerde studies aan energie- en elektronoverdrachtsreacties in moleculaire donor-acceptor combinaties, die de basis vormen voor deze applicaties, is immens maar nog steeds incompleet. Voor covalent gebonden donor-acceptor systemen kan controle over de energie- en elektronoverdracht verkregen worden, maar een extrapolatie van deze kennis om deze reacties ook in de vaste fase te begrijpen is lastig gebleken. Hiervoor is meer inzicht nodig in de intermoleculaire effecten in aggregaten van donor-acceptor moleculen zoals deze voorkomen in de vaste fase in organische halfgeleider systemen. Het doel van dit proefschrift is het bestuderen van fotogeïnduceerde elektronoverdrachtsreacties tussen donor en acceptor chromoforen die relevant zijn voor fotovoltaïsche cellen met bijzondere aandacht voor de ontwikkeling van deze eigenschappen van molecuul tot materiaal. Daarom behandelt dit proefschrift niet alleen moleculair opgeloste donor-acceptor combinaties, maar ook de eigenschappen in zelfgeassembleerde nanoaggregaten.

Hoofdstuk 2 behandelt de kinetiek van fotogeïnduceerde ladingsoverdracht in fullereen-donor-fullereen triades met een elektronrijke pyrroolring in de donoreenheid, bestudeerd met fotoluminescentie en tijdsopgeloste fotogeïnduceerde absorptie. De snelheid van de ladingsscheiding varieert tussen  $10^9 \text{ s}^{-1}$  en  $10^{10} \text{ s}^{-1}$ , afhankelijk van de polariteit van het oplosmiddel en de chromofoorafstand. Voor de recombinatiesnelheid kon alleen een waarde sneller dan  $2 \times 10^{10} \text{ s}^{-1}$  worden vastgesteld aangezien de bijdrage van de  $S_n \leftarrow S_1$  overgang van de fullereen ( $C_{60}$ ) een meer accurate benadering verhindert.

De kinetiek van fotogeïnduceerde ladingsoverdracht in drie donor-acceptor systemen gebaseerd op oligo(*p*-fenyleen vinyleen) (OPV) en peryleen bisimides (PERY) in een symmetrische OPV-PERY-OPV configuratie staat beschreven in hoofdstuk 3. De reductiepotentiaal van deze drie donor-acceptor-donor moleculen verschilt aanzienlijk, afhankelijk van de substituenten op de 3,4:9,10 posities van de peryleenbisimide. De tijdsopgeloste fotogeïnduceerde absorptie-experimenten geven aan dat ladingsscheiding plaatsvindt vanuit de eerste singlettoestand van de PERY eenheid, naar de ladingsgescheiden toestand en de eerste aangeslagen toestand van de ladingsgescheiden toestand. Voor hoge drijvende krachten, verkregen door verandering van oplosmiddel, wordt zowel de voorwaartse als teruggaande elektronoverdrachtsnelheid verlaagd bij toenemende drijvende kracht. Daarom vertonen deze OPV-PERY-OPV triades een uitzonderlijk voorbeeld van moleculen waarbij zowel de ladingsscheiding als de ladingsrecombinatie dichtbij of in het Marcus-inverted gebied plaatsvinden.

Hoofdstuk 4 concentreert zich op de multistaps fotogeïnduceerde elektronoverdracht in twee symmetrische pentades bestaande uit twee oligoaniline(OAn)-OPV segmenten die gekoppeld zijn aan een centrale PERY eenheid via een directe (1) of verzadigde (2) covalente binding. Na fotoexcitatie geeft dit OAn-OPV<sup>+</sup>-PERY<sup>-</sup>-OPV-OAn als primaire ladingsgescheiden toestand. De ladingsscheidingsreactie is uiterst snel ( $> 1 \text{ ps}^{-1}$ ) in alle bestudeerde oplosmiddelen voor het systeem met de directe binding waar de recombinatiereactie zich in het Marcus-inverted gebied bevindt. De ladingsscheiding en recombinatie zijn langzamer in de configuratie met de verzadigde binding door de kleinere elektronische koppeling tussen de donor en acceptor. De initiële OAn-OPV<sup>+</sup>-PERY<sup>-</sup>-OPV-

OAn toestand reorganiseert na een ladingsverschuiving tot de OAn<sup>+</sup>-OPV-PERY<sup>-</sup>-OPV-OAn toestand met efficiënties van 0.22 en 0.28 voor respectievelijk 1 en 2, nauwelijks afhankelijk van de polariteit van het oplosmiddel. Als gevolg van de verwaarloosbare interactie tussen de redox-paren heeft deze toestand een lange levensduur en is meetbaar tot enkele microsecondes na excitatie.

De OPV-PERY-OPV verbindingen die in hoofdstuk 3 bestudeerd zijn in hun moleculair opgeloste toestand zijn in hoofdstuk 5 verder onderzocht als zelfgeassembleerde aggregaten. Dit maakt het mogelijk om veranderingen vast te stellen die ontstaan door intermoleculaire interacties van moleculen op korte afstand. De supramoleculaire organisatie van deze drie verbindingen is bepaald in methylcyclohexaan met behulp van absorptie en circulair dichroïsme spectroscopie. Zowel een verticaal gestapelde (H-type) als een afgeschoven (J-type) pakking van de OPV en PERY chromoforen konden geïdentificeerd worden. Moleculaire mechanica berekeningen bevestigen dat de substitutie van de PERY eenheid leidt tot een J-type pakking voor OPV-PERY-OPV verbindingen. De korte intermoleculaire OPV-PERY afstand in J-type aggregaten zorgt ervoor dat een zeer efficiënte ladingsscheiding ( $> 10^{12} \text{ s}^{-1}$ ) mogelijk is die duidelijk sneller is dan de intramoleculaire ladingsscheiding voor dezelfde moleculen in hun moleculair opgeloste toestand. De intermoleculaire OPV-PERY afstand is in H-type aggregaten niet kleiner dan de intramoleculaire afstand waardoor de snelheden van de elektronoverdrachtsreactie nauwelijks veranderen. De verschillen in afstand tussen de chromoforen geven tevens een verklaring voor de veranderingen van de ladingsrecombinatiesnelheden bij aggregatie.

Supramoleculaire structuren bestaande uit OPV donor en C<sub>60</sub> acceptor eenheden gekoppeld via de viervoudige ureïdo-pyrimidinon waterstofbruggenheid zijn beschreven in hoofdstuk 6. In deze dimeren resulteert een singlet-energieoverdracht van de OPV naar de fullereen in een sterke afname van de OPV luminescentie ( $\geq 90\times$ ). De ondergrens van de snelheid voor deze reactie ( $\geq 6 \times 10^{10} \text{ s}^{-1}$ ) kan worden verklaard met behulp van het Förster-mechanisme. Een fotogeïnduceerde elektronoverdracht kon voor deze dimeren niet vastgesteld worden. Deze afwezigheid wordt toegeschreven aan de geringe elektronische koppeling tussen de donor en acceptor als gevolg van de grote afstand tussen de chromoforen. Verder werd met behulp van <sup>1</sup>H-NMR en fluorescentie technieken de vorming van heterodimeren van bifunctionele OPV en C<sub>60</sub> ureïdo-pyrimidinon derivaten vastgesteld.

Hoofdstuk 7 beschrijft de fotofysische eigenschappen van ureïdo-pyrimidinon gekoppelde, moleculair opgeloste OPV-PERY heterodimeren. De snelheid van de energieoverdrachtsreactie kon in deze waterstofgebrugde systemen bepaald worden in verdunde oplossing door gebruik te maken van tijdsopgeloste fotogeïnduceerde absorptiespectroscopie. Een fotogeïnduceerde elektronoverdracht kon voor dit waterstofgebrugde dimeer niet vastgesteld worden. Het tweede gedeelte van dit hoofdstuk concentreert zich op de effecten van aggregatie op de ladingsoverdrachtsreacties in waterstofgebrugde OPV-PERY systemen. In de geaggregeerde waterstofgebrugde OPV-PERY systemen vindt een zeer efficiënte ladingsscheiding plaats, vermoedelijk via een intermoleculair pad in de J-type structuur van deze afgeschoven gestapelde OPV-PERY moleculen. Zoals blijkt uit de vergelijking tussen verschillende geaggregeerde systemen hangt de recombinatiesnelheid sterk af van nanoscopische verschillen in de J-type pakking. Daarom is een poging ondernomen om de invloed van deze kleine verandering te zien door het koppelen van de gegevens verkregen via absorptie, circulair dichroïsme en fotogeïnduceerde absorptiespectroscopie. Een model met gekoppelde oscillatoren is gebruikt in een

poging om mogelijke moleculaire ordeningen voor te stellen die consistent zijn met de experimentele waarnemingen.

Hoofdstuk 8 beschrijft de vorming van alternerende co-aggregaten van OPV en PERY moleculen in water, veroorzaakt door hydrofobe effecten en de aanleg tot het vormen van een ladingsgescheiden complex in de grondtoestand voor  $\pi$ -geconjugeerde donor en acceptor chromoforen. Met behulp van tijdsopgeloste spectroscopie kon in deze alternerende aggregaten een ladingsscheiding op een sub-picoseconde tijdschaal waargenomen worden.





# Curriculum Vitae



Edwin Beckers werd geboren op 28 november 1977 in Maastricht. Na zijn VWO-opleiding aan het Trichter College in Maastricht begon hij in 1996 met de studie Scheikundige Technologie aan de Technische Universiteit Eindhoven. Na een externe bedrijfstage bij het Research and Technology Center van Shell in Louvain-la-Neuve (B) werd deze studie in 2001 afgerond met een afstudeeronderzoek bij de vakgroep Macromoleculaire en Organische Chemie. Dit onderzoek werd in dezelfde vakgroep onder leiding van prof. dr. ir. R. A. J. Janssen en dr. S. C. J. Meskers voortgezet met een promotieonderzoek waarvan de belangrijkste resultaten beschreven staan in dit proefschrift.

Edwin Beckers was born on November 28<sup>th</sup>, 1977 in Maastricht. After finishing his secondary education at the Trichter College in Maastricht, he started with the study Chemical Engineering at the Eindhoven University of Technology in 1996. Following an external traineeship at the Shell Research and Technology Center in Louvain-la-Neuve (B), he finalized this study in 2001 with a graduation project at the Laboratory for Macromolecular and Organic Chemistry. He continued this research as a Ph.D. student in the same laboratory under supervision of prof. dr. ir. R. A. J. Janssen and dr. S. C. J. Meskers. The most important results of this work are presented in this thesis.



# List of Publications

*Photoinduced Intermolecular Electron Transfer between Oligo(p-phenylene vinylene)s and N-methylfulleropyrrolidine in a Polar Solvent*

Paul A. van Hal, Edwin H. A. Beckers, Emiel Peeters, Joke J. Apperloo and René A. J. Janssen, *Chemical Physics Letters*, **2000**, 328 (4-6), 403-408.

*Singlet-Energy Transfer in Quadruple Hydrogen-Bonded Oligo(p-phenylene vinylene)-Fullerene Dyads*

Edwin H. A. Beckers, Paul A. van Hal, Albertus P. H. J. Schenning, Abdelkrim El-ghayoury, Emiel Peeters, Minze T. Rispens, Jan C. Hummelen, E. W. Meijer and René A. J. Janssen, *Journal of Materials Chemistry*, **2002**, 12(7), 2054-2060.

*Orientalional Effect on the Photophysical Properties of Quaterthiophene-C<sub>60</sub> Dyads*

Paul A. van Hal, Edwin H. A. Beckers, Stefan C. J. Meskers, René A. J. Janssen, Bruno Joussetme, Philippe Blanchard and Jean Roncali, *Chemistry, a European Journal*, **2002**, 8(23), 5415-5429.

*Preferential Hetero-Dimer Formation and Equilibrium Dynamics of Self-Complementary Bifunctional Oligo(p-phenylenevinylene) and C<sub>60</sub> Ureido-Pyrimidinone Derivatives in Solution*

Edwin H. A. Beckers, Albertus P. H. J. Schenning, Paul A. van Hal, Abdelkrim El-ghayoury, Luis Sánchez, J. C. Hummelen, E. W. Meijer and René A. J. Janssen, *Chemical Communications*, **2002**, 23, 2888-2889.

*Singlet-Energy Transfer in Quadruple Hydrogen-Bonded Oligo(p-phenylenevinylene) Perylene-Diimide Dyads*

Edda E. Neuteboom, Edwin H. A. Beckers, Stefan C. J. Meskers, E. W. Meijer and René A. J. Janssen, *Organic and Bioorganic Chemistry*, **2003**, 1(1), 198-203.

*Supramolecular Fullerene Architectures by Quadruple Hydrogen Bonding*

Minze T. Rispens, Luis Sánchez, Edwin H. A. Beckers, Paul A. van Hal, Albertus P. H. J. Schenning, Abdelkrim El-ghayoury, Emiel Peeters, E. W. Meijer and René A. J. Janssen and J. C. Hummelen, *Synthetic Metals*, **2003**, 135-136, 801-803.

*Charge Transfer Kinetics in Fullerene-Oligomer-Fullerene Triads Containing Alkylpyrrole Units*

Edwin H. A. Beckers, Paul A. van Hal, Anantharaman Dhanabalan, Stefan C. J. Meskers, Joop Knol, J. C. Hummelen, René A. J. Janssen, *Journal of Physical Chemistry A*, **2003**, 107(32), 6218-6224.

*Supramolecular Control over Donor-Acceptor Photoinduced Charge Separation*

Alicia Marcos Ramos, Stefan C. J. Meskers, Edwin H. A. Beckers, Ryan B. Prince, Luc Brunsveld and René A. J. Janssen, *Journal of the American Chemical Society*, **2004**, 126(31), 9630-9644.

*Charge Separation and Recombination in Photoexcited Oligo(p-phenylene vinylene) – Perylene Bisimide Arrays close to the Marcus Inverted Region*

Edwin H. A. Beckers, Stefan C. J. Meskers, Albertus P. H. J. Schenning, Zhijian Chen, Frank Würthner, and René A. J. Janssen, *Journal of Physical Chemistry A*, **2004**, 108(34), 6933-6937.

*Supramolecular p-n-Heterojunctions by Co-Self-Organization of Oligo(p-phenylene vinylene) and Perylene Bisimide Dyes*

Frank Würthner, Zhijian Chen, Freek J. M. Hoeben, Peter Osswald, Chang-Cheng You, Pascal Jonkheijm, Jeroen v. Herrikhuyzen, Albertus P. H. J. Schenning, Paul P. A. M. van der Schoot, E. W. Meijer, Edwin H. A. Beckers, Stefan C. J. Meskers, and René A. J. Janssen, *Journal of the American Chemical Society*, **2004**, 126(34), 10611-10618.

*Photoinduced Multistep Electron Transfer in an Oligoaniline–Oligo(p-phenylene vinylene)–Perylene Diimide Molecular Array*

Alicia Marcos Ramos, Edwin H. A. Beckers, Ton Offermans, Stefan C. J. Meskers, and René A. J. Janssen, *Journal of Physical Chemistry A*, **2004**, 108(40), 8201-8211.

*Charge Transfer in Supramolecular Co-Aggregates of Oligo-(p-phenylenevinylene) and Perylenebisimide in Water*

Edwin H. A. Beckers, Pascal Jonkheijm, Albertus P. H. J. Schenning, Stefan C. J. Meskers, and René A. J. Janssen, *ChemPhysChem*, **2005**, 6, 2029-2031.

*Sequential Energy and Electron Transfer in Aggregates of Tetrakis-[Oligo(p-phenylenevinylene)]-Porphyrins and C<sub>60</sub> in water*

Martin Wolffs, Freek J. M. Hoeben, Edwin H. A. Beckers, Albertus P. H. J. Schenning and E. W. Meijer, *Journal of the American Chemical Society*, **2005**, 127, 13484-13485.

*Organoselenium Substituted Poly(p-Phenylenevinylene) (PPV)*

Nicolai Stuhr-Hansen, Edwin H. A. Beckers, Lars Engman, René A. J. Janssen, *Heteroatom Chemistry*, **2005**, 7, 656-662.

*The Influence of Intermolecular Orientation on the Charge Transfer Kinetics in Self-assembled Oligo(p-phenylene vinylene)-Perylenebisimide Arrays*

Edwin H. A. Beckers, Stefan C. J. Meskers, Albertus P. H. J. Schenning, Zhijian Chen, Frank Würthner, and René A. J. Janssen, *Journal of the American Chemical Society*, in press.

*The Importance of Nanoscopic Ordering on the Kinetics of Photoinduced Charge Transfer in Aggregated  $\pi$ -Conjugated Hydrogen-Bonded Donor-Acceptor Systems*

Edwin H. A. Beckers, Stefan C. J. Meskers, Pascal Jonkheijm, Albertus P. H. J. Schenning, Zhijian Chen, Frank Würthner, and René A. J. Janssen, *manuscript in preparation*.

# Dankwoord

Allereerst ben ik natuurlijk dank verschuldigd aan mijn promotor René Janssen. Niet alleen omdat hij mij tijdens dit promotieonderzoek altijd met raad en daad heeft bijgestaan, maar in het bijzonder omdat hij voor een werkplek zorgt waarbij al het nodige voorhanden is. René, geweldig dat je zoveel tijd wil besteden aan vergaderingen, rapporten en andere bureaucratische rompslomp om een haast perfect lab te creëren terwijl je eigenlijk liever zelf met gereedschapskist, spiegels en cuvetten in de weer zou zijn.

Aan de basis van veel van de experimenten die beschreven staan staat de nooit opdrogende bron van creativiteit van Stefan Meskers. Ik ben je zeer erkentelijk voor de kritische discussies waarbij het even laten zien van een meting snel weer leidde tot een volgeplande nieuwe week vol “mogelijkheden”. Hopelijk heb ik een paar van je vragen op kunnen lossen, maar ik denk dat er nog steeds een flinke kast vol met uitdagingen ligt te wachten op nieuwe AIO's, die er zeker geen spijt van zullen krijgen als ze met jou in zee gaan.

Mijn interesse voor dit vakgebied werd aangewakkerd door mijn begeleider van het eerste uur Paul van Hal. Veel respect voor de tijd die je hebt genomen om mij gedurende 4 jaar de wondere wereld van de fotofysica te laten zien. Soms leken de discussies met jou als sparrings-partner veel tijd te kosten, maar uiteindelijk was het netto wel de productiefste tijd van mijn promotieonderzoek.

Aangezien ik zelf op zijn zachtst gezegd geen syntheses wonder ben is de aanwezigheid van een uitstekend syntheseslab een uitkomst. Daarom wil ik Bert Meijer en Albert Schenning graag bedanken voor de fantastische moleculen die altijd voor handen waren en het kritisch in het oog houden van de (supra)moleculaire kant van mijn verhalen. Wanneer ik hierbij persoonlijk zou moeten uitleggen wie elk molecuul gesynthetiseerd heeft zou het dankwoord flink uit de hand gaan lopen. Dit neemt echter niet weg dat ik het ongelooflijk waardeer dat Pascal Jonkheijm, Alicia Marcos Ramos, Edda Neuteboom, Emiel Peeters, Maarten Pouderoijen, Abdelkrim El-Ghayoury, Freek Hoeben, Jeroen van Herrikhuizen, Martin Wolffs, Anantharaman Dhanabalan en Asha Syamakumari hun met bloed, zweet en tranen gemaakte verbindingen aan mij durfden toe te vertrouwen.

Naast de moleculen uit Eindhoven is ook een belangrijk deel van het hier beschreven werk tot stand gekomen door samenwerkingen met andere universiteiten. Speciale dank is hierbij op zijn plaats voor de fullerenen van Minze Rispen, Luis Sánchez en Kees Hummelen van de Rijksuniversiteit Groningen die beschreven staan in de hoofdstukken 2 en 6. I would like to show my appreciation to Zhijian Chen and Frank Würthner of the University of Würzburg who provided a considerable share of the perylene chromophores mentioned in this thesis. In addition, I would also like to acknowledge Philippe Marsal, David Beljonne and Jérôme Cornil of the University of Mons-Hainaut for the calculations described in Chapter 5.

I'm honored that Michael Wasielewski and Jan Verhoeven were willing to participate as members of my committee. I would like to stress here that this is not only for reading and discussing my manuscript but also, probably without knowing, for being an inspiration with their own work.

Tijdens mijn promotietijd ging het gebruik van de verschillende apparaten zoals dat eigenlijk hoort niet altijd vlekkeloos. Daarom ben ik enkele mensen zeer dankbaar dat zij een prima vangnet vormden om steeds snel ervoor te zorgen dat alles weer naar behoren functioneerde. Hierbij wil ik met name Hans Damen en Martijn Wienk noemen, maar zeker ook de mensen van de technische dienst van de TUE en de immer hulpvaardige en zeer deskundige Hans Regeer en Paul Graff van Spectra Physics.

Als extra randvoorwaarde om naast het technische gedeelte ook alle andere zaken perfect te verzorgen is geen beter team denkbaar dan Henk Eding, Hannie van der Lee, Joke Rediker, Hanneke Veldhoen, Ingrid Dirx en Carine van der Vaart.

Een belangrijke steun en toeverlaat tijdens een promotie is de kamergenoot. Jos, onze verschillen in opvatting over zo ongeveer elk denkbaar onderwerp leverden vaak mooie discussies op. De combinatie Paulusse-Beckers resulteert daarom in een kippenhok waar menig theekransje jaloers op zou zijn. Hopelijk heb ik je niet teveel van je zoektocht naar supramoleculair katalyse afgehouden, in ieder

geval heb je er nog een fijne lijst met levenswijsheden voor de toekomst aan overgehouden, doe er je voordeel mee zou ik zeggen.

Naast geweldig onderzoek kun je bij SMO ook terecht voor een flinke invulling van je vrije tijd. Ik wil hierbij dan ook speciaal Linda, René, Anouk, Jeroen, Pascal, Hinke, Michel, Patricia, Sander, Mathieu, Chris en Dirk bedanken voor de fietstochten, bioscoop- en Liquidbezoeken, CL-breaks, koffiepauzes in de mannenhoek, bijstand bij zwemkilometers op de vroege ochtend, etentjes en uit de hand gelopen kerstborrels.

Het belang van een geïnteresseerd en stimulerend thuisfront is natuurlijk ook een niet te onderschatten factor. Pap, mam, Bianca en Erwin, bedankt voor de niet aflatende steun en waardevolle adviezen die jullie sinds jaar en dag aan me geven.

Als laatste woord staat hier meestal een verontschuldiging voor het gebrek aan aandacht dat de betreffende vriend of vriendin heeft moeten doorstaan tijdens de vele uurtjes schrijftijd die in een proefschrift gaan zitten. Wencke, in dit geval is dat geloof ik niet op zijn plaats, aangezien jij vooral grote concurrentie was voor het eindelijk gereedkomen van dit proefschrift. Vaak was het erg lastig om mijn roze bril af te zetten om me toch echt eens efficiënt met schrijven bezig te gaan houden. Uiteindelijk is mijn boekje toch afgekomen en hoef ik dus eigenlijk geen moment spijt te hebben van die iets minder productieve tijden. Ik kan nu weer met een gerust hart wegdromen bij de mooie toekomst die wij samen ongetwijfeld tegemoet gaan.

Edwin

